Spectral and ocellar inputs to honeybee motion-sensitive descending neurons

by

Yu-Shan Hung

Jan 2012

Supervisor: Professor Michael Ibbotson

A thesis submitted for the Degree of Doctor of Philosophy of The Australian National University

Declaration

Chapters 2 and 3

Professor Michael Ibbotson played a supervisory role. I did all of the measurements for the optical work, performed all of the work associated with the anatomy of the cells, including filling, processing and sectioning the tissue. I did all of the neural and ocellar 3D-reconstructions. I wrote-up the work.

Chapter 4 and 5

Prof. Michael Ibbotson played a supervisory role. Dr. Gert Stange and Robert Parker designed and built the wide-field LED display. Dr. Joshua van Kleef helped me to program the LED display for the visual stimuli. He also supervised and helped me with writing and developing the analysis codes for the physiological data. However, I conducted all the electrophysiological recordings, performed the data analysis, did the anatomy work for the neural identifications and wrote up the work.

Chapter 6

This chapter was published in 2011 by Yu-Shan Hung, Joshua P. van Kleef and Michael R. Ibbotson in the Journal of Comparative Physiology (Vol. 197(12) pp.1173–1187)

Prof. Michael Ibbotson played a supervisory role. Yu-Shan Hung performed and analysed the experiments on the physiology and anatomy of the reported neurons. Joshua van Kleef helped develop the visual stimuli

that were presented on the LED display. The manuscript was written and edited by Yu-Shan Hung and Michael Ibbotson.

I certify that the material presented in this thesis, unless acknowledged above, is my own work.

Yu-Shan Hung 12/01/2012

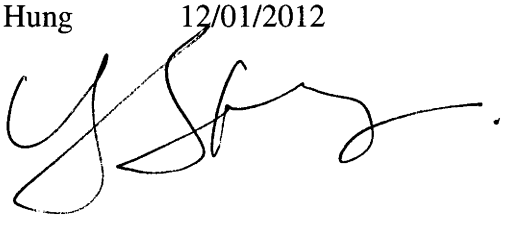

Acknowledgements

First and foremost I would like to thank my supervisor Professor Michael Ibbotson who made this thesis possible with his support, optimism and regular editing. I would also like to thank my advisors: Ted Maddess, Jan Hemmi and Joshua van Kleef, for their helpful words. The panoramic LED display which is crucial to this study was designed and built by Gert Stange and Robert Parker, for which I thank them. Thanks to Joshua van Kleef who programmed the LED display and helped me with writing the MATLAB scripts for the analysis of the data. Thanks also to Richard Berry, who showed me how to do the back-focal length measurements and neural histology, Shaun Cloherty, for sharing MATLAB codes and advice, and Markus Hietanen who gave me sound advice on the statistical analysis. Thanks to Alex Hadjinicolaou and Raymond Wong who proof read the drafts for me and, for their company when I needed it. Last but not least, I give thanks to my wonderful family, my parents and two sisters, for their encouragement, continued support and love.

Abstract

Optomotor reflexes have been observed in many insects and in some cases the neural pathways that mediate these reflexes have been identified physiologically and anatomically. In honeybees Kaiser (1975) established that the spectral sensitivity of optomotor responses in bees almost exactly matched that of the green photoreceptors, suggesting an exclusive input from green photoreceptors. However, physiological studies showed that the motion detectors in the optic lobes have a secondary response peak in the UV region of the spectrum suggesting that there may be more than one type of photoreceptor involved in the optomotor response. Thus in this thesis, I investigate the neural basis of motion and spectral wavelength processing in motion-sensitive descending neurons, which are on the optomotor response pathway, to reveal the neural contributions from other spectral receptor types. In this study, intracellular recording techniques were utilised. The stimuli consisted of a wide-field LED (light emitting diode) display in which green (peak 530 nm) and short-wavelength (peak 380 nm) LEDs were mounted in pairs across a wide visual area. Six types of motion-sensitive descending neurons were recorded and anatomically identified, including two pitch-sensitive neurons ($Locth_3$, $DNII_2$), two roll-sensitive neurons ($DNIV_2$ and $DNIV_3$) and two yaw-sensitive neurons ($DNVII_1$ and $DNVII_2$). The results show that for the vertical sensitive (pitch and roll) neurons, the cells have equal-sized excitatory responses to motion when using short-wavelength or green motion stimulation. However, for the horizontal sensitive (yaw-sensitive) neurons excitatory responses only occurred for the green stimulus in the preferred direction. The short-wavelength stimulus induced clear inhibitory responses for all tested motion directions. The results suggest that besides green photoreceptors, the

motion-sensitive descending neurons also receive inputs from the short-wavelength photoreceptors, but only for motion detectors tuned for vertical motion.

Honeybees, like most flying insects, have three ocelli (simple eyes) located on the top of the head, in addition to the compound eyes. However, the exact function of the bee ocelli and the information computation between the ocelli, compound eyes and central brain remain unclear. In this thesis, I investigate the ocellar properties morphologically, anatomically and physiologically. Semi-thin sections and focal length measurements were performed on both median and lateral ocelli, a 3-dimensional reconstruction model of the honeybee ocellar lenses and retinas was developed to understand the visual fields of the ocelli. Intracellular electrophysiology experiments were carried out on descending neurons to understand the information processing between the ocelli and compound eyes. Cell responses to different stimuli were recorded with and without the ocelli covered. It is shown that the ocellar input provides a faster response to motion stimuli than with compound eye stimulation alone, and also increases the amplitude of responses to flashed stimuli. In the case of the $DNII_2$ neuron, it is also shown that the ocelli provide a directional contribution to the responses.

Contents

Chapter 1

General Introduction

Vision, the ability to see, provides most animals with a remarkably rich source of information about the environment in which they live and is crucial for their survival (Gibson, 1979). Vision enables animals to orientate and spatially navigate as well as detect smaller targets like predators, prey or conspecifics (Vorobyev and Brandt 1997; Kelber 1999; Vorobyev and Menzel 1999; Cronin et al. 2000; Olberg et al. 2000; Srinivasan et al. 2000b). It is perhaps for this reason that diverse types of animals from vertebrates to invertebrates have devoted a significant portion of their nervous system to processing visual signals (Barton et al. 1995). Vision processing begins when light reaches the sensory cells, the photoreceptors, where photoconversion of a molecule into its active state begins a chemical cascade that leads to an electrical response, a process called phototransduction. The visual information collected by the photoreceptors is transmitted to consecutive levels of the nervous system through synaptic and electrical connections. Ultimately the knowledge transmitted by the visual system subserves a particular behavioural function.

1.1 Honeybees as a model of visual studies

The European honeybee, *Apis mellifera* L., is renowned for its impressive repertoire of visually guided behaviours. Karl von Frisch first demonstrated that bees could be trained to distinguish the different wavelengths of light

('colours') reflected from surfaces, independent of the brightness (von Frisch 1914, 1967). Von Frisch also showed that honeybees can orient to the polarization pattern in the sky and use it as a compass (von Frisch, 1949). Since von Frisch, many behavioural experiments have utilized honeybees to ask fundamental questions about visually guided behaviour (for an overview see Horridge, 2009). These include pattern recognition (Horridge, 2000) odometry (Srinivasan et al., 1996, 2000a), flight control (Srinivasan et al., 1996) and gaze control (Böddecker and Hemmi, 2010).

Besides the well established behavioural patterns and cognitive capabilities mentioned above, honeybees have a relatively simple nervous system whose structure has been mapped extensively. This makes it a good model system for analysing the neural circuits and mechanisms that underlie certain behaviours. Honeybee brain anatomical studies can be traced back to 1850, when Dujardin dissected the brain from the head capsule. Since then, there have been extensive works on the honeybee brain anatomy using various techniques and approaches (e.g. Kenyon 1896; Cajal and Sanchez 1915; Flanagan and Mercer 1989; Hammer and Menzel, 1995; Menzel, 2001; Ribi et al. 2008). The function of many of the structures and regions are now well established (Fig. 1 shows an X-ray microCT image of a honeybee brain (adopted from Ribi et al. 2008). For example, the antennal lobes are responsible for processing olfactory information (e.g. Flanagan and Mercer 1989); the mushroom bodies are the main area for learning and memory (for a review, see Hammer and Menzel 1995; Menzel 2001) Last, and importantly for us here, the optic lobes that process visual inputs from the compound eyes (e.g. Hertel and Maronde 1987) have been anatomically mapped in exquisite detail.

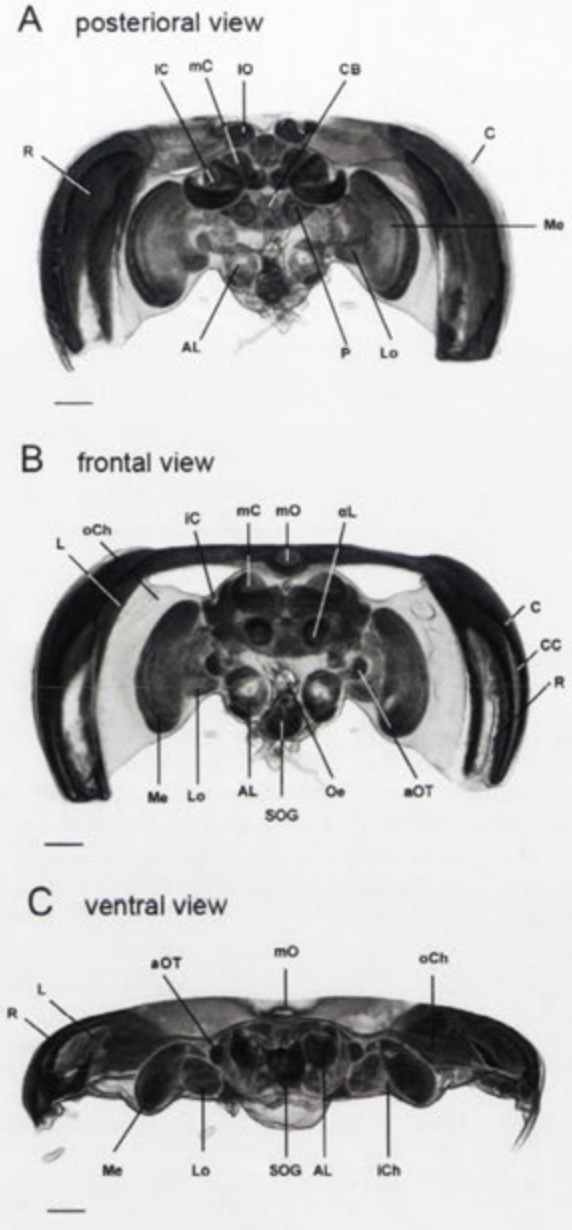

Figure 1.1: X-ray micro CT of honeybee brain (figure adopted from Ribi et al. 2008). A: posterior view; B. frontal view; C: ventral view. ***Abbreviations*:** AL, antennal lobe; aOT, anterior optic tubercle; C, cornea; CB, central body; CC, crystalline cone area; iCh, inner chiasma; lC left lateral calyx; αl, α lobe; L, lamina; Lo, lobula; lO, left lateral ocellus; mC, left median calyx; Me, medulla; mO median ocellus; oCh, outer chiasma; Oe, oesophagus; P, right pedunculus; R, retina; SOG suboesophageal ganglion. Scale bar 100μm.

1.2 Visual systems of honeybee

Honeybees, like most other insects, are equipped with two visual subsystems: the compound eyes and ocelli. Each of these subsystems has different optical and anatomical characteristics, visual pathways and appears to serve different functions. The compound eyes are known to be responsible for colour vision, form vision, target detection, and motion detection, while the exact function of the honeybee ocelli is as yet not completely understood.

1.2.1 Compound eyes

In insect compound eyes, the ommatidia are the basic structural-functional units that receive visual information from the environment; they contain photoreceptors that transfer the optic information into visual neuronal signals and then forward the neuronal signals into the brain for further processing. There are two types of compound eye design in the Insecta: apposition the superposition compound eyes (for review, see Warrant 2006, 2008; Horridge 1980). In apposition compound eyes each ommatidium is shielded and isolated from its neighbours by a sleeve of screening pigments, thus preventing light reaching the photoreceptors from all but their own corneal lens (Fig 1.2A). The superposition eye on the other hand, forms a clear zone between the corneal lenses and the photoreceptors. The light focused by the corneal facets and the crystalline cones then run across the clear zone toward a single photoreceptor in the retina. In the case of the superposition eyes, a single photoreceptor would receive light from many facets (Fig 1.2B). Superposition compound eyes are designed to enhance light signals; usually hundreds or even thousands of facets service a single retinal cell. Thus the superposition compound eyes have high sensitivity to light, but poor spatial resolution. Apposition compound eyes on the other hand, allow high spatial resolution but are less sensitive to light. The

apposition compound eyes are usually found in diurnal (day-active) insects which live in bright habitats, while superposition compound eyes are usually found in nocturnal insects.

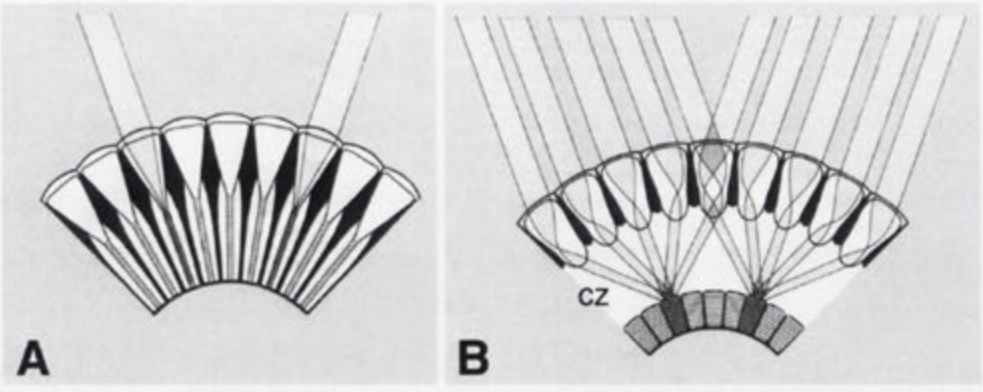

Figure 1.2: Schematic diagrams of the two main compound eye designs (figure adopted from Warrant 2008). A: The apposition compound eye: light reaches the photoreceptors exclusively from the cornea directly above. B: The superposition compound eye: light is collected and focused by the corneal facets and crystalline cones. As the light travels across the clear zone (CZ) of the eye it reaches a single photoreceptor.

Honeybees, as day-active insects, are equipped with apposition compound eyes. Physiological studies on honeybee compound eyes show that the honeybees, like humans, are trichromatic with photoreceptors maximally sensitive at wavelengths of 350nm (ultraviolet, UV), 440 nm (blue), and 540 nm (green) (see **Fig 1.8B**; Autrum and von Zwehl 1964; Menzel and Blakers 1976; Menzel et al. 1986). There are about 5,500 ommatidia in a worker bee's compound eye, and 9 photoreceptors in each ommatidium (Gribakin 1969ab). The main photoreceptors (R1-8) contribute their microvilli to the entire length of the rhabdom, while the basal R9 contributes microvilli only at the base of the ommatidium (Gribakin 1969ab; Menzel and Snyder 1974). Depending on the types of R1-8 they contain, the

ommatidia can be divided into three types (type I, type II, and type III). Every type of ommatidia has six green receptors, while type I ommatidia contain one ultraviolet and one blue receptor, type II ommatidia contain two ultraviolet receptors, and type III ommatidia contain two blue receptors. Each type is distributed rather randomly in the ratio of 44:46:10 over the retina (Wakakuwa et al. 2005).

The optic lobes

Histological studies on insect brain structure started in the late nineteenth century (e.g. Leydig 1885). Hickson (1885) was the first to describe the three optic lobes in *Musca*. Early histological studies were usually carried out using Golgi techniques and methylene-blue, however, the use of modern techniques for example the nuclear magnetic resonance (NMR; honeybee brain, Haddad et al. 2004), micro-X-ray-computed tomography (honeybee brain, Ribi et al. 2008) and the development of 3-dimensional atlases (fly brain, e.g. Peng et al. 2011) has helped to understand the more detailed structures. Three-dimensional atlases of insect brains can also be used to develop the standard-shape of insect brains (e.g. locust, el Judi et al. 2009; *Drosophila*, Rein et al. 2002; honeybee, Brandt et al. 2005). In this section, I will introduce the structure of the honeybee compound eye pathway, the optic lobes, based on previous histological and neural anatomical studies.

The optic lobes of honeybees contain three layers of neuropile, known as the lamina (the 1st optic ganglion), medulla (the 2nd optic ganglion) and lobula (the 3rd optic ganglion). The optic lobes consist of thousands of parallel and identical channels, providing the neural machinery for visual information processing (Hertel and Maronde 1987). The ganglia are successive stages of signal processing. From the retina to at least the lobula, each successive ganglion is a retinotopic array with different processing capacities (Meinertzhagen 1976). Neuroanatomical studies showed that the axons of retinal cells from one ommatidium remain together and are associated with neurons originating in the lamina and the medulla to form a cartridge (Ribi 1974). While each cartridge receives sensory axons

only from one ommatidium, the nine receptor cells in each ommatidium end as six short visual fibers (svfs) in the lamina, and three long visual fibers (lvfs) in the medulla (Ribi 1979). Electrophysiological recordings from the monopolar cells in the bee lamina also indicated that the input of the monopolar cells are from more than one photoreceptor type, and the spectral sensitivity is wider than that of a single receptor (Menzel 1974; de Souza et al. 1992).

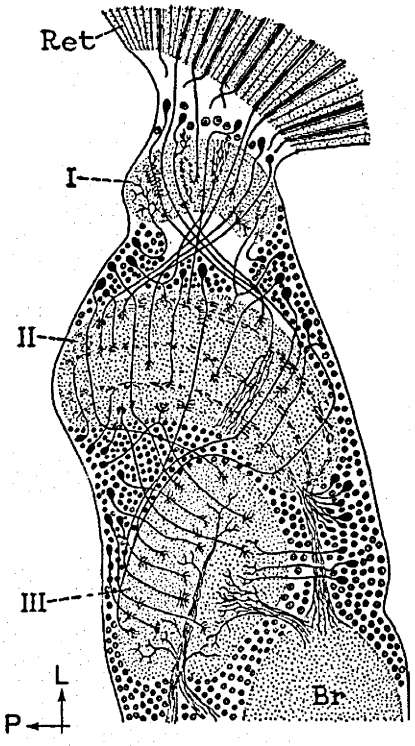

Figure 1.3: Schematic diagram of the compound eye pathway (Figure adopted from Snodgrass 1956). Behind the retina (Ret), there are three successive neuropiles known as the lamina (the 1st optic ganglion, I), the medulla (the 2nd optic ganglion, II), and the lobula (the 3rd optic ganglion, III). The ganglia form successive stages of signal processing. From the retina to at least the lobula, each successive ganglion is a retinotopic array with different functions.

***Abbreviations*:** Br, brain; L, lateral; P, posterior; Ret, retina

The medulla and the lobula contain higher order visual neurons, which have a precise neuronal arrangement (Ribi and Scheel 1981). The lobula receives the outputs of the medulla and transfers them onto extrinsic fibres that leave the optic lobes and project into the protocerebrum for further signal processing (Hertel and Maronde 1987). While in flies, moths and butterflies, the lobula is divided into two parts (the lobula and lobular plate), as shown in Figure 1.4B, the honeybee lobula is a complex stratified ganglion with six clear layers (Cajal and Sanchez 1915; Ribi and Scheel 1981; Strausfeld and Blest 1970; Strausfeld 1970). In bumblebees, it has been shown that both the medulla and the lobula can be morphologically

divided into layers (see Fig 1.4A; Paulk et al. 2008, 2009a). The eight layers in the medulla process increasingly complex aspects of the visual image as they get closer to the central brain. Moreover, the neurons in different layers (grouped as layer 1–4 and layer 5–6) have different roles within the lobula (Paulk et al. 2008, 2009a). Physiological studies showed that the neurons in layers 1–4 are usually insensitive to colour (i.e. not colour opponent; see section **1.4.1** for introduction of colour opponency) but are sensitive to motion, while those in layers 5–6 are sensitive to both colour and motion cues. The results suggest that the anatomical layers in the bumblebee lobula form the structural basis for the segregation of visual information into colour and motion (Paulk et al. 2008, 2009b). Bumblebee brain structure is very similar to that of honeybee (Mares et al. 2005).

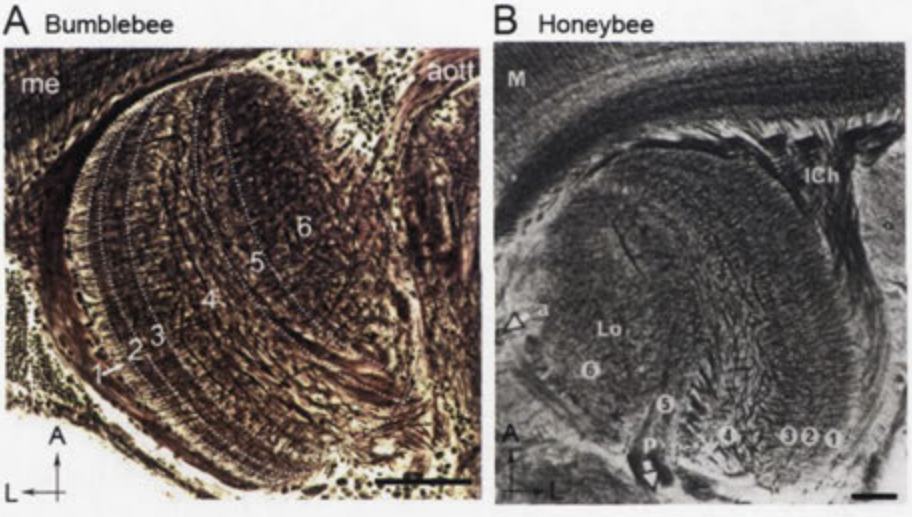

Figure 1.4: The lobula structure of bees. A: Horizontal section of a reduced silver Bodian stained **bumblebee** (left lobula, adopted from Paulk 2008). B: Horizontal sections of a Golgi stained **honeybee** (right lobula, adopted from Ribi and Scheel 1981). It can be seen that the lobula structures of the bumblebee and the honeybee are very similar. In both cases, six morphological layers can be seen clearly. It can also be seen that the lobula sends two nerve tracks out to both the anterior (A: the anterior optic track, aott; B: *arrow* a) and posterior (B: *arrow* p) side of the brain. ***Abbreviations*:** A, anterior; acott, anterior optic track; ICh, inner chiasma; L, lateral; Lo, lobula; m and me, medulla. Scale bars: A, 500 µm; B, 50 µm

Kaiser and Bishop (1970) first recorded from honeybee visual interneurons in the compound eye pathway and found light-sensitive and direction-selective units in the honeybee optic lobes. After their discovery, many physiological studies were carried out on the honeybee optic lobes to reveal the response properties of neurons and the mechanisms leading to visual information processing within the three ganglia. In honeybees both medulla and lobula neurons are found that have spectral wavelength-specific coding mechanisms and respond to motion stimulation in a direction-selective manner (e.g. DeVoe et al. 1982; Hertel 1980; Paulk et al. 2008, 2009ab). The wavelength-specific coding shows that response intensity is coded only for strictly limited spectral wavelengths of light. The cells can be classified based on their response types: broad-band and narrow-band. The former receive signals from two or more photoreceptors. The latter receive signals from one type of photoreceptor only and are colour opponent neurons (Hertel 1980; Kein and Menzel 1977ab; Paulk et al. 2008; Yang et al. 2004). The direction-selective neurons (i.e. they have excitatory responses to motion in one direction, and either little or an inhibitory response to motion in the opposite direction) in the compound eye pathway have never been found at the photoreceptor or the lamina levels. However, many insects, such as locusts (Osorio 1986a), flies (e.g. DeVoe 1980; DeVoe and Ockleford 1976), butterflies (Ibbotson et al. 1991), moths (Collett 1971) and honeybees (e.g. Hertel 1980) have been found to have direction-selective units in the medulla, suggesting that motion computation starts at the medulla level. Although both medulla and lobula neurons show motion-sensitive characteristics, the neurons have characteristic differences between the two structures. For example, direction-selective neurons found in the medulla have smaller receptive fields than those found in the lobula (flies, Collett and King 1975).

1.2.2 Ocelli

Ocelli are also known as dorsal ocelli, or simple lens eyes. Most flying insects are equipped with three ocelli together with the two larger compound eyes. The morphology and the numbers of the ocelli differ between species; it could be different within the same insect order or, even in the same insect family (reviewed in Goodman 1981). Honeybees have three ocelli on the dorsal surface of the head between the compound eyes; each ocellus consists of approximately 800 retinal cells (Toh and Kuwabara 1974). They are simple lens eyes and the photoreceptors in the retinas have peak spectral sensitivities at 340 (UV) and 490nm (green) (Goldsmith and Ruck 1958). The exact roles of the ocelli are still unclear.

Ocellar interneurons

Pan and Goodman (1977), using the cobalt sulphide technique, reported the anatomy of the ocellar projections within the honeybee central nervous system. In their study they found that despite there being approximately 800 retinal cells in each ocellus (Toh and Kuwabara 1974), the honeybee has very few second order neurons (see Fig 1.5). Dividing the neurons by the size of the fibres, they showed that there are 5 large fibres that have dendrites in the retina of the lateral ocellus and 12 that have dendrites in the retina of the median ocellus. As for medium sized fibres, there are 9 in each of the lateral ocellar retinas and 12 in the median ocellar retina. Both the large and medium size fibres project terminal arborisations into the brain and form two different ocellar association areas in the brain. The large ocellar fibres have wide-field terminal arborisations in the ocellar association areas on either side of the median posterior protocerebrum (mpp, terminology and brain anatomy see Chapter3, Figure 3.2). The median size ocellar fibres form a second ocellar association area close to the dorsal lobes on each side of the oesophageal foramen. There are also a group of fine

fibres in the ocellar nerves that arborise just below and anterior to the protocerebral bridge.

Also, the honeybee has 5 pairs of ocellar interneurons, which run from the ocellar retina through the ocellar nerve tracks to the pro- and mesometathroacic ganglia (Pan and Goodman 1977; Milde and Homberg 1984). The distinct 5 pairs of honeybee ocellar descending neurons include one pair that have dendrites in the median ocellar retina (Mocth) and four pairs that have dendrites in the lateral ocellar retinas ($Locth_{1-4}$). Physiological studies have shown that the ocellar interneurons in the honeybee are sensitive to light, and are direction sensitive to upward motion (Goodman et al. 1987; Milde 1984; Milde and Homberg 1984; Goodman et al. 1990). At least two of these neuron types, $Locth_1$ and $Locth_2$, were found to be multisensory, responding to both ocellar and compound eye input, and a variety of mechanosensory stimulation (Milde 1984; Goodman et al. 1987). The morphology and physiology of these neurons were shown to be similar in honeybees and a second hymenopteran insect, the European wasp (Goodman et al. 1987).

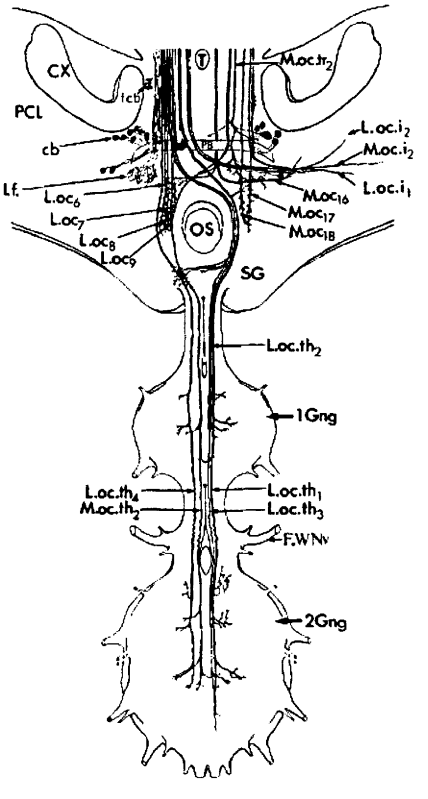

Figure 1.5: Schematic diagram of the pathways of honeybee ocellar interneurons (figure adopted from Pan and Goodman 1977).

The function of ocelli

Speculations about insect ocellar function started long ago. The speculations were proposed based on different aspects of the ocellar structure (optical properties), neural anatomy, physiological characteristics (for example, spectral sensitivity of the ocellar retinular cells or the light and motion response of ocellar neurons), to behavioural studies with the ocelli occluded. However, the exact functions of insect ocelli remain controversial.

Thus far, the most convincing hypothesis for ocellar function in flying insects is the **single sensor** hypothesis. The hypothesis was originally proposed by Wilson (1978), based on his research on locust ocelli. The term 'single sensor' was coined later by Stange et al. (2002). The fundamental core of the single sensor hypothesis proposed that the ocelli are not resolving spatial details of the environment. Instead, each ocellus is considered as a highly sensitive light detector which functions to detect global illumination levels from wide regions of visual space around the head of the insect. Certain aspects of the ocelli appear to be specifically designed to filter out unwanted spatial information. The hypothesis was supported by optical, anatomical and behavioural studies (see below).

The ocelli are typically considered to have very poor spatial resolving power because of their optical design. Homann (1924) reviewed the available literature on ocellar optics at the time, together with his own observations. Across several insect types he found that the lack of spatial resolving power is predominately due to under-focused dioptrics. The ocellar lenses in all the insects he tested were found to form images well beyond the location of the retina. This conclusion has been further proved by several more recent studies on locusts and blowflies (Berry et al. 2007b; Cornwell 1995; Parry 1947; Wilson 1978; Schuppe and Hengstenberg 1993). The large aperture of the ocellar lenses make them ideal for capturing light, thus allowing better sensitivity to illumination. Wilson (1978) used electrophysiological measurements to measure the neural sensitivity and estimated that the ocellar L-neurons in locusts are 5000 times more

sensitive to extended sources of light than compound eye lamina neurons. Moreover, in addition to the under-focused lenses, the ocelli are also characterised by high rates of convergence from first- to second-order neurons. For example, there are about 800 retinal cells in each of the honeybee ocelli (Toh and Kuwabara 1974), while only 30 large/medium sized ocellar neurons originate from the 3 ocelli (Pan and Goodman 1977). The high convergence ratios in combination with underfocused lenses presumably exclude the possibility of processing detailed spatial information in the ocelli. Therefore, each of the ocelli can be considered as a single optical sensor for illumination rather than consisting of individual pixels.

Parry (1947) concluded that the ocelli act as non-specific excitatory organs, which enhance visual responses mediated by the compound eyes in dim light. This view has been largely supported behaviourally in more recent times by Kastberger and Schuhmann (1993). By training honeybees flying through a certain feeding area and then to their hive, normal and ocelli-occluded bees were tested with side-light stimulation. It was found that the flight behaviour changed when the ocelli were occluded. The ocelli-occluded bees were only weakly affected by the side-light illumination (i.e. fewer turning responses), while the normal bees performed a quick positive turning response toward the stimuli (i.e. they turned toward the side-light during flight). In dragonflies, it was also shown that when the ocelli were occluded the animals had an unstable flight attitude and stalled when in the presence of a single light source with small angular dimensions (Mittelstaedt 1950).

Foraging activity in honeybees has been shown to be affected by two factors: the weather and the light intensity (Schricker 1965). The first and last of the daily flights is dependent upon the intensity of light. The occlusion of the honeybee ocelli however interferes with the timing of the first and the last foraging flight. Bees with ocelli occluded start to collect food later in the morning and cease collecting earlier in the evening than

normal workers (Renner and Heinzeller 1979). The behavioural studies suggest that ocelli play a regulatory role in diurnal activity through enhancing brightness sensitivity. In other insect species the ocelli were also shown to have an important role in modulating flight muscle coordination (locust: Taylor 1981b), and evoking head reflexes (dragonfly: Stange and Howard 1979; Stange 1981; locust: Taylor 1981a).

The single sensor hypothesis proposes that the ocelli are capable of high sensitivity but that they were not designed to process high spatial resolution information. However, growing evidence has challenged the applicability of the single sensor hypothesis based on more recent observations of the spatial resolving power of ocelli. Schuppe and Hengstenberg (1993) showed that although the ocelli are under-focused, the ocellar lenses of the blowfly (*Calliphora erythrocephala*) allow a limited degree of spatial resolution to be utilised by the retinal layer. Stange et al. (2002) also presented both anatomical and optical evidence from the dragonfly median ocellus and found that the dragonfly median ocellus is specifically adapted to detect horizontally extended features. More recently, studies have also shown that ocelli are able to resolve some spatial information, e.g. dragonflies (Stange et al. 2002; Berry et al. 2006; Berry et al. 2007a; Berry et al. 2007b; van Kleef et al. 2008) and wasps (Warrant et al. 2006). The capacity for some ocelli to resolve spatial features suggests that ocellar function may be more complex than previously suggested by the single-sensor theory.

Several insect species were found to have ocellar systems that were sensitive to both the UV and green range of spectral wavelengths, e.g., tobacco hornworn moths (Pappas and Eaton 1977) and dragonflies (Chappell and DeVoe 1975). Most of these insects are capable of flight. However, there are also some insects that only have green photoreceptors (cricket: Abner and Trouth 1989; nocturnal bee: Berry et al. 2011). The difference may have evolved because of the spectral composition of their habitant and visual environment in relation to some specific behaviour. The

honeybee ocellar system has developed receptor neurons with peak spectral sensitivities at 340 (UV) and 490nm (blue-green) (Goldsmith and Ruck 1958; Milde 1984), which occupy the same region of the spectrum as other flying insects. For flying insects, it is generally believed that ocellar UV sensation is for maximum contrast between the sky and ground, while green sensitivity is to detect contrast in low light conditions (Chappell and DeVoe 1975).

1.3 Optomotor response

Many animals, including humans, have a particular reflexive behaviour in which they follow the passive motion of the whole visual field with their eyes, heads and bodies. Such movements can occur within six degrees of freedom, three translational (forward/backward, up/down, side-to-side) and three rotational (roll, pitch or yaw; see Figure 1.6), when the visual field is moved unexpectedly.

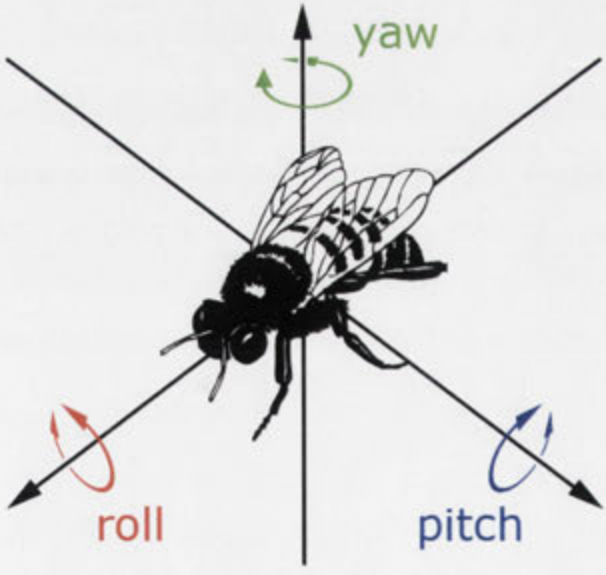

Figure 1.6: The rotational axes: roll, pitch and yaw. A 3-dimensional body can be rotated about three orthogonal axes, which are roll rotation about the *x-axis*; pitch rotation about the *y-axis*; and yaw rotation about the *z-axis*.

This behaviour is referred to as the optomotor response in insects and its equivalent in vertebrates is referred to as the optokinetic eye

response. The initiation of the optomotor response mostly relies on optic flow, which is the motion moving across an animal's eyes as the results of its locomotion or changes in the visual environment (review from Taylor and Krapp 2008). For example, if an animal makes a pitch upward movement, it generates a downward optic flow in the frontal visual field. The optic flow contains rich visual information such as speeds, directions, and distances to surfaces or edges. Behavioural studies have shown that on the basis of optic flow, insects are able to control their flying speeds (e.g. Srinivasan et al. 1996; Fry et al. 2009), their lateral position in a tunnel (e.g. Srinivasan 1991), or their height (e.g. Srinivasan et al. 1996, 2000b; Portelli et al. 2010).

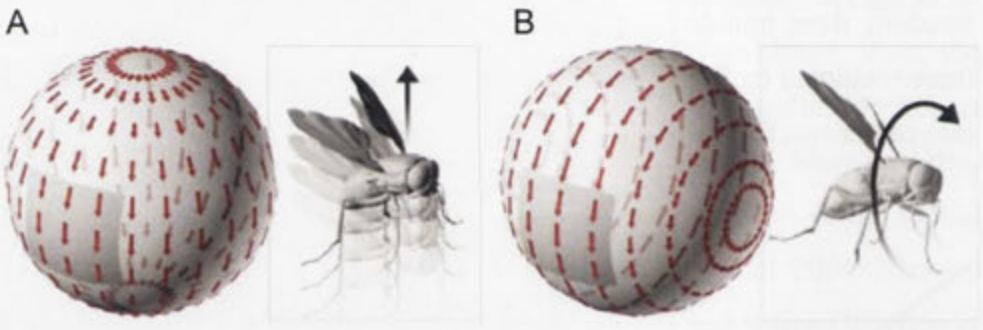

Figure 1.7: Optic flow fields generated by two manoeuvres- A: an upward vertical lift or pitch movement (frontally); B: leftward roll movement. The optic flow fields are presented by red arrow vector diagrams projected on a globe, which represents the visual fields of the animal. (Figure adopted from Zbikowski 2005)

The role of optomotor responses is to help animals stabilize the images on the retina and compensate for sudden movements of the visual environment, to maintain their orientation relative to the visual world. In general, the optomotor response consists of eye, head, or whole body movements. However, in insects, the eyes are fixed within the head capsule,

which allows virtually no eye movements (Hengstenberg 1972). It is therefore particularly important for insects to be able to detect self-movements relative to the visual environment because they are required to move their entire head or body to compensate, which requires far more musculature than the movement of the vertebrate eyeball within the eye socket.

The optomotor response has been observed in many flying insects (e.g. honeybees, Kunze 1961; flies, Eckert 1971; locusts, Robert 1988). The rotational motions around the yaw axis have been thoroughly studied in several insect species including honeybees (Kunze 1961; Kaiser and Liske 1974). Many insects have also been shown to generate torque in the roll and pitch axes (Musca: Srinivasan 1977; Drosophila: Blondeau and Heisenberg 1982; Locusta: Robert 1988). The term "optomoter response" was first coined by Schlieper (1927) and since then this behaviour has been used to study the mechanisms of motion vision and as a test for colour vision in early studies (Schlieper 1927). Schlieper had tested a number of insect species with rotating drums with alternating coloured and grey stripes. He found that in all the tested species, there was a particular combination of colour and a certain shade of gray that did not elecit the optomotor response, i.e. these insect species may be colour blind. Later, when he tested the honeybee optomotor response he discovered that although it was already well established that honeybees possessed colour vision (von Frisch 1914) the optomotor response appeared 'colour blind'.

Honeybees demonstrate strong optomotor responses (Kunze 1961, Schlieper 1927). The behavioural experiments suggested that the honeybee optomotor reactions show no colour-specific reactions and are "colour blind", but highly contrast-sensitive (Schlieper 1927; Kaiser and Liske 1972). From insects to vertebrates, optomotor responses have been widely observed to be colour blind, e.g. flies (e.g. Yamauchi et al 2008), goldfish (Schaerer and Neumeyer 1996), zibrafish (Krauss and Neumeyer 2003) and turtle (Schaerer and Neumeyer 1996). In the case of honeybees, Kaiser and

Liske (1974) subsequently measured the spectral sensitivity of the honeybee optomotor response for motion in the horizontal plane and found a single optimum performance at a spectral wavelength of 540 nm. As shown in Figure 1.8, this wavelength closely matched the peak of the spectral sensitivity function measured for green photoreceptors in honeybees (Kaiser and Liske 1974; Autrum and von Zwehl 1964; Menzel and Blakers 1976; Menzel et al. 1986). Thus, it has been suggested that honeybees use only one photoreceptor type (green) to drive the motion detectors that provide input to the optomotor system, thereby explaining the apparent colour blindness of the optomotor response (Kaiser 1974).

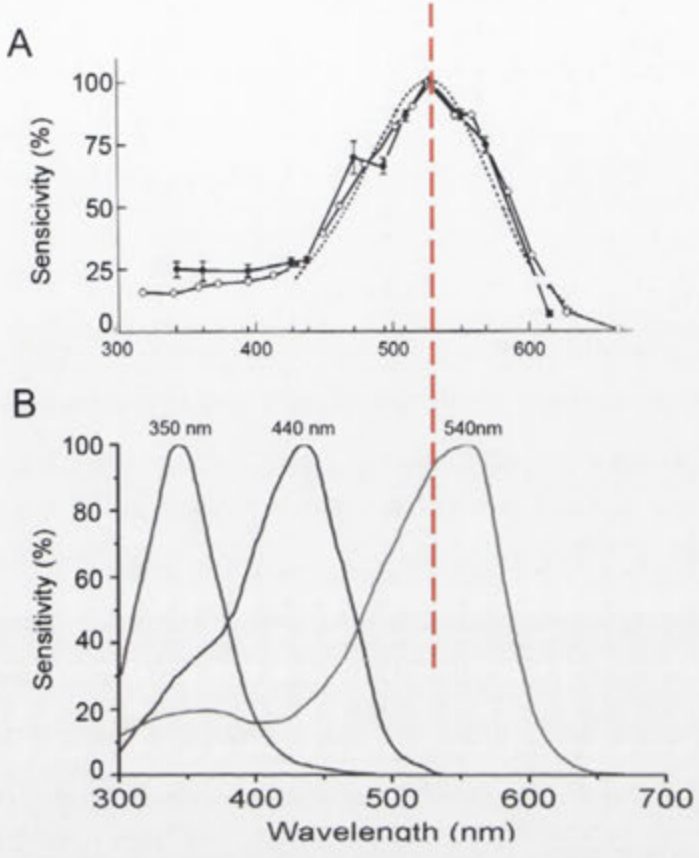

Figure 1.8: Spectral properties of honeybee. A: the action spectrum of the optomotor response (figure adopted from Kaiser 1974). B: the spectral sensitivity for honeybee photoreceptors (compound eyes). The three photoreceptor types (UV, blue and green) have maximum sensitivities at wavelengths of 350, 440, and 540 nm, respectively (Autrum and von Zwehl 1964; Menzel and Blakers 1976; Menzel et al. 1986). *Red dashed line* indicates the peak of the optomotor response. It is shown that the spectral sensitivity of the honeybee optomotor response (for motion in the horizontal plane) has optimum performance at a spectral wavelength of around 540 nm.

1.3.1 Colour vision

From vertebrates to invertebrates, different colours may have different kinds of meanings. For example, bright colours such as yellow and red for mating choice of fishes and birds, and some particular colours as cues for flower recognition and selection in insects (Chittka et al. 2001). Colour vision is a receptor-neural strategy, which enables an animal to detect or recognize objects with differences in spectral composition (Menzel and Backhaus 1991). However, not all animals possess colour vision, only those that are equipped with an appropriately designed visual system are able to discriminate colours. Colour vision is defined as the capability to discriminate spectral wavelengths based solely on the perception of the difference in the spectral distribution of the stimuli, independent of the relative intensities (Menzel 1979). The neural mechanism for colour vision is founded on the existence of two or more photoreceptor types maximally absorbing in different spectral ranges (Pichaud et al. 1999; Kelber et al. 2003). The absorption spectrum of photopigment can be read as the probability with which a photon of certain energy (related to the wavelength of the light) is going to be absorbed; in other words, the photopigment responds with the same change of neural response independent of the energy of the photon, and relates to the number of photons. Each photoreceptor is actually colour blind, and the central nervous system can compute the 'perception' of colours only by comparing the outputs of two or more of the different photoreceptor types. The phenomenon in essence follows the principle of Univariance: *The output of a receptor depends upon its quantum catch, but not upon what quanta are caught* (Rushton 1972; Naka and Rushton 1966).

However, it is not easy to determine whether an animal has colour vision, and colour discrimination is not present in all aspects of visual orientation (e.g. Zhang and Srinivasan 1993). For human, we can easily test colour vision using communication in terms that were first proposed by Newton to classify colours in 1672, such as red, blue and yellow etc; but we

cannot ask an animal what colours it sees. Thus, behavioural experiments are used to test colour discrimination in animals (Autrum and Thomas 1973). Because of the difficulties associated with behavioural training, so far, there are only a few invertebrate species that have been studied sufficiently to conclude that they have true colour vision, e.g. bees (von Frisch 1914), wasps (Chittka et al. 1992), flies (e.g. Troje 1993), butterflies (for example, Kolb and Scherer 1982; Kelber and Pfaff 1999).

As in the visual system of vertebrates, the output signals of insect photoreceptors are compared to assess how they differ in their spectral sensitivity by means of colour opponent cells (COCs) in the central nervous system (Buchsbaum and Gottschalk 1983; Menzel and Backhaus 1991). The COCs respond differently according to the stimulating spectra: the responses are excited by some wavelengths but are inhibited by others (for an example, see Figure 1.9). From earlier studies on vertebrate visual systems it is suggested that the colour opponency is one of the important neural mechanisms for processing colour information (e.g. de Valois 1973). The COCs provide the ability to extract the information about the spectral quality received by the photoreceptors. Spectral opponent mechanisms have been discovered in several insect species at the neural level (e.g. Locust: Osorio 1986b, 1987; cockroach: Edwards 1982; Mote and Rubin 1981). Honeybees have also been proved through both behavioural and physiological experiments to have similar colour opponent response patterns in the optic lobes (Chittka et al. 1992; Menzel and Backhaus, 1991; Kein and Menzel 1977ab; Paulk et al. 2008, 2009ab; Yang et al. 2004). However, scientists found that the receptive fields of the recorded COCs did not have centre-surround configurations, as had been found in vertebrates (Kein and Menzel 1977ab; de Valois 1973).

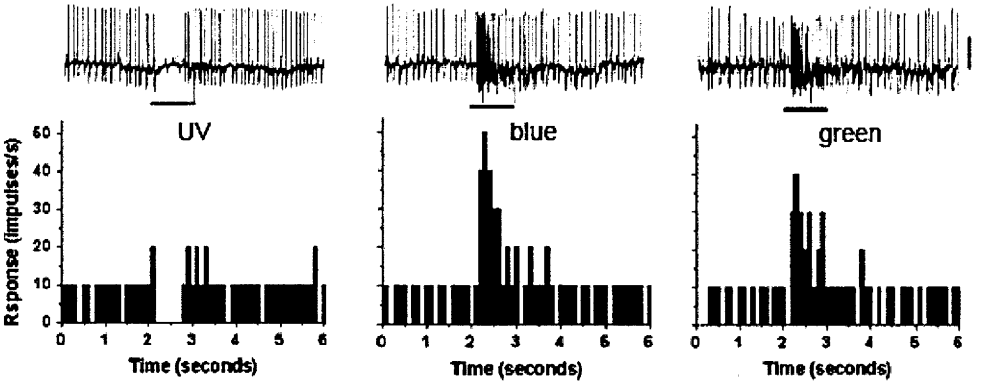

Figure 1.9: Responses of a colour opponent cell to flashes of three different spectra (UV, blue and green). The cell shows an inhibitory response to UV flashes, but tonic excitatory responses to blue and green flashes. (Figure adopted from Yang et al. 2004).

1.3.2 Motion detection and parallel processing of colour and motion signals

In many animals, motion detection is crucial for behaviours such as escape reactions, fixation, tracking, landing or prey capture. The response properties of motion detectors of different insects varies according to their visual ecology and have different response properties which allow them to detect motions at higher or lower velocities (O'Carroll et al. 1996). The study of motion processing in insects has a rich history with the first formal model (the correlation model, also known as the *Reichardt* model) was proposed by Hassenstein and Reichardt (1956). This model was based on behavioural observations first on a beetle (*Clorophanus*), then later on *Drosophila* and *Musca*. They used different moving patterns and measured the torque movement generated by the animals (i.e. the optomotor response). The core conclusions of the model are: 1. A sequence of two light stimuli on adjacent receptors is crucial for evoking an optomotor response; 2. The relation between stimuli to the receptors and the optomotor response follows

the rule of algebraic multiplication; 3. The strength of the optomotor response is proportional to the product of the two stimuli. The model has been extremely influential within the visual sciences. For example, similar models have been proposed to underlie motion detection in the primary visual cortex of mammals (van Santen and Sperling, 1985) and electrophysiological recordings suggest that neurons in the primary visual cortex do in fact perform the computations as predicted by the Reichardt model (Emerson et al., 1992).

The fundamental requirements for visual motion detection are that the image be sampled from at least two spatial locations, that there is a temporal asymmetry in the signals from these two spatial locations and finally that these signals are combined nonlinearly (Borst and Egelhaaf, 1989). Although it has been difficult to locate exactly where these computations are being performed within the insect visual system, recordings from the lobula suggest that higher-order visual cells do integrate the outputs of many spatially smaller units that perform these tasks (Borst and Egelhaaf, 1989).

The neural circuitry of motion processing involves the segregation of different types of visual information into retinotopic pathways that are found in primates and insects. The so-called parallel processing of different features of visual signals is well known in the visual systems of primates (e.g. Livingstone and Hubel 1988; van Essen and Gallant 1994), as well as insects (e.g. Douglass and Strausfeld 1995; O'Carroll 2001; Strausfeld and Lee 1991; Pfeiffer and Kinoshita 2012; Paulk 2008, 2009ab). The parallel processing of visual motion and colour information can be proven behaviourally (Srinivasan et al. 1993b; Lehrer 1994; Lehrer et al. 1990), neural anatomically, and electrophysiologically (e.g. Douglass and Strausfeld 1995; O'Carroll 2001; Strausfeld and Lee 1991; Pfeiffer and Kinoshita 2012; Paulk 2008, 2009ab). In honeybees, several motion-sensitive behaviours, such as optomotor responses (Kaiser and Liske 1974;

Kaiser 1974), and movement-avoidance responses (Srinivasan and Lehrer 1984) are proven to be chromatically independent (i.e. achromatic).

In flies, the parallel subdivisions of the retinotopic pathways to the lobula plate have been suggested from anatomical studies (e.g. Strausfeld and Lee 1991). The similar lobula structure can also be found in the lobula of honeybees and bumblebees (Ribi and Scheel 1981; Paulk 2008, 2009ab). It is shown that many of the motion-sensitive descending neurons that are connected to motor control centres position their dendritic fields in the posterior protocerebrum (Strausfeld and Bassemir 1985; Ibbotson 2001; Schröter et al. 2007; Hung et al. 2011). In bumblebees, it is found that most neurons in the lobular layers 1-4, which contain motion-sensitive interneurons, send their axons through the posterior protocerebrum. Conversely, the neurons in lobular layers 5-6, which are mostly colour-sensitive neurons, send their axons through the anterior optic track to the anterior side of the brain (Paulk et al. 2008).

1.4 Motion-sensitive descending neurons

In insect brains the intersegmental descending neurons (DNs) play an important role in integrating the multisensory inputs, including visual signals that project into the central brain and transmit information to motor ganglia in the thorax. The term 'descending neuron' is used exclusively for those neurons that have cell bodies and dendritic fields in the brain or suboesophageal ganglion and whose axons carry the information to the thoracic or abdominal ganglia (descending neurons do not make direct contact with muscles). In dipterous insects, it is also found that some DNs with dendrites in the optic lobes project directly into the thoracic ganglia (Nässel and Strausfeld 1982). The DNs, as higher order interneurons play an important role in integrating signals from different sensory systems, including visual systems, and then transmitting the computed information to the motor ganglia. It is generally believed that the motion-sensitive

descending neurons are responsible for the sensory-motor transformations required for optomotor and other visually driven orientation reflexes (e.g. Bidwell and Goodman 1993; Ibbotson and Goodman 1990; Olberg 1981ab; Wertz et al. 2008).

Descending interneurons that respond in a direction-selective fashion to visual motion have been reported in a range of insects, including moths and butterflies (Singarajah 1988), locusts (Kein 1974; Rowell and Reichert 1986), praying mantis (Yamawaki and Toh 2009) and dragonflies (Olberg 1981ab; 1986). Honeybee motion-sensitive descending neurons were reported extensively (Goodman et al. 1987; Goodman et al. 1990, 1991; Ibbotson and Goodman 1990; Ibbotson 1991ab), however, the field has been relatively quiet in the last 20 years. The anatomies of honeybee descending interneurons were first reported by Pan and Goodman (1977), in which they described the anatomy of five ocellar descending neurons in the honeybee that had cell bodies in the midbrain, dendrites close to the ocellar retinae and projected into the thoracic ganglia. Later on, Goodman et al. (1987) described the brain anatomies of six more groups of motion-sensitive descending neurons in the honeybee. Those neurons all confined their dendrites to the central brain area (protocerebrum). Although the detailed morphology of cells within different categories of neurons are distinct, it is clear that all the neurons descend from the brain into the thoracic motor centres, reaching as far as the most posterior tip of the metathoracic ganglion (Pan and Goodman 1977; Ibbotson 1989, 1991ab; Ibbotson and Goodman 1990). At that time 10 of the descending neurons had been recorded from and filled, and were placed into six groups based on their anatomical similarities (the classes were: DNI, DNII, DNIII, DNIV, DNV and DNVI). Ibbotson (1991b) then described the physiology and morphology of a new anatomical category of motion-sensitive descending neurons called DNVII. Besides the seven classes of honeybee descending neurons published in the open literature, Ibbotson (1989) also reported the morphology and physiology of another two classes of cells, each containing many individual neurons in his PhD thesis (DNVIII and DNIX). The

DNVIII category contains a particularly large number of cells (at least 8). The naming system of the honeybee descending neurons allows comparison across different authors and time periods. Therefore, the classification scheme described by Goodman and Ibbotson is used throughout this study (Pan and Goodman 1977; Goodman et al. 1987; Ibbotson and Goodman 1990; Ibbotson 1991ab).

The other distinctive feature is that most of the DNs recorded from so far are wide-field direction-selective motion sensitive cells. Target-selective descending neurons (i.e. responding only to movements of small patterns) have also been observed in honeybees and other insects, but to date their response properties have only been reported in detail in dragonflies (Olberg 1986). The directional response characteristics of honeybee descending neurons can be divided into two general classes: vertically tuned and horizontally tuned motion-sensitive DNs (Figure 1.9). It is also the case that the neurons have different receptive field properties, which are associated with their directional preferences. For example $DNII_2$ responds maximally to upward motion primarily in the frontal visual field, while $DNIV_2$, which is roll sensitive, has stronger responses to motion in the lateral fields of view (Figure 1.10). Vertical motion over the frontal field occurs when animals make pitching movements (or lift/descent), while vertical motion in opposite directions over the lateral fields of view occur when the animals make rolling movements (also see Figure 1.6).

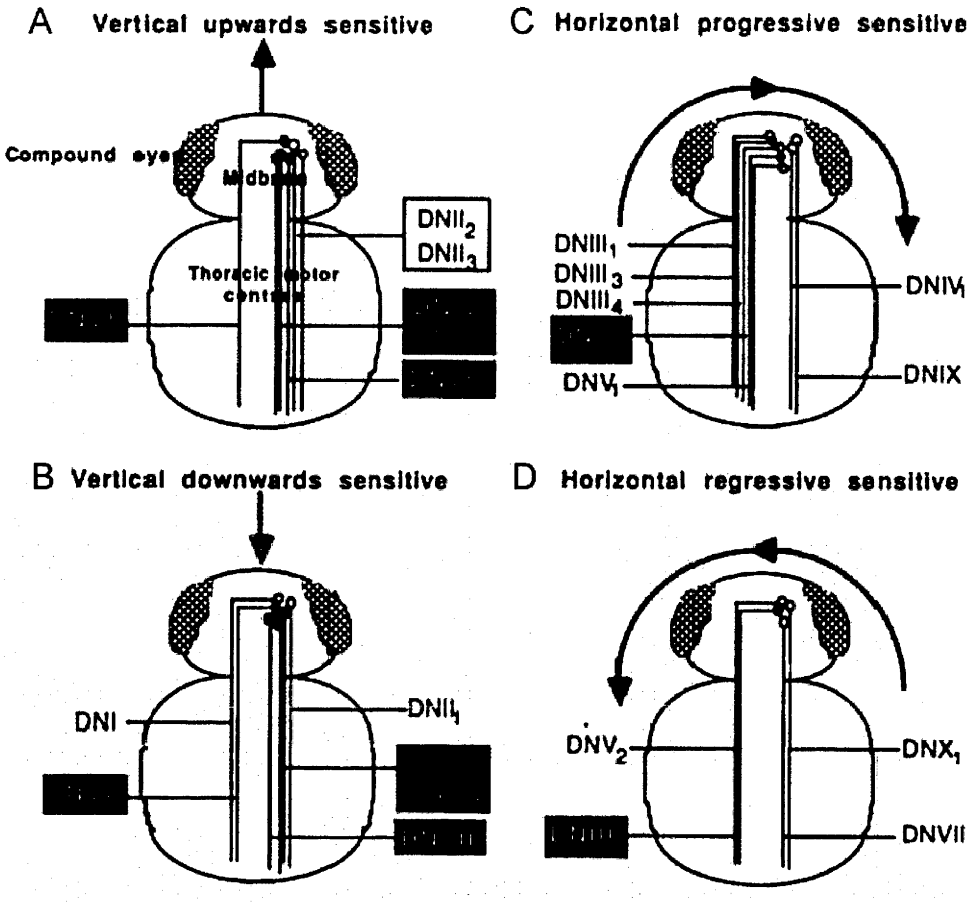

Figure 1.10: A diagrammatic figure, which shows the preferred directions of the identified honeybee descending neurons, as reported in the mid-1990s (figure adopted from Bidwell and Goodman 1993). Figure A and B show the neurons that are sensitive to vertical motion - A: upward motions; B: downward movements. Figure C and D show the neurons that are sensitive to horizontal movements - C: progressive motions; D: regressive motions. The cell bodies of the neurons that respond to **one direction** over the frontal or the lateral visual field are represented by *empty circles*; while for the neurons that respond to more than one direction, the cell body is represented by *filled circles* and *shaded annotations*.

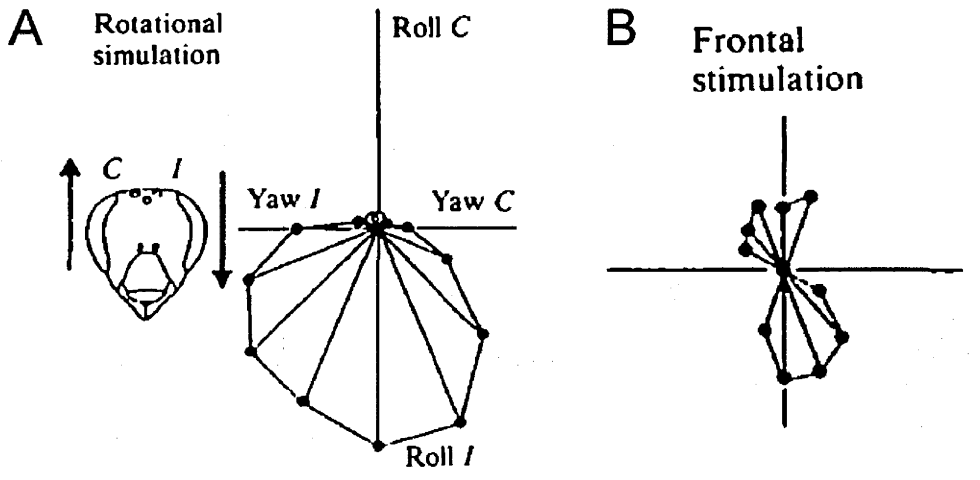

Figure 1.11: Direction tuning of a roll-sensitive neuron $DNIV_2$ (Figure adopted from Ibbotson and Goodman 1990). A: The maximum response occurred when it was stimulated by upward motion over the lateral portion of one eye and downward motion over the lateral portion of the other eye. B: When the neuron is stimulated by frontal vertical motion it generated small responses to both upward and downward directions, as a result of its respective inputs from each eye.

The honeybee motion-sensitive descending neurons can be divided into those that are tuned to velocity and those that are tuned to contrast frequency. The first group are thought to be involved in estimating distance (odometry) and flight speed control (Ibbotson 2001). The second group, which we will focus on in this thesis, is thought to play an important role in the optomotor response (Ibbotson and Goodman 1990; Ibbotson 1991b). The optomotor responses of insects are known to depend upon the contrast frequency of the moving stimulus rather than on its velocity (e.g. Buchner 1984). The contrast frequency is the ratio between angular velocity and the spatial period of the pattern. The tuning of the contrast frequency response function of the bee behavioural optomotor response matches that of those descending neurons. The contrast frequency tuning of optomotor responses varies between species. For example, in *Musca*, the yaw torque response

peaks between 1–2 Hz with a cut-off frequency of between 10 Hz and 20 Hz, while the roll torque response peaks between 1–2 Hz, but with a cut-off frequency of 3 Hz (Fermi and Reichardrt 1963; Eckert 1973; Srinivasan 1977). The contrast frequency sensitivity of the honeybee optomotor response peaks at higher temporal frequencies. A high cut-off value of 200 Hz was observed for the turning behaviour of walking bees (Autrum and Stoecker 1950). The yaw torque response generated by flying bees peaked at between 8 and 10 Hz, with a cut-off frequency at around 100 Hz (Künze 1961). These match the responses of the horizontally tuned descending neurons $DNIV_1$ and $DNVII_1$ (Ibbotson and Goodman 1990; Ibbotson 1991b), which peak at 8–10 Hz. Together with the specialised optic flow sensitivity of the DNs, the contrast frequency tuning provides strong evidence that the neurons are involved in transmitting the essential information required to drive optomotor responses. The DNs carry the information between the visual centres in the optic lobes and brain and the motor centres in the thorax.

1.5 Honeybee neck motor system

In insects head movements are mediated mainly by muscles in the prothorax, which is a compartment at the front of the thorax. Some muscles outside the prothorax, such as those that superficially control foreleg movements are also involved (Berry and Ibbotson 2010). From anatomical and physiological work, it is believed that the insect neck motor neurons are innervated primarily by the descending neurons (Gronenberg et al. 1995; Gronenberg and Strausfeld 1990ab; Gronenberg and Strausfeld 1991; Schröter et al. 2007; Hung et al. 2011). In flies, head movements are controlled by 22 pairs of neck muscles driven by motor neurons that have their arborisations situated in the brain, suboesophageal ganglion and the dorsal prothoracic ganglion (Strausfeld et al. 1987; Gronenberg et al. 1995). In honeybees, 12 pairs of neck muscles are involved in head movements

(Snodgrass 1942). Among them, 5 are direct muscles (muscles 40-44), which connect the thorax and the head while the other 7 (muscles 45-51) are indirect muscles that connect different parts of the prothorax to flex the exoskeleton and thus enable head movements (Schröter et al. 2007; Snodgrass 1942; Strausfeld 1992). Recent studies involving 3-dimensional reconstruction of the honeybee head-neck revealed the detailed muscular and neural anatomy. This work provided a method for interpreting the functions of each muscle in coordinating head movements (Berry and Ibbotson 2010). Comparing the digital atlases of the honeybee head-neck systems (muscular and neural systems), and previous anatomical studies, it was shown that all of the neck muscles are innervated by the motor neurons in the first and second cervical nerve (IK1 and IK2) as well as the first of the prothoracic nerves, IN1 (Berry and Ibbotson 2010; Markl 1966; Snodgrass 1942). Figure 1.11 shows the honeybee neck motor system - A: the neck muscular system; B: the neck nervous system.

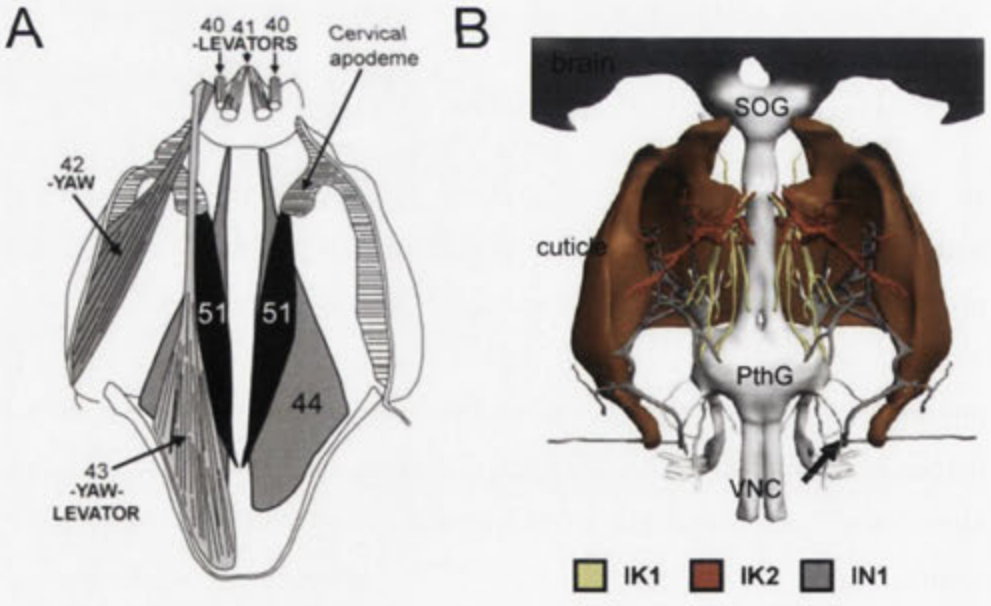

Figure 1.12: The honeybee neck motor system. **A:** Schematic plan view of the honeybee neck muscles based on Snodgrass (1942). Muscles 40-44 directly connect the thorax and the head (direct muscles) while muscle 51 is an indirect muscle that connects to the cervical apodeme with the rear of the

prothorax (Figure adopted from Schröter et al. 2007). **B:** dorsal view of the brain (including the suboesophageal ganglion, SOG), prothoracic ganglion (PthG), ventral nerve cord (VNC), and the nerves innervating the neck muscles. Nerves in *light yellow* are IK1, *orange* are IK2, and *grey* are IN1, which meets IN6 (*black arrow*). Figure adopted from Berry and Ibbotson (2010).

The present work on honeybee neck motor neurons (Chapter 6) is focused on the neurons in IK1, which innervate muscles 44 and 51. The work is based on knowledge from two relatively old anatomical studies (Snodgrass 1942; Markl 1966) and two recent studies on the honeybee neck motor system, in which they back filled motor neurons from the muscles (Schröter et al. 2007) and reconstructed the whole honeybee neck motor system (Berry and Ibbotson 2010).

Muscle 44 is the largest direct muscle in the honeybee neck motor system. It consists of 5 muscle subunits that each have an anatomically distinct attachment point (Fig 1.12A). It attaches to the head via a long tendon. Constriction of the muscle results in depression of the head (Snodgrass 1942; Markl 1966; Berry and Ibbotson 2010). The innervation patterns of muscle 44 are provided exclusively by IK1. Muscle 51 was previously thought to be a single muscle (Snodgrass 1942; Markl 1966), but the two recent studies found that it could be divided into two closely related but anatomically distinct subunits, 51a (dorsal) and 51b (ventral). Anteriorly, they are divided by a dense, forward projecting branch of IN1; posteriorly, they are divided by the supraneural bridge of the endosternum (SNBE) (Fig 1.12B). It is suggested that when muscle 51 contracts it moves the cervical apodeme inwards toward the prothoracic cavity, therefore allowing outward deformation of the exoskeleton. It then generates indirect head yaw movement to the ipsilateral side (Schröter et al. 2007; Berry and Ibbotson 2010).

There are 8 motor neurons in IK1, which can be divided into three classes according to the location of their cell bodies (review from Schröter et al. 2007). They are named M1-2 (median-), C3 (contralateral-), and L4-7 (ipsilateral side of the suboesophageal ganglion). Among the 8 neurons in IK1, 6 of them (M1, C3, and L4-L7) innervate muscle 44, while two (M2 and L8) innervate muscle 51. Each of the neurons innervates a specific subunit of the muscle (Fig 1.13A). M1 innervates only the lateral subunit of muscle 44. The L4-L7 group, although it is difficult to distinguish them based on their morphology within the suboesophageal ganglion, can be identified by their target subunits in muscle 44: L4 innervates the lateral fibre of the ventral subunit; C3 innervates the dorsal fibre of the ventral subunit; L5 innervates the dorsal-B subunit; L6 innervates the dorsal-A subunit; and L7 innervates the lateral subunit of muscle 44 (Fig 1.13B). For the other two motor neurons that innervate muscle 51, L8 innervates exclusively the ventral subunit and M2 innervates the dorsal subunit of muscle 51 (Fig 1.13C).

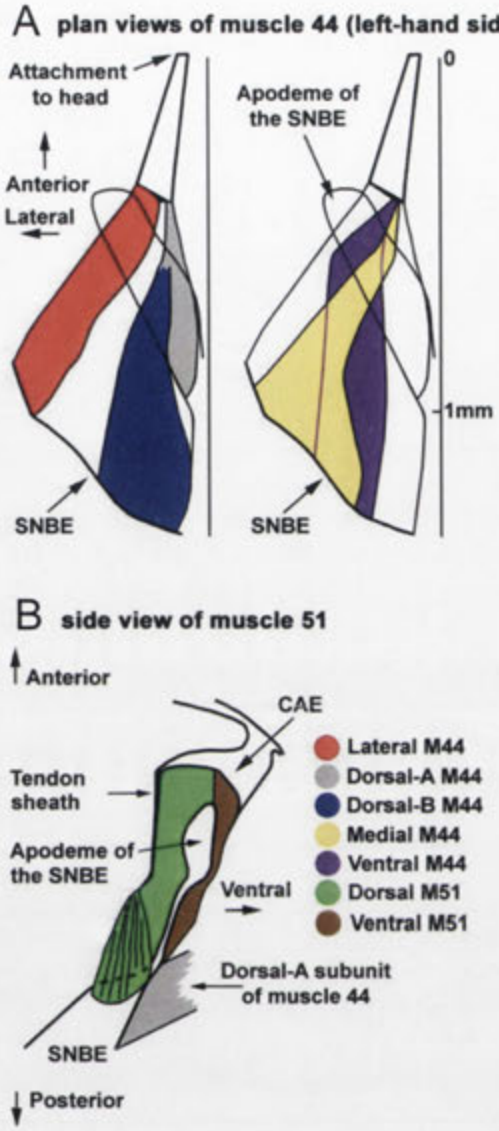

Figure 1.13: Schematic drawings of muscle 44 and 51. **A:** Plan views of muscle 44. The figure on the left hand shows the lateral and dorsal subunits. It can also be seen that the dorsal unit is further divided into another two subunits, A and B. The figure on the right hand shows the medial and ventral units of muscle 44. **B:** A side view of muscle 51. It is shown that the muscle is divided by the supraneural bridge of the endosternum (SNBE) posteriorly into dorsal and ventral subunits. Figure adopted from Schröter et al. (2007). *Abbreviations*: CAE, cervical apodeme of the endosternum; SNBE, supraneural bridge of the endosternum; M44, muscle 44; M51 muscle 51

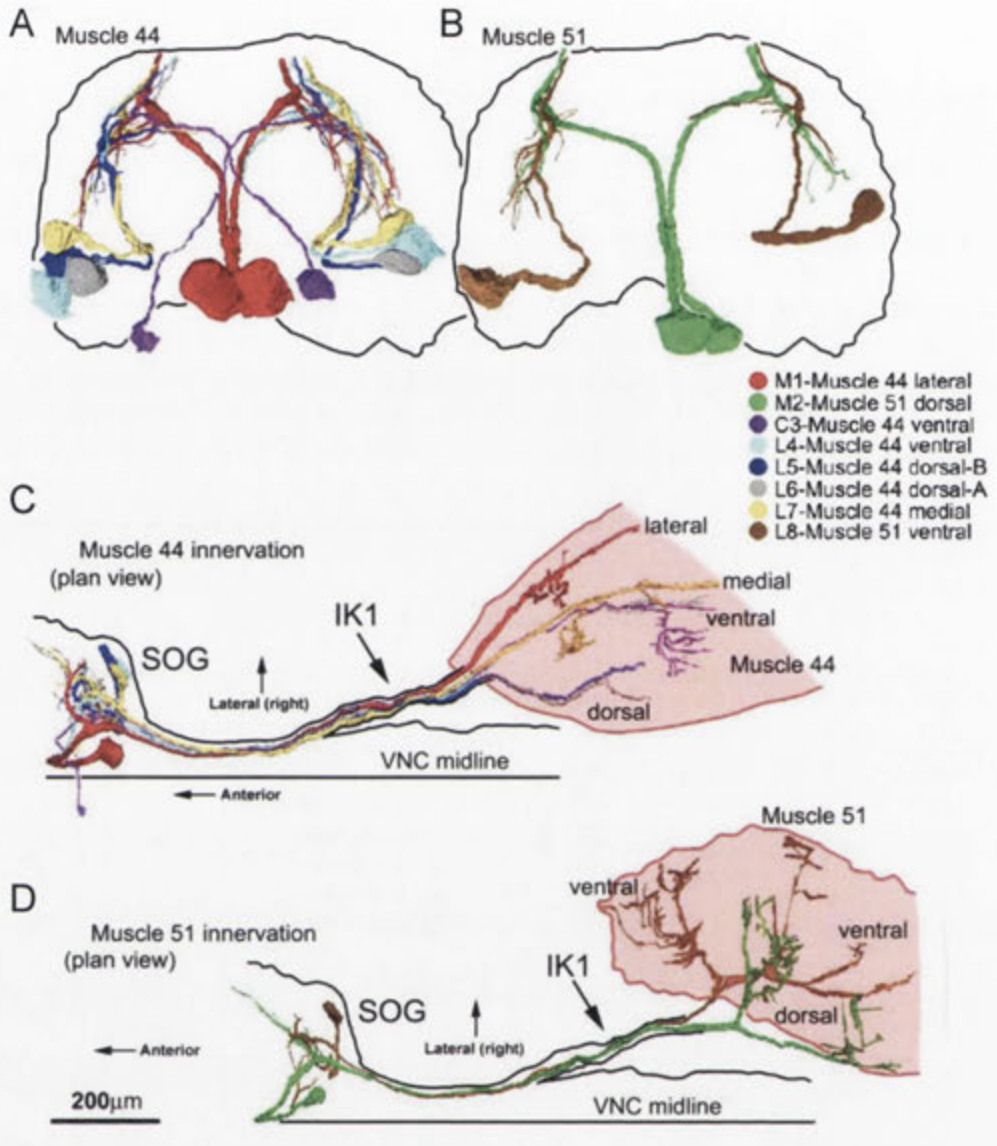

Figure 1.14: Reconstructions of the neurons that innervate muscle 44 and 51 (Figure adopted from Schröter et al. 2007). A: Plan view of the 6 reconstructed motor neurons that innervate muscle 44 in the suboesophageal ganglion. B: Plan view of the two motor neurons that innervate muscle 51. In C and D only the right hand side of the nervous system us shown. *Abbreviations*: SOG, suboesophageal ganglion; VNC, ventral nerve cord

1.6 Thesis outline

This thesis is focused on the neural basis of motion and spectral wavelength processing in the output from the two visual systems of honeybees, the compound eyes and the ocelli.

Chapter 2 examines the morphology and anatomy of the honeybee ocelli by using scanning electron microscopy and semi-thin sectioning techniques. From the serial sections of honeybee head and ocelli, a 3-dimensional reconstruction model of the honeybee ocelli is developed to understand the ocellar fields of vision. In addition to the morphology and anatomy, the optical properties of the ocelli were revealed using the well-established hanging-drop method.

In Chapter 3 I report the detailed morphology of five honeybee motion-sensitive descending neurons ($DNII_2$, $DNIV_2$, $DNIV_3$, $DNVII_1$ and $DNVII_2$) and one lateral ocellar descending neuron ($Locth_3$). Among those cells, $DNVII_2$ is a new cell type in which the morphology is reported for the first time. For the other neurons, basic anatomical descriptions already exist but this thesis shows their 3-D characteristics based on serial optical sections after filling with fluorescent dye.

In Chapters 4 and 5 I focus on the physiological responses to visual stimulation of the ocelli and compound eyes in the neurons described in Chapter 3. I recorded the neural responses to different types of visual stimuli, including flashes and motion. Moreover, the stimuli provided selective stimulation in two distinct bands of spectral wavelengths: short-wavelength (peak 380 nm) and green (peal 530 nm). The neurons in these two chapters are grouped according to their directional selectivity. In Chapter 4, the responses of two pitch-sensitive neurons, $DNII_2$ and ocellar descending neuron $Locth_3$, are reported. Both neurons responded to upward motion in the frontal visual field, which simulates the optic flow that would occur during forward and downward pitch. In Chapter 5, the physiology of two roll-sensitive neurons ($DNIV_2$ and $DNIV_3$) and one yaw-sensitive neuron

are reported. The roll sensitive neurons are maximally sensitive to upward motion over one eye and downward motion over the other. The yaw neuron was maximally sensitive to forward horizontal motion over one eye and backward horizontal motion over the other.

In Chapter 6 I investigate the physiology of the honeybee neck motor neurons that innervate two neck muscles (m44 and m51). The two muscles are involved in generating honeybee head yaw movements. I present neural responses to flashes and gratings moving in different directions.

In the physiology chapters (Chapter 4-6), cell responses with and without ocellar stimulation are reported to reveal the interactions that occur between the two visual systems and the possible roles that ocelli play in visual processing.

Chapter 2

Anatomy of honeybee ocelli

2.1 Abstract

Honeybees, like most flying insects, have a visual system composed of three ocelli (simple eyes) located on the top of the head, in addition to two large compound eyes. Although numerous experiments have been conducted to investigate the role of the ocelli within the visual system, their exact function remains controversial. In this study, the three-dimensional structures of the honeybee ocelli are mapped with the aim of assisting in determining the role of the ocelli in that species. I investigate the morphological and optical characteristics of honeybee ocelli using scanning electron microscopy, semi-thin sections and focal length measurements of both the median and lateral ocelli. Three-dimensional reconstructions of honeybee ocellar lenses and retinas were also generated from serial sections of the ocelli. Each type of ocellus has two retinas, the dorsal and ventral. The study assesses for the first time the spatial resolution of both retinas using the hanging drop technique. By using the 3-D model that is presented, it was possible to determine the visual fields of the various retinas. The dorsal retina views the horizon while the ventral retina views the sky, suggesting quite different roles in attitude control. It was found that the dorsal retina has a higher spatial resolution than the ventral retina in both ocellar types, consistent with the need to assess spatial detail on the horizon.

The lateral ocellus was also found to have a higher resolution than the median ocellus.

2.2 Introduction

Honeybees (*Apis mellifera*), like most of the flying insects possess two visual systems: the compound eyes and an additional set of simple lens eyes (ocelli). The morphology of the ocelli varies across insect orders and even within the same family (reviewed in Goodman 1981). The lack of optical resolving power, however, represents one morphological feature that is consistently observed in ocelli of different insects. Homann (1924) examined the ocelli in several different insect types and found that the focal planes of the ocellar lenses were well beyond the proximal limit of the retina in all cases. The same feature was subsequently found in locust (Parry 1947; Wilson 1978; Cornwell 1995; Berry et al. 2007b), blowfly (Cornwell 1955; Schuppe and Hengstenberg 1993), nocturnal bee and diurnal wasp (Warrant et al. 2006). The function of these under-focused lenses is not yet entirely clear, although speculation about their roles began over 100 years ago (Müller 1826; Lowne 1870). Wilson (1978) proposed a convincing hypothesis of ocellar function based on his work on locust ocelli, which is referred to as the 'single-sensor' hypothesis (Stange et al. 2002). It suggests that the ocelli do not resolve spatial details of the environment: instead, each ocellus functions as a highly sensitive light detector of illumination levels from a wide region of visual space. Their large aperture and field of view suggest that they are designed to detect overall brightness while minimising the effect of small objects in the visual field (Wilson 1978).

However, even though the focal planes of many ocellar lenses lie behind the retina, this does not necessarily exclude the possibility of detecting form, or motion vision. Schuppe and Hengstenberg (1993) examined blowfly ocelli (*Calliphora erythrocephala*) and found that despite the under focussing of the ocellar lens, low spatial frequency patterns could

be imaged on the retinal plane. Other studies have also shown that ocelli are able to resolve some spatial information, e.g. dragonflies (Stange et al. 2002; Berry et al. 2006; Berry et al. 2007a; Berry et al. 2007b; van Kleef et al. 2008), and wasps (Warrant et al. 2006). The capacity for some ocelli to resolve spatial features suggests that ocellar function may be more complex than previously suggested by the single-sensor theory.

The honeybee ocelli are located as a triplet on the dorsal surface of the head between the compound eyes; each ocellus consists of approximately 800 retinal cells (Toh and Kuwabara 1974). Although the basic morphology and anatomy of the honeybee ocelli has been studied previously (Toh and Kuwabara 1974; Pan, PhD thesis 1980; Ribi et al. 2011), these studies were focused on the ocellar structure in relation to the synaptic terminals of ocellar nerve fibers. The optical characteristics of the honeybee ocelli remain unclear. Therefore, in this study, the internal morphologies of the ocellar lens and retinal structure are examined by combining serial sections and three-dimensional reconstructions of honeybee ocelli. This is important because it is evident that each ocellus has more than one retina, potentially with different roles. Additionally, the dioptrics of honeybee ocelli is investigated using optical techniques. What sets this study apart from earlier investigations, including one conducted during the tenure of my PhD candidature (Ribi et al. 2011), is that I have measured the actual spatial resolving capacity of the ocellar retinas and have created a three-dimensional (3-D) model of the ocelli that offers the capacity to observe the full 3-D structure of the lenses and their relationship with the associated retinas. The 3-D model will be made available through the website of the journal that publishes the work.

2.3 Methods and materials

2.3.1 Experimental animals

Experiments were conducted on worker honeybees, *Apis mellifera*, that had been actively foraging. Hives were situated at The Australian National University in Canberra, Australia. Prior to experimental preparation, each bee was lightly anaesthetized by cooling in a refrigerator at 5°C for about 20 minutes.

2.3.2 Histology

Light microscopy and scanning electron microscopy (SEM) were performed using standard methods. Freshly removed heads were partially dissected; after removing the mouthparts, frons and the cuticle from the back of the head, the head capsule was kept in primary fixative (2.5% glautaraldehyde and 4% paraformaldehyde in 1M phosphate buffer saline, PBS) for three hours. After fixation, the samples were post-fixed in 1% phosphate buffered osmium tetroxide to enhance the contrast and through an ethanol series (50%-100%) for dehydration. The samples were then embedded in hard Epoxy resin (Epon®812) and carefully oriented at different angles for sectioning. Semi-thin sections of 1 μm were cut using either a glass or diamond knife on a Reichert-Jung ultramicrotome. Sections were post-stained with toluidine blue and imaged on a Zeiss Axioskop (light microscope) with a SPOT RT digital camera.

2.3.3 Three-dimensional reconstructions of honeybee ocelli

A set of selected longitudinal serial sections of honeybee heads was used to generate three-dimensional (3D) reconstructions. The images were manually aligned relative to each other in Amira 5.3.3 (Visage Imaging GmbH). After

alignment, each image was segmented into discrete components by manually tracing outlines of the cuticle, lenses and retina. Mesh models of each structure were then generated from the segmented images. Images of the reconstructions were obtained via the Blender rendering engine (http://www.blender3d.com).

2.3.4 Focal length measurement

The hanging drop method described by Homann (1924) was used to measure the optics of honeybee median and lateral ocelli. The lenses of the median and lateral ocelli were carefully dissected and cleaned using honeybee saline (111.22 mM NaCl, 3.35 mM KCl, 1.37 mM $CaCl_2$, and 1.89 mM Na_2CO_3) to minimize osmotic flow out of or into the lens. The ocellar lenses were then suspended from a droplet of bee saline, which was suspended from a glass cover slip (Fig 2.1). The lens was oriented with the inner surface facing the saline, and the outer surface facing the air. The cover slide with the lens was then sealed onto a rubber O-ring attached to a glass slide with vacuum grease. The distances between the inner surfaces of the lens to the best focused plane (Back focal distance, BFDs) were determined by using the pattern "F", which provides both vertical and horizontal stripes. The "F" was printed onto rice paper and placed on the foot of the microscope at a distance of 9.5cm from the lens. Sufficient illumination was applied so that the object was imaged by the ocellar lens. The distance required to shift the focus of the microscope objective from the inner lens to the best focal plane was measured. The results were then corrected by multiplying with the reflective index of the immersion medium (1.34 for saline). The focal length (f) of each lens was also determined by transverse magnification using the equation:

$$f = s\frac{\lambda i}{\lambda o}, \qquad (1)$$

where s is the distance between the test object and the lens, λ_o is the size of the object, and λ_i is the size of corresponding image at the plane of best focus.

An LCD monitor was used to deliver wide field stimuli consisting of sinusoidally-modulated black and green gratings of spatial wavelengths ranging from 1° to 20° (1°, 2°, 4°, 8°, 12°, and 20°) and utilizing a 50% duty cycle such that the average intensity of light passing through the grating was constant. Because the object images were projected over a wide plane which covers a large visual angle, these patterns were corrected (mathematically warped) so that the angular size reamins constant from the lens point of view. The images formed by the ocellar lenses were captured by a digital camera. The images formed from different distances from the back of the lens were collected.

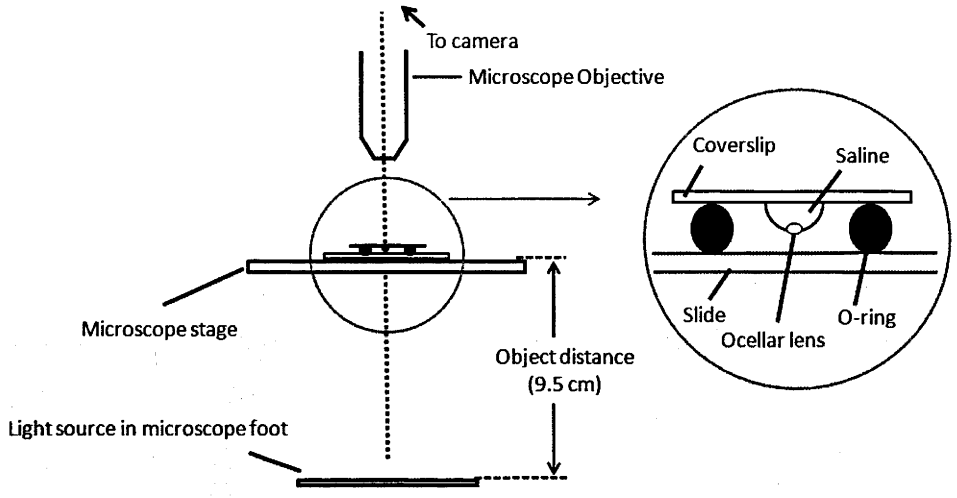

Figure 2.1: Schematic diagram of the hanging-drop setup used for optical analysis of the ocellar lenses. Circular inset to the right shows an enlargement of the lens chamber. The ocellar lens is suspended in a drop of saline from a coverslip, and the coverslip is separated from the slide by a rubber O-ring. Two types of stimuli were used to test the ocellar lenses: 1) a pattern printed on the rice paper directly placed onto the light source on the microscope foot, and 2) an LCD display for the wide field stimuli. Both types of stimuli were placed 9.5 cm from the slide. The image plane of the ocellar lens was magnified by the microscope objective and imaged by a digital camera. The vertical dashed line indicates the optical axes of the ocellar lens and the microscope.

2.4 Results

2.4.1 External morphology

The honeybee ocelli are located on the vertex of the head capsule between the compound eyes. Based on measurements from SEM photographs I determined that the distance from the midline of the head to the inner edge of the lateral ocelli was 237 μm (n = 2; 250, 224). Therefore, the lateral ocelli are 474 μm apart (inner edge to inner edge). The vertical distance between the bottom edge of the lateral ocelli and the bottom edge of the median ocellus is 217 μm (n = 2; 194, 241). Both the median and lateral ocelli are ellipse-shaped from the external view, with the median ocellus slightly larger than the lateral ocelli (Fig 2.2AB). The semi-major axis of the median ocellus is 312 μm and the semi-minor axis is 268 μm, while the measurements for the lateral ocellus are 300 μm and 238 μm, respectively (n = 2, measured from SEM pictures).

When viewing a honeybee from the front, only the median ocellus can be seen because the lateral ocelli are occluded by the sensory hair on the head capsule (Fig 2.2A). After carefully removing all the sensory hairs from the bee head, all three ocelli were exposed and three bald areas devoid of sensory hair were revealed. The hairless area for the median ocellus is a triangle-shape pointing anteriorly, while the lateral ocelli have hairless areas that are rectangle-shaped, pointing laterally (Fig 2.2B). As a single lens eye, the light could come from all angles. The dense and long sensory hair, as well as the hairless zone at certain area around the three lenses may help reduce the light coming from unwanted angles (noise), thus enhance the signals that needed for flying or walking. Although no direct measurements have been made for the visual field of the honeybee ocelli, it appears, from the relative positions of the ocelli and the hairless zone, that the median ocellus looks up- and forward, while the lateral ocelli look upwards and to either side of the head. The modelling that follows will demonstrate these features in greater accuracy.

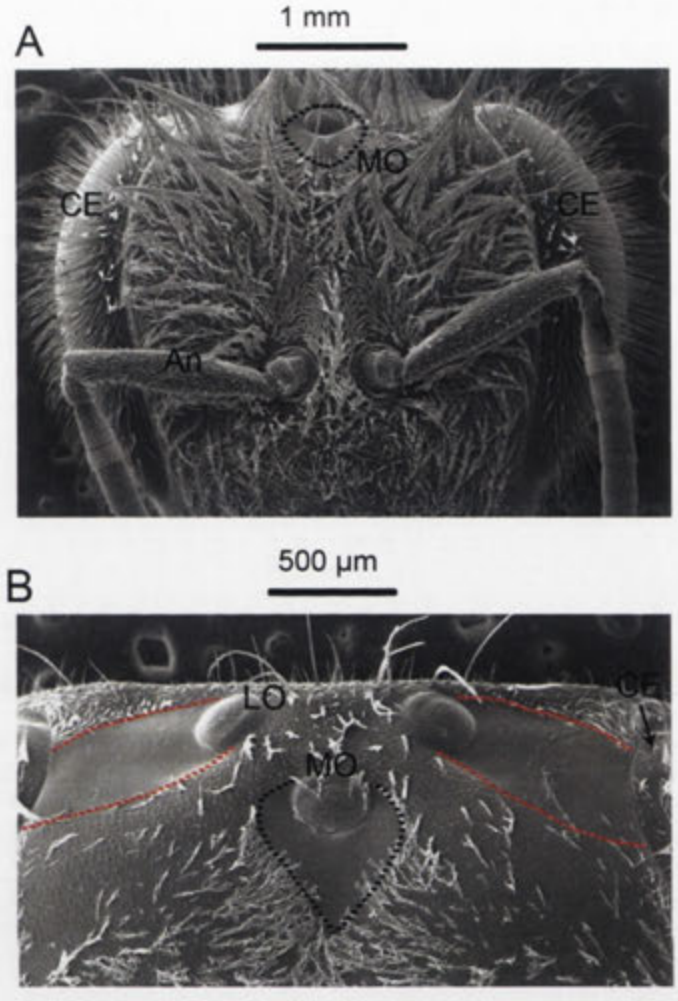

Figure 2.2: Scanning electron microscope image of the honeybee head. A: Frontal view of honeybee head. The black dashed circle indicates the median ocellus and also the hairless area. The honeybee ocelli are located between the compound eyes (CE), however, because of the coverage of sensory hairs on the capsule, only the median ocellus can be seen from the frontal view. B: Frontal view of honeybee ocelli without the sensory hairs. Three clean areas devoid of sensory hair can be seen around the ocelli. The edges of these hairless areas are marked by dashed lines (red: lateral; black: median ocellar area). ***Abbreviations*:** An, antenna; CE, compound eye; LO, lateral ocellus; MO, median ocellus. Scale bars: (A) 1 mm; (B) 500 µm.

2.4.2 Anatomy - internal morphology of the ocellar lens and retinal structure

The three-dimensional (3-D) reconstructions, together with the sections of the three ocelli illustrate both the internal and external morphologies of the honeybee ocelli and provide a complete visualisation of the retinal structures and their relation to the lenses. From horizontal sections of the ocelli, the 3-D reconstructions and the associated retinal layers, it is evident that the lens and retina of the median ocellus project inwards toward the dorsal side of the brain. In the lateral ocelli the retina projects side-ways and inwards toward the midline of the brain (Fig 2.3A and 2.4C). It is also shown that although the external surfaces of the median and lateral ocellar lenses appear as a simple smooth surface; both the inner surfaces of the lenses are convoluted in a more complicated fashion. The median ocellar lens curves and elongates downward, while the lateral ocellar lens curves sideways toward the midbrain.

Median ocellus

In all previous studies only longitudinal sections have been presented of the honeybee ocellus. From these sections of the median ocellus the lens appears to be a thick, dome shaped, spherical biconvex corneal lens (Fig 2.3C). However, from the 3-D reconstruction of the median ocellus, it is shown that below the level of the surrounding cuticle of the median ocellar lens, the inner surface of the lens curves downward and forms a complex non-spherical shape (Fig 2.6A).

Adjacent to the inner surface of the median ocellar lens is a transparent space called the vitreous chamber, which separates the corneageal ocellus. In the median ocellus this chamber is smaller than in the lateral ocelli, and the shape of the chamber is pointed around the midline. The corneagal cells lie between the vitreous chamber of the ocellar lens and the tip of the retinula cells. They contain dark pigmented granules and act as

a mobile iris mechanism during adaptation that can filter light that passes to the retinal cells (Stavenga et al. 1979). The retinal cells of the median ocellus are directly behind the corneagal cells. It is found that the retinal region can be divided into two parts, the dorsal and ventral retinas, according to the length of the retinula cells and the relative position to the lens (Fig 2.3C). The limit of the rhabdomeric zone (marked by pigment accumulated along the edges of the retina: Fig 2.3C) from the inner surface of the lens for the dorsal retina (dr) is 92 μm, while that for the ventral retina (vr) is 55 μm. In both cases this was measured from the longitudinal section of the median ocelli, n = 2. These differences are important in setting the limits for spatial resolution in the ocelli, as will be shown later for the dorsal and ventral retinas.

Lateral ocellus

From the sections it can be determined that the outer surface of the lateral ocellar lens is convex, but the inner surface of the lens curves toward the midline of the brain, as it becomes more asymmetrical (Fig 2.3B). This feature is shown clearly by the 3-D reconstruction: under the surrounding cuticle of the lateral ocellar lens, the inner surface curves and becomes thicker toward the midline of the brain (Fig 2.5AB).

The vitreous chamber of the lateral ocellus is located between the ocellar lens and the corneagal cells. The chamber follows the inner surface of the lens and forms a transparent space that is stained light blue by Toluidine Blue. Adjacent to the corneagal cells, the rhabdomeric zone of the retina forms layers that allow a measurement from the rear surface of the lens. Importantly, the lateral ocellar retina can also be divided into dorsal and ventral parts (Fig 2.3B). The rhabdomeric zone follows the asymmetrical inner surface, where the thickening of the lens is correlated to the thickening of the retina. The furthest extent of the ventral retina is 78 μm and the furthest extent of the dorsal retina is 148 μm.

2.4.3 The 3-D reconstruction of the honeybee ocelli

The 3-D reconstruction of the honeybee ocelli provides a thorough description of the ocellar inner structure. As mentioned in previous sections, it is shown that both median and lateral ocellar lenses curve below the surface of the cuticle to form complex non-spherical shapes (Fig 2.5A, 2.6A). The median ocellar lens curves downward while the lateral ocellar lens curves toward the midline of the brain, which allows the light to be guided to different regions of the retinas through diffraction. From the semi-thin sections of the ocelli, it is shown that the retina of both the median and lateral ocelli can be divided into two parts: the ventral and lateral retinas. Therefore in this study, besides seeing the lateral or median ocellar retina as one section (Fig 2.4), I also performed 3-D reconstructions of the divisions of the retinas (i.e. the dorsal and ventral retinas). Figure 2.5AB show the 3-D reconstruction model of the **lateral** ocellus from the frontal view. It is shown that the lens of the lateral ocellus curves toward the mid-line of the brain; the dorsal retina (shown in purple) and ventral retina (shown in blue) follow the inner surface of the lens and are also pointed toward the middle of the brain (Fig 2.5AB). Figure 2.6AB show the lateral view of the **median** ocellar lens in relation to the two retinas (dorsal retina, shown in purple; ventral retina, shown in blue). Using the 3-D ocellar model it is possible to predict the fields of view of the retinas by rotating the model and viewing the retinal locations through the window created by the lens opening in the cuticle. This technique is generally useful but does not take account of the diffractive capacity of the lens.

As shown in Figure 2.5B, the **lateral** ocellar retinas are positioned inwardly toward the midline of the brain, so the frontal visual fields for the lateral ocelli are very limited. Figure 2.5C-G simulates a rolling movement of the head. The observer is viewing the bee from its left-hand side. The left-most image shows the head in the normal position (ocelli uppermost). It is clear that only the blue dorsal retina is in view. Even taking refraction into account, it is unlikely that the ventral retina would be able to obtain very

much information from the horizon. The important result here is that the dorsal retina is positioned to observe the horizon when the head is in its 'normal' attitude. As the head rolls to the side (dorsal towards the viewer) the dorsal retina slowly turns out of view and the ventral retina becomes evident. When the head is turned fully through 90 degrees, such that the top of the head points directly towards the viewer, only the ventral retina can be seen. Therefore, when the head is in its normal position the ventral retina views directly upwards towards the sky. The dorsal retina has very little input from above the head.

In Figure 2.6C-F the **median** ocellus is seen from the front of the head (as if the bee were flying towards the observer). The simulation shows what would be seen from the frontal view as the bee makes a pitching movement (dorsal downwards and forwards). It is clear that when the head is in its normal position (Fig 2.6C) only the dorsal retina (purple) can be seen through the lens aperture. As the head tilts forward more of the ventral retina becomes evident. By the time the head is tilted forward by 90 degrees, only the ventral retina (blue) is visible from the front. Again, as with the lateral ocelli, the dorsal retina views the horizon, while the ventral retina views the sky directly above the head. Therefore, while the visual fields of the lateral ocelli point latero-dorsally and the median ocellus points fronto-dorsally, they share a common feature: the ventral retinas of both lateral and median ocelli view the sky above, while the dorsal retinas view the horizon. While this has been inferred previously, it has never been demonstrated in a quantitative fashion.

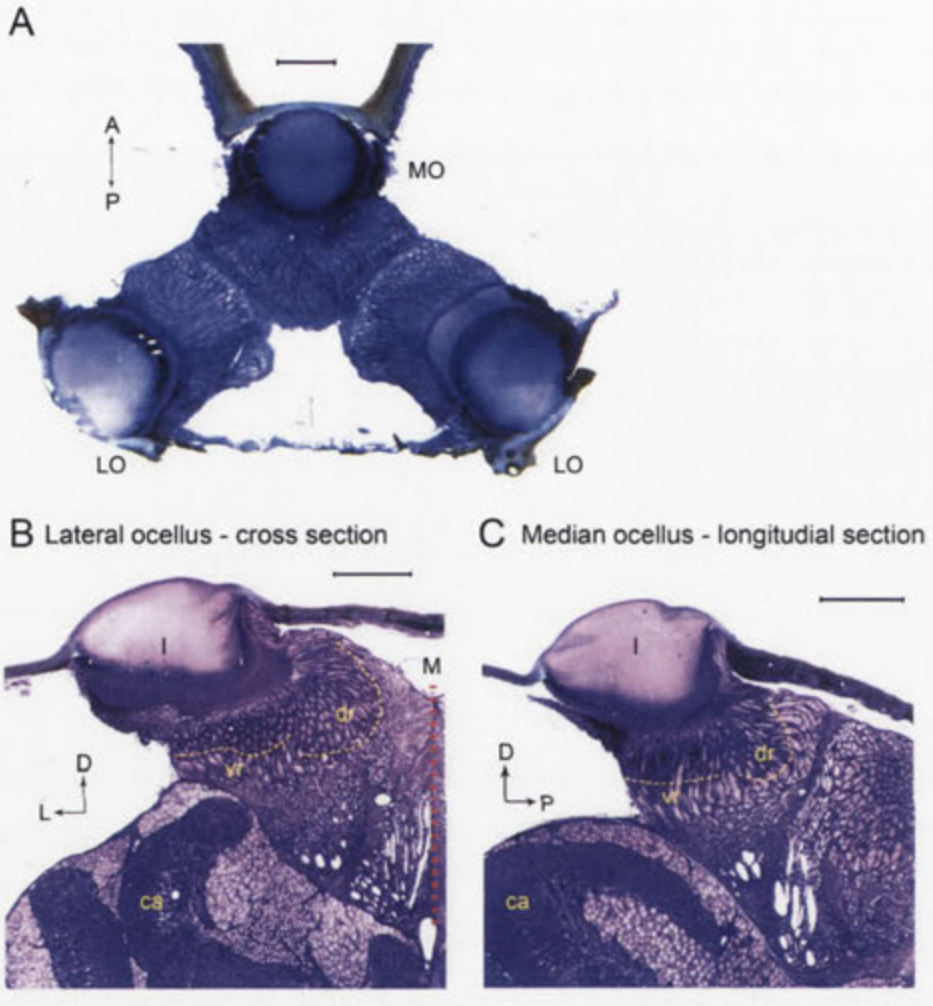
A
A
P
MO
LO
LO
B Lateral ocellus - cross section
C Median ocellus - longitudial section
l
M
dr
vr
D
L
ca
l
dr
vr
D
P
ca

Figure 2.3: Light micrographs of honeybee ocellar semi-thin sections. A: The horizontal section of the three ocelli. It is shown that the lens and retina of the median ocellus project dorsally while the lateral ocelli project slightly ventrally and toward the midline of the brain. B: Cross section of the lateral ocellus. It is shown that the outer surface of the ocellar lens is smooth and convex, but the inner surface curves asymmetrically toward the midline of the brain (M). C: Longitudinal section of the median ocellus. It is shown that the lens is a thick, dome shaped, spherical biconvex corneal lens. The black dashed line in (B) and (C) indicate the edge of the screening pigment of the retina. It is shown that in both median and lateral ocelli, the retina is divided into two regions (dr and vr). ***Abbreviations*:** A, anterior; ca, calyces; CE, compound eye; D, dorsal; dr, dorsal retina; I, lens; L, lateral; LO, lateral ocellus; M, midline of the brain; MO, median ocellus; P, posterior; vr, ventral retina. Scale bars: all 100 μm.

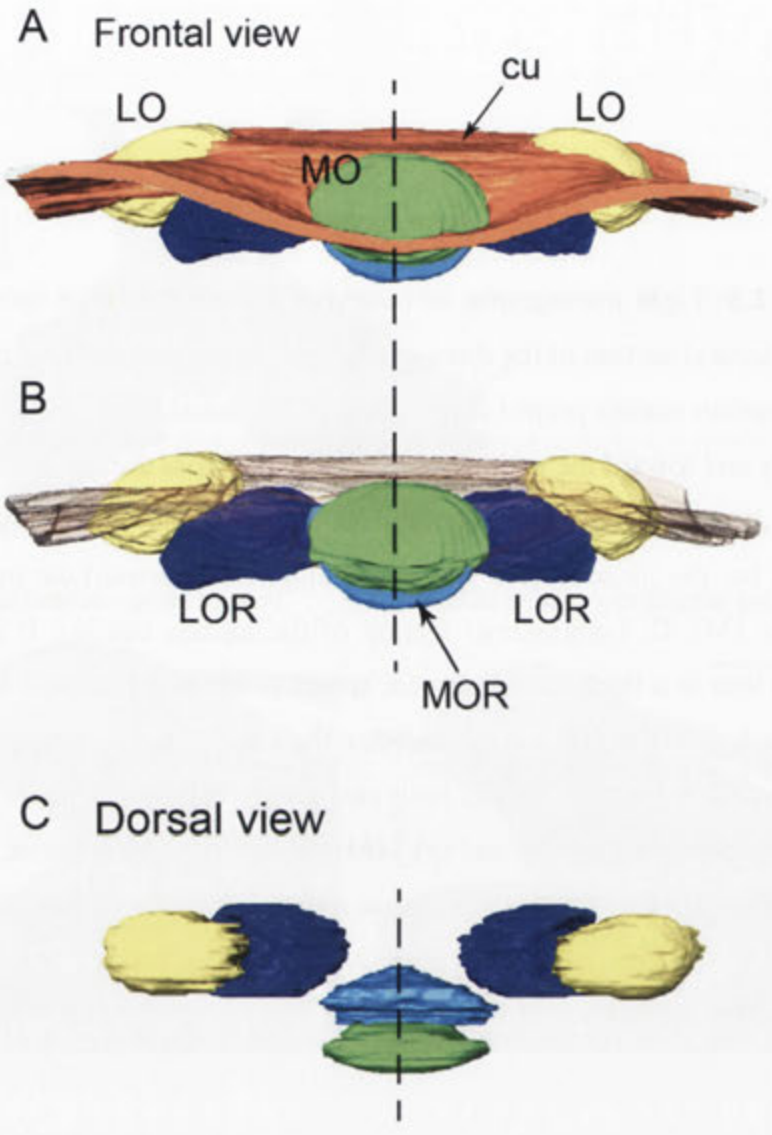

Figure 2.4: The three-dimensional reconstruction of honeybee ocelli. Reconstructions were generated from serial sections through the head of honeybee. (A, B) Front view of all three ocelli and the ocellar retina. (C) Dorsal view of the three ocelli and the ocellar retina. The dashed line indicates the mid-line of the brain. It is shown that while the retina of the median ocellus is positioned posteriorly to the median ocellar lens, the retina of the lateral ocellar lens is positioned laterally to the lens toward the midline of the brain. ***Abbreviations*:** cu, cuticle; LO, lateral ocellus; LOR, lateral ocellar retina; MO, median ocellus; MOR, median ocellar retina.

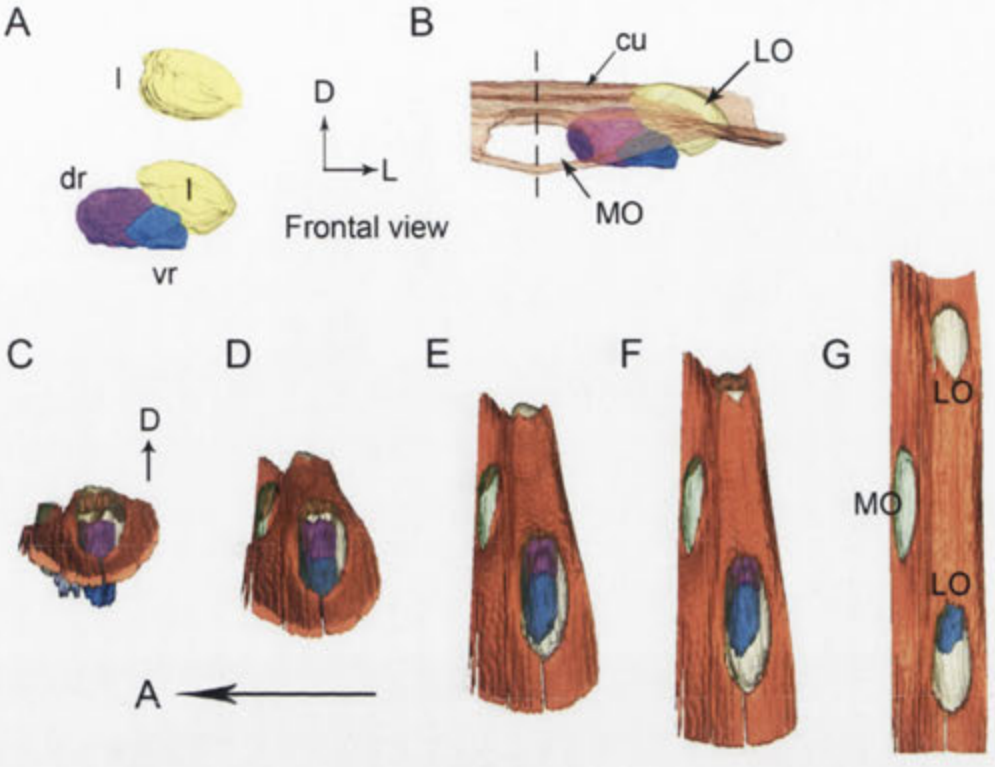

Figure 2.5: The 3-D reconstruction of the honeybee **lateral ocellus**. A, B: frontal views of lateral ocellar lens and retinas. A: the inner surface of the lens (l, shown in yellow) of the lateral ocellus is asymmetrical, the dorsal (dr, shown in purple) and ventral (vr, blue) retinas follow the inner surface of the lens and are pointing toward the mid-line of the brain (dashed line in B). C-G: Simulation of the rolling movement of the model. The ocelli are viewed from the side of the head. To the left the ocelli are dorsal. To the extreme right the head has been rolled downwards by 90 degrees to reveal all three ocelli. C: A lateral view of the lateral ocellus, only the dorsal retina can be observed. G: A dorsal view of the three ocelli, only the ventral retina can be observed. ***Abbreviations*:** A, anterior; cu, cuticle; D, dorsal; LO, lateral ocellus; MO, median ocellus.

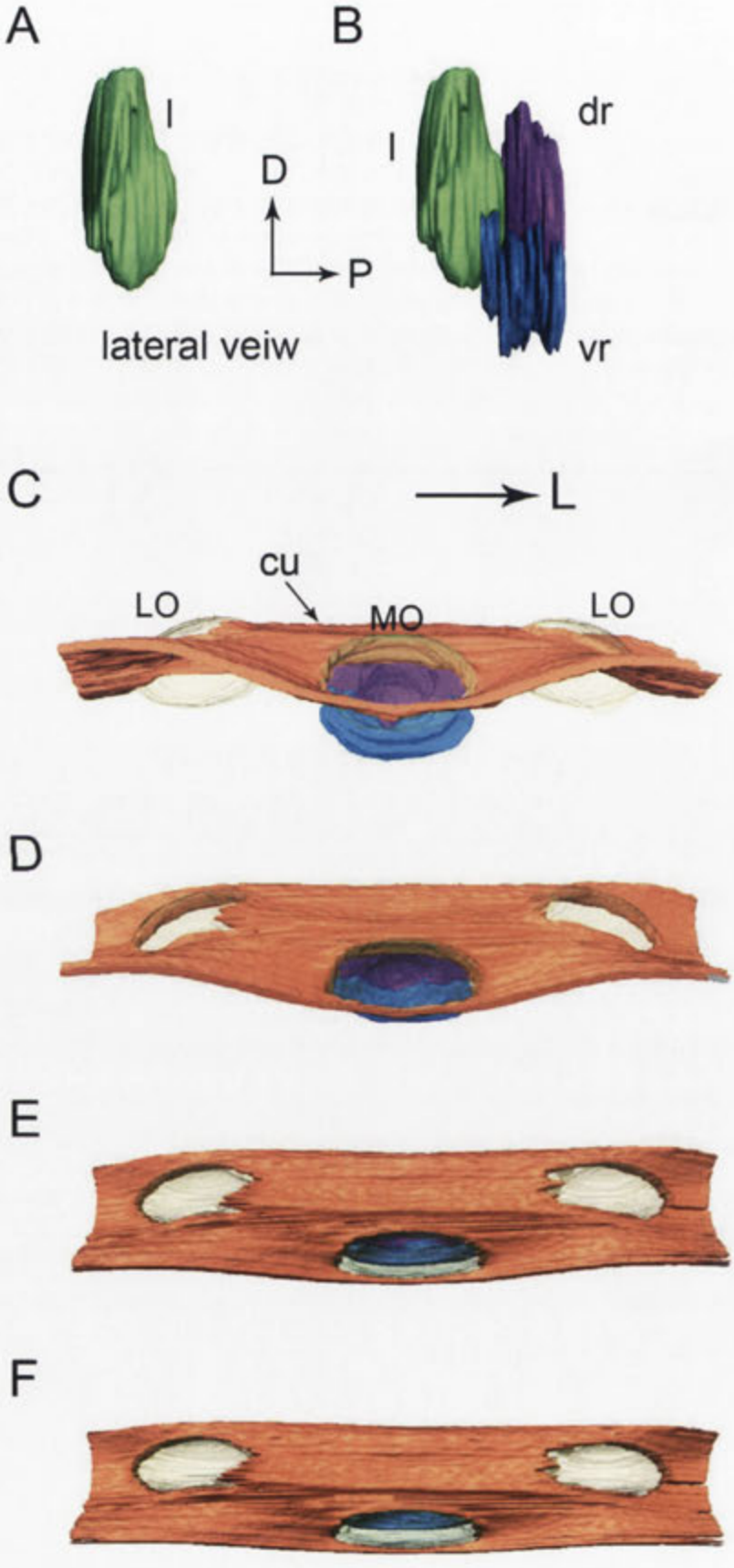
A
B
l
D
P
l
dr
vr
lateral veiw
C
L
cu
LO
MO
LO
D
E
F

Figure 2.6: The 3-D reconstruction of the honeybee **median ocellus**. A, B: lateral views of median ocellar lens (l, shown in green) and dorsal (dr) and ventral (vr) retinas. It is shown that while the lens of the median ocellus is elongated downward, the retinas are positioned downwardly and posteriorly in relation to the lens. C-F: Simulation of a pitching movement of the model. C: A frontal view of the median ocellus, only the dorsal retina can be seen through the median ocellar lens (the ventral retina is under the cuticle). F: A dorsal view of the ocelli, only the ventral retina can be seen. ***Abbreviations*:** cu, cuticle; D, dorsal; LO, lateral ocellus; MO, median ocellus; P, posterior.

2.4.4 Focal length of the ocellar lenses

Utilising the hanging-drop method to directly examine the image produced by the ocellar lenses, and by testing with the 'F' pattern, it can be seen that the images formed by the honeybee median and lateral ocelli are similar. The ocellar lenses form a single image, which is sharp laterally but out of focus in the middle (Fig 2.6). However, differences were shown when testing the lenses with different spatial patterns. For example, testing the radial pattern (spatial frequency = 0.2 cycles per degree, cpd) on the best focus plane, it can been seen that images formed by the median ocellar lens split into fragments in the middle, while the lateral ocellar lens forms a better image, which shows an '8' shape in the middle. The results hint that the lateral ocelli have better spatial resolution than the median ocellus.

Measuring the focal length with the 'F' pattern reveals that the focal distance of the lateral ocellus is significantly longer than the median ocellus ($F_{(1,65)} = 166.73$, $p = 0$). The distances between the back of the lens to the focal plane (back focal distance, BFD) is 209 ± 40 μm for the median ocellus and 320 ± 46 μm for the lateral ocelli (mean ± s.d., $n = 10$). The focal length (f) calculated from equation (1) showed that the focal lengths for the median and lateral ocellar lenses were 293 ± 35 and 393 ± 26 μm (mean ± s.d., $n = 5$). As the rhabdoms are no more than 100 and 150 μm behind the median and lateral ocellar inner surfaces, this suggests that the honeybee ocellar lenses form a focal plane well beyond the proximal limit of the retina in both cases.

Images on the retinal plane

The ocellar section and back focal measurement results show that the ocellar lenses of honeybees are extremely under focused with respect to the retina. The focal planes are roughly 100 μm beyond the retinal level in both median and lateral ocelli. Therefore, imaging through the ocellar lenses at the retinal level was examined using the hanging drop method to verify the spatial

resolving power of honeybee ocelli. The images formed by wide-field gratings with different spatial wavelengths were recorded at the level of the retina with a digital camera. In all cases the resolving capacity was studied for both vertical and horizontal gratings.

To provide accurate measurements of spatial resolution over a wide range of back focal distances (BFDs) I took photographs of the gratings through the lenses at 20 μm intervals from the back of the lens to 200 μm below the back surface of the ocellar lenses. The dorsal retina and ventral retina in each lens type are located at different distances from the back of the lens. In the description below I show data at BDF of 60 μm (ventral retina) and 100 μm (dorsal retina) for the median ocellus and 80 μm (ventral retina) and 140 μm (dorsal retina) for the lateral ocellus. These values approximately match the BDF measurements given above.

It was found that both the median and lateral ocellar lenses were able to resolve spatial information at the dorsal and ventral retinal levels but that the dorsal retina had better resolution for both types of ocelli (Fig 2.7 and 2.8). In all cases we found no difference in the capacity to resolve horizontal or vertical gratings. Therefore, the data for both are presented in the figures but they are discussed together.

For the dorsal retina of the median ocellus contrast information is available at a spatial frequency of 0.25 cpd (4° spatial wavelength) but it is poorly focused (Fig 2.8A-H). The ventral retina of the median ocellus cannot resolve a grating below a spatial frequency of 0.125 cpd (Fig. 2.8I-P). The dorsal retina of the lateral ocellus could resolve gratings presented at spatial frequencies as high as 0.5 cpd (spatial wavelength 2°) (Fig. 2.9A-H). Gratings at 1 cpd could not be resolved (data not shown). The ventral retinas of the lateral ocelli were not capable of resolving a 0.5 cpd grating but were able to resolve a grating of 0.25 cpd (spatial wavelength 4°) (Fig. 2.9I-P).

In both the lateral and median ocelli, the images show some fragmentation in the middle of the image, which corresponds to the middle of the lens (Fig 2.8 and 2.9).

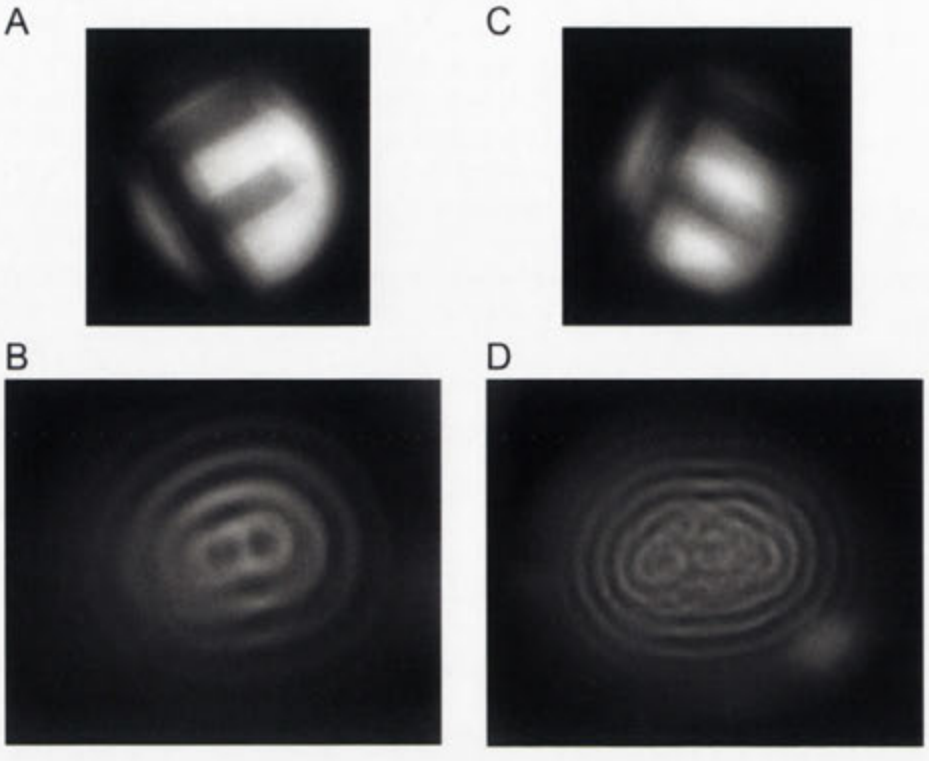

Figure 2.7: Imaging through the lateral and median ocellar lenses of honeybee. (A) and (B): Images formed by the **lateral** ocellar lens. (C) and (D): Images formed by the **median** ocellar lens. (A) and (C) show the image of a single "F" seen at the focal plane. (B) and (D) show images of angularly corrected stimuli of 5° spatial wavelength on a wild field LCD monitor as seen through the lenses on the focal plane. Both the median and lateral ocellar lenses form a single image although, when testing the lenses with the radial pattern, the centres of the images spilt in both cases.

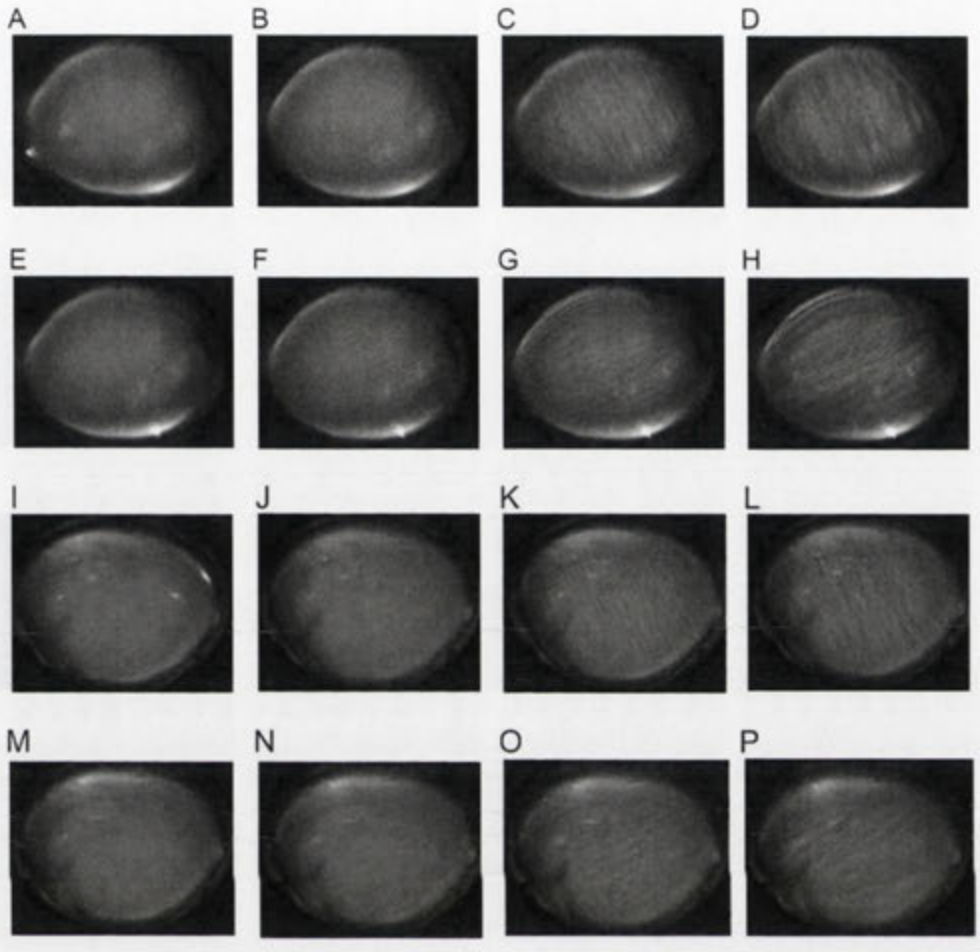

Figure 2.8: Grating images through the honeybee **median** ocellus at the dorsal retinal level (A-H; 100 μm away from the back of the lens) and ventral retina (I-P; 54 μm away from the back of the lens).

Spatial wavelength: (A) (E) 2°; (B) (F) 4°; (C) (G) 8°; (D) (H) 12°

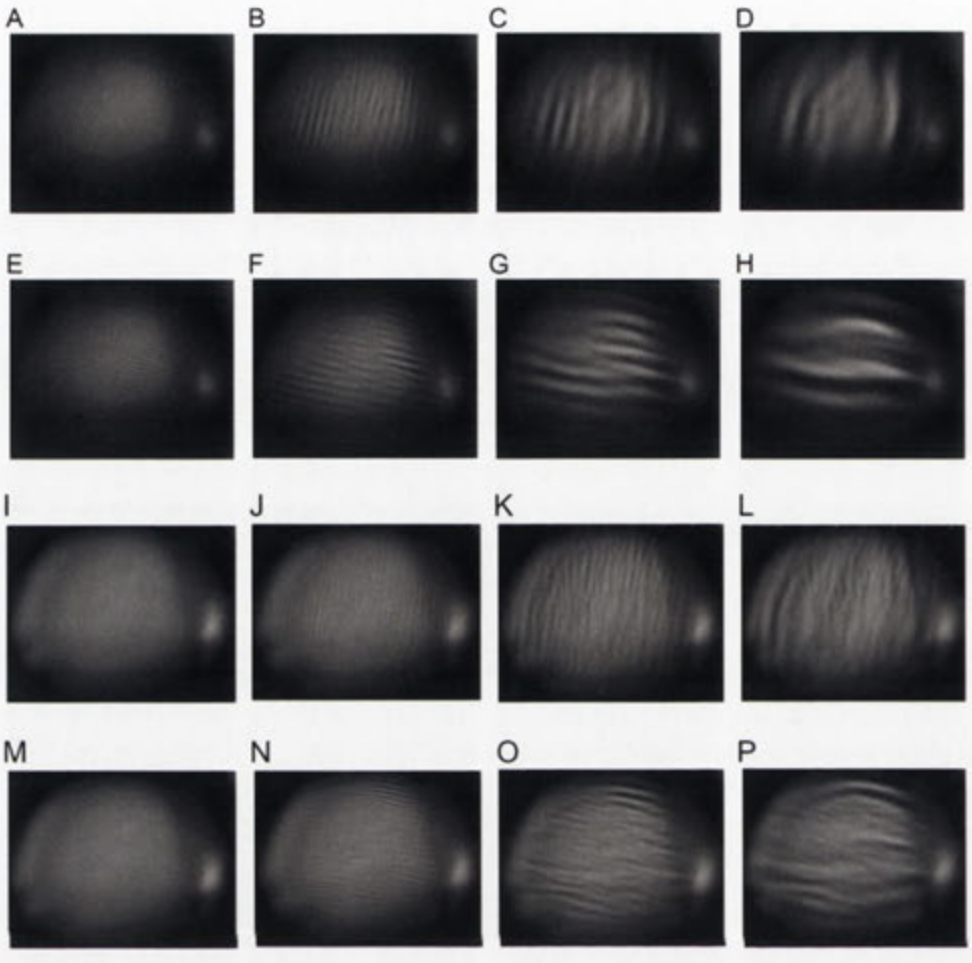

Figure 2.9: Grating images through the honeybee **lateral** ocellus at the dorsal retinal level (A-H; 140 μm away from the back of the lens) and ventral retinal level (I-P; 80 μm away from the back of the lens).

Spatial wavelength: (A) (E) 2°; (B) (F) 4°; (C) (G) 8°; (D) (H) 12°

2.5 Discussion

2.5.1 The morphology of honeybee ocelli – lens and retinal structure

The structural organisation of ocelli is varied (reviewed in Goodman 1981). The gross morphology of the honeybee ocelli has been investigated in three previous studies (Toh and Kuwabara 1974; Pan, PhD thesis 1980; Ribi et al. 2011), the last of which was conducted at the same time as my thesis. The data in Ribi et al. was published in 2011 and presents similar anatomical data to that obtained by me through independent experiments. While that paper removed the novelty of discovering two retinas in bee ocelli, they did not produce a 3-D model of the ocelli and they did not measure the spatial resolving power of the ocelli. The histological sections from the previous studies are similar to those obtained here. The lateral ocellar lens has a convex ellipsoid outer surface and an asymmetric inner surface while the median ocellar lens is a flattened spheroid. However, the three-dimensional reconstructions of the ocelli presented for the first time here show that the median ocellar lens is elongated downward and forms a complex non-spherical shape. The three-dimensional reconstruction of the three ocelli that I have performed is more useful than the traditional techniques used in all previous studies as it allows the lenses and retinas to be viewed in three-dimensions and can be combined in the future with ray tracing technology to give accurate mapping of the visual fields of the retinas.

Berry et al. (2011) found that the ocellar lenses of a nocturnal bee (*Megalopta genalis*) consist of at least three structurally distinct components, named the outer, middle and inner layer. The outer layer is stained lightly with Toluidine Blue; the middle layer is similarly composed of tightly layered tissue and stained more densely with Toluidine Blue. The inner layer stains with the highest density of Toluidine Blue among the three layers. In honeybees, the semi-thin sections through the ocelli showed that it

has a similar layered structure. The density of Toluidine Blue staining showed that honeybee ocellar lenses lack the middle layer and only possess the outer and inner layers. However, the boundaries between the layers are difficult to define; the staining density of Toluidine Blue indicates the density of organic material within the lens. It is still not known whether the different layers have different optical properties (Berry et al. 2011), but it is possible that the non-homogeneous components of the ocellar lens may help focus the images closer to the retinal plane (Berry et al. 2007ab).

The dragonfly lateral ocellar lens has an asymmetrical inner surface, which reflects the underlying division of the retina into two regions, as also observed in dragonflies (Berry et al. 2007a). Both the honeybee lateral and median ocellar lenses have been shown here to have an asymmetrical inner surface. The retina has two major regions, each with different lengths of rhabdomeres, which correspond with the shape of the lens. These two regions are referred to as the dorsal and ventral retinas. For the median ocellus, the retinal layer lies around the elongated side of the inner surface of the lens; for the lateral ocellus the retinal layer is on the inner surface of the lens that is close to the midline of the brain. In both cases the ocellar structure allows light from the horizon to travel further in the lens before it reaches the dorsal retina, as compared to light from above, which lands on the ventral retina. The increased path length to the dorsal retinas may enable a more focused image on the retina through increased refraction. A very recent study on the ocelli of worker and drone honeybees has also shown the two separate retinal regions (i.e. dorsal and ventral retinas: Ribi et al. 2011). Their work showed that the retinas form two distinctly separate nerve bundles as they pass to the first synaptic plexus where they make contact with second-order interneurons (Ribi et al. 2011). Combining the 3-D structural reconstruction that I have done here and the anatomical results (both mine and those in Ribi et al. 2011), I suggest that the two retinal regions may have different roles in processing visual information. It is possible that the dorsal retina has evolved for receiving information about the horizon while the ventral retina has evolved to detect more general

information regarding intensity changes in the sky above (Stavenga et al 1979, Berry et al 2007a, Ribi et al. 2011). The ventral retina may well be involved in the ocellar dorsal light response, as demonstrated in dragonflies (Stange and Howard 1979).

Previous studies have found that the structural morphology of Hymenopteran insects reflects their ecological niche. For example, it has been shown that two nocturnal species (halictid bee *Megalopta genalis* and paper wasp *Apoica pallens*) have a distal retinal surface that is positioned close to the proximal surface of the lens; while in the diurnal wasp (*Polistes occidentalis*) there is a gap between the retina and the proximal lens surface (Warrant et al., 2006). Cross- and longitudinal-sections of honeybee ocelli reveal a similar structure as the diurnal wasp: both the median and lateral ocelli possess corneagal cells that contain screening pigments and a vitreous chamber that separates the inner surface of the lens and the retinal layer.

Although no direct measurements have been made of the visual field of the honeybee ocelli, it is possible to predict the field of vision based on the relative position of the ocelli, the hairless zone that surrounds the ocelli, the morphology of the lens and its relation to the retina. From the results here, it appears that the median ocellus looks up- and forward (covering the horizon), while the lateral ocelli look upwards and to either side of the head (again, also encompassing the horizon). More specifically, the modelling exercise has revealed that the ventral retinas of all ocelli take their primary input from the region directly above the head. Under normal flying conditions this would equate with the sky above the animal. However, when the animal's head rolled to one side the lateral ventral retina on one side would view the far darker horizon, possibly providing a strong clue to the animals orientation. The dorsal retinas of all ocelli exclusively view the horizon. As described below, this feature corresponds with a higher spatial resolution, suggesting that more sophisticated processing might be possible through the dorsal retinas. This processing may well include the detection of motion, as has been found to be the case in dragonfly ocelli (van Kleef et al.

2008). A neuron that has its dendrites in the ventral retina of the lateral ocellus is described in Chapter 3. Even this neuron, which does not get direct dorsal retinal input shows evidence of the capacity to code motion in a direction-selective manner (see Chapter 4). Other ocellar second-order neurons have been observed in bees that receive their primary input from the dorsal ocellar retinas (see Chapter 3; Milde and Homberg 1984; Heinzeller 1976). Unfortunately, the directional properties of these neurons are currently unknown.

2.5.2 Ocellar resolution

It has been consistently observed in a wide range of species that ocelli lack optical resolving power (Parry, 1974; Wilson, 1978; Cornwell, 1995; Berry et al., 2007ab; Schuppe and Hengstenberg, 1993; Warrant et al., 2006). However, this view has recently been re-examined, with several studies showing that despite their poor focus, ocelli can still provide a certain level of spatial resolution (blowfly *Calliphora erythrocephala*: Schuppe and Hengstenberg 1993; diurnal and nocturnal wasps: Warrant, 2006; locusts *Lousta migratoria*: Berry et al., 2007b; Dragonflies: van Kleef et al., 2005; Berry et al., 2006). From the back focal measurement results and the semi-thin sections of honeybee ocelli, it has been shown that both the honeybee median and lateral ocellar lenses form focal planes well beyond the proximal limit of the retina.

Although, a recent study on honeybee ocelli suggested that the focal plane of the honeybee median ocellus falls on a more dorsally located retina, thus expanding the available focal distance, it was not clear that this improved the capacity to form focused images (Ribi et al. 2011). Comparing the back-focal-distances (BFDs) measured from the present study and that of Ribi et al., it is apparent that the BFDs for the lateral ocellar lenses are similar (both studies showed a BFD with a length of 330 μm). However, the BFDs for the median ocellar lens differed by approximately 40 μm. The variation between the two studies may be due to the limitations of the

hanging drop method as it is not possible to fully control the position and angle of the final observation. The position of the tested lens on the saline drop is set by the surface tension of the drop and by gravity.

The important findings presented here are that the dorsal retinas, which view the horizon, have higher spatial resolution than the ventral retinas, which view the sky above. It is also the case that the lateral ocelli have higher spatial resolution than the median ocellus. It makes sense that the dorsal retinas would have higher resolving power than the ventral retinas because they view the horizon, which usually contains some spatial texture. Conversely the sky has little in the way of useful texture. Clouds can provide texture but they offer little assistance in maintaining orientation relative to the ground, other than to offer input to a simple light reflex (Stange et al. 2002). It is not immediately obvious why the lateral ocelli have higher resolving power than the median ocellus. During flight the lateral portions of the visual field will move very rapidly, thus degrading the spatial information in the image. Conversely, the stationary pole of the optic flow field during forward flight will be directly ahead of the animal. It might, therefore, be expected that the median ocellus should have the best spatial resolution as it looks at the most stable part of the visual field. In fact, exactly the reverse is the reality.

The results presented in this chapter, together with previous and recent studies on other insects, provide growing evidence that some level of form vision is an integral part of ocellar function in insects. Given that prior chapters showed that directional signals appear to arise from ocellar input in the honeybee system, it might have been expected that some spatial resolving capacity should have been available from the ocelli, as this is essential in calculating a motion signal (Borst and Egelhaaf 1989). The results show that the honeybee ocelli do indeed have a reasonable level of form vision, certainly sufficient to calculate motion signals using low spatial frequency inputs. In the chapters that follow we reveal that the ocelli provide an important visual input to numerous large direction-selective

descending neurons in the bee. Interestingly, some of these neurons are selective about which ocellar retina they receive input from (Chapter 3). Thus, the gross anatomy of the sensory structure itself is carried on through the nervous system, presumably leading to specific behaviours.

Chapter 3

Anatomy of honeybee motion-sensitive descending neurons

3.1 Abstract

Nine classes of descending neurons (DN) have been previously reported in the honeybee and these are labelled as DNI_x through to $DNIX_x$. The roman numerals indicate the class label and the subscript numbers indicate specific identifiable neurons within each class. While the neurons in each of the nine classes have anatomical similarities, thus placing them in a class, they also have distinct anatomical features that allow them to be distinguished from each other. Each of the nine classes of cells contains 1-8 identifiable neurons, with approximately 30 cells having been observed in total. Here, the anatomical characteristics of five identified motion-sensitive descending neurons from the nine classes are described. Four cell types, $DNII_2$, $DNIV_2$, $DNIV_3$ and $DNVII_1$, were repeatedly recorded and identified by iontophoretic dye injection. The cell morphology of these four cells is described separately and the inter-individual variations are considered. A newly identified cell that clearly fits into the DNVII class was also identified and is described in this chapter ($DNVII_2$). In addition to the nine classes of direction-selective descending neurons, there are five large descending neurons that receive their primary input from the ocellar retinas. These are termed Mocth or $Locth_{1-4}$. In this classification, M and L

represent the median or lateral ocellus (oc) and 'th' denotes the fact that the neurons descend into the thorax. Here, the specific anatomy of a lateral ocellar descending neuron, $Locth_3$ is reported. The dendritic field of the $Locth_3$ neuron was carefully mapped to show that the neuron receives inputs specifically from the ventral retina of the lateral ocellus. Having made this discovery, and armed with the new knowledge about the retinas of the honeybee ocelli, I went back into the literature and found that it was possible to establish which retina provided the inputs to $Locth_{1-2}$ and Mocth. These new revelations, based on published data are also presented in this chapter. The three dimensional morphology of all filled cells was determined for the first time by combining intracellular dye injection techniques and confocal microscopy. By comparing the detailed spatial geometry within the brain the results provide a better understanding of the dendritic inputs onto honeybee motion-sensitive descending neurons and the targets of their axonal outputs.

3.2 Introduction

Honeybees rely on their ability to sense visual cues in the surrounding environment. These visual cues may be static, such as patterns of colour (von Frisch 1914), contrast (Srinivasan et al. 1993) or polarisation (von Frisch 1914), or dynamic, such as optic flow (Esch et al. 2001). The visual detection of motion is particularly important for flying bees, enabling them to control flight and maintain spatial orientation (Srinivasan et al. 1996; Baird et al. 2005). Vision also plays a role in flight stabilising reflexes such as the optomotor response, where visual stimulation with wide-field image motion produces reflexive body movements in the same direction as the image motion (Schlieper 1927; Kaiser and Liske 1974). These visually guided flight behaviours require sensory-motor transformation of the visual motion signals into useful signals for the motor system. In insect brains the intersegmental descending neurons (DNs) play an important role in

integrating the multisensory inputs, including visual signals, and transmitting that information to motor ganglia. The term 'descending neuron' is used exclusively for those neurons that have cell bodies and dendritic fields in the brain or suboesophageal ganglion and whose axons carry the information to the thoracic or abdominal ganglia (descending neurons do not make direct contact with muscles). It is believed that the motion-sensitive descending neurons are responsible for the sensory-motor transformations required for optomotor and other visually driven orientation reflexes (Ibbotson and Goodman 1990; Wertz et al. 2008).

Descending interneurons that respond in a direction-selective fashion to visual motion have been reported in a range of insects, including moths and butterflies (Singarajah 1988), locusts (Kein 1974; Rowell and Reichert 1986), and dragonflies (Olberg 1981ab). Honeybee motion-sensitive descending neurons have also been reported (Goodman et al. 1987; Goodman et al. 1990, 1991; Ibbotson and Goodman 1990; Ibbotson 1991ab). Pan and Goodman (1977) described the anatomy of five descending neurons in the honeybee that had cell bodies in the midbrain, dendrites close to the ocellar retinae and projected into the thoracic ganglia. Subsequent analysis showed that at least one of these neurons was also direction-selective when stimulated with wide-field moving gratings (Goodman et al. 1987). Goodman et al. (1987) later described the brain anatomies of six more groups of motion-sensitive descending neurons in the honeybee. These neurons were distinguished from the ocellar descending neurons by the fact that none of them sent dendrites up into the ocellar retinae: all confined their dendrites to the central brain area. At that time 10 of these 'non-ocellar' descending neurons had been recorded from and filled, and were placed into six groups based on their anatomical similarities (the classes were: DNI, DNII, DNIII, DNIV, DNV and DNVI). Ibbotson (1991a) then described the physiology and morphology of a new anatomical category of motion-sensitive descending neurons called DNVII. Besides the seven classes of honeybee descending neurons published in the open literature, Ibbotson (1989) also reported the morphology and physiology of another two classes

of cells, each containing many individual neurons in his PhD thesis (DNVIII and DNIX). The DNVIII category contains a particularly large number of cells (at least 8). Although the detailed morphology of cells within different categories of neurons are distinct, it is clear that all the neurons descend from the brain into the thoracic motor centres, reaching as far as the most posterior tip of the metathoracic ganglion (Pan and Goodman 1977; Ibbotson and Goodman 1990). The other distinctive feature is that most of the DNs recorded from so far are highly direction-selective.

The available information from previous work takes the form of 2-dimensional drawings of the neurons from the posterior aspect, which reveals their general shape but not their 3-dimensional (3-D) characteristics. Therefore, my aim here was not to re-describe the general cellular morphological properties, but rather to use modern fluorescent dye-filling and optical sectioning to gain an accurate identification of the recorded cells and to add some useful information about the 3-D shape of the neuron within the central brain and prothoracic ganglion. The 1µm optical slices provide valuable depth information for dendrites and axon collaterals within the nervous system that was not previously available. The spatial reference in relation to the brain was obtained by applying the newly available virtual atlas of the honeybee brain (honeybee standard brain; Rybak et al. 2010). The labelled brain area, and the terminology used in this study will be described in the methods and materials section.

In this chapter, I report the cell types recorded in this study. All dye-filled neurons were classified on the basis of both their physiological characteristics and cell morphology. The classification scheme described by Goodman and Ibbotson is used throughout this study (Pan and Goodman 1977; Goodman et al. 1987; Ibbotson and Goodman 1990; Ibbotson 1991ab).

3.3 Methods and Materials

3.3.1 Visualisation of stained neurons

All experiments were performed on worker honeybees, *Apis mellifera*. The ventral nerve cord was exposed from the dorsal side of the neck, between the suboesophageal and prothoracic ganglia, so that a recording electrode could be vertically inserted into it. The morphology of the neurons were obtained using fluorescent dye-filling and optical sectioning (confocal imaging). Cells were impaled at random with no visual guidance at the single-axon level using intracellular recording technique. Electrode tips were filled with 3-10% Lucifer Yellow CH (lithium salt, Invitrogen™) in 1% LiCl (by capillary action), and back-filled with 1M LiCl. Recordings were attempted from 300 bees. From these, complete fills were obtained on 43 occasions and data from this sub-population is presented here. Upon successful completion of an intracellular recording, cells were filled with Lucifer Yellow by iontophoretic injection of 5-10 nA (negative injection) for at least 15 minutes. Following the current injection the brain, suboesophageal ganglion and thoracic ganglia were carefully dissected in fixative (3.7% paraformaldehyde in phosphate buffered saline) and then transferred to 3.7% paraformaldehyde in methanol for 45 minutes. The samples were then dehydrated through an ethanol series of 80%, 90% and 100% for 10 mins each, and mounted in methyl salicylate. Filled neurons were observed and optically sectioned on a confocal microscope (LSM Pascal, Zeiss). The image series were processed in Lieca LCS and Zeiss AxioVision software to produce 2D projections of neurons at different angles.

3.3.2 Terminology

Directional terms

Figure 3.1 (adopted from Berry and Ibbotson 2010) shows the 3-dimensional reconstruction of the honeybee head and thorax both externally and internally (the nervous system including the brain, ventral nerve cord and thoracic ganglion). The honeybee has two visual systems: the relatively large compound eyes located on the lateral sides of the head and three simple eyes (ocelli) located on top of the head. When the animal is facing to the front, the head appears to be vertically positioned while the thorax and abdomen are relatively horizontal. The head and the thorax are connected by the neck forming an angle of about 90 degrees. As the animal can change orientation with respect to its environment, the head and thorax position shown in Fig 3.1A is defined as the standard anatomical position throughout this study. Anatomically, the anterior end of the nervous system is dorsally positioned relative to the normal body orientation. Therefore, the top of the head capsule will be referred to as dorsal and the mouth parts ventral. The directional terminology of the nervous system, the brain, the ventral nerve cord and the thoracic ganglia, will be referred to in this same manner. The honeybee nervous system is shown in Fig 3.1B. The antennal lobes are positioned at the ventro-anterior side of the brain (lower front), the mushroom bodies are on the dorsal side of the brain (upper), and the suboesophageal ganglion is on the posterior side of the brain.

Honeybee brain anatomy

In insect brain anatomy the different brain segments are determined according to the segmental origin of brain neuropils. Modern developmental studies on *Drosophila* suggest that the protocerebrum is the first segmental neuropil, the deutocerebrum is the second, and the tritocerebrum is the third (the segmental origin of the optic lobes is not yet fully understood). The results also suggest the positions of regions and boundaries of the segments (Hirth et al. 2010). The terminologies of brain segmental regions from

Drosophila were adopted and used to describe the neural morphology in previous studies on honeybee descending neurons (Goodman 1987; Ibbotson and Goodman 1990; Ibbotson 1991ab). However, in recent honeybee studies, different anatomical terminologies are used to describe brain anatomy (e.g. Maronde 1991; Paulk et al 2008; Rybak 2010). Therefore, for further comparisons of neural projections, the latter honeybee terminology is used throughout this study. Figure 3.2 shows the standard bee brain (adopted from Rybak et al. 2010), with the brain chambers labelled with different colours. Briefly, the honeybee brain can be divided into optic lobes (including lamina, medulla, and lobula; the lamella is not shown in the standard brain), central body, protocerebrum, and deutocerebrum (including antennal lobes and dorsal lobes). The protocerebrum is further divided into the mushroom bodies and three regions: the median protocerebrum and two lateral protocerebra (after Maronde 1991). Throughout this account the half of the brain in which the descending axon lies is termed ipsilateral, and the opposite is termed the contralateral side. This convention is more useful than using the cell body location as the identifier of brain lateralisation when discussing descending neurons. The reason for this is that the cell body can often arise in very distant parts of the nervous system, while the axon offers a very clear defining feature of each neurons location in the nervous system.

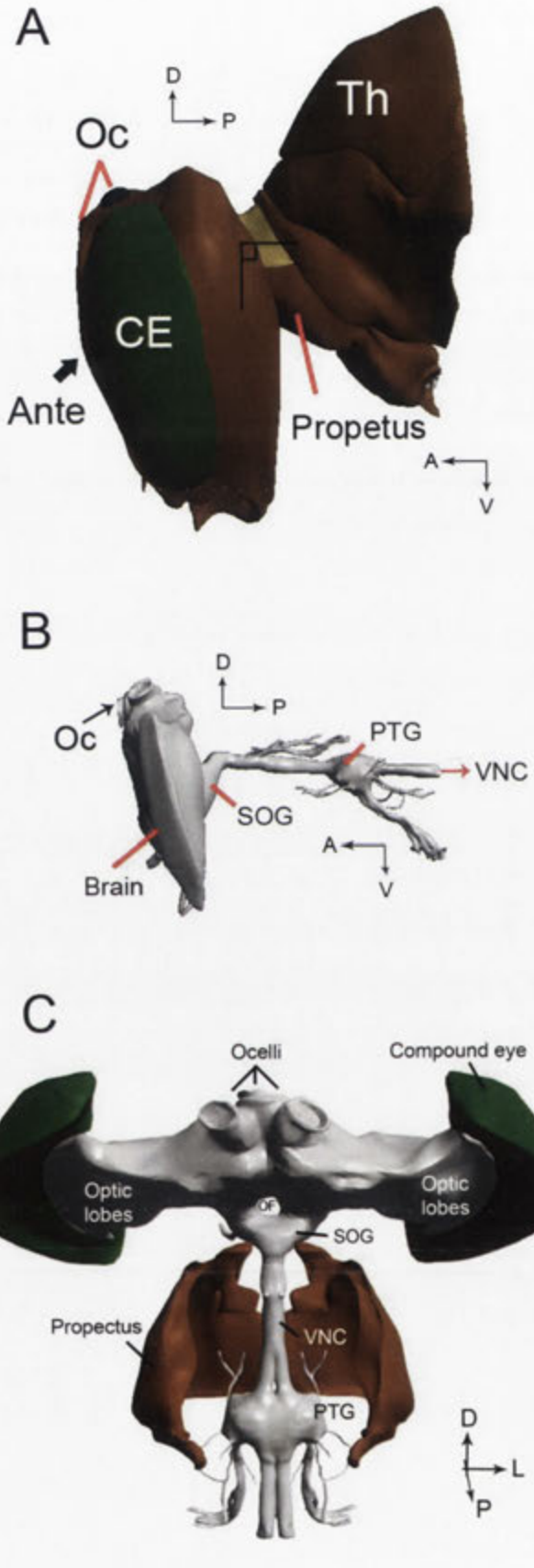
A
D
P
Th
Oc
CE
Ante
Propetus
A
V
B
D
P
Oc
PTG
VNC
SOG
A
V
Brain
C
Ocelli
Compound eye
Optic lobes
Optic lobes
OF
SOG
Propectus
VNC
PTG
D
L
P

Figure 3.1: The 3-dimensional reconstructions of honeybee head and thorax (adopted from Berry and Ibbotson 2010) and the standard anatomical position of honeybee. A: The external 3-dimentional reconstruction of a honeybee. The head and thorax (Th) position forming an angle of 90° is defined as the standard anatomical position (body axis). The antennae (Ante) are at the anterior end. The top of the head capsule where the ocelli (Oc) are located will be referred to as dorsal, while the mouth parts will be ventral. B and C: Internal (the nervous system) 3-D reconstruction of honeybee head and thorax to the same scale as the external drawing in A (B: lateral view; C: dorsal view). The directional terminology of the nervous system, the brain, the ventral nerve cord (VNC) and the pro-thoracic ganglion (PTG), will be referred to in the same manner as the body axis. ***Abbreviations for all figures:*** A, anterior; D, dorsal; OF, oesophageal foramen; P, posterior; SOG, suboesophageal ganglion; V, ventral

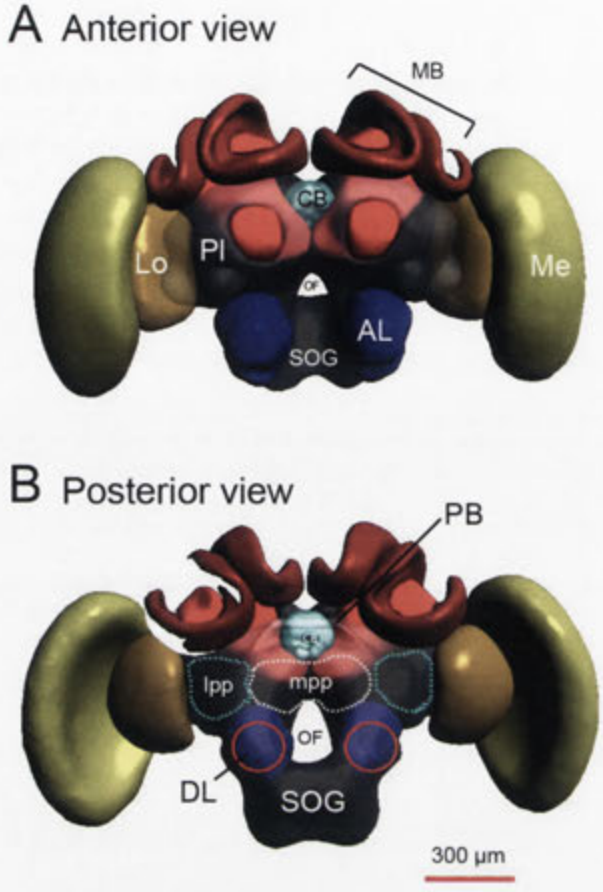

Figure 3.2: The virtual atlas of the honeybee brain (standard bee brain; adopted from Rybak et al. 2010). A: The anterior view of the honeybee brain. The brain chambers are labelled with different colours. The honeybee brain consists of the optic lobes (including lamella, medulla, and lobula; the lamella are not shown in the atlas), protocerebrum, deutocerebrum (including antennal lobes and dorsal lobes), and suboesophageal ganglion. B: The posterior view of the honeybee brain. The different regions in the protocerebrum are labelled. ***Abbreviations for all figures:*** AL, antenna lobes; CB, central body; DL, dorsal lobes; Lo, lobula; lpp, lateral posterior protocerebrum; MB, mushroom bodies; Me, medulla; mpp, median posterior protocerebrum; OF, oesophageal foramen; PB, protocerebral bridge; Pl, protocerebrum; SOG, suboesophageal ganglion

3.4 Results

Four types of honeybee descending neurons $DNII_2$, $DNIV_2$, $DNIV_3$, $DNVII_1$ were recorded and identified as single fills repeatedly in this study. The selection of these four cells was purely random and probably relates to the fact that they have particularly large axons, which made penetration with an intracellular electrode more likely. The cell morphology of each cell type within the brain and suboesophageal ganglion will be reported individually in this section. For $DNII_2$ and $DNIV_3$ cells, the dye was successfully filled into the prothoracic ganglion. The morphology in the brain and prothoracic ganglion of a fifth, newly identified cell that fits into the DNVII category is also presented. This cell is referred to as $DNVII_2$. The cell morphology of $DNVII_2$ within the brain region and the prothoracic ganglion is described. In this chapter, where possible, the morphological variation between the same neuron-type in different preparations is examined based on multiple fills. The physiological characteristics of these cells are reported separately in the following chapters.

3.4.1 $DNII_2$

The $DNII_2$ cell type was identified as a single fill in 12 preparations and the axon was filled in the prothoracic ganglion in 3 preparations. The following description of the neural anatomy is based on information derived from those preparations.

The variability of individual cell types between different preparations is remarkably small. Figure 3.3 shows one of the preparations in detail with three characteristic branches marked with arrows (1-3). All of these branches were identified in all twelve preparations. The first branch (1) comes out from the major joint and projects toward the dorsal-posterior protocerebrum on the ipsilateral side. The second branch (2) also extends out from the major joint, projecting downward toward the ipsilateral dorsal lobe. The third branch (3) is located on the terminal of the dendrite on the

contralateral side branching from the major trunk of the dendritic arbors. An analysis of the branch length was conducted. The total variation of the selected branch lengths between preparations was small: branch 1: 163 ± 14 μm; branch 2: 151 ± 21 μm; branch 3: 112 ± 15 μm. Based on the observations and measurements on the selected dendritic branches, we are confident that we have recorded from and filled the same neuron type in every preparation. Therefore, the physiology reported in subsequent chapters is based on the same neuron type across 12 preparations.

$DNII_2$ lies on the posterior side of the brain with the cell body located on the lateral edge of the protocerebral bridge, close to the calyx of the mushroom bodies (Fig 3.3A). In Figure 3.3C the cellular structure is coded in different colours to show its depth in relation to the surface of the suboesophageal ganglion. It is shown that the cell body lies about 18 μm under the posterior surface of the brain. The trunk of the dendritic arbors with fine branches projects to both halves of the brain in the postero-medial protocerebrum, dorsal to the oesophageal foramen while the major branches lie at a depth of about 25 μm relative to the posterior brain surface. It also projects anteriorly for approximately 100 μm into the brain. As the cell's axon travels down to the suboesophageal ganglion the terminal arbores branch into the lateral suboesophageal neuropile, which is approximately 50 μm away from the posterior surface of the suboesophageal ganglion. The terminals of those branches thicken, forming knob-like blebs (see Fig 3.3A, black arrows). Figure 3.3D shows the presynaptic terminals (black arrows) observed from a second preparation.

The section of $DNII_2$ within the prothoracic ganglion was successfully filled in three preparations. Figure 3.4 shows the axon of $DNII_2$ and its branches in the prothoracic ganglion. It is shown that the axon lies on the very dorsal side of the cervical nerve cord and sends out two pairs of branches to both the ipsilateral and contralateral sides of the neuropile. Rehder (1988) did a comprehensive analysis of the anatomical compartments within the honeybee prothoracic ganglion. The 3-D

reconstruction reveals that the blebbed axon collaterals of $DNII_2$ occupy a very distinct region of the dorsal prothoracic ganglion (Fig. 3.4AB) that is associated with the dendrites of motor neurons that innervate the wing musculature (Pan, 1980). While it is impossible to say, based on the present data, if there is a connection between $DNII_2$ and those motor neurons, the proximity of the terminals suggests a potential link.

For reference, I use the 3-D model of honeybee nervous system previously developed in our laboratory (Berry and Ibbotson 2010), the location of the $DNII_2$ neuron is shown to scale in the 3-D reconstruction of the brain and prothoracic ganglion (Fig 3.5).

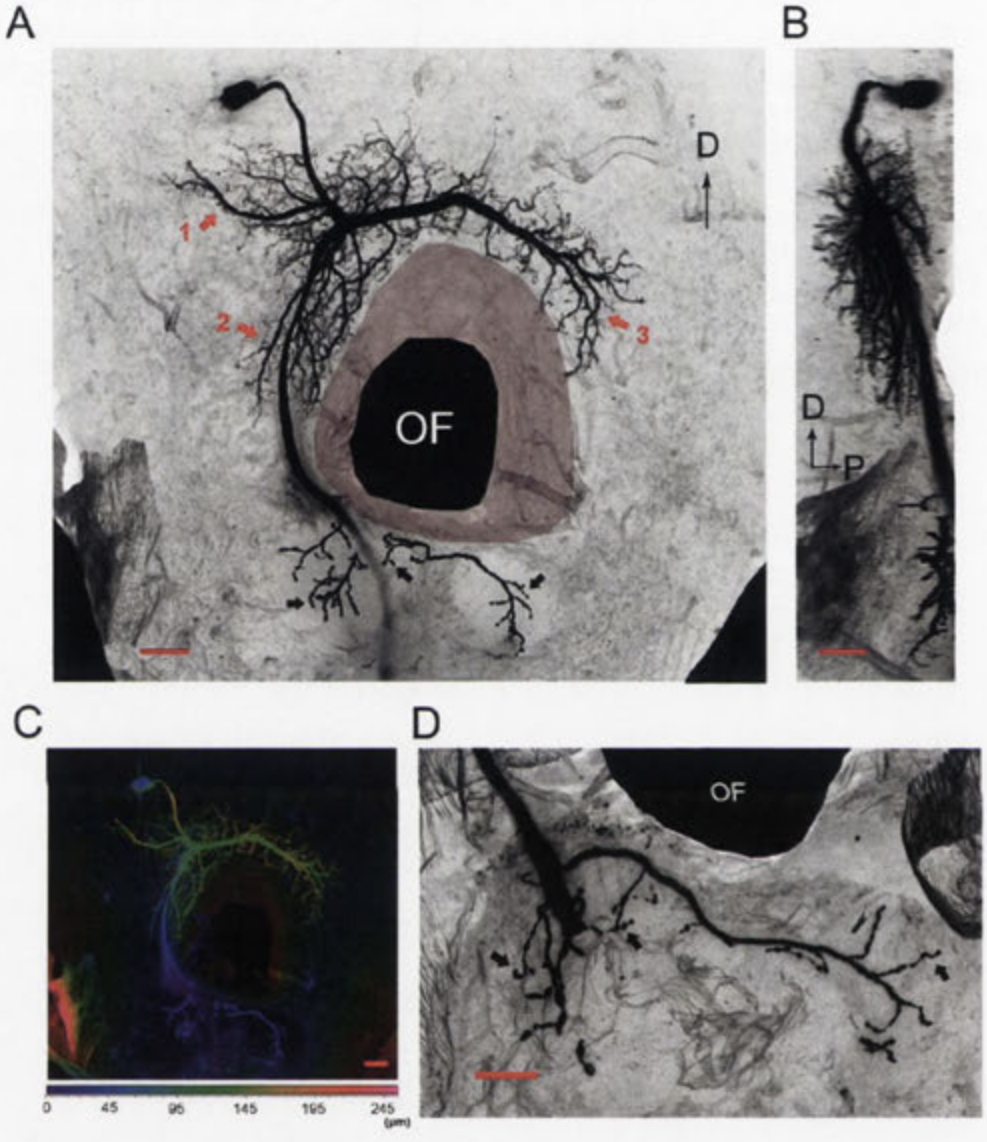
A
B
D
1
2
3
OF
D
P
C
D
0
45
95
145
195
245
(µm)
OF

Figure 3.3: The z-projections of the lucifer yellow stained cell $DNII_2$ within the brain region viewed from the posterior (A, C, D) and lateral (B) aspects. The projections were generated from serially optically sectioned slices (1 μm thick). It was therefore possible to obtain accurate depth information. It is shown that the cell branches extensively on both sides of the brain and suboesophageal ganglion. The main dendritic field is located above the oesophageal foramen (OF) and is 100 μm below the posterior surface of the brain (B). The colour-coded image (C) also shows the depth information of cellular structures in relation to the posterior surface of the suboesophageal ganglion.

In the middle of A is the oesophageal foramen (OF). The anterior circumference of the OF is shown in black, while the extent of the posterior OF is shown as a transparent overlay. Three selected characteristic branches were marked with red arrows in (A) to verify the morphological variability between preparations.

The black arrows marked in (A) and (D) show the knob-like blebs found at the terminal of branches (presynaptic terminals) in the suboesophageal ganglion in two different preparations. Scale bars: all 50 μm.

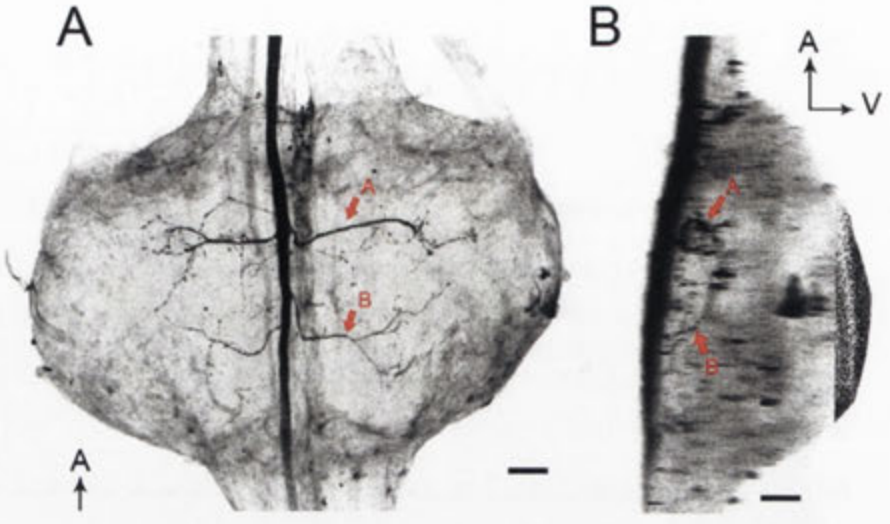

Figure 3.4: The projections of cell $DNII_2$ in the prothoracic ganglion (PTG) viewed from dorsal (A) and lateral (B) aspects. The optical scan did not reach to the most ventral region of the PTG. Therefore, the ventral end of the ganglion was traced by hand and marked as the grainy-black shaded area in (B). It is shown that the axon of $DNII_2$ has two pairs of branches (red arrows, labelled as A and B in both figures) projecting to both sides of the ganglion and the axon collaterals from branch A and B invade similar areas on both sides. It is also shown that the axon and the collaterals are positioned very dorsally in the prothoracic ganglion (B). Scale bar: all 50 μm.

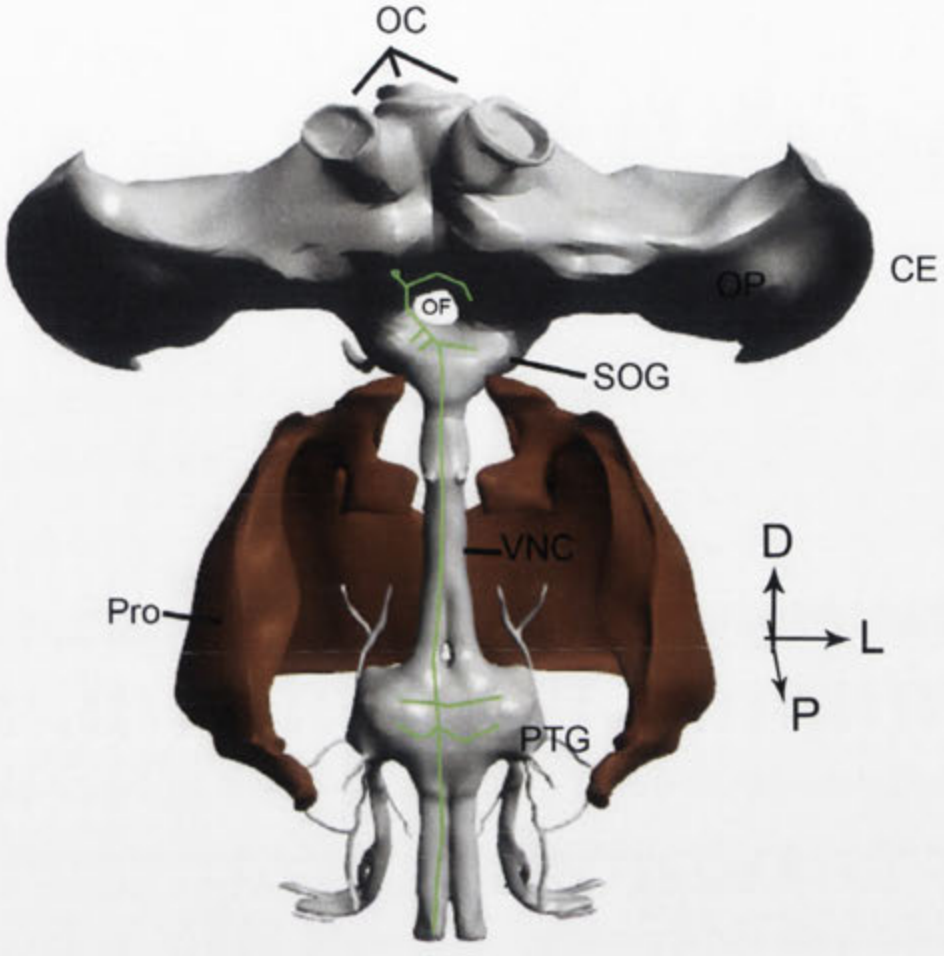

Figure 3.5: A 3-D reconstruction of the bee nervous system showing the brain and prothoracic ganglion from the dorsal perspective. The green schematic drawing shows the location of $DNII_2$. The 3-D model of the honeybee nervous system was developed in our laboratory (Berry and Ibbotson 2010).

Abbreviations: CE: compound eye; D: dorsal; OC: ocelli; L: lateral; OF: oesophageal foramen; OP: optic lobe; P posterior; Pro: prospectus; PTG: prothoracic ganglion; SOG: suboesophageal ganglion; V: ventral; VNC: ventral nerve cord.

To reveal the spatial relations between $DNII_2$ and the neck motor neurons, one experiment was successfully conducted in which a recording from $DNII_2$ was followed by a recording and fill of a neck motor neuron from the first cervical nerve (IK1) in the same preparation. The two cells were recorded and filled separately in the same bee. The cell from IK1 was identified as M1, which is one of the eight neurons in that nerve (see Chapter 6, Hung et al. 2011 and Schröter et al. 2007). Fig 3.6A shows the relative positions of $DNII_2$ and M1 in the brain and the suboesophageal ganglion. The axon of $DNII_2$ arborizes on both sides of the midline in the suboesophageal ganglion. In Fig 3.6B, the axon collaterals of $DNII_2$ were traced manually and outlined in red. It is shown that the M1 has its cell body in the ventral cell body group of the labial neuromere of the SOG close to the midline. The primary neurite of M1 travels posteriorly along the midline and arborizes in the dorsal suboesophageal ganglion. Figure 3.6C shows the neurites from the two different cells with the colour indicating the depths of the structures. It is shown that the axon branches of $DNII_2$ on the ipsilateral side run in close association with the dendrites of M1, the neurites from the two cells meet at 115-125 μm from the posterior surface of the suboesophageal ganglion.

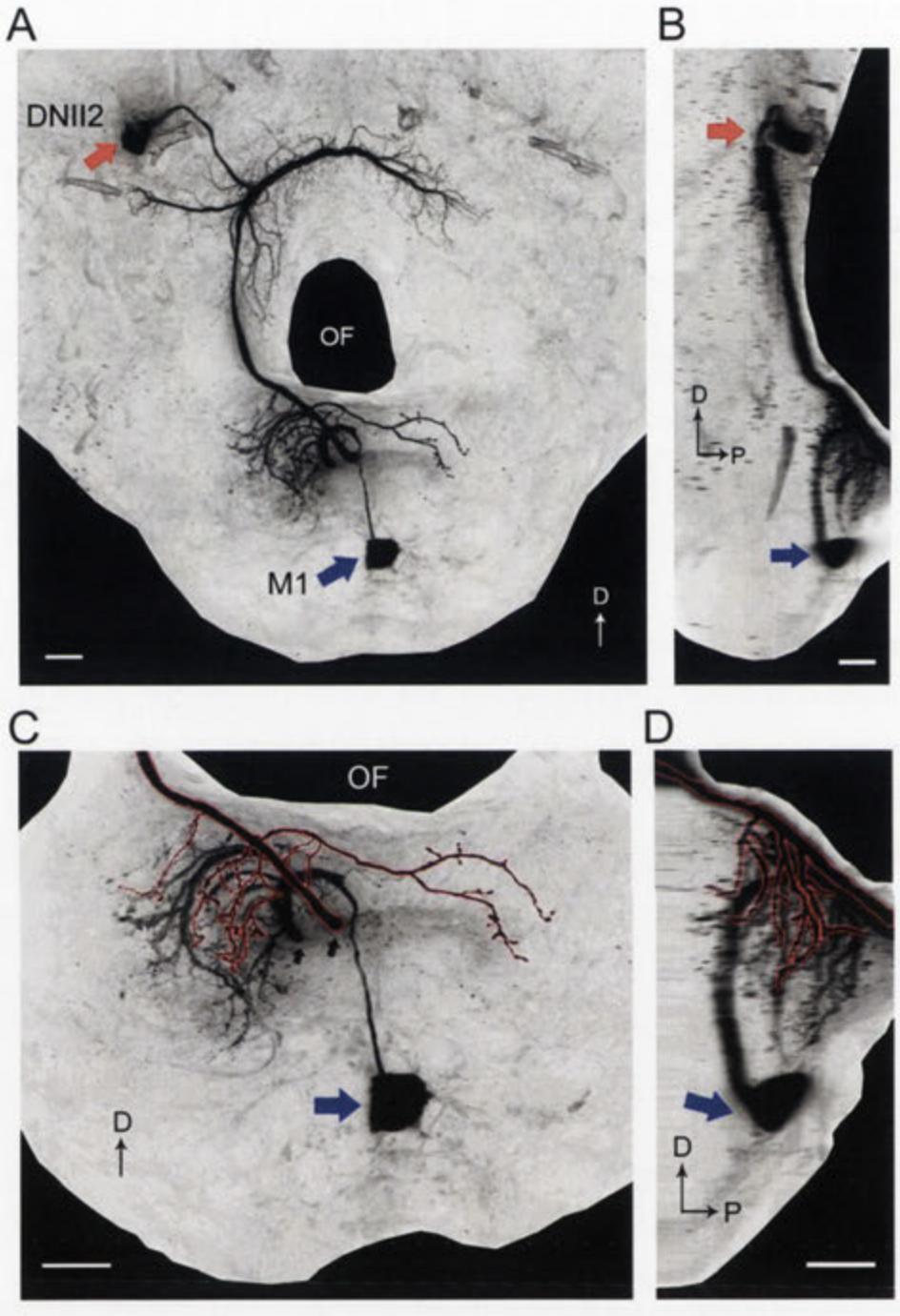
A
DNII2
OF
M1
D
B
D
P
C
OF
D
D
D
P

Figure 3.6: The spatial relations between motion-sensitive descending neuron $DNII_2$ and a neck motor neuron M_1 (from the first cervical nerve IK_1). The projections of the brain (A) (B) and the suboesophageal ganglion (C) (D) are viewed from both the posterior (A and C) and lateral (B and D) aspects. The dashed line in (A) indicates the edge of the posterior surface of the brain. It is shown that while the soma of $DNII_2$ originated from the posterior protocerebrum, the soma of M_1 originated from the ventral suboesophageal ganglion close to the mid-line of the ganglion (the soma of each cell was labelled and marked with black arrows in ABCD). As the axon of $DNII_2$ descends down to the suboesophageal ganglion, the axon collaterals have an overlap with the dendrites of the motor neuron M_1 on the ipsilateral side. (C) and (D) show a magnified section of the suboesophageal ganglion. The axon collaterals from $DNII_2$ were manually traced and marked with red outlines in both figures. From the posterior (C) and lateral (D) views of the suboesophageal ganglion, it is shown that the spatial distribution of the two cells in the suboesophageal ganglion is very close, suggesting a possible route for signal transmission between $DNII_2$ and M_1. Scale bars: 50 μm

3.4.2 $DNIV_2$ and $DNIV_3$

Both $DNIV_2$ and $DNIV_3$ have each been identified in 5 preparations as single fills. $DNIV_2$ and $DNIV_3$ are grouped in the same DNIV group based on their general cell morphologies. Figure 3.7 ($DNIV_2$) and Figure 3.8 ($DNIV_3$) show the cell morphologies. Two characteristic branches from each cell type were carefully marked (see arrows marked in Fig 3.7A and Fig 3.8A). For both types, the first branch (1) is a large branch that comes out from the major joint, projecting ventrally toward the ipsilateral dorsal lobe. In $DNIV_2$, branch 2 also emanates from the major joint, and projects laterally toward the soma. Branch 2 in $DNIV_3$ is a rather smaller dendritic arborisation projecting dorsally toward the ocellar tract. Branch 1 was found in all the preparations for both $DNIV_2$ and $DNIV_3$. The branch lengths for both types were similar with a length of 140 ± 28 μm and 148 ± 36 μm, respectively. The length of branch 2 in $DNIV_2$ was 56 ± 9 μm. Branch 2 in $DNIV_3$ was also found in all preparations, with a length of 115 ± 41 μm. Although the measurements of branch length varied due to the quality of the staining, the selected branches were identified throughout all the preparations, which showed that the within-type morphology is similar from preparation to preparation.

$DNIV_2$ and $DNIV_3$ have similar anatomical characteristics within the brain region; they have cell bodies in the lateral posterior protocerebrum and have major dendritic fields in the median posterior protocerebrum. The dendrites are restricted to the ipsilateral side of the brain. Although there are similarities in morphology, each cell has certain unique characteristics that make it easy to distinguish based on the brain anatomy alone. The most important feature is that $DNIV_2$ sends a large branch antero-ventrally towards the dorsal lobe, whereas $DNIV_3$ has its arborizations confined exclusively to the medial posterior protocerebrum. The $DNIV_2$ cell sends branches down towards the dorsal lobe, while $DNIV_3$ sends several dendrites up towards the protocerebral bridge. In the two preparations shown in the figures, both $DNIV_2$ and $DNIV_3$ have their cell bodies located

20 μm beneath the posterior surface of the brain. However, the main dendritic branch of $DNIV_2$ lies more dorsal than $DNIV_3$; the distances between the posterior surface of the brain and the main branches are 20 and 50 μm, respectively. By measuring the size of the dendritic fields in the brain region, it was determined that the conjugate diameter of $DNIV_3$ was 177 μm, and it therefore has a larger dendritic field than $DNIV_2$ (with a conjugate diameter of 157 μm).

Figure 3.9A shows $DNIV_3$ in the prothoracic ganglion. As the axon travels on the ipsilateral side to the prothoracic ganglion, it sends out three branches to the ipsilateral side of the ganglion. The first and the second branches project horizontally toward the side with a maximum length of 198 and 90 μm, respectively. The third branch projects downward and has a maximum length of 98 μm. All three branches from the axon are positioned on the dorsal side of the prothoracic ganglion. Bleb-like structures were found on the terminals of the branches. The location of the $DNIV_2$ and $DNIV_3$ neuron are shown to scale in the 3-D reconstruction of the brain and prothoracic ganglion (Fig 3.10). The 3-D model of the honeybee nervous system was developed in our laboratory (Berry and Ibbotson 2010).

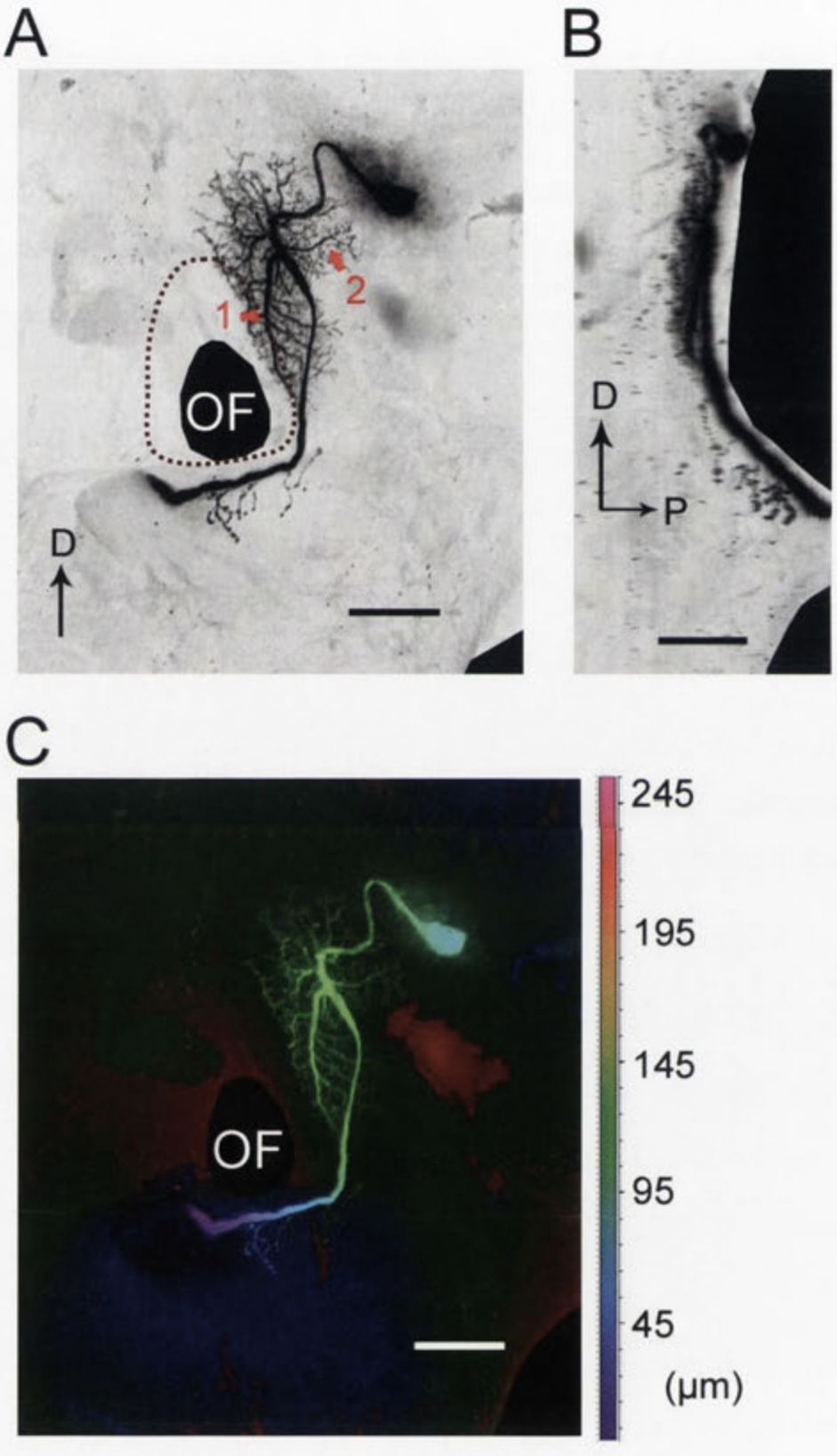
A
B
C
1
2
OF
D
D
P
OF
245
195
145
95
45
(μm)

Figure 3.7: The 2-D projection of a lucifer yellow stained neuron DNIV2 in the brain region from both posterior (A and C) and lateral (B) aspects. Dashed circle in (A) indicates the posterior surface of the brain. It is shown that the positions of the cell body and dendritic field of $DNIV_2$ are restricted to the ipsilateral side of the brain (A), and both of them are positioned at the posterior rim of the brain (B). By colouring the cellular structure with different colours to show the depth information in relation to the posterior surface of suboesophageal ganglion (C), it is also shown that all dendritic arborisation are in the same plane in the brain. Scale bars: 100 μm.

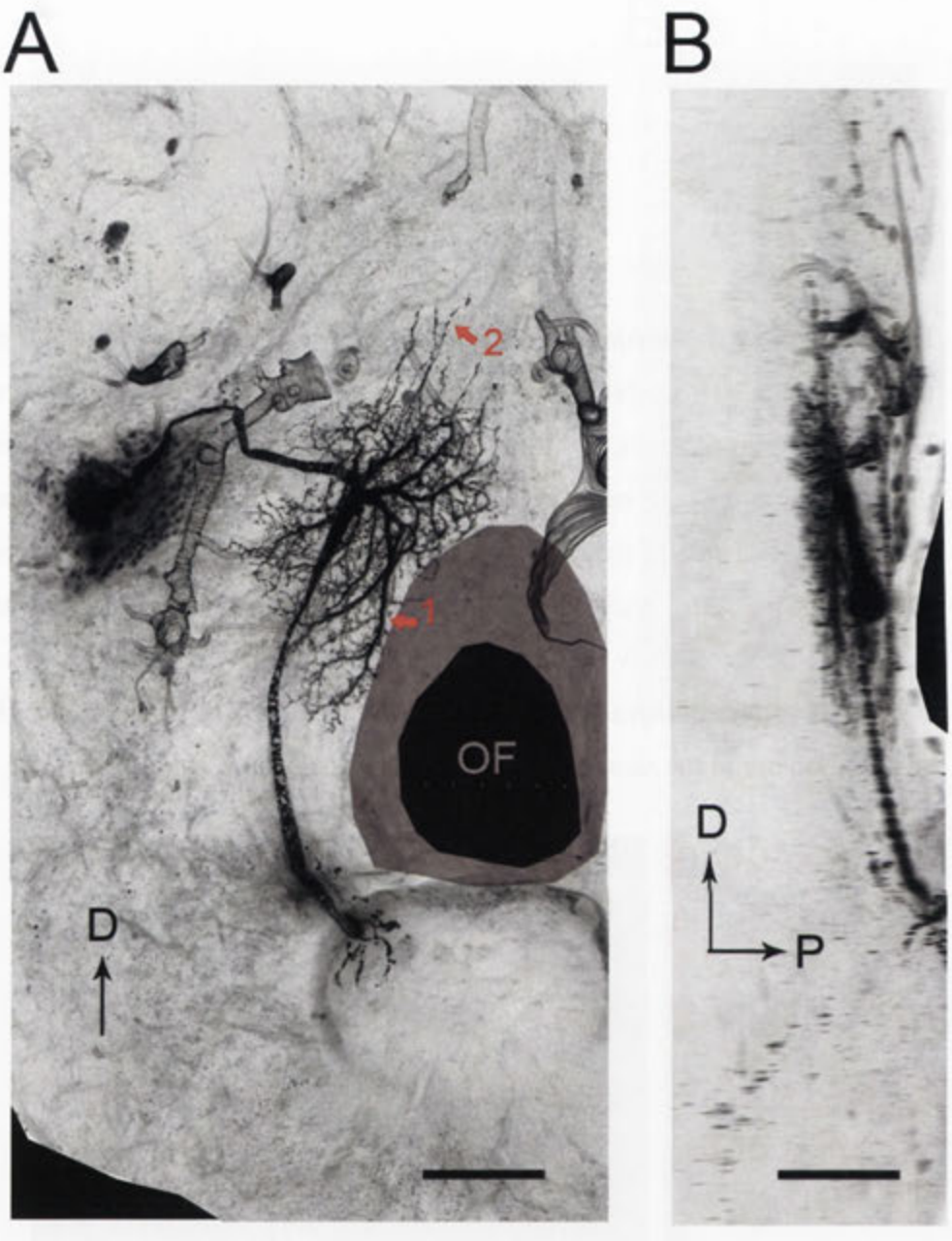
A
B
2
1
OF
D
D
P

Figure 3.8: The z-projection of cell $DNIV_3$ within the brain region from the posterior (A) and lateral (B) view. The edge of the shadow area in (A) indicates the posterior surface of the brain. It is shown that the cell arborizations are confined to the ipsilateral half of the brain. Fine branches (red arrow, 2) were observed extending dorsally to the base of the ocellar tract. Two characteristic dendritic branches were marked with red arrows to identify the variability of the morphology between preparations. Scale bars: 100 μm.

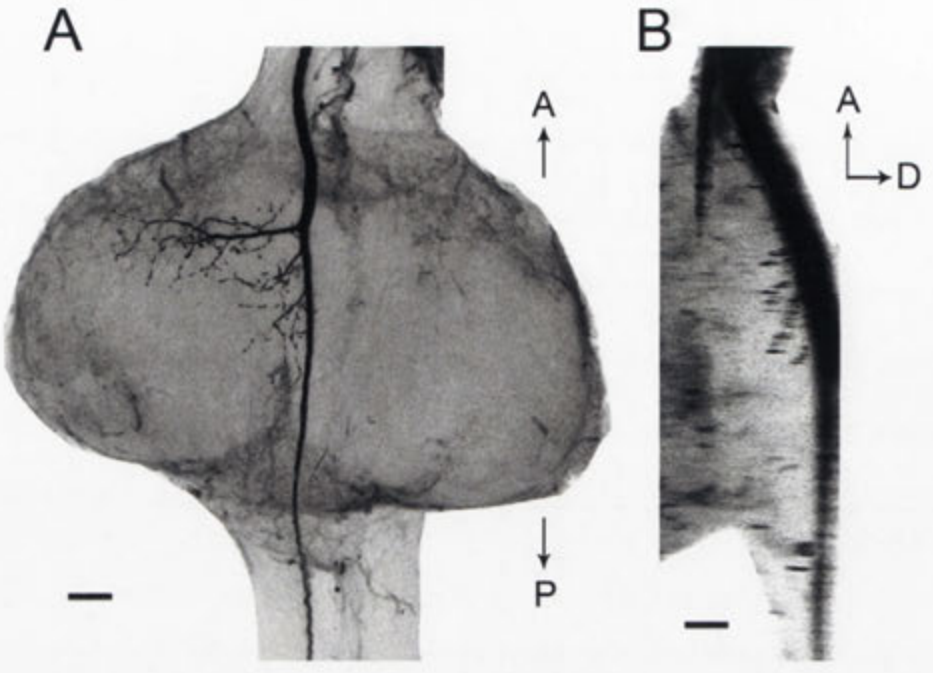

Figure 3.9: The 2-D projection of $DNIV_3$ in the prothoracic ganglion. The dorsal view (A) of the ganglion shows that all the axon collaterals branching out from the major trunk are restricted to the ipsilateral half of the ganglion. These three branches were consistent between preparations. The lateral view (B) of the ganglion shows that the axon trunk and the collaterals are positioned dorsally in the median dorsal tract. Scale bar: all 50 µm.

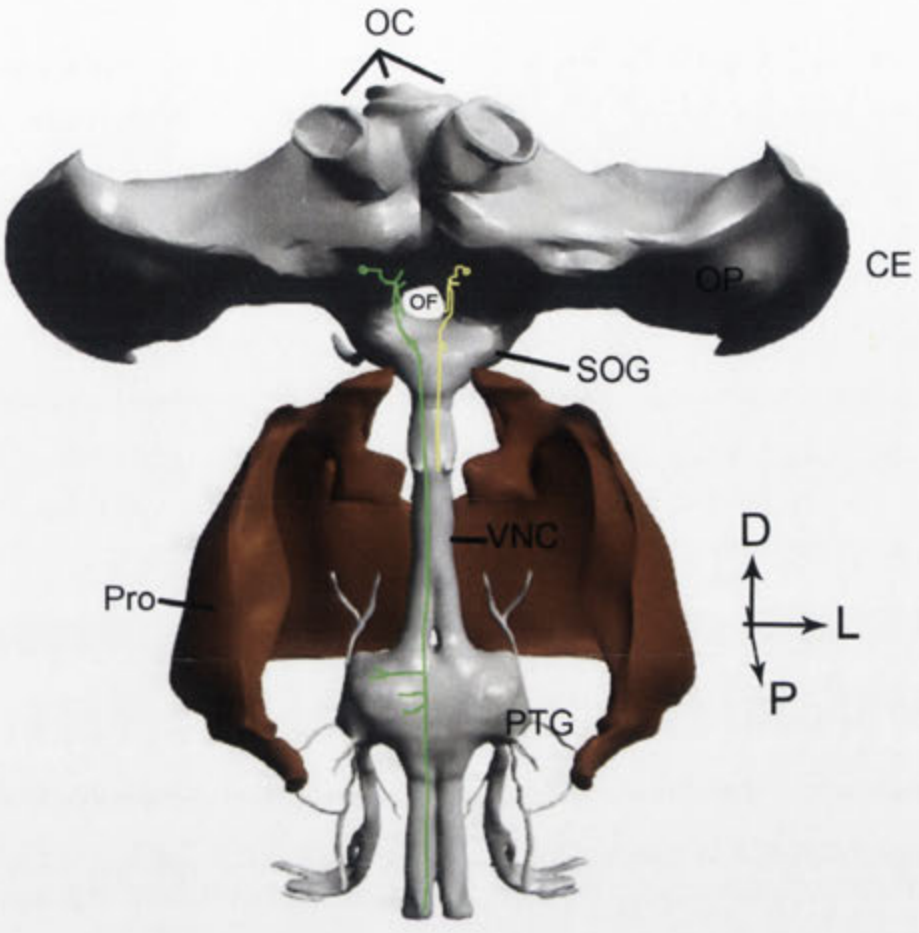

Figure 3.10: A 3-D reconstruction of the bee nervous system showing the brain and prothoracic ganglion from the dorsal perspective. The green and yellow schematic drawing shows the location of $DNIV_3$ and $DNIV_2$ respectively. The gross morphology $DNIV_3$ was shown in both the brain and ptothoracic ganglion, while the $DNIV_2$ was only shown in the brain region. The 3-D model of the honeybee nervous system was developed in our laboratory (Berry and Ibbotson 2010).

Abbreviations: CE: compound eye; D: dorsal; OC: ocelli; L: lateral; OF: oesophageal foramen; OP: optic lobe; P posterior; Pro: prospectus; PTG: prothoracic ganglion; SOG: suboesophageal ganglion; V: ventral; VNC: ventral nerve cord.

3.4.3 $DNVII_1$

$DNVII_1$ was identified as a single fill on two occasions. Figure 3.9 shows a reconstruction of a $DNVII_1$ cell. It is shown that the cell body lies in the anterior protocerebrum on the edge of the oesophageal foramen. The depth information of the cell structure relative to the brain area is shown in Fig 3.9B. This figure shows that the distance from the posterior surface of the brain to the cell body is about 400 μm. The dendritic field of the cell lies in the dorsal lobe area close to the oesophageal foramen (posterior protocerebrum) and is restricted to the ipsilateral side of the brain. The dendritic territory is restricted to a region approximately 100 μm below the posterior surface of the brain.

3.4.4 $DNVII_2$

In this study I identified a second neuron that had characteristics that made it logical for it to be placed into the DNVII class. While it was similar to $DNVII_1$, it had features that clearly distinguished it from $DNVII_1$. The main distinguishing feature is that it has a differently shaped dendritic arbor, as is clearly evident when comparing $DNVII_1$ with the new neuron (compare Fig 3.10A and 3.10B). Therefore, the cell has been classified as $DNVII_2$. As it has not been previously described, it is important to note its general physiology. As with the other descending neurons shown here it was direction-selective when gratings were moved through its visual field. Unfortunately, only preliminary tests were possible before the recording began to deteriorate and it was filled. From these preliminary physiological tests, it was shown that the $DNVII_2$ cell was sensitive to progressive motion (e.g. gratings moving from the contralateral side to the ipsilateral side of the animal in the frontal horizontal plane). It did not respond to motion in the opposite direction (regressive) and upwards and downwards motion produced relatively small responses. These characteristics are similar to those reported for $DNVII_1$ (Ibbotson 1991a). Figure 3.10B and Figure 3.11A

show the 3-D reconstruction of the filled $DNVII_2$. Like $DNVII_1$, the cell body of $DNVII_2$ is located on the edge of the oesophageal foramen in the anterior protocerebrum and is approximately 450 μm away from the posterior surface of the brain (Fig 3.11A). Figure 3.11B-F show the neural reconstructions at different depths of the brain (each plane is indicated using dashed lines in Fig 3.11A). The dendritic field is restricted to the ipsilateral side of the brain, 60 μm beneath the posterior brain surface; it projects dorsally along the oesophageal foramen, reaching the median posterior protocerebrum. As the axon travels downwards it curves into the dorsal lobe and is approximately 50 μm more anterior than the branching point from the dendrites. The axon then projects into the SOG and branches extensively in the ipsilateral posterior-dorsal region. The axon collaterals are distributed around 40 μm beneath the surface of SOG, and bleb-like structures are found on the terminals of the branches.

A side-by-side view of the prothoracic projection of $DNVII_1$ and $DNVII_2$ is shown in Figure 3.12; the drawing of prothoracic ganglion of the $DNVII_1$ (Fig 3.12A) was adopted from Ibbotson (1991a). As the $DNVII_2$ axon travels on the ipsilateral side to the prothoracic ganglion, it sends out branches to both the ipsilateral (2 main branches) and contralateral (4 main branches) sides of the neuropile asymmetrically. The first branch on the contralateral side is 174 μm long, projecting across the midline of the ganglion while the other three branches are roughly the same length (74 μm). The two branches on the ipsilateral side are shorter than those on the contralateral side, with lengths of 95 and 66 μm respectively. Comparing the prothoracic projection from $DNVII_1$ and $DNVII_2$, it is shown that while the axon collaterals of $DNVII_1$ are confined to the ipsilateral side of the ganglion, the axon collaterals of $DNVII_2$ invade both sides of the ganglion asymmetrically. For comparison, schematic drawings $DNVII_1$ and $DNVII_2$ neurons are scaled in the 3-D reconstruction of the brain and prothoracic ganglion (Fig 3.15). The 3-D model of the honeybee nervous system was developed in our laboratory (Berry and Ibbotson 2010).

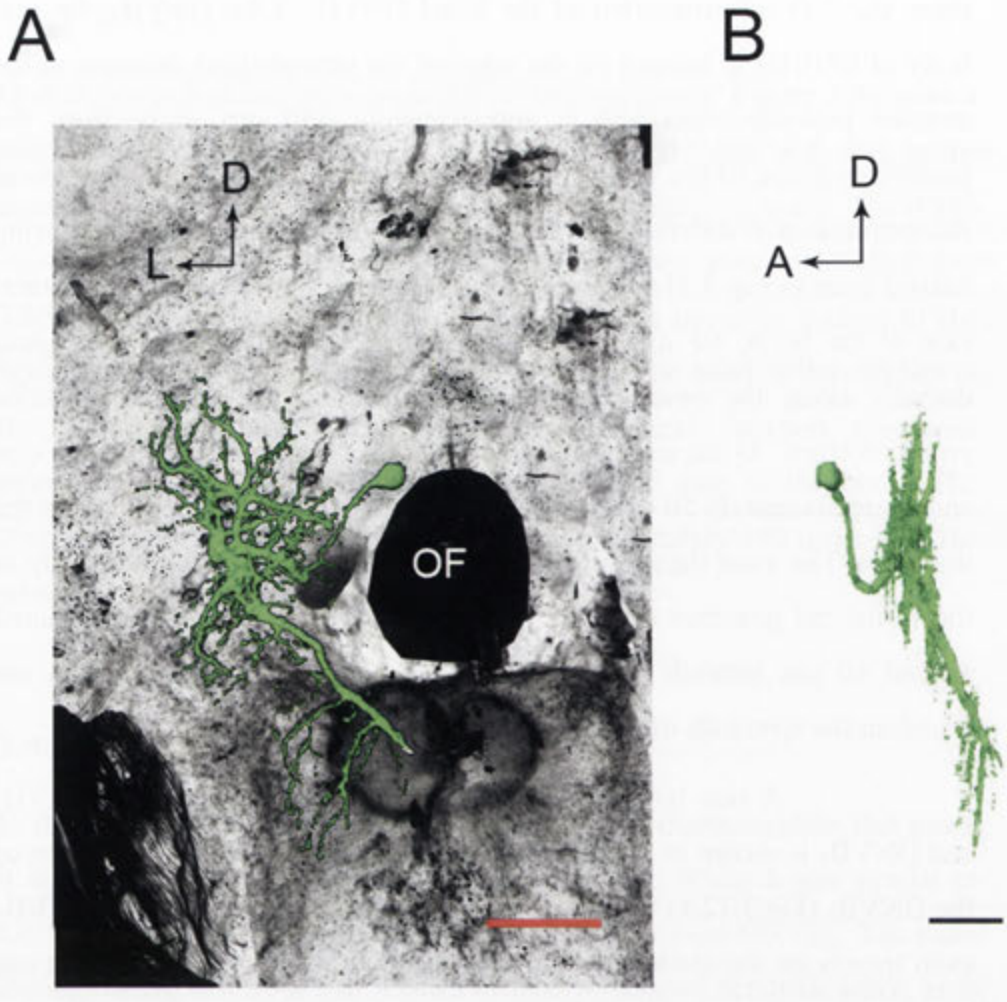

Figure 3.11: The 3-D reconstruction of $DNVII_1$ in the brain region. A: The 3D-reconstruction of a $DNVII_1$ neuron was superimposed on a section of a honeybee brain. B: A lateral view of the reconstructed $DNVII_1$ neuron. Scale bars: A: 100 µm; B: 200 µm.

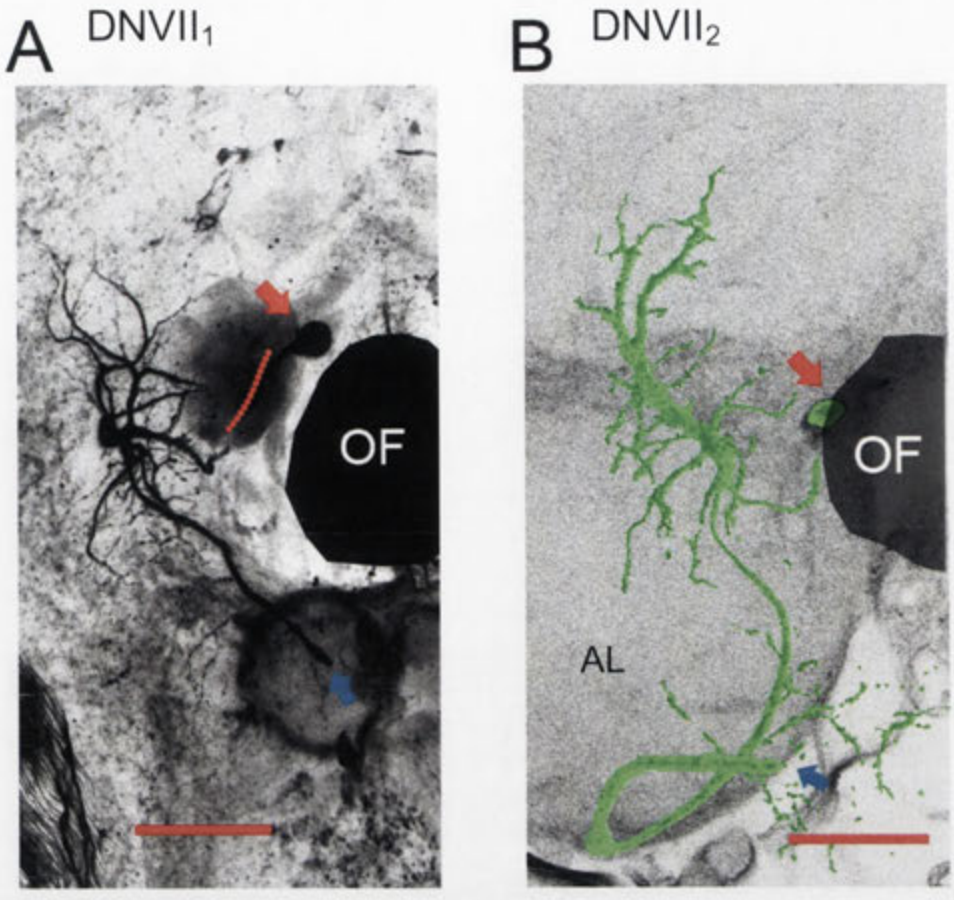

Figure 3.12: The morphology of $DNVII_1$ and $DNVII_2$ from the posterior view. A: the projected 2-D morphology of $DNVII_1$. It is shown that the cell has its cell body (red arrow) very close to the oesophageal foramen (OF) and the dendrites are restricted to the ipsilateral side of the brain. The red dashed line connecting the soma and the major dendritic branch was made by careful observation and tracing throughout the optical sections. B: the 3-D reconstruction of $DNVII_2$ with a red arrow indicating the soma location. It is shown that the soma of $DNVII_2$ is located very anterior on the edge of the ipsilateral antennal lobe (AL). The dendritic field of the cell is also confined to the ipsilateral half of the brain. The blue arrows in both (A) and (B) indicate the axonal output from the brain. Scale bars: 100 μm.

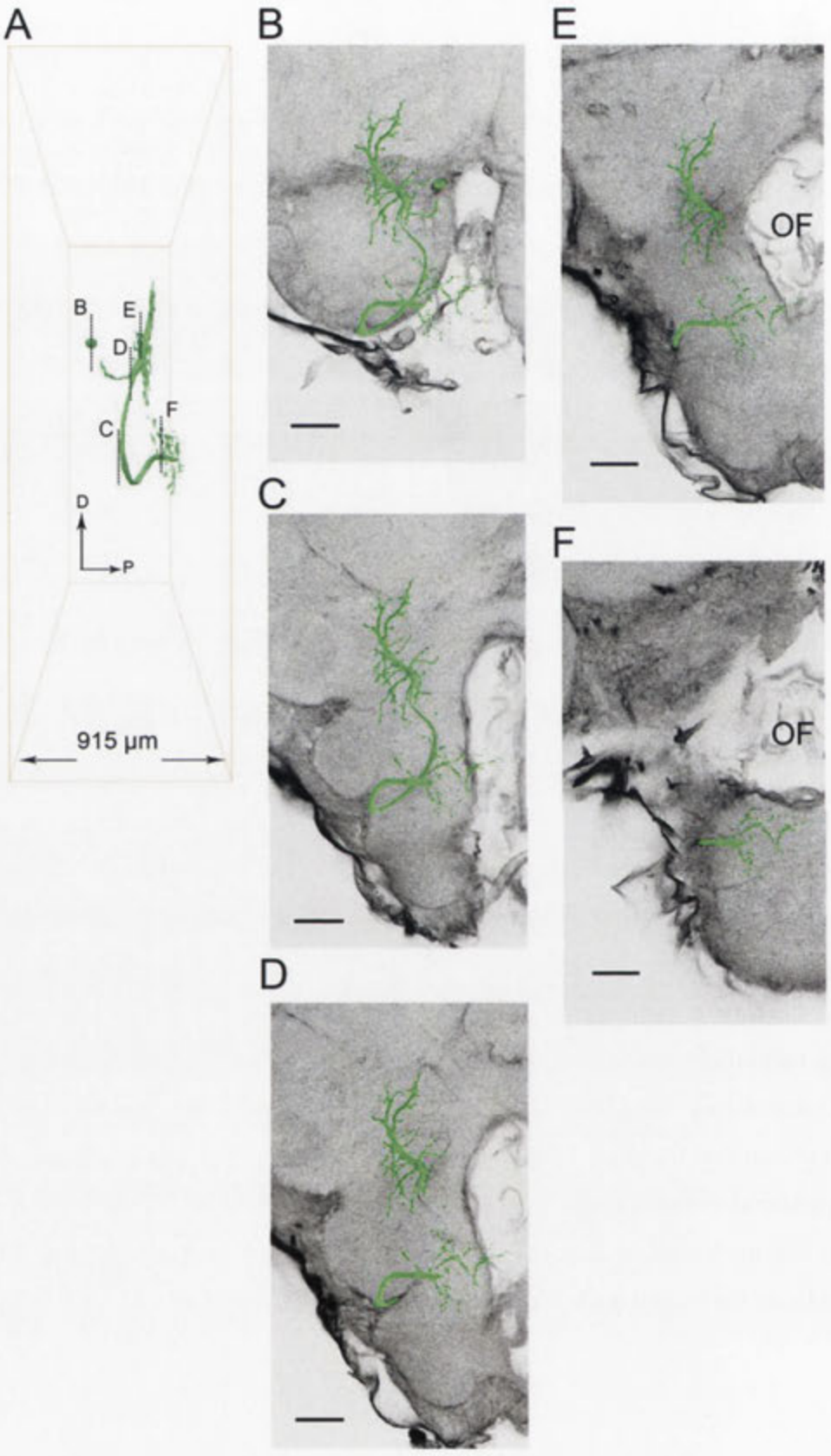
A
B
E
D
C
F
D
P
915 µm
B
E
OF
C
F
OF
D

Figure 3.13: The 3-D reconstruction of $DNVII_2$ in the brain region. A: The lateral view of the reconstructed neuron. The orange bounding box shows the total scanned volume, which measures 915 μm in z-axis. The dashed lines (B-F) on the cellular structure indicate the different depth planes in the brain. The marked planes are shown in figure (B) - (F), respectively. Each of the planes indicates a depth of 453 μm (B), 189 μm (C), 135 μm (D), and 61 μm (E) beneath the posterior surface of the brain. The plane (F) indicates a depth of 41 μm from the surface of the suboesophageal ganglion. Scale bars: 100 μm.

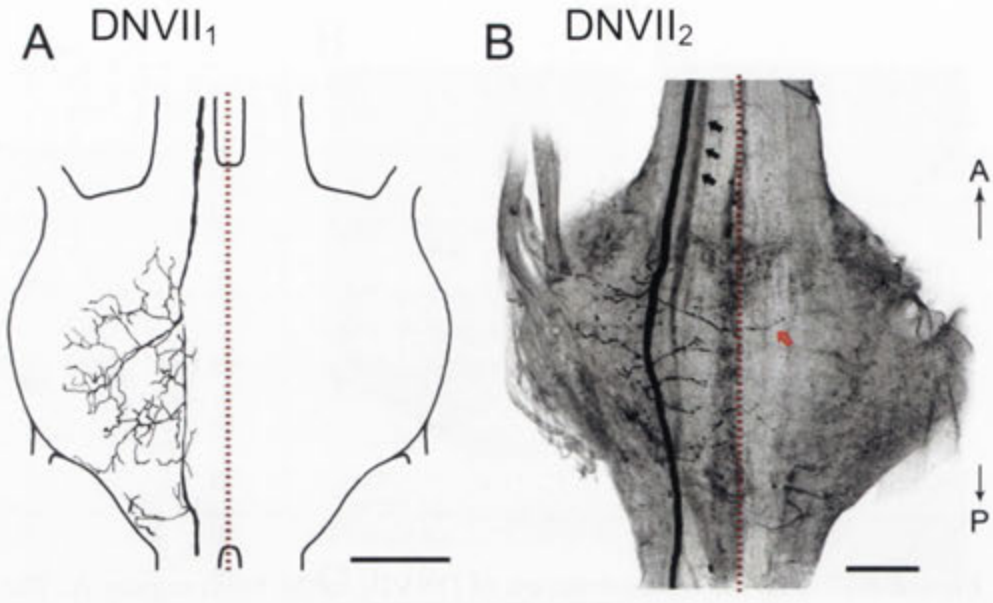

Figure 3.14: The dorsal view of the prothoracic projections of $DNVII_1$ (A) and $DNVII_2$ (B). The drawing of $DNVII_1$ in A is adopted from Ibbotson (1991a) for comparison to the newly identified $DNVII_2$ shown in (B). It is shown that while the axon collaterals of $DNVII_1$ are confined to the ipsilateral side of the ganglion, the axon collaterals of $DNVII_2$ branch on both sides of the axon asymmetrically, with a fine branch (red arrow in B) extending across the midline into the contralateral side of the ganglion. The black arrows in (B) indicate a shadow filled axon from another cell. Scale bars: 100 μm.

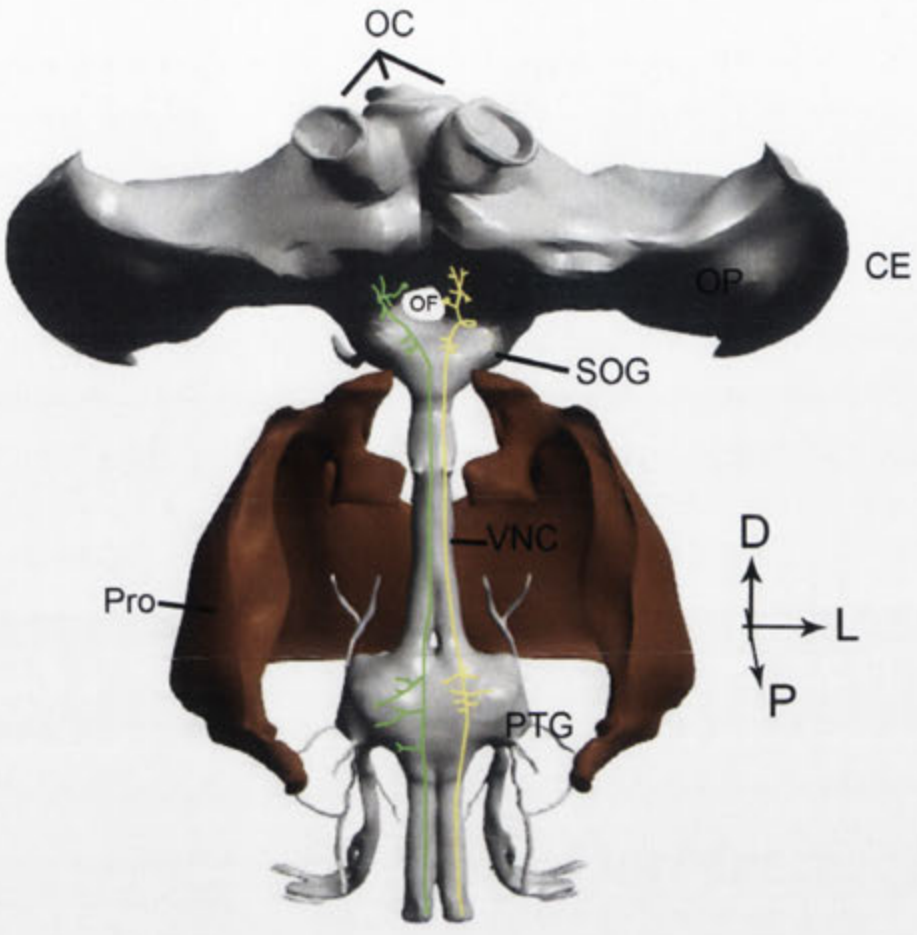

Figure 3.15: A 3-D reconstruction of the bee nervous system showing the brain and prothoracic ganglion from the dorsal perspective. The green and yellow schematic drawing shows the location of $DNVII_1$ and $DNVII_2$ respectivly. The gross morphology both $DNVII_1$ and DNVII2 were shown in the brain and ptothoracic ganglion regions. The 3-D model of the honeybee nervous system was developed in our laboratory (Berry and Ibbotson 2010).

Abbreviations: CE: compound eye; D: dorsal; OC: ocelli; L: lateral; OF: oesophageal foramen; OP: optic lobe; P posterior; Pro: prospectus; PTG: prothoracic ganglion; SOG: suboesophageal ganglion; V: ventral; VNC: ventral nerve cord.

3.4.5 Lateral ocellar descending neuron ($Locth_3$)

The honeybee possesses 5 pairs of distinct ocellar descending neurons, which receive direct inputs from the ocellar retina and descend directly to the thoracic ganglia (Pan and Goodman 1977; Milde and Homberg 1984). These neurons were given the classification L or M, meaning lateral or median ocellus. The letter combination 'oc' was the code given to indicate 'ocellus' and 'th' was used to denote that the neurons descend into the 'thorax'. At least two of these neuron types, Locth1 and Locth2, were found to be multisensory, responding to both ocellar and compound eye input, and a variety of mechanosensory stimulation (Milde 1984; Goodman et al. 1987). The morphology and physiology of these neurons were shown to be similar in honeybees and wasps (Goodman et al. 1987). In addition to responding to brightness changes, some were reported to be direction-selective during combined compound eye and ocellar stimulation with moving gratings (Goodman et al. 1987; Goodman et al. 1990). In all cases they responded to upward motion in the frontal visual field.

In the present study, the $Locth_3$ neuron was identified as a single neuron in three preparations. On all occasions enough dye was injected to clearly identify the unique shape of this neuron (Fig 3.13A). However, as is common with such dye filling it was not of sufficient quality to allow a detailed 3-D reconstruction. For comparison between my neurons and previous work, Figure 3.13B shows a drawing of a cobalt-filled ocellar Locth3 neuron (adapted from Goodman et al. 1990). It is clear that, despite the poor fills that I obtained, they were without doubt Locth3. The Locth3, as a second order neuron, receives input from the retina of the of lateral ocellar plexus on the contralateral side of the body (relative to the axon). Figure 3.13AB shows the dendritic field of Locth3 is restricted to a certain region of the retinal plexus. From the semi-section and the 3-D reconstruction of the lateral ocelli presented in chapter 2, it is apparent that $Locth_3$ receives input from the ventral retina of the lateral ocellus. The cell body of $Locth_3$ lies 38.4 μm beneath the posterior surface of the brain. As

the major branches travel down to the mid brain, the depth of the major branch changes from 79.4 to 56.4 μm (in relation to the posterior surface of the brain). The axon travels down to the midbrain where it arborises on both sides of the oesophageal foramen in the median posterior protocerebrum. The branches on both sides are 38.445.1 μm away from the posterior surface of the brain. Through the optical sectioned images, the arborizations on the contralateral side (Fig 3.13A, arrow C) were found to be bleb-like structures, while in the ipsilateral side (Fig 3.13A, arrow D), no bleb-like structures were found. The observations suggest that the arborizations on either side of the oesophageal foramen may serve different purposes: the ones on the contralateral side are dendritic branches which may receive input from the contralateral compound eye, while on the ipsilateral side the arborizations may serve as axonal branches, which send signals out to other interneurons. Figure 3.13B shows that the axon then descends down to the pro- and mesometa-thoracic ganglia, where it sends out axon collaterals only into the ipsilateral side of each ganglia.

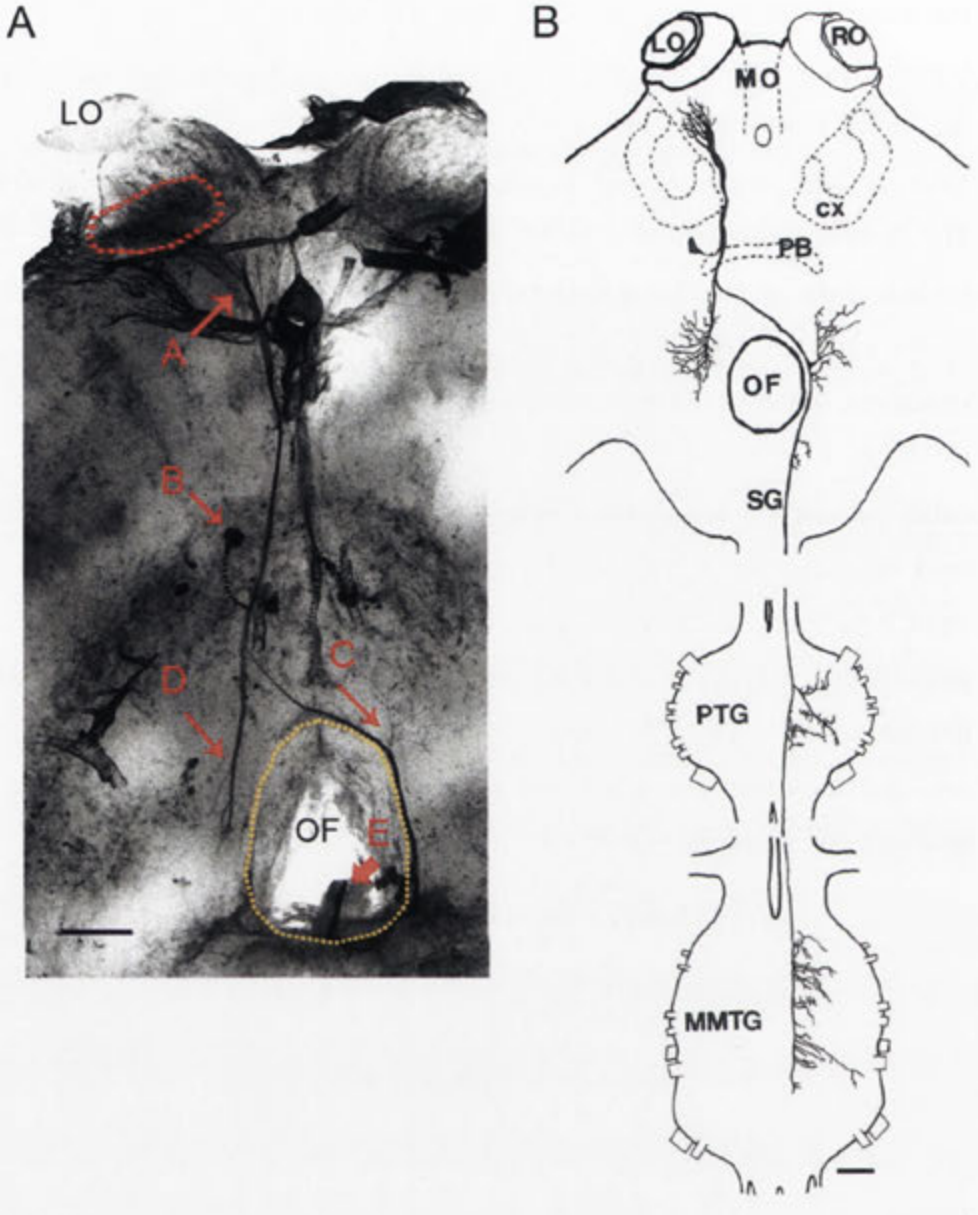
A
LO
A
B
C
D
OF
E
B
LO
RO
MO
CX
PB
OF
SG
PTG
MMTG

Figure 3.16: Morphology of the ocellar neuron $Locth_3$. A: z-projection of an optically sectioned neuron $Locth_3$. The red dashed circle shows the dendritic field of $Locth_3$, and the red arrow (A) below indicates the major dendritic branch. The cell body (arrow B) of the neuron is located on the contralateral side of the brain (relative to the axon shown by the arrow marked E). The yellow dashed circle indicates the surface of the brain, which shows that the axon travels on the edges of the oesophageal foramen (OF). B: Drawing of a cobalt-filled neuron $Locth_3$ (figure adopted from Goodman et al. 1990). The neuron receives signals directly from the contralateral side of the lateral ocellar retina and sends out branches to both sides of the OF as it travels down to the midbrain (see arrows CD). The main axon branch travels on the ipsilateral side of the suboesophageal ganglion (SOG) and descends directly down to the prothoracic (PTG) and mesometathoracic (MMTG) ganglia. Scale bar: all 100 μm.

3.5 Discussion

In this study, the detailed morphology of 6 neurons, including one lateral ocellar descending neuron were reported ($DNII_2$, $DNIV_2$, $DNIV_3$, $DNVII_1$, $DNVII_2$, and Locth3). It is shown that although $DNII_2$, $DNIV_2$, $DNIV_3$, DNV_1, $DNVII_1$ and $DNVII_2$ have their cell bodies in the protocerebrum, the cell bodies of $DNII_2$, $DNIV_2$ and $DNIV_3$ lie in the lateral posterior cell body rind, while the cell bodies of $DNVII_1$ and $DNVII_2$ lie anteriorly in the median protocerebrum. The ocellar descending neuron $Locth_3$ has the cell body positioned on the contralateral side of the median posterior protocerebrum and was found innervating the ventral retina of the lateral ocellus.

3.5.1 Variability

One of the advantages of studying insect nervous system is the ability to repeatedly identify individual neurons from different animals based on the distinct anatomical and functional (physiological) features (Hoyle 1977). The number of neurons stained in this study permits some comment on the amount of variability in the morphology of honeybee descending neurons ($DNII_2$, $DNIV_2$, and $DNIV_3$). As described in the Results section, careful observations and analyses were performed on selected dendritic branches to reveal the variability between different preparations. These results can be compared with previous reports on the cell morphology, where the same selected branches can also be identified (Goodman et al. 1987; Ibbotson 1991b). Although neurons of the same type that stained in different preparations have some small variations in the fine branching pattern of both the dendrites and the axon arborizations, the patterns of the dendritic field and major branching structures are consistent throughout the samples observed. The location of the cell body and the course of the axon descending through the brain remain very similar. As I show in later

chapters, the anatomical reliability is carried over to the physiology, which also shows little variation between preparations.

3.5.2 Neuroanatomy as a predictor of function

Previous studies of descending neurons showed that the cells have strong responses to visual stimulation of the compound eyes (e.g. Ibbotson and Goodman 1990; Ibbotson 1991ab). As will be shown in later chapters, this has now been extended to show that the directional properties persist at both short (UV/Blue) and long (Green) wavelengths of light. The direction tuning characteristics of the cells are similar to those described for lobula units in bees (Kaiser and Bishop 1970; DeVoe et al. 1982; Hertel and Maronde 1987; Ibbotson and Goodman 1990). This suggests that the visual motion information carried from the lobula is transferred to the descending neurons. Several studies on the properties of descending neurons in the dragonfly and locust suggest that the descending neurons involved in course control receive signal inputs from more than one sensory system (Olberg 1981b; Rowell and Reichert 1986; Wertz et al. 2008). It was shown that the descending neurons of the dragonfly and locust integrate inputs from the compound eyes, ocelli and wind-sensitive hairs to provide an optimal response signal to the relevant motor units. In this study, the detailed anatomy of the honeybee descending neurons makes it possible to suggest functions for the neurons by observing the dendritic and axon arborization distributions, which may provide information for experimental designs for physiological studies.

Previous studies using silver-intensified cobalt-filled neurons show impregnation of the very finest of dendritic twigs. It is believed that it is possible to identify the synaptic specialisations according to the structure of the neural terminals, such as fine branches (spines) and blebs. It has been suggested that spines represent the postsynaptic while the blebs are presynaptic terminals (Strausfeld 1971; Guy et al. 1979; Hausen et al. 1980).

In this study, by using the fluorescent dye lucifer yellow, similar structures were observed in the associative areas, such as the very fine branches in the brain, and 'bleb'-like axon arborisation terminals in the suboesophageal and thoracic ganglia, suggesting that previous observations on synaptic properties can be applied in this study. Therefore, by observing the spatial geometry of the cell dendritic fields and the axon collateral terminals (blebs), it is possible to make predictions about the inputs to the neurons from various sensory structures, and the neural signal outputs.

DNII$_2$

$DNII_2$, in contrast to $DNIV_2$ and $DNIV_3$, branches extensively in both halves of the brain, suboesophageal and prothoracic ganglia. The trunk of its dendritic tree lies on the median posterior protocerebrum arching with extensive arborizations above the oesophageal foramen, and extends toward the edge of the lobula on the ipsilateral side. The median posterior protocerebrum contains neurons projecting from the antennal lobes (Suzuki 1975), the medulla, lobula (Hertel and Maronde 1987ab) and ocellar interneurons (Pan and Goodman 1977; Milde 1987). The multisensory inputs in the brain area suggest that $DNII_2$ may receive information from both the olfactory system and the two visual systems. Electrophysiological evidence of the motion detecting abilities of $DNII_2$ showed that the cell is direction-selective with the preferred direction being upward image motion (see Chapter 4). It was also shown that the cell had its maximum response when the frontal regions of both compound eyes were stimulated (Ibbotson and Goodman 1990). The physiological results suggest that the cell receives inputs from both compound eyes and may be responsible for detecting image motion during pitching movements of the head and body (i.e. downward pitch). Lobula fibres carry the motion information from both compound eyes and project to the median posterior protocerebrum. The dendrites of $DNII_2$ are located exactly in this part of the brain suggesting that the cell integrates the visual signals and transfers the signals to neck and thoracic motor neurons.

The neck motor neurons, such as M1, have dendrites in the regions of the suboesophageal ganglion that are invaded by the terminals of the $DNII_2$ neuron. Snodgrass (1942) described the honeybee musculature, and later on Markl (1966) described the innervations of the 12 neck muscles. It has been shown that muscles 44 and 51 are innervated by IK1 and different cells in IK1 innervate different subunits of the muscles (Schröter et al., 2007). Muscle 44 is a direct muscle that connects the prothorax to the head capsule. The anatomy of muscle 44 in the bee suggests a role in depressing the head (i.e. downward pitch) and unilateral adduction control (Snodgrass 1942; Schröter et al., 2007; Berry and Ibbotson 2010). As M1 innervates the lateral subunits of muscle 44 (Schröter et al., 2007), the anatomical results shown in Fig 3.6 suggest that the axon terminals of $DNII_2$ meet with the dendrites of M1, providing further evidence that $DNII_2$ may be involved in the control of head pitching movements. It is possible that the motion signals from the paired $DNII_2$ are sent to both the ipsi- and contralateral sides of the suboesophageal ganglion and thoracic ganglia providing the symmetrical signals that would be required to drive corrective wing and body movements to correct against pitching movements of the head and body.

$DNIV_2$ and $DNIV_3$

$DNIV_2$ and $DNIV_3$ have their dendrites restricted to the ipislateral side of the median posterior protocerebrum, suggesting that they primarily receive signals from the ipsilateral side of the sensory system, i.e. the ipsilateral compound eye, lateral ocellus and antenna. However, it has been established that neurons exit the bee lobula and travel to the opposite protocerebral region, thus offering a route for contralateral motion information (Hertel and Maronde 1987a). The axon arborisations in the prothoracic ganglion ($DNIV_3$) are also restricted to the ipsilateral side of the ganglion. Although, these two cells share very similar dendritic field patterns, it is shown that $DNIV_2$ sends a dendritic branch to the ipsilateral dorsal lobe, while some $DNIV_3$ dendrites extend toward the midline of the median protocerebrum.

From previous studies on neural projections, it is known that the dorsal lobe receives projections from the ipsilateral antenna (Suzuki 1975), and also motion-sensitive lobula projection neurons from the ipsi- and contralateral optic lobes (Hertel and Maronde 1987a; Maronde 1988). From this neuroanatomical observation, it is also plausible that both the cells may receive motion signals from not only the ipsilateral eye, but also the contralateral eye. Electrophysiological experiments support this anatomical observation: while both cells are direction-selective to downward moving patterns, $DNIV_2$ and $DNIV_3$ showed the strongest direction-selective excitatory response when laterally positioned gratings moved simultaneously in a downward direction over the ipsilateral eye and in an upward direction over the contralateral eye (Ibbotson and Goodman 1990). So both neuroanatomical and electrophysiological results suggest that these cells may be responsible for detecting image motion that occurs when the animal rolls around its longitudinal body axis.

DNVII$_1$

$DNVII_1$ has a dendritic field restricted to the ipsilateral deutocerebrum (dorsal lobe) suggesting that it may receive signal inputs from both the olfactory (antenna) and the compound eye visual system (both sides of the optic lobes). Electrophysiological experiments show that the cell generates its maximum response when both sides of the compound eyes were stimulated simultaneously with yaw stimulation, i.e. the pattern moved regressively over the ipsilateral eye and progressively over the contralateral eye (Ibbotson 1989; 1991a). From the anatomical and electrophysiological results, it is suggested that $DNVII_1$ receives visual inputs from both the ipsi- and contralateral sides of the compound eyes.

DNVII$_2$

$DNVII_2$ is a new type of motion-sensitive neuron that was described for the first time in this chapter. $DNVII_2$ has a dendritic field that is restricted to the ipsilateral protocerebrum next to the oesophageal foramen. The dendrites

project dorsally toward the median posterior protocerebrum, which contains fibers from the medulla, lobula (Hertal and Matonde 1987ab; Maronde 1988), and ocellar interneurons (Pan and Goodman 1977; Milde 1987). This suggests that the $DNVII_2$ neuron may receive signals from the ipsilateral compound eye, and the ocelli. The bleb-like structures found in the neuronal terminals suggested that the cell may have signal outputs in the SOG and prothoracic regions. In the 9 cell types reported in previous studies (Ibbotson 1989; Ibbotson and Goodman 1990; Ibbotson 1991ab), only 4 types of cell ($DNII_2$, $DNIV_2$ $DNVI_1$, and $DNVIII_1$) were found to have axonal branches that project laterally from both sides of the axon. The neural morphology of $DNVII_2$ in the prothoracic ganglion showed that the axon projects collaterals to both ipsilateral and contralateral sides of the axon.

3.5.3 Ocellar descending neurons

The honeybee processes 5 pairs of ocellar descending neurons: one pair of the median fibres (Mocth), and four pairs of lateral fibers (Locth1-4). They are considered as medium/large-size fibers which run from the ocellar retina through the ocellar nerve tracks to the pro- and mesomemathroacic ganglia (Pan and Goodman 1977; Milde and Homberg 1984). In this study, combining the neural anatomy and the ocellar 3-D reconstruction model presented in Chapter 2, it was shown that the dendritic field of the ocellar descending neuron $Locth_3$ is positioned in the ventral retina of the lateral ocellus, which suggests that Locth3 receives inputs exclusively from the ventral retina. Ribi et al. (2011) showed that the retinas of different regions in the honeybee ocelli form two distinctly separate nerve bundles as they pass to the first synaptic plexus where they make contact with the second-order interneurons. While in this study, I was not able to record and stain other ocellar descending neurons, the morphology of 3 other ocellar neurons were shown in previous studies. Milde and Homberg (1984) described the morphology of the ocellar neurons Locth1 and Locth2. They did careful

drawings of the cells. While at the time there was no knowledge of the ocellar retinas having multiple retinal zones, their drawings clearly reveal that the dendritic fields of these neurons were restricted to the region that is close to the mid-line of the brain (Fig 3.14, neural morphology adopted from Milde and Homberg 1984). This region is now known to be occupied by the dorsal retina, based on the reconstructed model. Heinzeller (1976) reported three types of honeybee second-order ocellar neurons in the brain. One of the cells which he referred to as the type C neuron was then reported and classified as the median ocellar descending neuron Mocth (Pan and Goodman 1977). Figure 3.15 (neural morphology adopted from Heinzeller 1976) shows the morphology of the Mocth neuron and the 3-D reconstruction model of the median ocellus. It is clear that the dendrites of the Mocth neuron originate from the ventral retina of the median ocellus. Ocellar descending neurons that originated from different regions of the retinas suggest that they may serve different roles in detecting different visual cues. As shown in Chapter 2, the dorsal retinas, which view the horizon, have higher spatial resolution; therefore, the 2 lateral ocellar descending neurons $Locth_1$ and $Locth_2$ may be motion sensitive and have properties that make them useful for observing movements of the horizon. The pair of lateral and median descending neurons ($Locth_3$ and Mocth), which have their dendrites in the ventral ocellar retinas may be more sensitive to luminance and light as the ventral retinas view the sky and above. Although no physiological evidence has been done to show the direction selectivity of the $Locth_1$ and $Locth_2$, the flashed responses of the two cells showed that they process an inhibitory response to 300 ms flash (intensity above -1.9 logI), and no OFF response (i.e. a phasic response to light OFF) was observed (Milde and Homberg 1984). The tonic inhibition responses during the light on found in the $Locth_{1-2}$ were also found in Locth $_3$ neuron, however, the $Locth_3$ showed strong OFF response to flashes (see Chapter 4). It is believed that the phasic response is related to enhancing contrast, while the tonic response is responsible for the sustained property stimulus (Hertel and Maronde 1987). The results suggested that the neurons

which originated from the ventral retinas may be more sensitive to light changes. Stange and Howard (1979) showed that by applying dorsal light and as well as motion stimuli on the dragonfly ocelli, it was able to initiate the head movements. It is possible that those ocellar descending neurons, as the pre-motor units, may play an important role in corrective flight responses that orient the animals.

3.6 Conclusions

The honeybee motion-sensitive descending neurons were first reported by Pan and Goodman (1977) and were extensively investigated in the late 1980s and early 1990s (Goodman et al. 1987; Goodman et al. 1990, 1991; Ibbotson and Goodman 1990; Ibbotson 1991ab). The morphological features and cell classifications were established in these studies. However, until now the unique morphology of honeybee descending neurons has not received significant attention. In this study, I used modern fluorescent dye injection and confocal microscopy techniques to provide a 3-dimensional view of the cell geometry and structure, which completes the cellular morphological profile for five of the DNs. The depth information in the brain region for the cell types described ($DNII_2$, $DNIV_2$, $DNIV_3$, and $DNVII_1$) were shown for the first time. The morphology of a newly identified cell type $DNVII_2$, which belongs to the DNVII class, was also described for the first time.

Combining the 3-D reconstruction model of the honeybee ocelli and the morphology of the ocellar descending neurons, it is suggested that the Locth3 receives inputs exclusively from the ventral retina of the lateral ocellus. It has also been inferred from previous studies that Mocth also receives input from the ventral retina of the median ocellus and that $Locth_{1\text{-}2}$ receive input from the dorsal retina of the lateral ocellus.

A

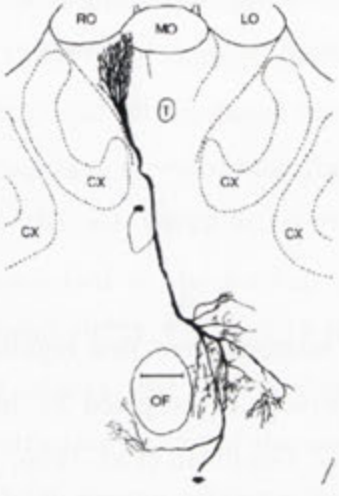

Locth1

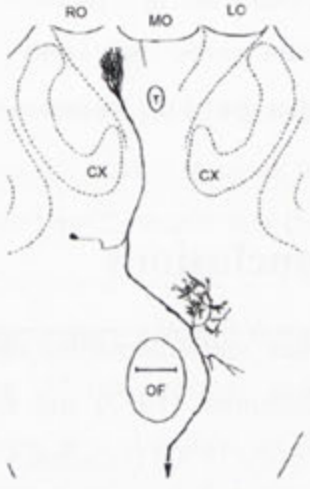

Locth2

B

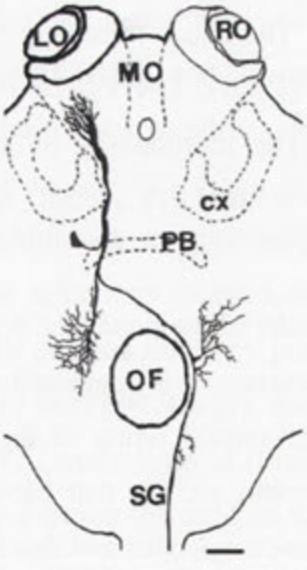

Locth3

Figure 3.17: The morphology of three lateral ocellar descending neurons with the 3-D reconstruction model of the lateral ocellus and the retinas. A: Frontal view of two lateral ocellar descending neurons Locth1 and Locth2 (adopted from Milde and Homberg 1984). It is shown that the two neurons have the dendritic field positioned in the dorsal retina (dr) of the lateral ocellus. B: Posterior view of the lateral ocellar descending neuron Locth3 (adopted from Goodman et al. 1990). It is shown that the neuron has its dendritic field positioned in the ventral retina (vr) of the lateral ocellus. ***Abbreviations***: cx, calyx; dr, dorsal retina; l, lens; LO, left lateral ocellus, MO, median ocellus; OF, oesophageal foramen; PB, protocerebral bridge; RO, right lateral ocellus; SG, suboesophageal ganglion; T, central trachea; vr, ventral retina. Scale bars: all 100 μm.

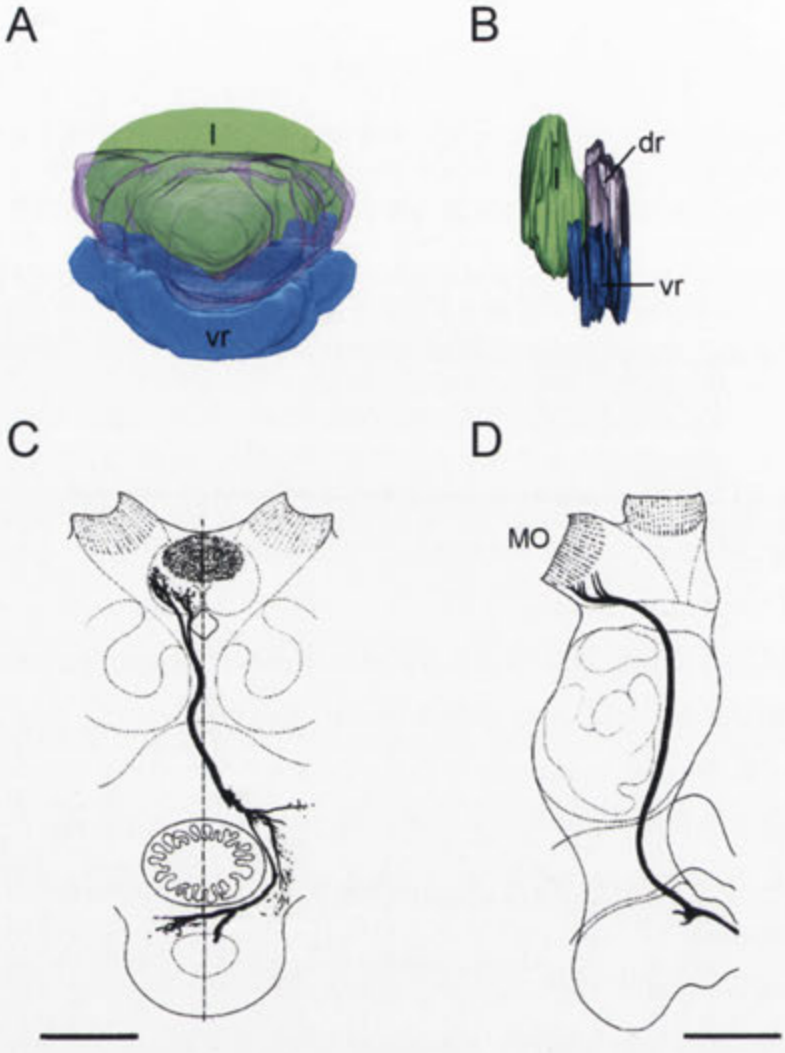

Figure 3.18: The morphology of a medial ocellar decending neuron Mocth (adopted from Heinzeller 1976) and the 3-D reconstruction model of the median ocellus (MO). A, B showed the posterior and the later view of the reconstruction of the median ocellar lens (l) and the retinas (dr, dorsal retina; vr, ventral retina). C, D showed the frontal and lateral view of the neuron Mocth. By comparing the reconstructed 3-D median ocellus model and the neural morphology, it is clearly shown that Mocth has its dendritic field positioned in the ventral retina of the median ocellus. Scale bars: 200 μm

Chapter 4

Evidence for short-wavelength receptor inputs to two pitch-sensitive descending neurons in the honeybee

4.1 Abstract

Optomotor reflexes have been observed in many insects and in some cases the neural pathways that mediate these reflexes have been identified physiologically and anatomically. In honeybees Kaiser (1975) established that the spectral sensitivity of optomotor responses in bees almost exactly matched that of the green photoreceptors, suggesting an exclusive input from green photoreceptors. Here, I present the responses of two neurons in the optomotor pathway of bees ($DNII_2$ and $Locth_3$) that selectively respond to the optic flow fields generated by a downward pitch of the head or body, i.e. both cells are sensitive to upward image motion in the frontal visual field. In contrast to the dogma regarding spectral inputs of the optomotor pathway, the present study shows that both neurons respond strongly to short-wavelength stimulation as well as to green stimulation. Although green photoreceptors in bees have spectral sensitivities that stretch into the UV region of the spectrum, their short-wavelength responses are relatively

weak. Given the very strong short-wavelength (380 nm) responses in the identified optomotor neuron, the results suggest a strong contribution from short-wavelength photoreceptors in addition to those from green photoreceptors. The present account describes the velocity tuning and contrast frequency response characteristics of the neurons for both green and short-wavelength light. The latency and spectral ocellar contributions to the responses of these neurons are also shown for the first time. The ocellar input provides a faster response to motion stimuli (lower latency) than with compound eye stimulation alone, and also increases the amplitude of responses to flashed stimuli. The ocelli provide a directional contribution to the responses of at least one of the neurons ($DNII_2$).

4.2 Introduction

Visual information is critical for the survival of most animals. Vision enables crucial behaviours such as foraging for food, detecting predators, finding mates and distinguishing between individual conspecifics. The visual cues used may be static, such as colour and contrast, or dynamic, such as the motion of prey. Maintaining a stable image on the retina in spite of continual body movements is a particularly important behaviour (Guitton, 1992; Hengstenberg, 1993). Optomotor responses compensate for unintentional movements of the head and body. For example, during normal flight bees hold a steady course for short periods interspersed with rapid saccade-like head and body movements that are intentional turns aimed at changing course direction (van Hateren and Schilstra, 1999; Boeddeker and Hemmi 2010; Boeddeker et al. 2010). This mode of flight has an important role in separating the optic flow that occurs across the retina into rotational and translational components, thus simplifying spatial vision during locomotion (Kern et al. 2005; Karmeier et al. 2006; Lindeman et al. 2008). During pure translational flight the bees attempt to keep their retinal image stable, which is where optomotor head turning reflexes play a key role. While flying the head and body vibrate due to the flight motor, thus leading

to a loss of flight stability. Also, external influences, such as air currents can blow the animal away from its intended flight course. During pure translational phases any unintentional head and body movements will induce image rotation. For example, an unintended deviation of the head or body to the right will induce leftward image rotation. The optomotor reflex drives the head and body in the direction of the image movement, thus compensating for the unintentional deviation.

A key step in forming the optomotor responses is the ability to detect the motion of the retinal image (Clifford and Ibbotson 2003). This motion signal is then transformed and sent to the motor system to generate appropriate muscle contractions that lead to compensatory head and body movements in the same direction as the retinal image movements. Recordings from direction-selective neurons have been made from multiple steps in this optomotor pathway in honeybees (optic lobes: Kaiser and Bishop 1970; Kaiser 1970; Menzel 1973; Hertel and Maronde 1987; descending intersegmental neurons: Ibbotson and Goodman 1990; Ibbotson 1991ab; motor neurons: Schroeter et al. 2007). Insects cannot move their eyes independently of their head as they are fixed within the head capsule (Hengstenberg 1972). It is therefore particularly important for insects to be able to detect self-movements relative to the visual environment because they are required to move their entire head and/or body to compensate, which involves the control of a very large number of muscles – far more than is required to move the mammalian eyeball!

The optomotor response has been observed in many flying insects (flies, Eckert 1971; locusts, Robert 1988; honeybees, Kunze 1961). It has been used to study the mechanisms of motion vision (Schlieper 1926) and as a test for colour vision in early behavioural experiments (Schlieper 1927). The latter study tested the honeybee optomotor response and reported that although it was already well established that honeybees possessed colour vision (von Frisch 1914) the optomotor response appeared 'colour blind'. Kaiser and Liske (1974) subsequently measured the spectral sensitivity of

the honeybee optomotor response for motion in the horizontal plane and found a single optimum performance at a spectral wavelength of 540 nm. This wavelength closely matched the peak of the spectral sensitivity function measured for green photoreceptors in honeybees. Thus, it has been suggested that honeybees use only one photoreceptor type (green) to drive the motion detectors that provide input to the optomotor system, thereby explaining the apparent colour blindness of the optomotor response (Kaiser 1975).

However, extracellular recordings from motion-sensitive interneurons in the honeybee optic lobe show that although their spectral sensitivity tuning is very similar to the green-photoreceptor sensitivity curve, some recordings suggested the presence of an additional peak in the ultraviolet (UV) region of the spectrum (Autrum and von Zwehl 1964; Kaiser 1975). Similarly, extracellular studies on motion-sensitive units in the fly optic lobe (McCann and Arnett 1972) and butterfly ventral nerve cord (Singarajah 1988) also show such secondary peaks in the UV region of the spectrum. These physiological data suggest that motion-sensitive interneurons may have inputs from both green and UV sensitive photoreceptors in a range of insect species, including the honeybee. Could short-wavelength-sensitive neurons be involved in optomotor responses in the bee despite the findings of Kaiser and colleagues?

Descending interneurons (DNs) that connect the central brain with the thoracic motor centres respond in a highly direction-selective manner to visual motion. They have been reported in a range of insects, including flies (Wertz et al. 2008), moths and butterflies (Singarajah 1988), locusts (Kein 1974; Rowell and Reichert 1986), dragonflies (Olberg 1981ab) and honeybees (Goodman et al. 1987; Goodman et al. 1990, 1991; Ibbotson 1991ab; Ibbotson and Goodman 1990). Moreover, it is believed that these direction-selective descending neurons are on the optomotor pathway because their directional, temporal and spatial tuning characteristics exactly match those of the honeybee optomotor response (Ibbotson and Goodman

1990; for optomotor tuning, see Kunze 1961). Thus, in this study, I use intracellular recordings from two frequently encountered motion-sensitive descending neurons to investigate the possibility that short-wavelength photoreceptors contribute to the optomotor responses of honeybees. It was recently established that dragonfly visual neurons tuned to detect vertical image motion receive input from photoreceptors sensitive to short-wavelengths (380nm) of light (van Kleef et al. 2010). The present account describes the fine anatomy, velocity tuning and temporal frequency response characteristics of two prominent DNs in the honeybee for both short-wavelength and green wavelengths of light. The relative contributions from the ocelli and compound eyes to the directionality of the DNs are also tested. The responses of these two neurons are presented together in this chapter because they both have similar directional tuning properties – they both respond to upward image motion frontally, which is the optic flow generated when the head and body pitch downwards and forwards.

4.3 Methods and materials

4.3.1 Experimental preparation

Experiments were conducted on honeybees, *Apis mellifera*, that had been actively foraging. Hives were situated at the Australian National University in Canberra, Australia. Each bee was lightly anaesthetised by cooling at 4°C for about 20 minutes. After removing the legs, the bee was placed horizontally (dorsal side up) on a metal holder, and the head and thorax were secured with a 3:1 mixture of beeswax and violin resin. A chlorinated silver wire was then inserted into the thorax to serve as the indifferent electrode for intracellular electrophysiological recordings (see below). Figure 3.1 shows a schematic diagram of the animal preparation. The ventral nerve cord was exposed from the dorsal side of the neck, between the suboesophageal and prothoracic ganglia, so that a recording electrode could be vertically inserted into it. Once prepared the bee was left for 15

minutes prior to making any recordings for the temperature to recover to room levels (22-24°C).

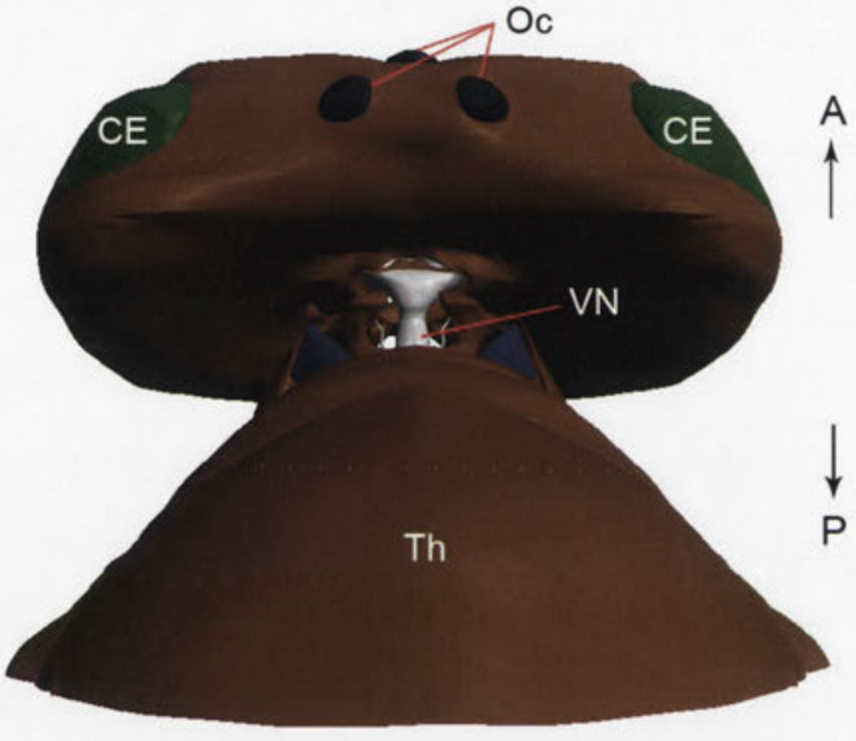

Figure 4.1: Dorsal view of a 3-D reconstructed honeybee head and thorax (adapted from Berry and Ibbotson 2010). The experimental animals in the present project were set up in the dorsal perspective for the dissection and experiment. The animals were horizontally secured on the stage with dorsal side up. The neck connective membrane and foregut were removed to expose the ventral nerve cord (VN). ***Abbreviations*:** A, anterior; CE, compound eye; P, posterior; Oc, ocelli; Th, thorax.

4.3.2 Electrophysiology

Honeybee motion-sensitive descending neurons have been described and classified previously according to their neuronal morphology (Pan and Goodman 1977; Goodman et al. 1987; Ibbotson 1991). The classification scheme and terminology described by Goodman and Ibbotson are used throughout this study. The recordings and results presented here are focused on two types of motion-sensitive descending cells, the so-called $DNII_2$ neuron and $Locth_3$ (the morphologies of the cells were described in Chapter 3). Through random selection these particular neurons were recorded from frequently and subsequently filled with dye, thus providing a strong statistical basis for comparisons between preparations.

Microelectrodes were pulled using a P-97 Flaming/Brown puller (Sutter Instruments) from borosilicate glass capillaries (GC100TF-10, Harvard Apparatus LTD). The electrode tips were filled 10% Lucifer Yellow CH (lithium salt; Invitrogen) in 1% LiCl solution and then backfilled with 1M LiCl solution, producing impedances of about 100 MΩ in honeybee saline (111.22 mM NaCl, 3.35 mM KCl, 1.37 mM $CaCl_2$, and 1.89 mM Na_2CO_3).

The microelectrode was inserted vertically into the exposed ventral nerve cord and lowered gently using a mechanical micromanipulator. Once the electrode was in position the microelectrode holder was tapped lightly to penetrate the cell membrane. Monitoring the electrode potentials on an oscilloscope was used to assess successful penetrations. When a cell's stable resting potential was detected, flashed wide-field visual stimuli were used to stimulate the eyes to confirm that the recorded cell was a visual neuron. All the recordings were done under room temperature.

4.3.3 LED display

A two-dimensional wide-field LED array described in Berry et al. (2006) was used to present visual stimuli during electrophysiological experiments

(Fig 4.2). Briefly, the display consisted of 9 columns of LEDs, and each column consisted of 12 pairs of UV (peak emission at 383 nm, Roithner Lasertechnik) and green (peak emission at 528 nm, Roithner Lasertechnik) LEDs (emission spectra of the LEDs are shown in Fig 3.2B). The emission spectrum of the green LEDs covered the peak region of the spectral sensitivity of honeybee green photoreceptors. It should also be noted that the lower-wavelength cut-off for the green stimulator coincided almost exactly with the upper cut-off of the honeybee blue photoreceptor. Therefore the green LEDs provided stimuli that were almost exclusively stimulating the green photoreceptors. The situation for the short-wavelength stimulus was far more complicated. It was not sufficient to just stimulate with flashes from single LEDs: rather, it was necessary to provide a wide-field motion stimulus. Therefore a stimulator array was constructed that could provide green and short-wavelength stimulation across a relatively wide field. The development of this device was complex and a decision had to be made early about which short-wavelength was most appropriate. The problem is that there is no safe and practical short-wavelength emission spectrum that would not provide some stimulation to the blue and the green photoreceptors (see Fig 3A). Also, we did not know if any short-wavelength input would come from the blue or the UV photoreceptors, so we did not want to prejudice our ability to record responses by, for example, selecting a very short-wavelength, only to find that it was the blue receptor that provided the input. With these considerations in mind, we selected a wavelength of light that provided near-equal stimulation for the UV and blue photoreceptors (380 nm). The theoretical quantum catch of the chosen LED is shown in Figure 3C (for calculation, see below). It is evident that it provides very strong input to the blue and UV and less input to the green photoreceptor.

LEDs on the display were arranged at 6 degree intervals on the circumference of a circle. The honeybee head was positioned at the centre of this circle. The intensity of each LED was controlled by individual voltage-to-current driver amplifiers and calibrated using either short-wavelength or

green-sensitive photodiodes (Electro Optical Components, EPD-365-0/2.5, and Centronic, series 15-5T, respectively). The LEDs were driven by individual voltage-to-current converting driver-amplifiers, and each driver-amplifier is independently controlled via a 32-channel D/A converter with 14-bit resolution (Analog Devices AD5532HS). The converter features a digital sample-and-hold on each channel so that pixels were only refreshed if they have changed values. The converter was driven via a microcontroller (IsopodTM, NewMicros Inc.), which communicates with the PC via a parallel port. Data from the PC were converted by the microcontroller into the serial format required by the D/A converter. The display was refreshed at a rate of 625 Hz. The PC is run on the Linux operating system (Debian), with a real-time module (RTAI) for synchronous data acquisition and control, interfaced with MATLAB for higher-level functions. After calibration, the intensity of each short-wavelength LED had a maximum flux of $\approx 1.2\times10^{14}$ photons cm^{-2} s^{-1} at λ= 383 nm and each green one had a maximum flux of $\approx 0.9\times10^{14}$ photons cm^{-2} s^{-1} at λ = 528 nm, at the position of the honeybee head.

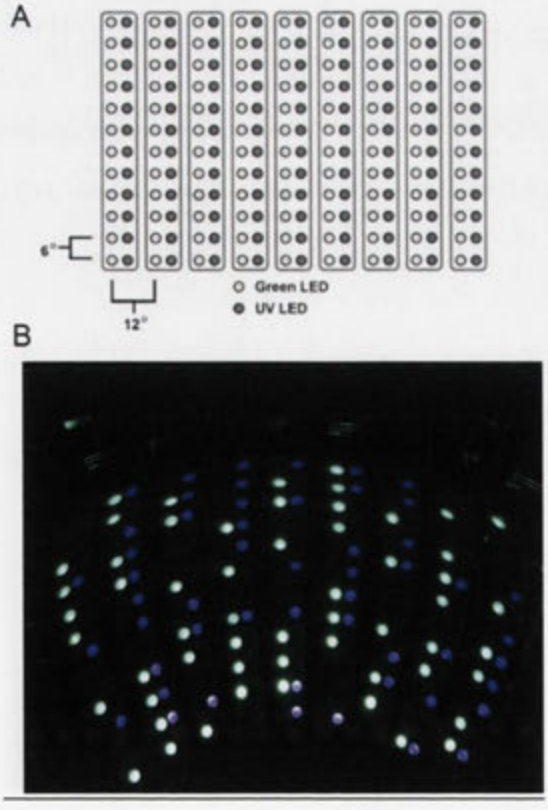

Figure 4.2: (A) A schematic diagram of the wide field LED display (figure adapted from Berry et al., 2006). The resolution of the display is 6° in vertical direction and 12° in horizontal direction.

(B) shows an example image of the display when the LEDs were randomly on.

Calculation of the relative quantum catches of the photoreceptors

The quantum catch for photoreceptors represents the number of quanta that are absorbed by a certain photoreceptor type, and is widely used as input for calculations and models of colour vision (e.g. Kelber 1999; Kelber et al. 2003). In this study, the relative quantum catch (Q) for a photoreceptor type i (where in honeybee, i = UV, blue or green receptors) to UV stimulation used in the experiments were calculated from the integral of the spectrum weighted by the receptor sensitivity curves:

$$Qi = \int_{300}^{700} S(\lambda)P(\lambda)d\lambda\,, \qquad (1)$$

Where $S(\lambda)$ is the emission spectrum of the UV LED, and $P(\lambda)$ is the spectral sensitivity curve of the photoreceptor. The spectral sensitivity curves of the honeybee (P) were generated using a vitamin A_1 template described by Stavenga et al. (1993) and considering the photoreceptors peak sensitivity (α-band) at the wavelength of 350, 440, and 540 nm (Autrum and Zwehl 1964; Menzel and Blakers 1976; Menzel 1986). It is worth noting that Menzel and Blakers (1976) did find variability in peak UV sensitivity of up to 30nm in bee retina. It is therefore possible that the quantum catch calculations could be slightly different from bee to bee.

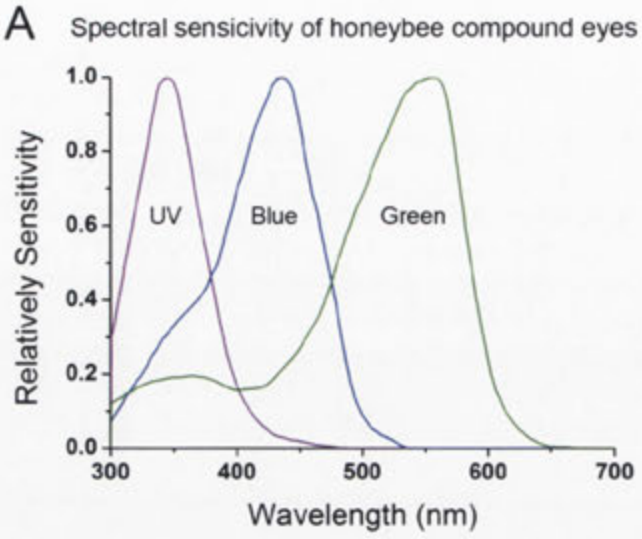
A
Spectral sensicivity of honeybee compound eyes
Relatively Sensitivity
1.0
0.8
0.6
0.4
0.2
0.0
UV
Blue
Green
300
400
500
600
700
Wavelength (nm)

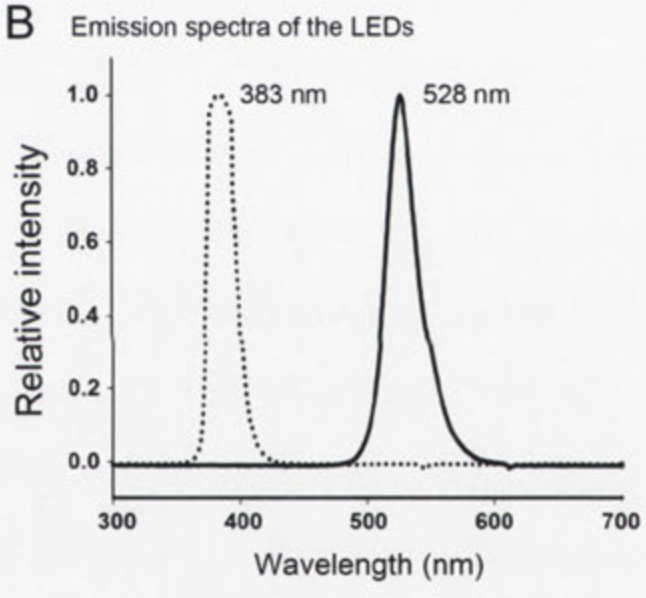
B
Emission spectra of the LEDs
Relative intensity
1.0
0.8
0.6
0.4
0.2
0.0
383 nm
528 nm
300
400
500
600
700
Wavelength (nm)

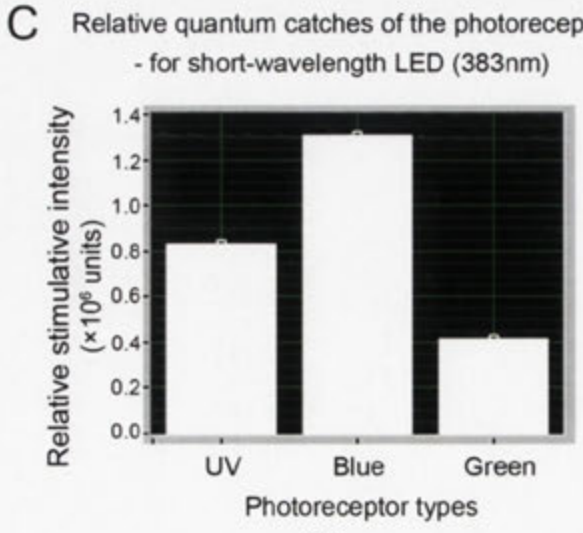
C
Relative quantum catches of the photoreceptors
- for short-wavelength LED (383nm)
Relative stimulative intensity
(×10⁶ units)
1.4
1.2
1.0
0.8
0.6
0.4
0.2
0.0
UV
Blue
Green
Photoreceptor types

Figure 4.3: The spectral profile of honeybee photoreceptors and stimulations (LEDs) used in the study. A: the spectral sensitivity for honeybee photoreceptors (compound eyes). The three photoreceptor types (UV, blue and green) have the maximum sensitivity at the wavelength of 350, 440, and 540 nm, respectively. B: The emission spectra of the two LEDs used in this study. The short-wavelength LED has the peak emission spectrum at 383 nm, while it is 528 nm for the green LED. C: The theoretical quantum catch of the honeybee receptors to the short-wavelength LED (383 nm). It is shown that the short-wavelength LED provides strong inputs to the blue and UV photoreceptor types and less input to the green photoreceptors.

4.3.4 Visual stimuli

Using the LED display described above, two different types of visual stimuli were employed in this study: wide-field flashed stimuli, and directional motion stimuli. To examine the ocellar contribution to the descending neuron responses, recordings were made with visual stimuli presented to both the compound eyes and the ocelli simultaneously and to the compound eyes alone (i.e. with the ocelli covered). It proved impossible to reliably and reversibly cover the compound eyes while leaving the ocelli uncovered. Stray light always managed to stimulate some part of the compound eye whatever the covering technique used. In contrast, it was possible, due to their small size, to cover the ocelli using a small cap, while leaving the compound eyes unaffected. The cap was made of a small (~3mm × 3mm) piece of aluminium foil on one side together with a same size of a black paper on the other side; it was also bended on the sides so that it can cover the ocelli completely. The small cap is put on top of the ocelli with the aluminium foil side out. The aluminium foil side acted to block any coming light from the environment; the black surface facing the ocelli can absorb bouncing light (if any) thus prevent any reflecting and scattering between the ocelli and the cap. All experiments were carried out under dim-light conditions (10^{-2} -10 cd.m^{-2}).

Flashed stimuli

Two types of flashed stimuli were used in the experiments. In the first (Type I), all 216 LEDs (i.e. both short-wavelength and green LEDs) were driven simultaneously to produce wide-field ON and OFF flashes that simultaneously used both the short-wavelength and green LEDs. The flashes were of 200 ms duration. In the second (Type II), the array of short-wavelength and green LEDs were modulated independently with a constant short-wavelength and green background set at 50% of their respective maximum intensities. Modulation of short-wavelength and green intensity

above and below this background was controlled by two independent sequences, one driving all short-wavelength LEDs simultaneously and one driving all green LEDs simultaneously. Increments (80% maximum intensity) or decrements (20% maximum intensity) of either the short-wavelength or green channel above or below the mean background were 38 ms in duration and 1 sec in interval. The sequence of the flashes was always as follows: short-wavelength increment, green increment, short-wavelength decrement and then green decrement (see Figure 4.4A).

Directional stimuli

Directional stimuli consisted of either single bars or gratings moving either vertically or horizontally at different speeds. Vertically moving bars were 6° wide and the horizontally moving bars were 12° wide. The bars could take several forms. We did not mix LED stimulation; any given stimulus was generated using LEDs of one wavelength (i.e. when using a green background, the bars also used green LEDS). When a particular wavelength was in use (green or short-wavelength) the LEDs for the other wavelength were inactive. Bright bars consisted of a moving bar of LEDs that had higher brightness than the background (positive contrast bars). Dark bars consisted of a moving bar of LEDs that had lower brightness than the background (negative contrast bars). The contrast of the bars was -0.82 (negative contrast). Bars were presented at 12 increasing speeds from 100 °/s to 3750 °/s, and then at decreasing speeds so that two samples of the response for each speed were obtained. This sequence could then be repeated to obtain additional experimental repeats for each speed. Bar stimuli at the speed of 341 °/s with 10 different contrasts (from +0.82 to -0.82) were also applied in some experiments.

Gratings had a square-wave profile with a Michelson contrast of 0.82 and spatial wavelengths of 24°, 36° or 60° in elevation (horizontal gratings), or 48°, 72° or 120° in azimuth (vertical gratings). The spatial wavelengths were chosen so as to produce an integer number of cycles on the display. Gratings were drifted vertically (horizontal gratings) or

horizontally (vertical gratings) at speeds of either 75 or 750 °/s. Gratings of each spectral wavelength and speed were moved up and down 5 times and held stationary for 500 ms between movements.

4.3.5 Data analysis

Electrode potentials were amplified (Getting Instruments, Model 5A), displayed on an oscilloscope and recorded digitally at a sampling rate of 5 kHz, on a PC using a 14-bit analogue-to-digital converter (Measurement Computing, PCI-DAS1001). The recorded data was analysed offline using Matlab. First, a neuron was judged to have occurred if the difference between consecutive measurements of the membrane potential (dV) exceeded a threshold. This threshold was set at three times the standard deviation of dV over the entire recording. Spikes were determined to occur at the zero crossing of dV that occurs immediately following the point at which dV exceeds the threshold. The spike density functions were calculated by convolving the spike arrival times with a Gaussian filter with a width at $1/e$ of the maximum of 10 or 5 ms. The 10 ms case was used for visual presentation in figures, while the 5 ms case was used when calculating timing events.

For the bar stimulus, the response rate was calculated as the number of spikes that occur during the stimulus time minus the spontaneous activity of the cell and normalised by the maximum response in the preferred direction. The spontaneous activity for each trial was estimated from the average spike rate during the 500 ms period before stimulus onset.

For the grating stimulus, we also used the directional index (DI) to analyse the directional response. DI was calculated as:

$$DI = \frac{R_p - R_n}{R_p + R_n}, \qquad (2)$$

where R_p is the number of spikes that occurred within the stimulus duration in the preferred direction and R_n is the number of spikes that occurred within the same period of time in the anti-preferred direction.

4.3.6 Visualisation of stained neurons

The methods used to stain and visualize the recorded neuron were described in Chapter 3. Briefly, after the completion of intracellular recording, cells were filled with Lucifer Yellow CH (lithium salt, Invitrogen™) by iontophoretic injection of 5-10 nA (negative injection) for at least 15 minutes. Following the general histological protocol, the honeybee brain was then optically sectioned by confocal microscope (LSM Pascal, Zeiss). The 3-D reconstruction model of the $DNII_2$ neuron shown in the results section was made using Amira 5.3.3 (Visage Imaging GmbH). The stained cell body and neurite on each slide were manually traced and segmented. The traced neuron was then reconstructed and rendered using the same program.

4.4 Results

In this study, recordings were made from 300 descending neurons and from this population 43 were filled and anatomically identified. Among the identified cells, 12 cells from separate preparations were classified as $DNII_2$. This was the largest subpopulation of an identifiable neuron that was reliably and repeatedly recorded from, and therefore, in this chapter I focus on the physiological responses of this particular cell-type. The $DNII_2$ neurons have a very distinct physiological profile that is highly repeatable from preparation to preparation. Therefore, I also analysed the responses of a further 16 recorded units that had responses that were not distinguishable from the anatomically identified $DNII_2$ neurons. While we cannot be certain

that these cells were $DNII_2$ neurons at the anatomical level, it is highly probable that they represent a reasonable additional population average from this cell type.

The second neuron that is considered in this Chapter is $Locth_3$. This neuron has its main dendrites in the retinal plexus of the lateral (L) ocellus (oc) and descends into the thoracic (th) motor centres. In total the bee has 5 ocellar neurons that descend on each side of the nervous system. For whatever reason, $Locth_3$ is by far the most commonly encountered and filled neuron among the 5 cell types. It is easy to distinguish this cell from the other four cell types because it receives input from the lateral ocellus on the contralateral side of the body compared to the descending axon and has a distinct dendritic morphology (see Chapter 3). It was encountered anatomically on three occasions in this study. More detail will appear in section 4.4.4, below.

4.4.1 $DNII_2$ morphology

The detailed morphology of the $DNII_2$ cell has been described in the previous chapter. In this chapter a 3-D reconstruction model of the neuron is presented (Fig 4.4). Briefly, the $DNII_2$ cell lies on the posterior side of the brain with the cell body located on the lateral edge of the protocerebral bridge, close to the calyx of the mushroom bodies. The trunk of the dendritic arbors with fine branches project to both halves of the brain in the postero-medial protocerebrum, dorsal to the oesophageal foramen. The axon travels down to the suboesophageal ganglion where the terminal arbores branch into both the ipsilateral and contralateral sides of the suboesophageal neuropile.

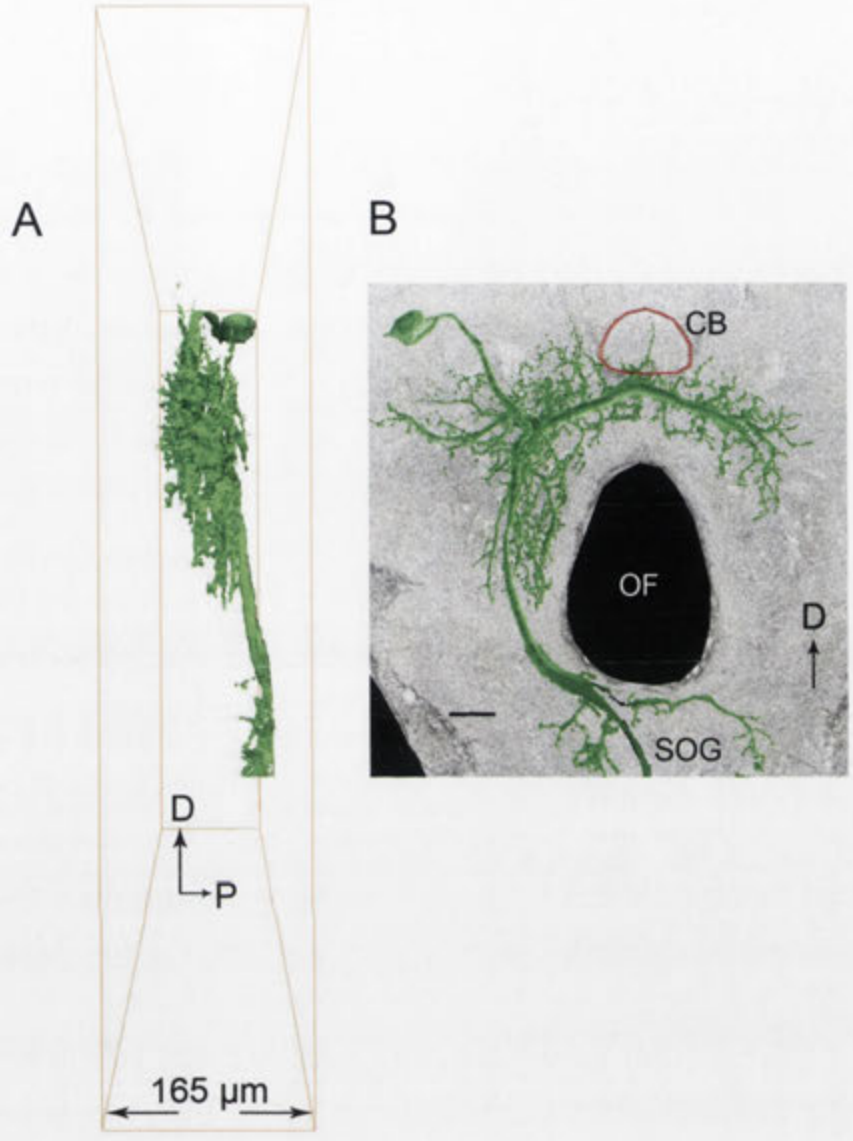

Figure 4.4: The 3-D reconstruction of motion-sensitive descending neuron $DNII_2$ in the brain region. A: The lateral view of the reconstructed neuron. The orange bounding box shows the total scanned volume with 165 µm in z-axis. B: The posterior view of the neuron. The dendritic trunk arches above the oesophageal foramen (OF) into both halves of the brain with fine branches projecting from both sides of the main trunk. As the axon travels down to the suboesophageal ganglion (SOG) terminal arbores branch into both sides of the ganglion. ***Abbreviations*:** CB, central body; D, dorsal; OF, oesophageal foramen; P, posterior; SOG, suboesophageal ganglion. Scale bar: 50 µm.

4.4.2 Responses to flashed stimuli

Responses to flashed stimuli

The type II flashed stimulus used in these experiments comprised of a 38 ms increment or decrement of luminance with respect to the background luminance. Short pulses of brightness change were used to prevent adaptation. However, the pulses generated both an increment and decrement (or *vice versa*) making it difficult to judge which part of the response resulted from an increment and which from a decrement. Therefore, only the response to the initial transition was considered as we could extract precise latency and amplitude information from the first burst of spikes. The flashes used either short-wavelength or green stimulation (the two sets of LEDS were not used together). Experiments were carried out while the ocelli were uncovered or covered.

Using the green stimulus, and with both compound eyes and ocelli stimulated simultaneously there were reliable and robust responses to brightness increments (Fig 4.5). The mean latency to peak response across 5 cells was 35.8 ms (SD = 6.2, n = 5). There was also a robust excitatory response following brightness decrements with a mean latency of 21.2 ms (SD = 3.5, n = 5). With stimulation of the compound eyes only there was little evidence for a response to brightness increments. There was, however, a robust response to brightness decrements with a mean latency of 27.6 ms (SD = 6.5, n = 5).

Using only short-wavelength stimuli, responses were more variable between preparations. With compound eyes and ocelli stimulated two identified neurons produced responses to brightness increments, while the other three showed no response. The latencies for the two cells that did show a response were 30 and 35 ms. All five tested cells showed robust responses to brightness decrements with a mean latency of 23.4 ms (SD = 3.4, n = 5). Once the ocelli were covered the results were mixed: four of five cells showed a clear ON response, while three showed a clear OFF response.

The mean latencies for the ON and OFF responses were 27.8 ms (SD = 1.7, n = 4) and 24.7 ms (SD = 4.0, n = 3), respectively.

Figure 4.6 shows a scatterplot of the maximum spiking rate in response to brightness increments (green: squares; short-wavelength: crosses) and decrements (green: circles; short-wavelength: plus symbols) with the ocelli covered (abscissa) and uncovered (ordinate). Response amplitudes in this figure come from five anatomically identified neurons and six non-identified neurons that had physiological tuning properties that identified them with high probability as arising from $DNII_2$ neurons. There is a significant decrease in the spiking rate when the ocelli were covered for both wavelengths and for both ON and OFF responses ($F_{(1,84)} = 13.5$, $p < 0.01$).

The results show that the descending neuron $DNII_2$ receives both green and short wavelength inputs. This is a novel finding because it was previously assumed that optomotor neurons such as $DNII_2$ would only respond to input from one colour channel (green). Therefore, we would have expected the response amplitudes at short-wavelengths to be relatively smaller than those at the peak of the green receptor. This was not the case. In fact the short and green-wavelength responses were not significantly different in amplitude (t-test, $p>0.05$). Moreover, a second novel finding is that the neuron receives robust input from both the compound eyes and the ocelli. When the ocelli were stimulated simultaneously with the compound eyes the response latency was reduced, suggesting a direct influence via a synaptic pathway that included very few stages from the ocellar retina to $DNII_2$.

Flash stimulation during dark adaptation: Having established the general response properties to flashed stimuli, further tests were conducted during which the animals were placed in the dark for 15 minutes prior to the presentation of flashed stimuli. The stimulus in this case was the Type I flashed stimulus, which consisted of simultaneous 200 ms presentations of short-wavelength and green light using all LEDs. The left column in Figure

4.7 shows a cell's response to simultaneous stimulation of the compound eyes and ocelli, and the right column shows the cell responses when only the compound eyes were stimulated (ocelli occluded). In both cases the stimulus was presented 40 times to obtain the data shown.

Under dark adaptation, when both compound eyes and ocelli were stimulated, the anatomically identified $DNII_2$ cell had a transient ON and OFF response to flashed stimuli (Fig 4.7AB). Figure 4.7 A shows the mean membrane potential across the 40 trails in the recording period of time. The membrane potential fluctuations show several phasic changes in membrane potentials which are directly correlated with bands of time-locked spike arrival times. When the ocelli were covered the response characteristics changed dramatically: the cell only showed a transient ON response (Fig 4.7CD).

The latencies of the recorded responses also differed between the different stimulus conditions. When the compound eyes and ocelli were stimulated the ON response exhibited three bands of time-locked action potentials in the response, the peaks occurring at 20, 34 and 54 ms (Fig 4.7AB). With only compound eye input the ON response also exhibited three time-locked bands of action potentials. These had longer latencies of 27 ms, 52 and 69 ms. For the OFF response with both compound and simple eyes stimulated there were two bands of time-locked action potentials with latencies of 14 and 34 ms (Fig 4.7B). It was not possible to measure latencies for the OFF response with the ocelli covered.

The results confirm that the cells are sensitive to brightness increments and decrements. A difference in comparison to the light adapted case was that the OFF response was absent when the ocelli were covered. This result suggests that during dark adaptation the ocelli provide a very large drive to the OFF circuit, perhaps because they are highly sensitive to light (Wilson 1978).

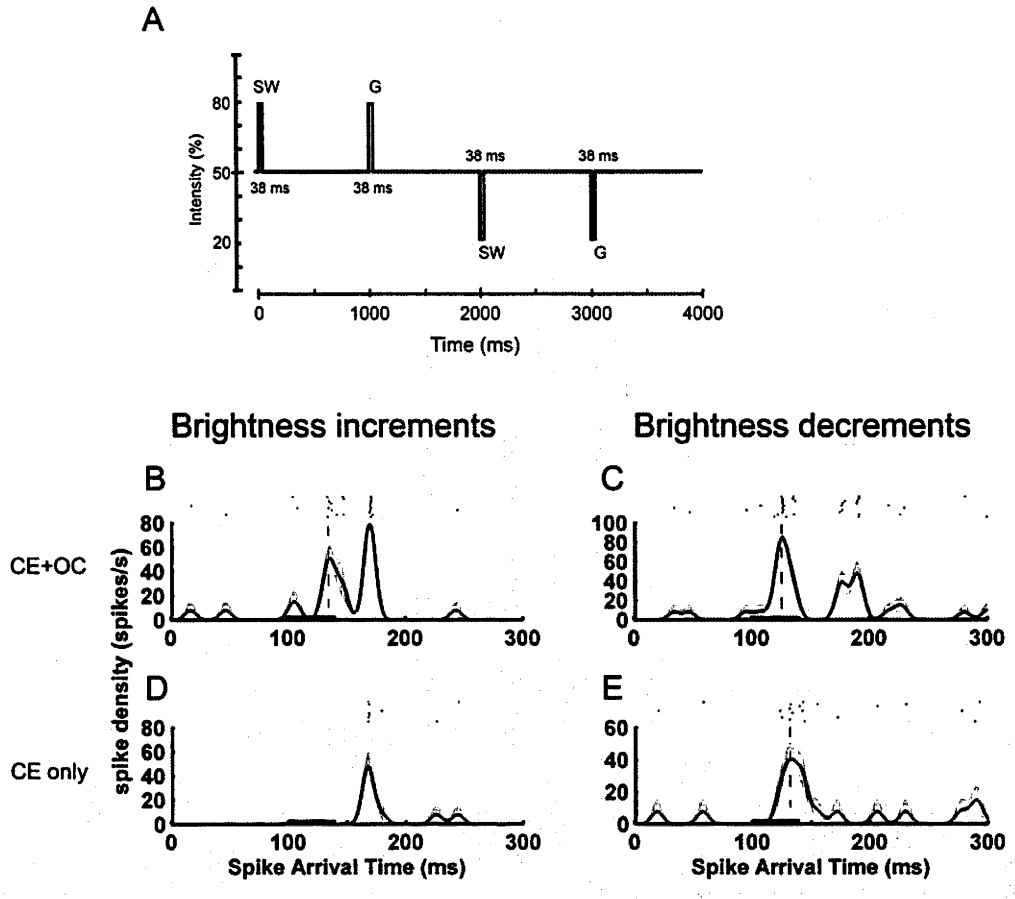

Figure 4.5: The time scale and intensity of flahes of the type II flashed stimulus (**A**). The type II stimulus are increments (80% maximum intensity) or decrements (20% maximum intensity) of either the short-wavelength (SW) or green (G) flashes above or below the mean background. The stimulus was 38 ms in duration and 1 sec in interval. The sequence of the flashes was: SW increment, G increment, SW decrement and then G decrement. **B-E** show the $DNII_2$ responses to green brightness increment and decrement flashes. Two conditions were applied in this test: both compound eyes (CE) and ocelli (Oc) were stimulated simultaneously (B and C); only compound eyes were stimulated (D and E). The black dashed lines indicate the response to the onset of the stimulus. The results showed that when both compound eyes and ocelli were stimulated there was an excitatory response to brightness increments and decrements while when only the compound eyes were stimulated the cell only responded to the green brightness decrements.

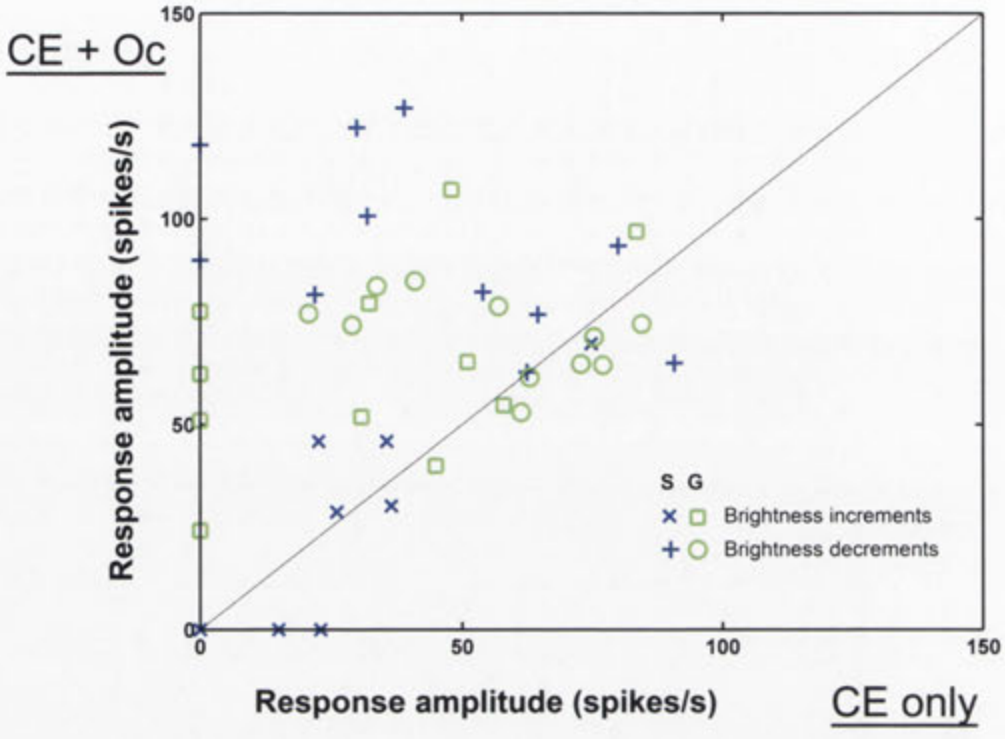

Figure 4.6: Scatterplot of the maximum spike rates in response to brightness increments (green: squares; short-wavelength: crosses) and brightness decrements (green: circles; short-wavelength: plus symbols) when only the compound eyes were stimulated (CE only, abscissa) and when both compound eyes and ocelli were stimulated (CE + Oc, ordinate). It is shown that when both compound eyes and ocelli were stimulated simultaneously, the response amplitudes were significantly larger than those when only the compound eyes were stimulated ($F_{(1,84)} = 13.5$, $p < 0.01$). The results were analysed from 5 anatomically identified $DNII_2$ neurons and 6 non-identified neurons that had identical physiological tuning properties to $DNII_2$ (total n = 11). **S**=short-wavelength; **G**=green.

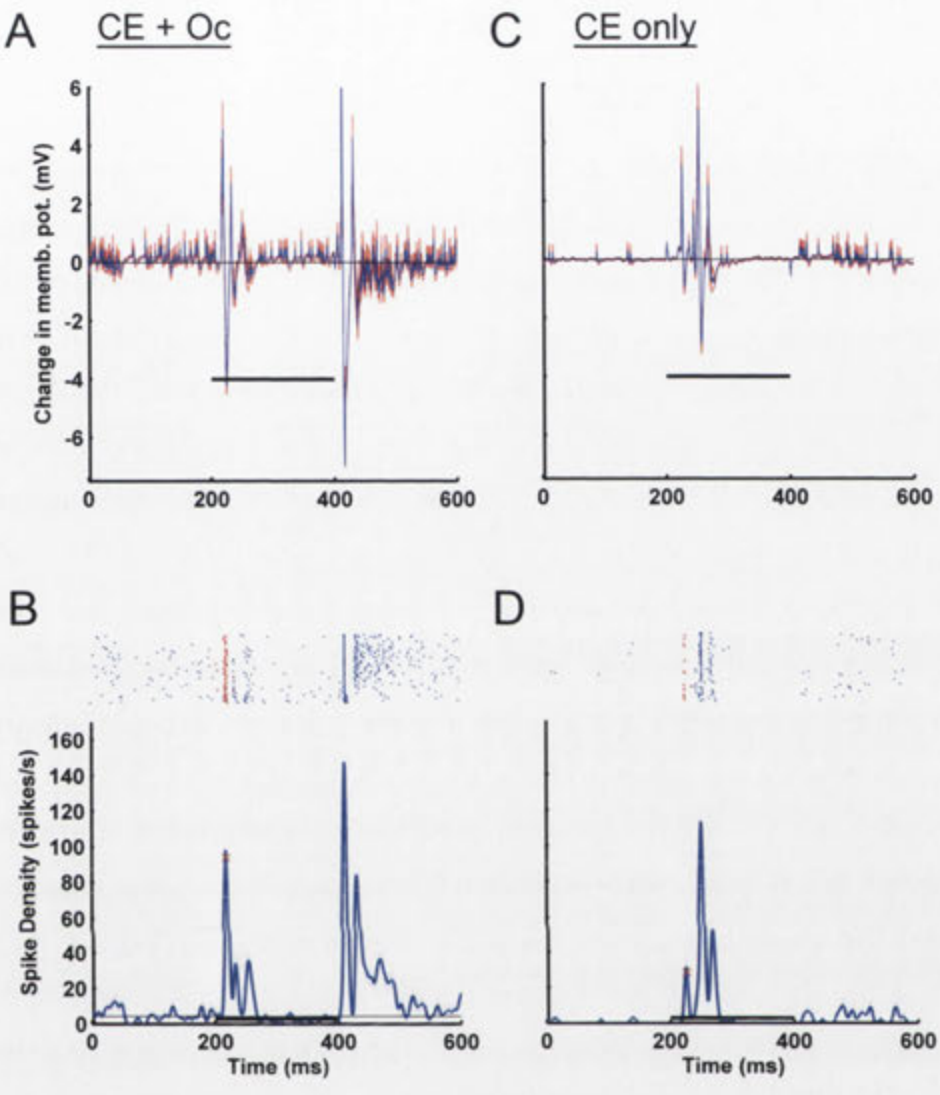

Figure 4.7: Flash response of the $DNII_2$ neuron under dark adaptation. The left column shows the cell response to 200 ms flashes when both compound eyes and ocelli were stimulated simultaneously, while the right column shows the response when only the compound eyes were stimulated (i.e. the ocelli were covered). It is shown that when the compound eyes and the ocelli were stimulated simultaneously the cell had robust transient responses to both stimulus ON and OFF with a latency of 20 ms (red cross and red rasters) and 13 ms, respectively. However, when only the compound eyes were stimulated, the cell only had a transient response when the stimulus was ON with a latency of 27 ms (red cross and red rasters).

4.4.3 Direction-selectivity

Responses to moving bars

In total twelve anatomically identified $DNII_2$ neurons were tested with moving bars. These included the five neurons presented in the light-adapted flashed stimulus section above. All of these $DNII_2$ neurons were strongly direction-selective, preferring upward moving bars when stimulated in the frontal visual field. The responses to upward and downward motion are presented in Figure 4.8 for 12 different image speeds using green bars and in Figure 4.9 using short-wavelength bars. The spike density functions and representative spike rasters are shown for each velocity tested. The cells generated an excitatory response to upward moving bars and their spontaneous activities were reduced during downward bar movement. Accordingly, the cells are classed as motion-opponent, direction-selective neurons. Prior experiments with the same anatomically identified cell type revealed that the preferred axis of motion was tightly tuned around the vertical, giving no response to horizontal motion (Ibbotson and Goodman 1990). To check the validity of those prior findings the same range of image velocities were tested for horizontal motion. These results revealed no significant response for either leftward or rightward motion (Fig 4.10 shows the cell responses to green horizontally moving bars). Upward motion will be referred to as the preferred direction, downward motion as the anti-preferred direction and horizontal motion as the cross-oriented direction.

In the following section I determine the velocity tuning and contrast sensitivity of $DNII_2$, and also determine the contribution of the ocelli to the generation of direction-selectivity.

Velocity tuning

The spike density functions for a representative cell are presented in Figure 4.8 and 4.9 for a wide range of stimulus speeds for two different coloured stimuli (Fig 4.8: green; Fig 4.9: short-wavelength). Speeds ranging from 268 to 3750 °/s were tested. It was problematic to use lower speeds because the

spatial interval between LEDs was such that the motion appeared in the form of apparent motion (i.e. the bar jumped from LED row to LED row rather than moving steadily. This led to time-locked, bursty firing patterns). Figure 4.11A shows the individual velocity-tuning functions for six anatomically identified $DNII_2$ neurons tested with vertical upward and downward motion. The cells responded over a similar range of speeds for moving green and short-wavelength bars. Some neurons showed a band-pass characteristic in which responses increased to a peak and then declined with further increases in image velocity. Others show a low-pass tuning in which the response amplitude declines as velocity increases. Figure 4.11B shows the result of averaging all of the cells together after normalising the responses to the maximum values obtained with short-wavelength stimulation. This average tuning shows a low-pass tuning characteristic.

The recordings from this section provide evidence for two key findings: 1) stimulation with moving green and short-wavelength bars generates responses of the same amplitudes and that responses occur over the same range of speeds for the two colours. 2) The peak velocity tuning is in the range 268 to 600 °/s, with a peak at 340 °/s.

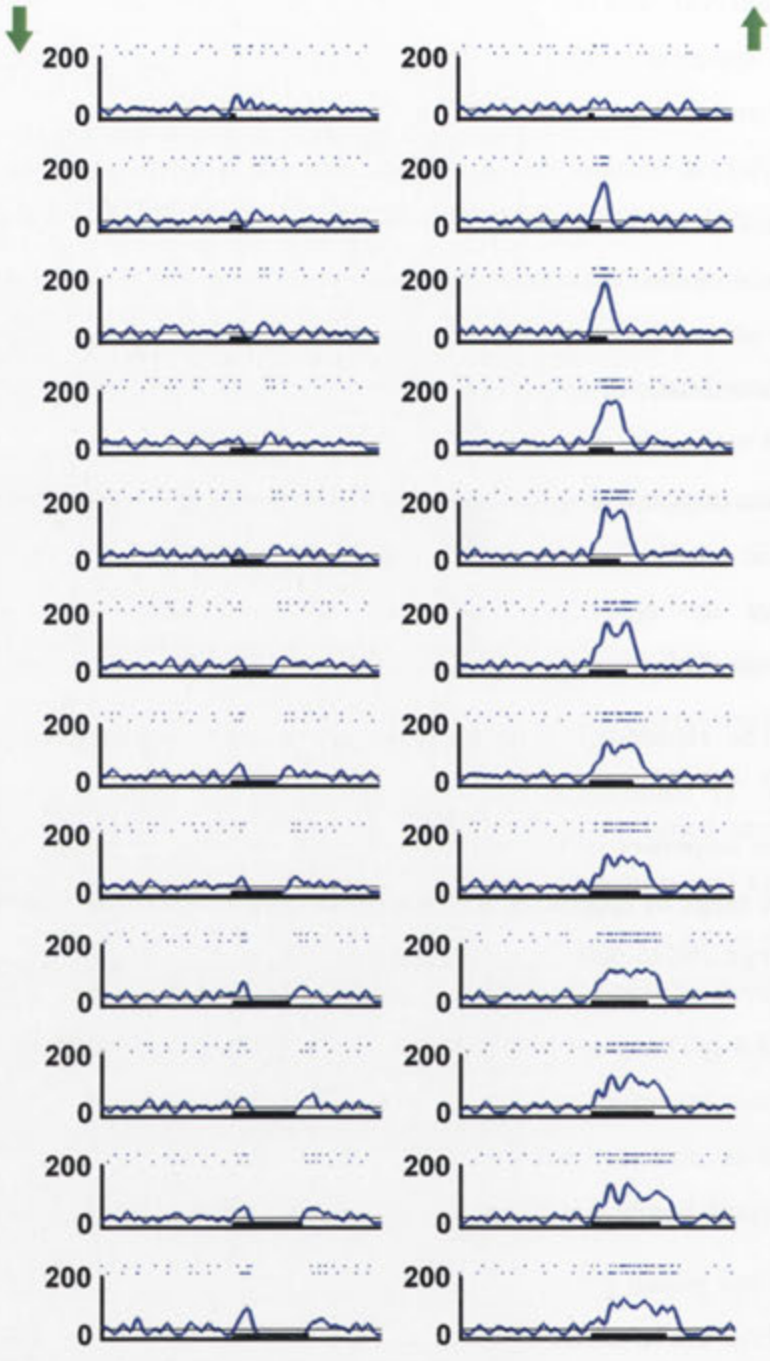

Figure 4.8: Responses of $DNII_2$ to a wide range of speeds of vertically moving **green** bars (contrast: -0.82). The directions of movement are shown by the green arrows (left column, downward moving bars; right column, upward moving bars). The test speeds ranged from 3750 (upper row) to 312 °/s (bottom row). The cell has an excitatory response to upward moving green bars and an inhibitory response to downward moving bars.

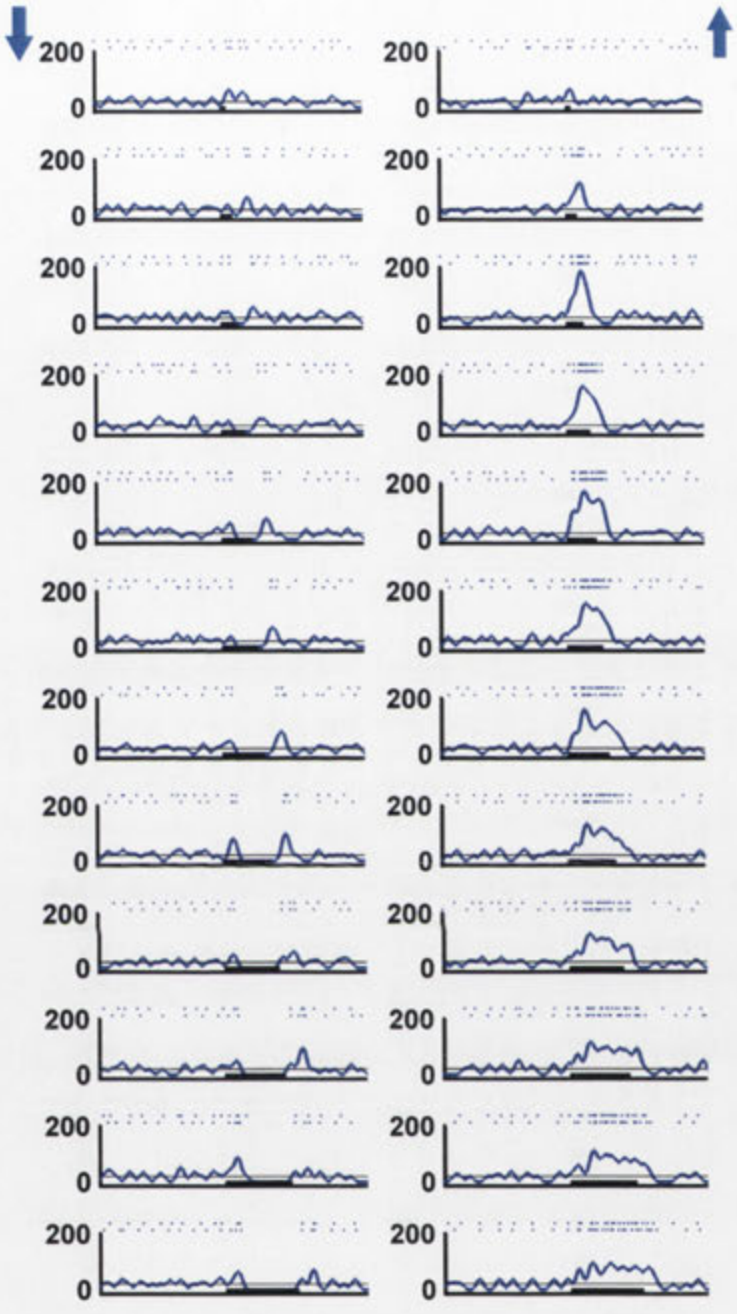

Figure 4.9: Responses of $DNII_2$ to a wide range of speeds of vertically moving **short-wavelength** bars (contrast: -0.82). The directions of movement are shown by the blue arrows (left column, downward moving bars; right column, upward moving bars). The test speeds ranged from 3750 (upper row) to 312 °/s (bottom row). The cell has an excitatory response to upward moving short-wavelength bars and an inhibitory response to downward moving bars.

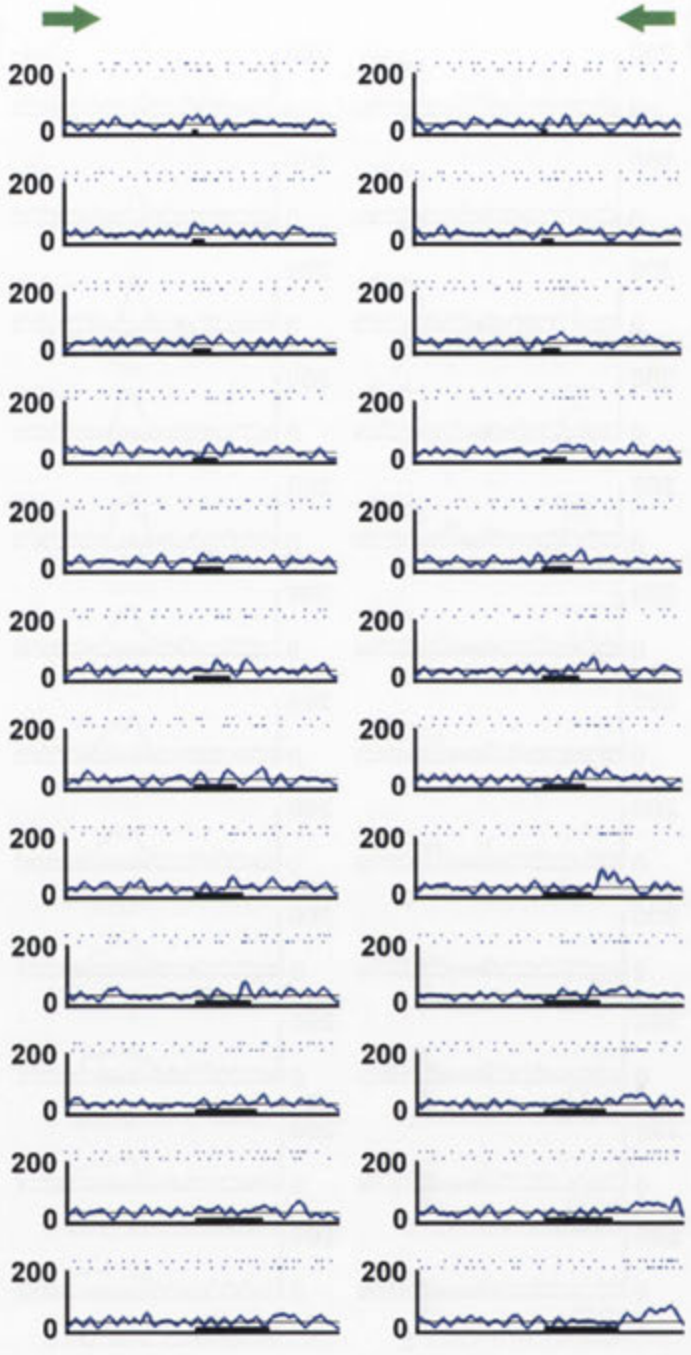

Figure 4.10: Responses of $DNII_2$ to a wide range of speeds of horizontally moving **Green** bars (contrast: -0.82). The directions of movement are shown by the green arrows (left column, rightward moving bars; right column, leftward moving bars). The test speeds ranged from 3750 (upper row) to 312 °/s (bottom row). The cell shows no significant response to horizontal movement in either of the directions for any speed of motion.

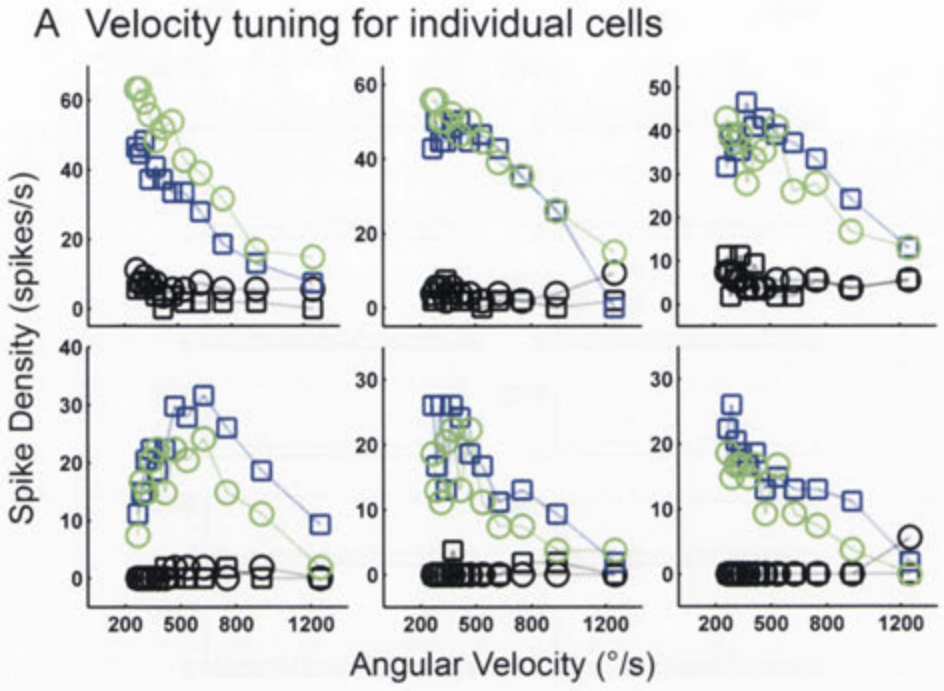
A Velocity tuning for individual cells
Spike Density (spikes/s)
Angular Velocity (°/s)
200 500 800 1200

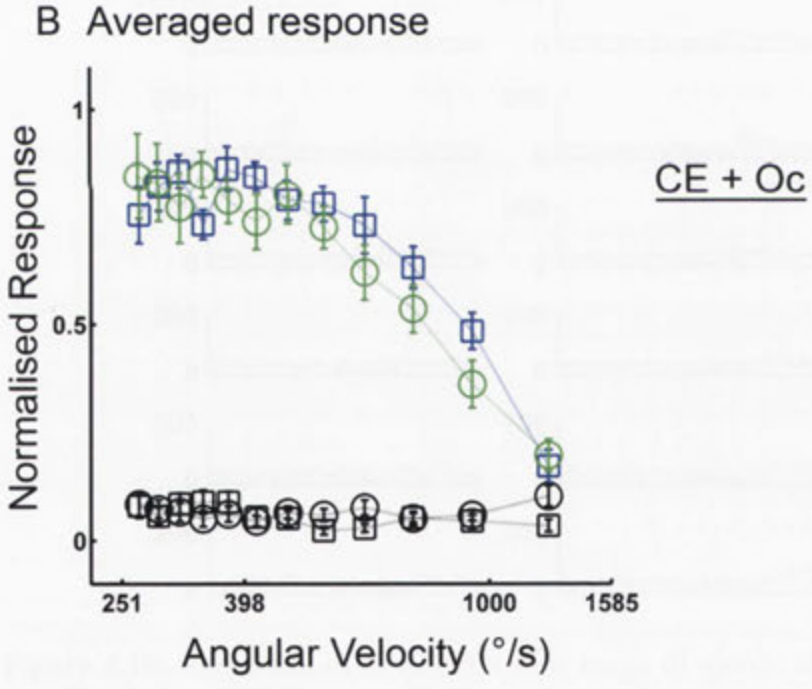
B Averaged response
Normalised Response
CE + Oc
251 398 1000 1585
Angular Velocity (°/s)

Figure 4.11: The velocity tuning of $DNII_2$ to vertically moving bars. The black symbols (squares: short-wavelength; circles: green) indicate the responses to motion in the anti-preferred direction (i.e. downward moving bars) while the coloured symbols (blue squares: short-wavelength, green circles: green) indicate the responses to motion in the preferred direction (i.e. upward moving bars). (A) shows the velocity curves from six anatomically identified $DNII_2$ neurons. (B) shows the results of averaging the six individual recordings after normalizing the responses to the maximum values. It is shown that although one of the individual velocity functions showed a band-pass tuning characteristic (lower left panel), the averaged tuning curve showed a low-pass tuning characteristic with maximum responses at speed around 340 °/s.

In the previous section all stimulation was provided to both compound eyes and the ocelli. In the next section we compare this case with compound eye only stimulation. To compare the response amplitudes between different stimulus conditions all responses were normalised with respect to the maximum response to short-wavelength bars moved in the preferred direction. The mean response rates and standard deviations shown in Figure 4.12 were calculated from 5 identified $DNII_2$ cells (these were a different population of anatomically identified $DNII_2$ neurons from those in the previous velocity tuning section). The results show that when both ocelli and compound eyes were stimulated, the velocity tuning functions for moving short-wavelength and green bars were very similar, and no significant difference was found ($F_{(1,160)} = 0.01$, $p > 0.05$). The cell was maximally tuned to detect upward moving bars with a velocity of 340 °/s.

When the ocelli were covered, the cell similarly showed an excitatory preference for upward moving bars. No significant difference was found between the amplitudes of the responses to short-wavelength and green stimulation ($F_{(1,160)} = 0.01$, $p > 0.05$). However, the standard deviations of the responses to green bar stimulation were higher than those to short-wavelength bar stimulation at low angular velocities. For example, when the ocelli were covered, at an image velocity of 312°/s the standard error was 0.05 for short-wavelength and 0.1 for green stimulation.

There was a significant difference between the amplitudes of the speed tuning curves for compound eyes and ocelli stimulation versus the compound eyes only stimulation ($F_{(1,160)} = 6.46$, $p = 0.012$). However, a closer examination on the size of this effect using partial ^{2} showed that only 3% of the difference in the normalised response was due to covering the ocelli. This result shows that the curves of normalized responses for both conditions are similar. This suggests, on first analysis, that the ocelli provide little in the way of input relevant for the calculation of directional responses.

However, based on careful examination of the time courses of the responses, a significant effect of response latency was identified between

the responses when the ocelli were simultaneously stimulated or just the compound eyes were stimulated ($F_{(1,280)} = 4.35$, $p < 0.0001$). Figure 4.13 shows a scatterplot of the response latencies for 11 neurons (5 anatomically identified $DNII_2$ cells and 6 non-identified neurons that have the same physiological characteristics) to different coloured bar stimuli (left: short-wavelength, right: green). The different velocities are represented by the different sizes of the circles. With both the compound eyes and ocelli stimulated with the green bars the response latencies were between 30 and 70 ms across 10 image velocities, while when the ocelli were covered the latencies were between 50 and 80 ms. When using the short-wavelength stimulus the latencies were between 30 and 65 ms for simultaneous compound eye and ocellar stimulation and between 55 and 85 ms when only the compound eyes were stimulated. There was no significant difference between the latencies for short-wavelength and green bar stimulation ($F_{(1,280)} = 1.55$, $p > 0.1$). There was no other main effect or any interactions between spectra, speeds of movement, and whether ocelli were stimulated or not ($F < 2$, $p > 0.05$). Thus, when the ocelli and compound eyes were simultaneously stimulated the latencies of the responses were shorter but this had only a small impact on the directional or velocity tuning of the cells based on amplitude measurements.

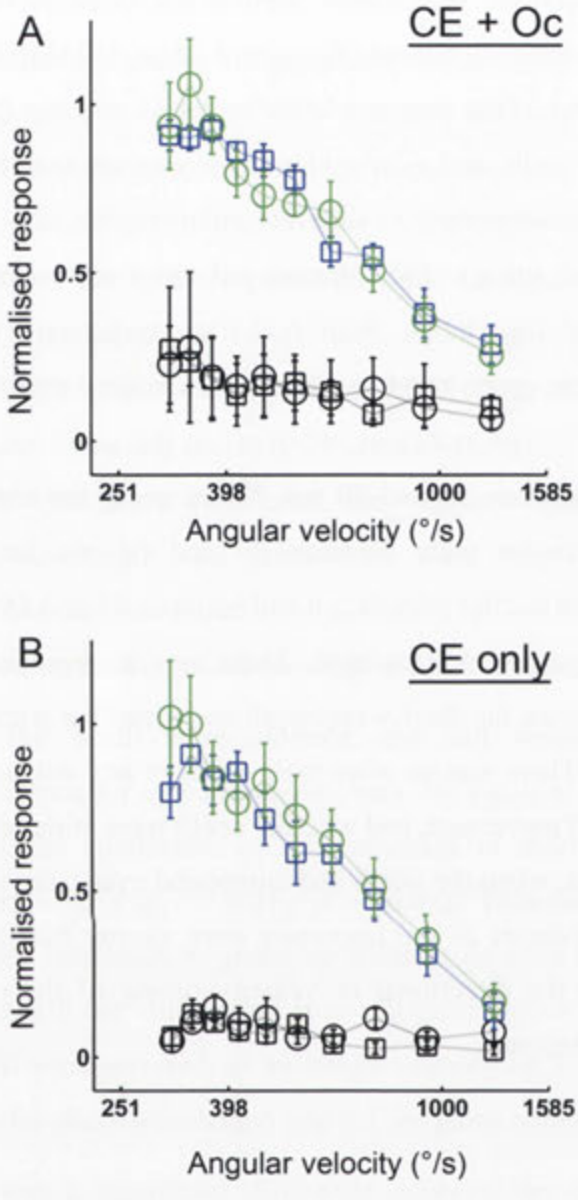

Figure 4.12: The velocity tuning function of 5 anatomically identified $DNII_2$ neurons to vertically moving bars of two different spectra. The black symbols (squares: short-wavelength; circles: green) indicate the responses to motion in the anti-preferred direction (i.e. downward moving bars) while the coloured symbols (blue squares: short-wavelength, green circles: green) indicate the responses to motion in the preferred direction (i.e. upward moving bars). The experiments were carried out with two experimental conditions: (A) when both the compound eyes and ocelli were stimulated simultaneously; (B) only the compound eyes were stimulated.

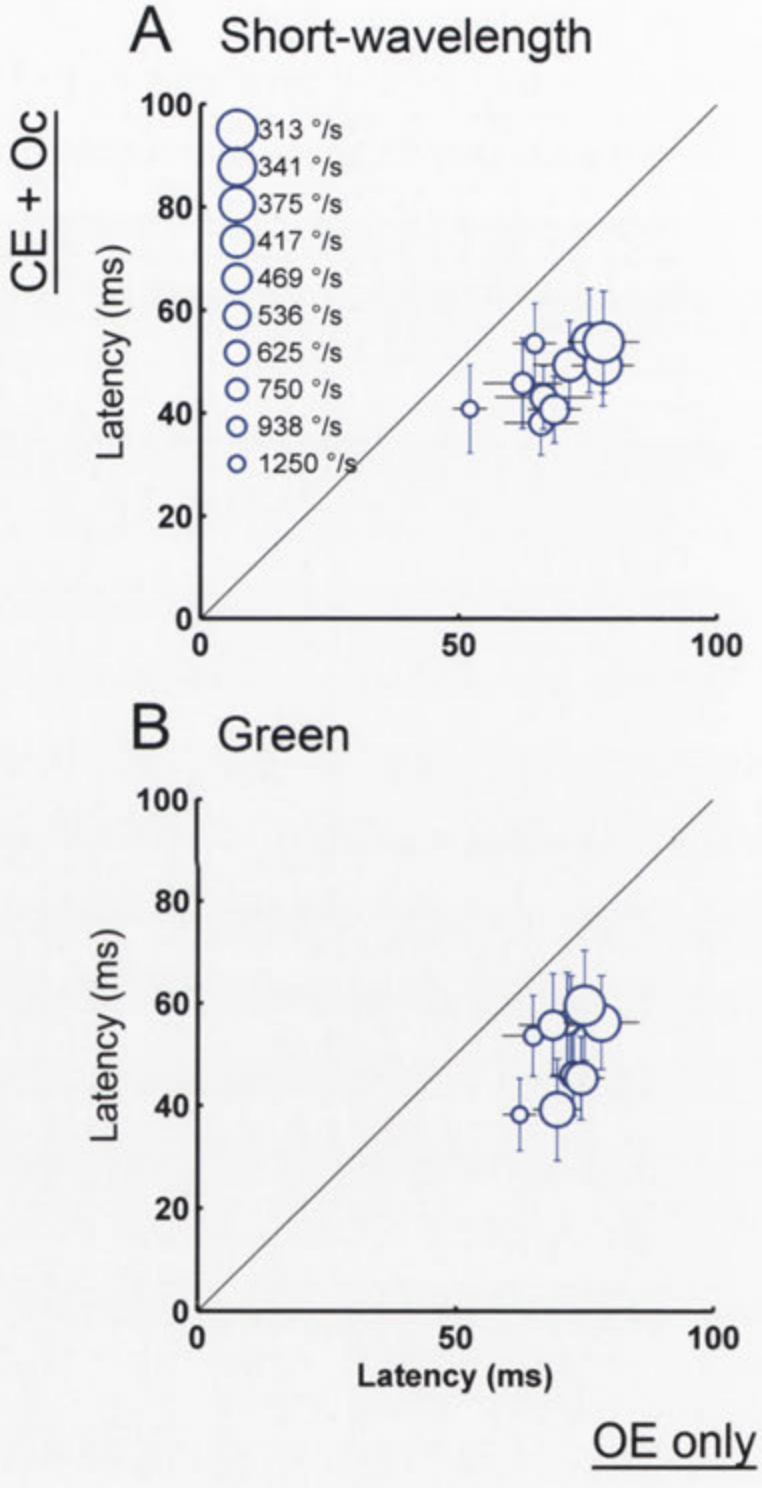
A Short-wavelength
CE + Oc
Latency (ms)
313 °/s
341 °/s
375 °/s
417 °/s
469 °/s
536 °/s
625 °/s
750 °/s
938 °/s
1250 °/s
0
20
40
60
80
100
0
50
100
B Green
Latency (ms)
Latency (ms)
OE only

Figure 4.13: Scatterplot of the response latencies to different coloured moving bars at different velocities. The experiments were carried out in two different conditions: the compound eyes were stimulated (CE only, abscissa) and both compound eyes and ocelli were stimulated (CE + Oc, ordinate). (A) shows the response latency to short-wavelength upward moving bars at different speeds, while (B) shows the latency to green upward moving bars at different speeds. The different sizes of the circles indicate the different bar velocities. When the ocelli were covered the response latencies were significantly longer than those when the compound eyes and ocelli were stimulated simultaneously ($F_{(1,280)} = 4.35$, $p < 0.0001$). In this figure, the mean and standard error were calculated from 5 anatomically identified $DNII_2$ neurons and 6 non-identified cells (n = 11).

Contrast response functions

In this experiment, the bar stimulus was moving at an angular velocity of 340 °/s, which matched the peak response observed in the velocity-tuning experiments. Contrast was presented in two forms: positive contrast was a bright bar on a mean background while negative contrast was a dark bar on the same mean background. For both polarities of contrast I increased contrast from 0.08 to 0.82. Full contrast response functions were obtained from 4 of the 12 identified $DNII_2$ neurons. Responses to positive and negative contrasts are shown in Figure 4.14. As response amplitudes were similar for all four cells only the normalised response profile is shown (as usual, responses were normalised to the maximum response to short-wavelength stimulation). A multi-way ANOVA test was applied to verify the interactions between different test conditions: contrast, contrast polarity (negative or positive contrasts), and test spectrum (short-wavelength or green). It is shown that there is no significant interaction between each condition ($F < 2$, $p > 0.1$), so the effects of the test conditions on the normalised response are independent of each other. A significant effect of contrast was shown because, for both positive and negative contrasts, the response amplitude increased when contrast increased ($F_{(4,140)} = 28$, $p < 0.0001$). Responses to negative contrasts for both green and short-wavelength stimulation had larger amplitudes compared to the positive contrast condition. The differences between the response amplitudes for the two contrast polarities were significant ($F_{(1,140)} = 15$, $p < 0.0001$).

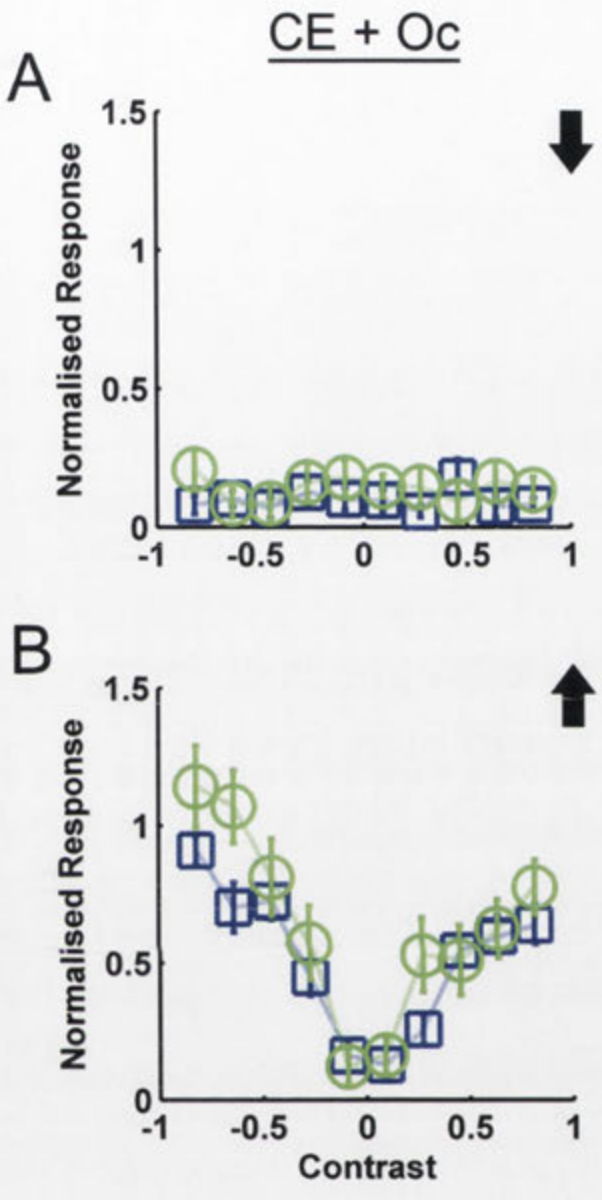

Figure 4.14: Contrast responses of $DNII_2$ to two different coloured moving bars; the direction of the vertically moving bars is shown with black arrows (A: responses to downward moving bars; B: responses to upward moving bars). Both negative and positive contrasts were tested; the test range was from -0.82 to 0.82 (for two polarities). The figure shows a result of averaging 4 anatomically identified $DNII_2$ cells together after normalising the responses to the maximum values obtained with short-wavelength stimulation. Green circles and blue squares represent the responses to green and short-wavelength stimuli respectively.

Responses to gratings

Figure 4.15A shows a typical spiking response of an anatomically identified $DNII_2$ neuron to a moving grating (spatial wavelength: 72°; speed: 75 °/s) travelling down (left) and up (right) across the stimulus array. Clearly this cell is directional, as can be seen by the difference in its responses to upward and downward gratings. The cell also responds strongly to the time-locked passage of the gratings for downward motion (Fig 4.15B). Given that this occurs during downward motion, despite the cell being direction-selective it suggests that the cell is quite responsive to the brightness change irrespective of whether the stimulus is moving. These responses could, therefore, be regarded as flicker response components. The directional index (DI) was used to quantify the directionality of the response (see Equation (2) in Methods). The mean DI and standard errors measured from two identified $DNII_2$ cells are shown in Figure 4.16. Each cell has 3, 5, or 7 repeats for spatial wavelengths of 120°, 72° and 48°, respectively. While the circular and square symbols represent the 75 °/s and 750 °/s gratings respectively, the colours of the grating stimuli are also indicated by different colours (green stimulus: green; short-wavelength stimulus: blue). In this experiment, both the ocelli and compound eyes were stimulated simultaneously.

A multi-way ANOVA test was performed to understand the interactions between each condition (speeds, spatial wavelengths and colours of the gratings). It is shown that there is a strong 3-way interaction between the three conditions ($F_{(2,108)} = 4.7$, $p = 0.01$), and a large interaction between grating speeds and spatial wavelengths ($F_{(2,108)} = 18.7$, $p < 0.0001$). At a speed of 75°/s the DI values do not depend on the colour of the grating and do not vary much with different spatial wavelengths ($F_{(1,108)} = 0.57$, $p > 0.05$). However, when the gratings are moving at 750 °/s it can be seen that there is a significant interaction between the light spectrum and spatial wavelengths ($F_{(2,59)} = 3.8$, $p = 0.029$), i.e. the cell responds differently to short-wavelength and green gratings at different spatial wavelengths. The response of the cell to short-wavelength gratings appears to be more

directional at low spatial wavelengths than it is to green gratings at a velocity of 750°/s.

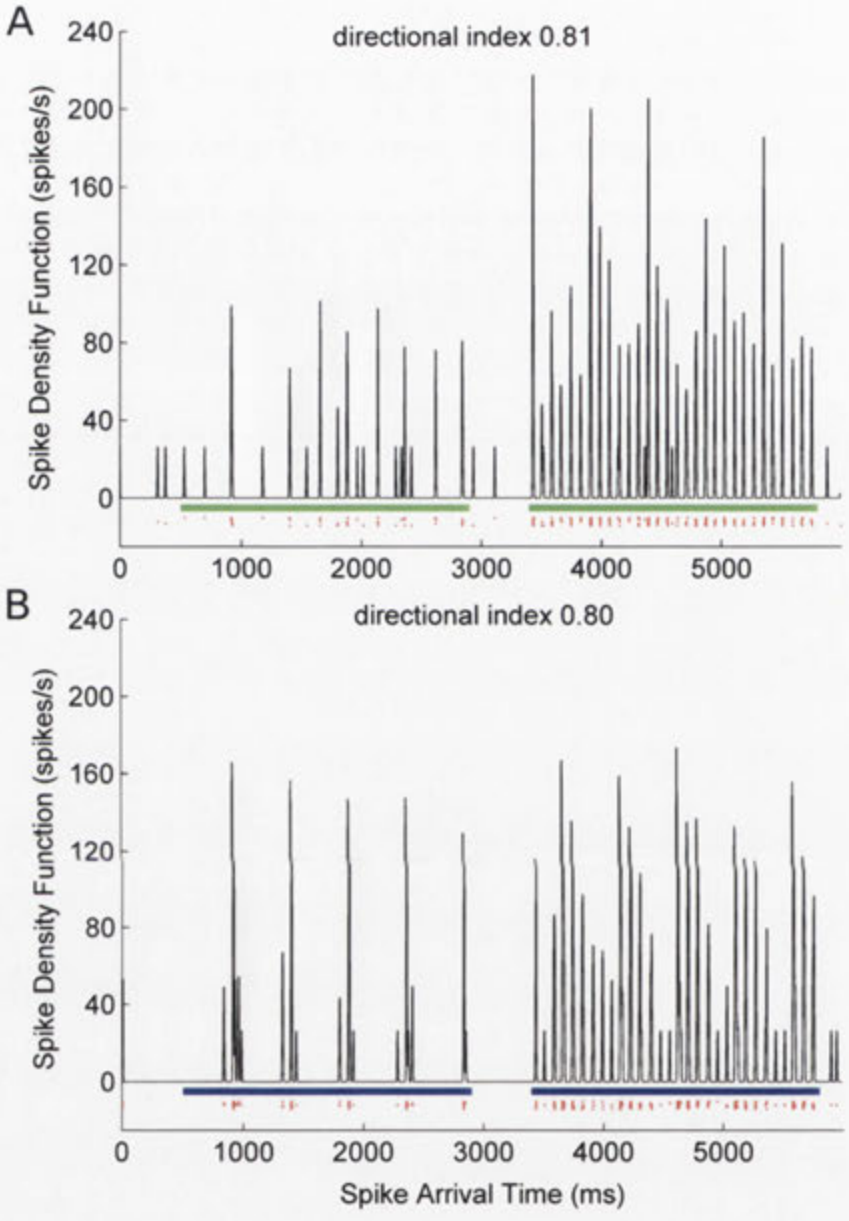

Figure 4.15: Spike density function of grating responses for an anatomically identified $DNII_2$ neuron. The gratings had spatial wavelengths of 72° (speed 75 °/s) and moved up (right) or down (left). A: response to **green** gratings. B: response to **short-wavelength** gratings. It is shown that while the cell response is highly directional to both gratings, the cell showed strong phase-locked excitatory responses for the short-wavelength grating during downward motion. The DIs were calculated from the spikes within the stimulus time for both directions of motion.

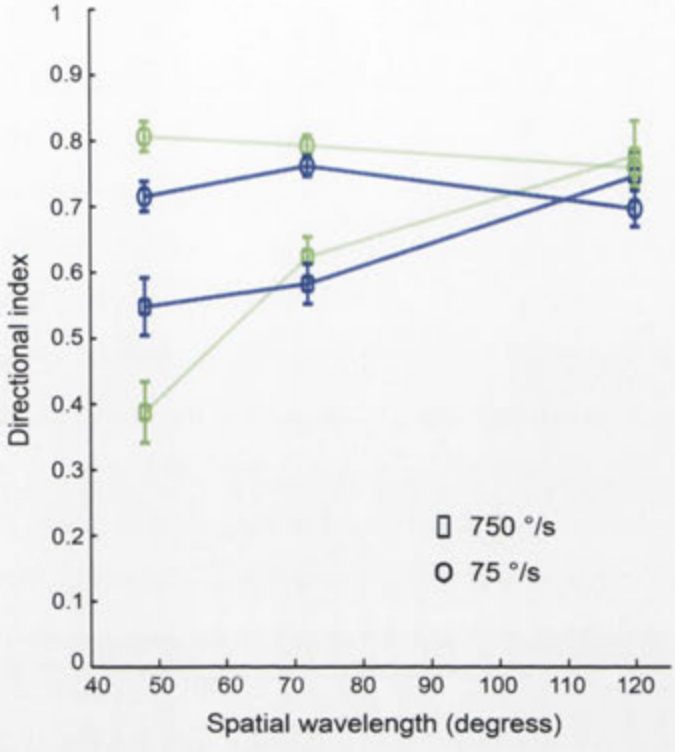

Figure 4.16: The directional index of two identified $DNII_2$ neurons to grating stimuli. The square symbols show the results from gratings moving at 750 °/s while the circles show results at 75 °/s. The spectra of the gratings are also shown in different coloured symbols: green: green gratings; blue: short-wavelength gratings. The DI for the cell remained similar for both green and short-wavelength gratings when the gratings moved at 75 °/s. At 750 °/s the cell response was more directional when using the short-wavelength gratings at a spatial wavelength of 48°.

Directional ocellar inputs to $DNII_2$

In the section above, it was suggested that the ocelli provide little input in terms of the amplitudes of the direction-selective responses. Those conclusions were, however, drawn from analysis in which the responses during the stimulus presentation were considered. Here, I consider the after-responses that occur once the stimulus is removed from the receptive fields of the recorded neurons. Figure 4.17 shows responses to green moving bars (contrast -0.82) in the preferred direction (top row) and the anti-preferred direction (lower row). When the ocelli were uncovered (left column) an excitatory rebound response was observed after the bar left the screen (Fig 4.17B). This rebound response was not present when the ocelli were covered (Fig. 4.17D). While the $DNII_2$ cell generates an excitatory response to upward moving bars, there was also an excitatory rebound response after motion in the anti-preferred direction (i.e. downward moving bars). To measure the rebound response, a 78 ms time window was utilised in the period immediately following the removal of the stimulus. The mean and standard error of the responses during this window are shown for 5 identified $DNII_2$ cells in Fig 4.18. The results show that when the ocelli were occluded, there was no response in the post-stimulus time window for motion in the anti-preferred direction (Fig 4.18D). However, when the ocelli were uncovered, an excitatory rebound response with a peak of around 20 spikes/s was generated after motion in the anti-preferred direction (Fig 4.18C). These responses were the same regardless of whether the bars were short-wavelength or green ($F_{(1,160)} = 0.46$, $p > 0.1$). Although there is some increased spiking activity after motion in the preferred direction this occurs because the tail of the excitatory response during the stimulus intrudes into the post-stimulus window (Fig 4.17AB). The responses after motion in the preferred direction showed no significant difference for the cases where the ocelli were covered and uncovered ($F_{(1,160)} = 1$, $p > 0.1$), showing that the ocellar effect is selective for the period after motion in the anti-preferred direction.

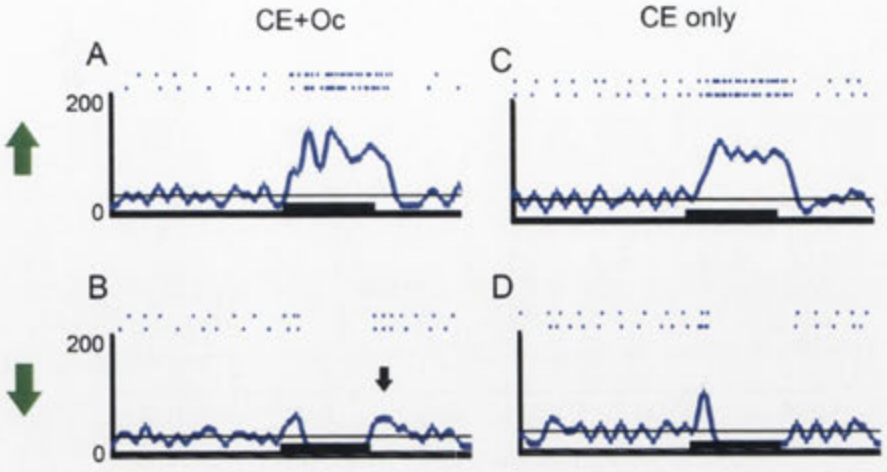

Figure 4.17: The spike density functions of an anatomically identified $DNII_2$ neuron to green vertical moving bars. The green arrows indicate the directions of the bar motion- upper row: upward moving bars (preferred direction); lower row: downward moving bars (anti-preferred direction). It is shown that when both the compound eyes and ocelli were stimulated simultaneously (left column; CE + Oc) there was a small after response for the anti-preferred direction (as indicated with the black arrow), while when only the compound eyes were stimulated, no after response was present. The black line in all the figures indicates the spontaneous response rate.

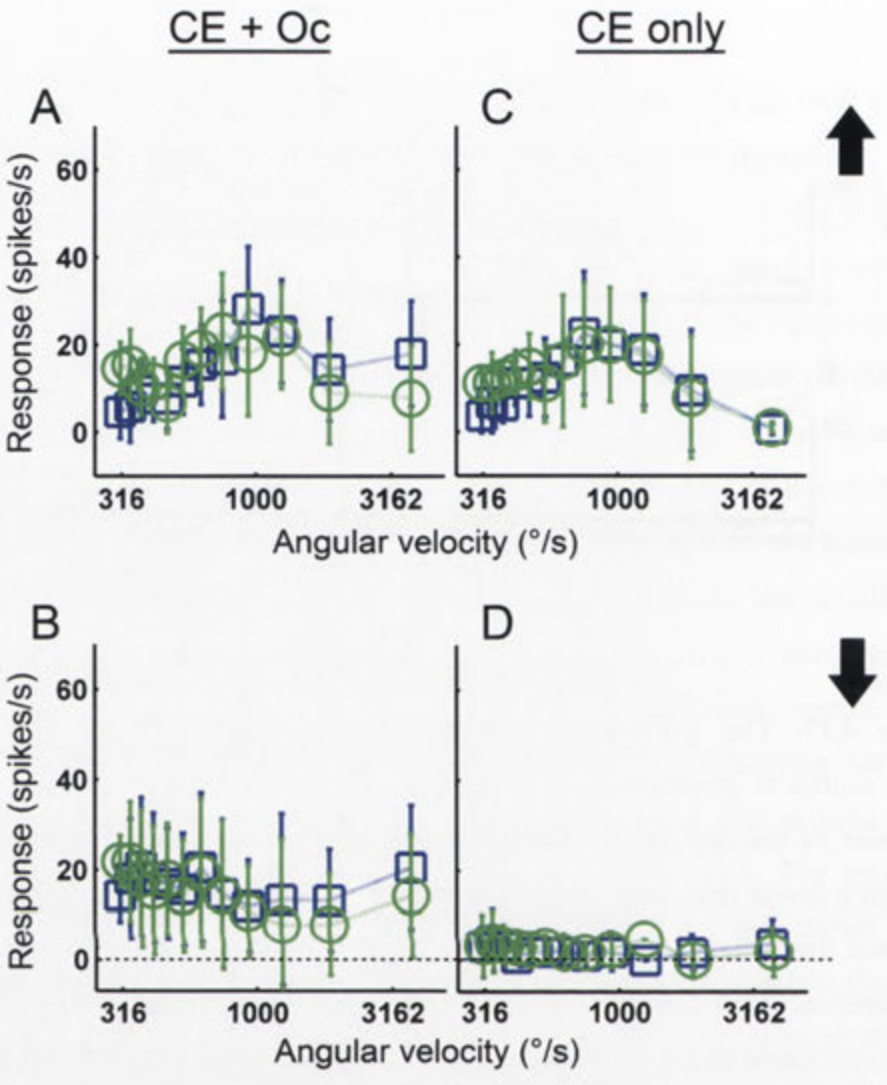

Figure 4.18: The after responses of 5 anatomically identified $DNII_2$ neurons. The responses in a 78 ms time window after the stimulus were measured. The upper row shows the responses after the preferred direction while the lower row shows the responses after the anti-preferred direction.

4.4.4 Lateral ocellar descending neuron (Locth3)

Flash response

Type I flashed stimulus: Two confirmed recordings were made from Locth3 using the type I flashed stimulus. In general the response characteristics were similar between preparations, except for one noticeable difference. For both neurons, when stimulating the compound eyes and ocelli simultaneously with a 200 ms flash (combined short-wavelength and green LEDs), the background firing rate was strongly inhibited during the stimulus. Soon after the stimulus was removed from the screen there was a robust excitatory OFF response. The latency to the onset of the inhibition and the OFF excitation was ~20 ms. However, one of the recorded cells also showed a highly phasic ON response with a 50 ms latency soon after the onset of the bright flash (Fig 4.19). The strong ON response occurred after the inhibitory phase had begun and the ON response was very brief, so for the remainder of the stimulus there was continued inhibition for part of the flash duration. The flash was followed by a strong OFF response with a latency of 19 ms. In this second preparation it is interesting to note from the raster plots that the OFF response is highly time-locked (i.e. all initial spikes occur within 10 ms of each other across 40 trials). In contrast, the ON response had a far more variable initial spike arrival time (i.e. within 30 ms across 40 trials), which perhaps suggests that the signal travelled on a more circuitous route that may have involved multiple synapses.

Type II flashed stimulus: The type II stimuli generated single spectrum (either short-wavelength or green) brightness increments or decrements (against a fixed background luminance of the same spectral type). By applying the stimuli, it is shown that the $Locth_3$ neuron generated small excitatory responses to both short-wavelength and green brightness decrements (right hand column, Fig 4.20). The time-to-peak for both the responses was around 20 ms. A clear OFF response was also evident after the offset of the short-wavelength increment (top row, left column). There

were no statistically reliable responses to brightness increments (left column).

Directional response

In the present study, I tested responses to bar movements in $Locth_3$ generated by the wide-field LED display at four different speeds (ranging from 288-2500 °/s) for vertical and horizontal moving bars (either short-wavelength or green). The contrast for all bar stimuli in this experiment was -0.82. Similar results were observed for both the short-wavelength and green stimuli (Figure 4.21, 4.22, 4.23). Figure 4.21 and 4.22 show the $Locth_3$ responses to short-wavelength and green vertically moving bars (there were 6 trials for each of the tested speeds). At moderate speeds (288-375 °/s), $Locth_3$ generated relatively weak, but significant (t-test, $p<0.01$), excitatory responses to upward moving bars and no significant change in spiking activity during downward motion. When the speed of the bar movement increased to 937 °/s, no response was observed for either spectra. It is also shown that in both spectra, there was an excitatory response shown for some of the speeds tested (375 and 288 °/s for short-wavelength bar stimuli; 536 °/s for green bar stimuli) with a latency of ~30 ms (black dashed line in Fig 4.21 and 4.22). The excitatory responses were then followed by a continuous tonic response. It is possible that the initial phasic responses shown were the responses to the bar moving into the receptive field (light OFF response; as it was a bar of negative contrast relative to the background), however, this response was not observed for any other bar stimuli (eg. downward moving bars or horizontal bar movements). The cell responses to horizontal movements were very small or absent (Fig 4.23). In summary, the directional responses of $Locth_3$ are similar to those of $DNII_2$ but the responses to moving bars are considerably less robust.

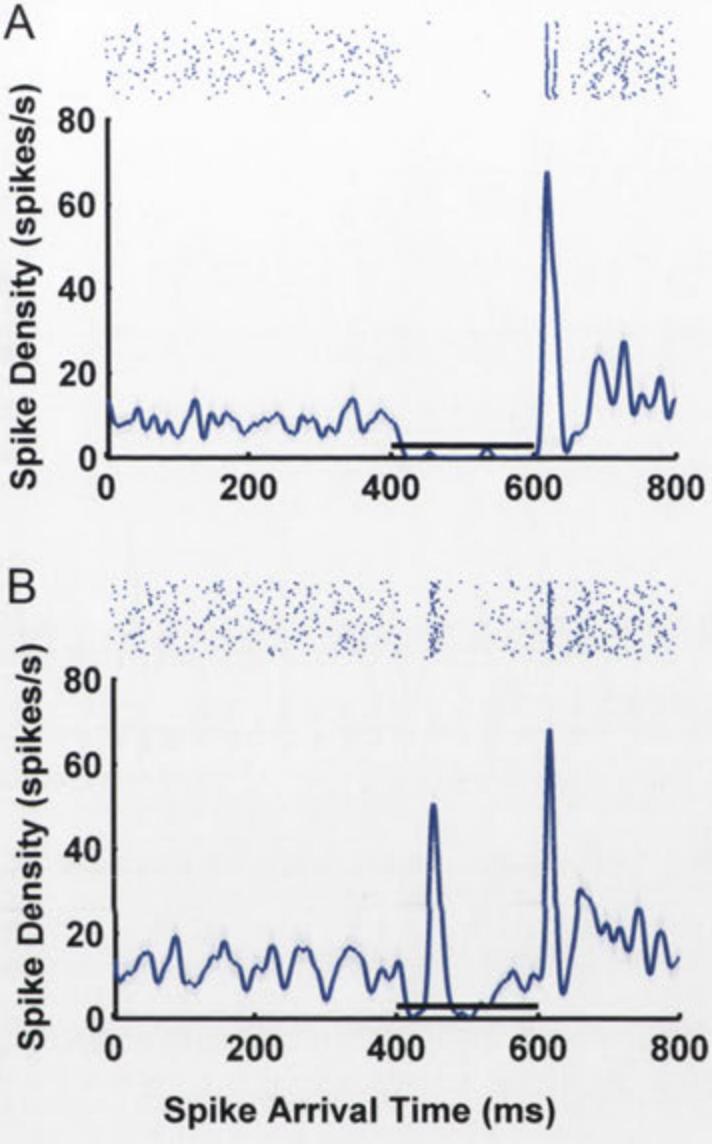

Figure 4.19: Responses of Type I flashed stimuli from two anatomically identified Locth$_3$ neurons. A: The Locth$_3$ showed a clear inhibitory response when the light was turned ON. A robust OFF excitatory response was also generated with a latency of 20 ms. B: In the other preparation, Locth$_3$ showed a robust ON response with a delay of 50 ms. An inhibition during the light ON period was also observed in this preparation.

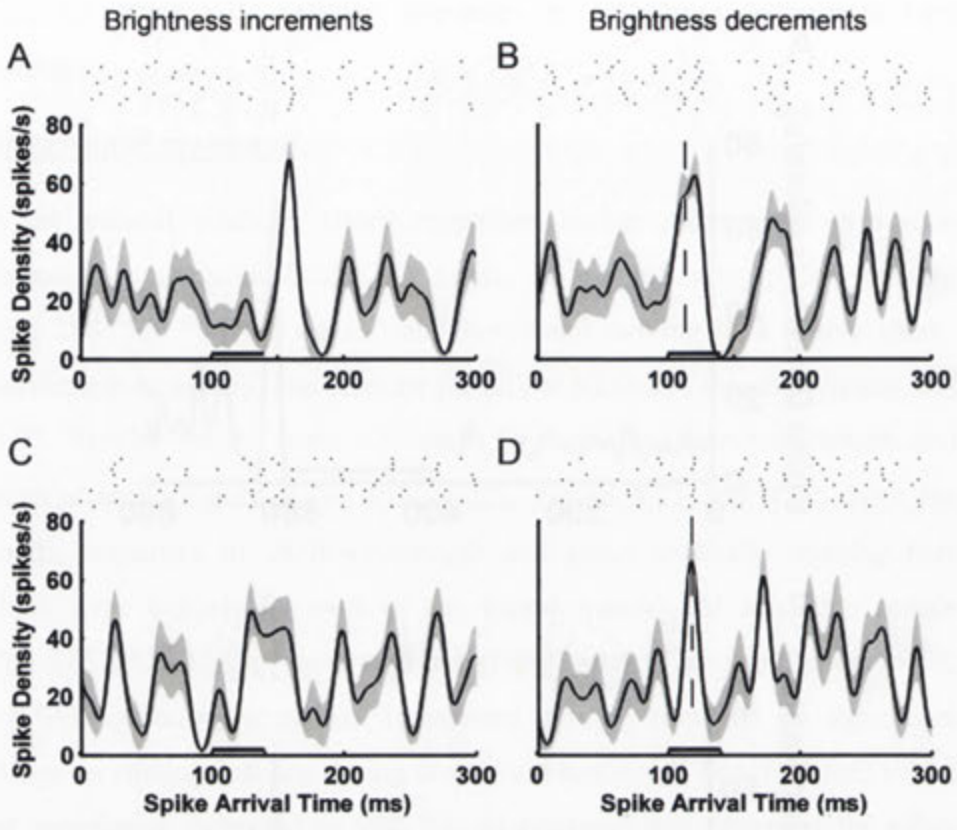

Figure 4.20: The Locth$_3$ responses to brightness increment and decrement flashes to either short-wavelength (upper row) or green (lower row). The gray areas show the standard error. The black dashed lines indicate the response to the stimuli. It is shown that Locth$_3$ responded to both the short-wavelength and green brightness decrements (right column) with latencies of ~20 ms. No excitatory response was observed for brightness increment flashes (left column).

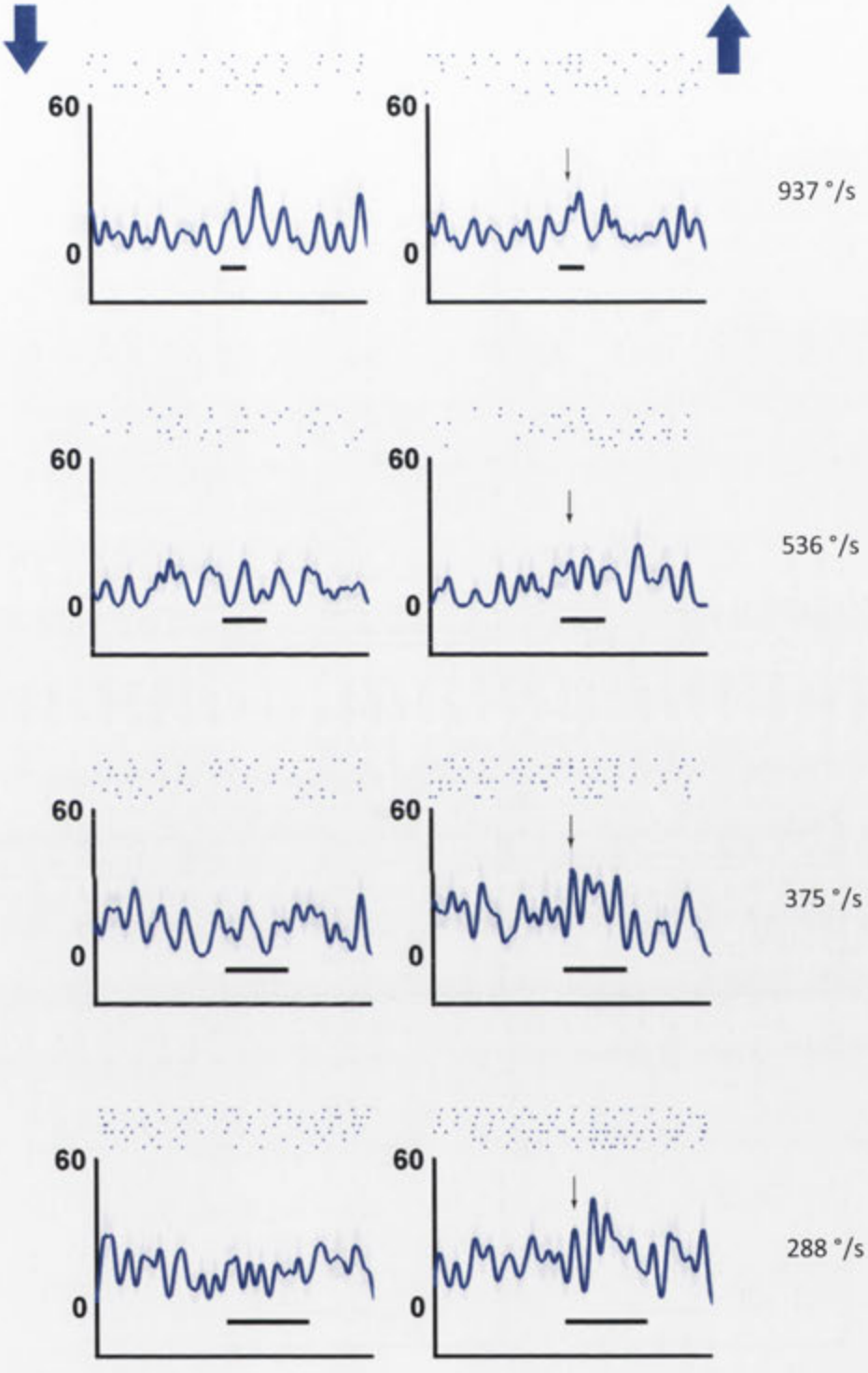

Figure 4.21: Responses of $Locth_3$ to vertically moving **short-wavelength** bars. It is shown that $Locth_3$ is motion-sensitive to upward motion for the tested speeds when stimulated by short-wavelength moving bars. The black dashed line indicates a latency of 30 ms.

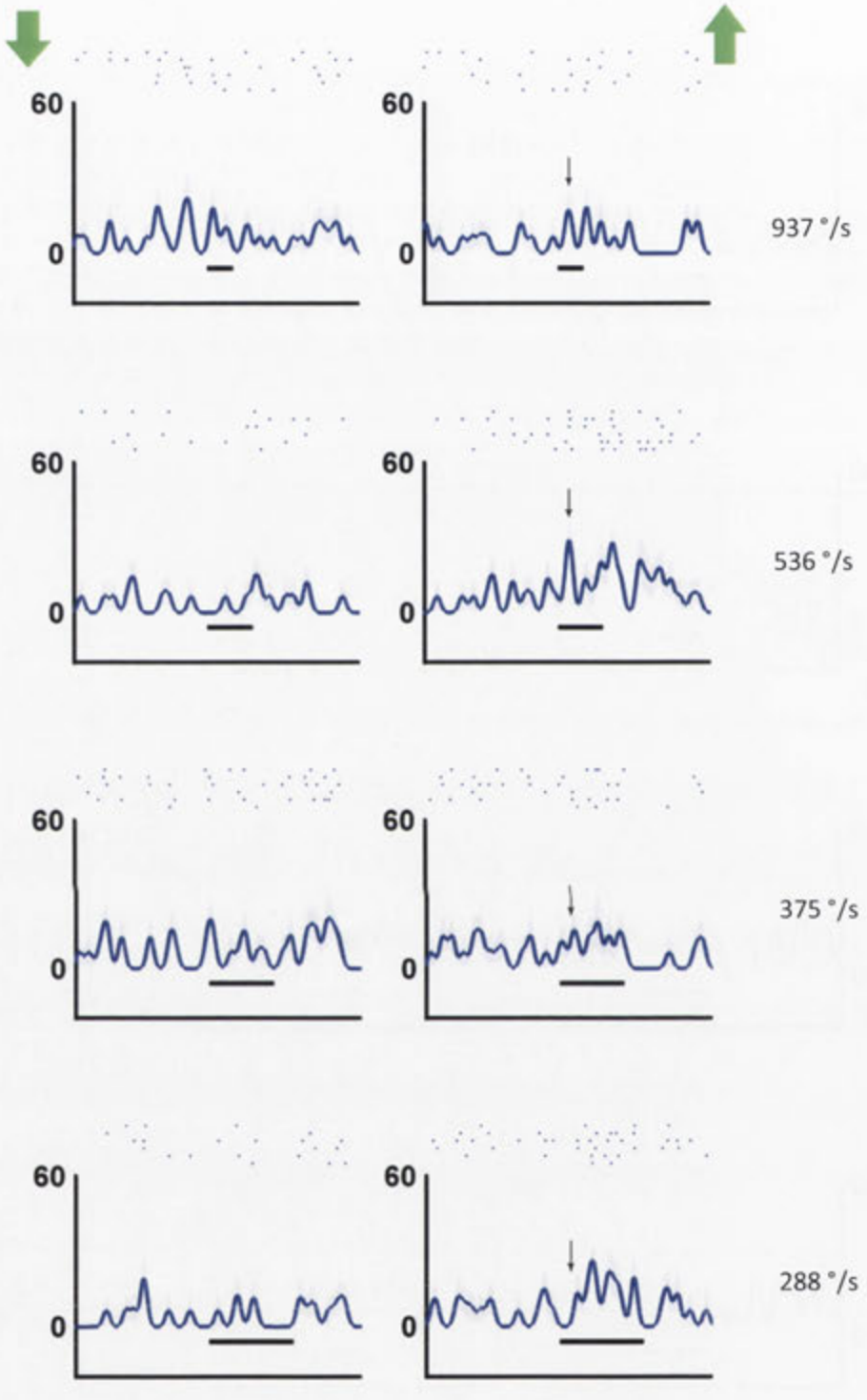

Figure 4.22: Response of $Locth_3$ to vertically moving **green** bars. It is shown that $Locth_3$ is motion-sensitive to upward motion at the tested speeds. The black dashed line indicates a period of 34 ms from stimulus onset, which approximately matches the latency of the cell across the four conditions.

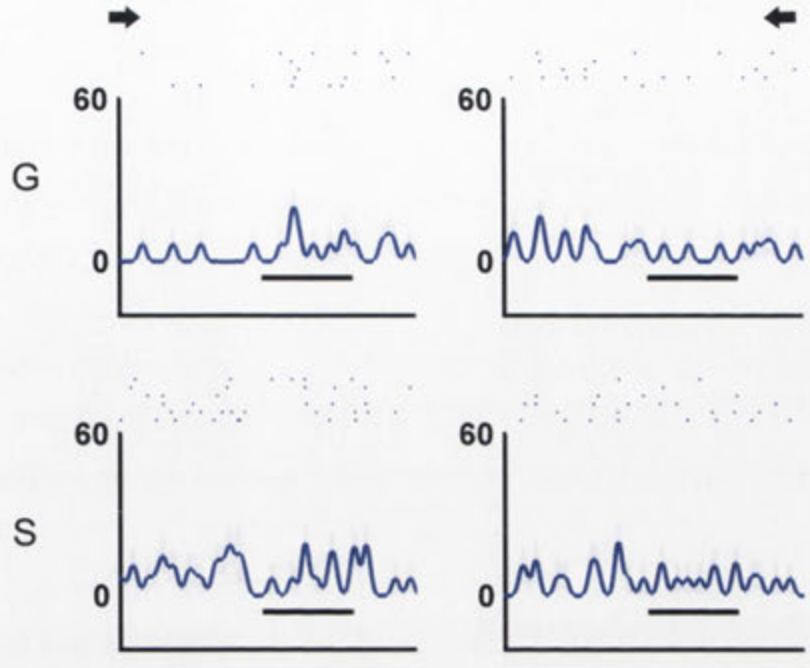

Figure 4.23: Responses of $Locth_3$ to horizontally moving bars at 577 °/s (horizontal motion). No significant response was generated during either green (G) or short-wavelength (S) horizontal motions.

4.5 Discussion

The fact that honeybee motion-sensitive descending neurons are directionally selective suggests that they play an important role in producing the compensatory movements that underlie course correction, like those seen in the optomotor response (Hengstenberg, 1993). A previous study of the honeybee $DNII_2$ neuron has provided a thorough characterisation of its responses to moving wide-field gratings (Ibbotson and Goodman 1990). That study showed that these neurons are highly direction-selective to upward motion and the response magnitude is dependent on the temporal frequency of grating motion (i.e. the ratio between angular velocity and the spatial period of the pattern). A previous study of the motion sensitivity of $Locth_3$ also revealed sensitivity for upward motion in the frontal visual field (Goodman et al. 1990). In that study the neuron was tested with speeds ranging from 90°/s to 300°/s. The cell was highly direction selective across all of this speed range. It has now been shown in the present Chapter that it is also direction-selective out to far higher speeds of >750°/s. As with $DNII_2$, $Locth_3$ is highly sensitive to high image speeds. Several studies have shown that flying insects can respond to rotations at angular velocities of up to 2000 °/s (Ibbotson 2001; Lewen et al., 2001; van Kleef et al., 2008). van Hateren and Schilstra (1999) observed the head and thorax movements of free flying blowflies and discovered that they perform a series of short, saccade-like turns at the rate of about 10 per second. These generate rotations in roll, pitch and yaw with angular velocities of up to 2000 °/s. Therefore, in this study, moving bar stimuli with a wide range of speeds were used to examine the velocity tuning in $DNII_2$ and $Locth_3$. The cells show clear velocity-dependent responses to motion in the preferred direction (upward motion) that peak at speeds around 300°/s. The response amplitude decreased to 50% of the peak when the speed had increased to around 1000°/s. Directional responses at the high speeds have been observed in insect neurons that receive compound eye input (Ibbotson 1991; Olberg 1981a; O'Carroll et al. 1996; Lewen et al. 2001). In dragonfly ocellar L-

neurons, van Kleef et al. (2008) also showed that the neurons were direction-selective to short-wavelength (380nm) bars moving as fast as 3750 °/s. However, in the present study the ocellar contribution to motion detection in $DNII_2$ was shown to be small because the velocity tuning curves obtained when the ocelli were covered remained similar to when they were uncovered (although there were significant differences, the relative change was small at ~3%).

4.5.1 The short-wavelength motion sensitive descending neuron $DNII_2$

In the mid-1970s Kaiser established that, for the honeybee, the behaviourally measured spectral sensitivity of the optomotor response almost exactly matched that of the green photoreceptors (R1-R6) found in the bee retina (Autrum and von Zwehl, 1964; Menzel and Blakers, 1976; Menzel et al., 1986; Kaiser and Liske, 1974; Kaiser, 1975). This suggested that the optomotor response was exclusively driven by the green photoreceptors. Similar results were obtained in dragonflies (Horridge et al. 1990) and recent results in *Drosophila* have shown that the motion pathway is exclusively mediated by the photoreceptors R1-R6 (which is the motion channel; color channel: R7/R8) and therefore is independent of color (Yamaguchi et al. 2008; Yamaguchi et al. 2010). However, this was very recently challenged by experiments demonstrating the involvement of other spectral classes of photoreceptors (R7-R8, Wardill et al. 2012). It was shown that instead of using just one class of photoreceptor, the R7 and R8 receptors also contribute to the motion pathway by convergence of all channels at the large monopolar cell level in the optic lobes. This convergence improves motion discrimination.

It has been suggested that for theoretical reasons motion processing is 'colour blind' (Srinivasan, 1985). This suggestion gave rise to some controversy because von Frisch (1914, 1967) had long before demonstrated

colour vision in honeybees. Recent studies of motion vision in *Drosophila* (Yamaguchi et al., 2008) and bumblebees (Paulk et al., 2008) have also shown that motion and colour processing pathways are segregated. However, Paulk et al. (2008) did find that some lobula cells were sensitive to both colour and motion, which suggested that although the motion and color information pathways are initially segregated they converge in bees in the higher order neurons. The convergence of the motion and color information pathways can also be proved by behavioural experiments. Stojcev et al. (2011) found that in honeybees and gold fishes, the short and medium wavelength receptors (color pathway) contribute to slower speeds (6 and 12 Hz) motion-sensitive behavioural responses; however at a higher speed of motion (24 Hz), it is found that the animals use long wavelength inputs exclusively for the motion-sensitive behavioural responses. In the present study, similar results were found on the $DNII_2$ grating responses, that is, the response of the cell to short-wavelength gratings appears to be more directional at low spatial wavelengths than it is to green gratings at high velocity gratings (750°/s).

In the present study I have demonstrated that two motion-sensitive cells, known to be on the optomotor pathway in bees, respond equally to short-wavelength and green moving patterns. Moreover, both green and short-wavelength flashed stimuli generate very strong responses in the cells. The evidence strongly supports the view that neurons on the optomotor pathway of the bee not only receive input from green receptor inputs but also from the UV or blue receptors. Although, we cannot be certain whether blue or UV receptors are responsible in this case (see Fig 4.2C for the theoretical quantum catch for photoreceptors to short-wavelength stimulation), the data clearly show that there is more than one type of photoreceptor involved in the honeybee optomotor response. The fact that selective stimulation of the system with only short-wavelength stimulation produces direction-selective responses suggests that short-wavelength inputs are integrated into the direction-selective motion detectors in the bee. This would not be consistent with a single-channel spectral system. Where might

these short-wavelength inputs arise? Would it be purely from the compound eyes, or are the ocelli contributing to the short-wavelength inputs?

Recently it has been shown that neurons receiving input from the ocelli of dragonflies are motion sensitive and direction-selective when stimulated by moving bars of light at 380 nm (van Kleef et al. 2008). Given that this occurs in another insect species it is plausible that in the honeybee, the short-wavelength responses of the descending neuron $DNII_2$ may also receive a directional signal from the ocelli. I have shown that the velocity tuning function of $DNII_2$ is the same when both the compound eyes and ocelli are stimulated simultaneously and when only the compound eyes are stimulated alone. Also, the responses to short-wavelength and green show no difference between the two stimulated conditions. Although, there is some evidence that the ocelli influence these signals in selected stimulus conditions (i.e. after-response in the anti-preferred direction), the results suggest that the primary input to the directional responses of the $DNII_2$ neurons for both green and short-wavelength stimulation arise in the compound eyes.

Electrophysiological evidence from several studies shows that UV signals arise from the compound eye pathway (optic lobes). The spectral sensitivity of honeybee lobula motion sensitive units has a green peak and a secondary peak in the UV region of the spectrum (Bishop 1970; Menzel 1973). Studies on fly (Australian Sheep Blowfly, *Lucillia cuprina*) optic lobes also provide physiological evidence that the motion sensitive units in the optic lobe are sensitive to green and short-wavelengths (Srinivasan and Guy 1990). That is, lobula motion sensitive units that respond to flashes as well as movement possess a dual-peaked spectral sensitivity in the UV and blue-green region of the spectrum (Srinivasan and Guy 1990).

The compound eyes of the worker honeybee consist of approximately 5500 ommatidia, with different eye regions looking at different portions of the visual environment. Although, the spectral heterogeneity of honeybee ommatidia show that the green photoreceptors

distribute equally throughout the compound eye, the UV- and blue-photoreceptors have different densities in different eye regions (Wakauwa et al. 2005). Only by applying behavioural tests can one reveal whether the final product of information processing is determined at the level of the receptors. Several behavioural studies show that honeybees use different eye regions to detect different colours, forms, and movements of an object (Giger and Srinivasan 1997; Lehrer 1998). However, in both flies and bees there is some evidence that pattern matching need not be retinotopic (Efler and Ronacher 2000; Campbell 2001; Tang et al. 2004).

With the wide-field LED display used in this study, the stimuli were restricted to frontal and dorsal eye regions, while Kaiser's experiments stimulated the ventral eye region only. Behavioural experiments on the fly *Musca domestica* have shown that the optomotor response was UV sensitive when the dorsal frontal region of the compound eyes was stimulated (Eckert 1971). In concurrence with this observation in flies, the data presented here suggests that the optomotor system of the bee receives input from more than the green photoreceptors but that this may be regionalised within the compound eyes.

4.5.2 Ocellar inputs to $DNII_2$ and $Locth_3$

Two spectral classes of photoreceptors have been identified in the ocellar retina of the bee, a green channel and an ultra-violet (UV) channel. The peak sensitivities of these channels are, respectively, 350 nm and 490 nm. There is no blue receptor in the honeybee ocellus, so we can be certain that any short-wavelength stimulation of the ocelli stimulated the UV channel. Our short-wavelength stimulus had a peak output at 380 nm with a bandwidth of 15 nm, while the green LED had a peak at 530 nm with a bandwidth of 30 nm. The output of the green LED did not overlap with the spectral sensitivity of the UV receptor, but no wavelength of light, even down to wavelengths as short as 300 nm is capable of selective UV-

stimulation without partially activating the green channel (see the spectral sensitivity in Fig 4.2A). Given that ocellar stimulation with the short-wavelength stimulus generated responses as large as those with the green LEDs, it is highly probable that the UV-photoreceptors in the ocellar retinae provide strong input to the descending neurons, as do the green ocellar photoreceptors.

Previous studies on honeybee motion-sensitive neurons have classified these neurons according to their neural morphology and physiological response characteristics. However, those studies were mainly focused on the neuronal responses to whole-field stimulation, which stimulated both the compound eyes and ocelli. Evidence from anatomical studies of ocellar neurons and the neuronal projections from the compound eye pathway suggest there may be connections between those two visual systems. For example, the arborisations of ocellar neurons have been discovered in several brain regions: posterior neuropil, optic lobes, and protocerebral bridge in different insects (locusts: Goodman 1974; Goodman and Williams 1976; cricket: Knoontz 1976; bee: Kenyon 1896; Cajal 1918; Heinzeller 1976; Pan and Goodman 1977; Milde 1981). Not surprisingly, electrical and synaptic connections between the compound eyes and ocelli have also been reported (fly: Strausfeld 1970; Parsons et al., 2006; bee: Heinzeller 1976; Pan and Goodman 1977; locusts: Goodman and Williams 1976; cricket: Koontz 1976) and the direct connection between ocellar neurons and cells in the ventral nerve cord (descending neurons) has been identified in the locust (Guy et al. 1977; Simmons 1981) and honeybee (Guy et al. 1979).

Unlike the compound eyes, which are known to be responsible for form vision and motion detection, early studies of insect ocelli have inferred from anatomical and optical evidence that the ocellar lenses are under-focussed, therefore, individual ocelli are not capable of processing directional information (Wilson 1978; Wehner 1981; Schuppe and Hengstenberg 1993). However, under-focused ocellar lenses do not

necessarily exclude the possibility of detecting form, or motion vision. Schuppe and Hengstenberg (1993) examined blowfly ocelli (*Calliphora erythrocephala*) and found that despite the under focussing of the ocellar lens, low spatial frequency patterns could be imaged on the retinal plane. Growing evidence has shown that the ocelli are able to resolve some spatial information, e.g. dragonflies (Stange et al. 2002; Berry et al. 2006; Berry et al. 2007ab; van Kleef et al. 2008), and wasps (Warrant et al. 2006). In honeybee, despite the under-focusing lenses that form a focal plane behind the retinal level, some spatial detail can still be formed on the retinal plane of the dorsal ocellar retinas (see Chapter 2). It is plausible that the honeybee ocelli may play a role in motion detection.

In this study I examined the possibility of there being ocellar inputs to the motion-sensitive descending neurons. This was achieved for $DNII_2$ by providing visual stimulation (flashed stimuli and motion) and comparing the neural responses when both the compound eyes and ocelli were uncovered with responses obtained when only the compound eyes were uncovered. It is shown that the ocelli contribute a robust OFF transient response to the $DNII_2$ neuron and provide a faster response to ON stimulation.

While it was not possible to do tests in which the ocelli were covered for $Locth_3$, an interesting finding was that there was a very clear and very short-latency OFF response after flashes of light (time to peak of ~20 ms). It should be noted that the measurements used here were time to peak, rather than using a threshold based on the spike density function. When a threshold was used the measured latencies were typically 10 ms less, but the measurements were less reliable. Thus, the short-latency responses could be as short as 10 ms before the first detectable change based on a population average across many trials. This suggests that these responses almost certainly arose from the ocellar input. Noticeably, the short-latency responses were very precise, with highly time-locked spike arrival times, suggesting a single-synapse pathway. In contrast the ON responses that were observed in one recording from $Locth_3$ were long-latency and the

arrival times were far more variable. While I cannot give a categorical answer to the origins of the ON response, the evidence points towards the input having come from the compound eyes via a slower, possibly multi-synaptic pathway. It has been observed in flies that the ocellar and lobula plate neurons are electrically coupled (Strausfeld 1976). It is plausible that this is the case in bees too.

Previously, using a flashed stimulus, Guy et al. (1979) had showed that the latency of ocellar and compound eye pathways was 6-9 ms in descending units based on intracellular subthreshold measurements, rather than spiking output. In this study I showed that when both compound eyes and ocelli were stimulated, the latency of the spiking ON transient response appeared to be 7 ms faster than compound-eye only stimulation. Similar observations on fly pre-motor descending neurons also suggest that fast electrical connections couple ocellar and compound eye visual interneurons (Parsons et al. 2006, 2010; Haag et al. 2007).

How optic flow is translated into motor system commands remains poorly understood. Theobald et al. (2009) measured the temporal dynamics of optomotor responses in tethered flies to optic flow and found that the flies reacted very quickly with pure delays in the order of ~20ms and with a maximum response (time-to-peak) of ~100ms. The time-to-peak response for pitch appeared to be faster than other directions with latencies of ~50ms. In honeybees, the latency of the optomotor response is unclear. In the $DNII_2$ neuron the response time-to-peak to motion in the preferred direction was measured as 30–70 ms for 10 different speeds. However, when the ocelli were covered the response time-to-peak increased to 50–80 ms. This suggests that the ocelli play a role in reducing the latency of motion signals and, therefore, may lead to a faster behavioural response.

Another feature of the ocellar input to $DNII_2$ was the weak but consistent directional effect noted after the cessation of the downward (anti-preferred) motion stimulus. Given that with static flashes the ocelli are known to provide a strong OFF-response, it is plausible that this component

of the ocellar input provides some feed into the direction-selective motion detecting circuits that form the input to $DNII_2$. In flies, Hu and Stark (1980) proposed that the ocelli act to modulate the sensitivity of the compound eyes. Goodman (1968) found that the descending units in locust, although responding to both compound eye and ocellar stimulation, could not be driven by ocellar stimulation alone. The modulating role of the ocelli has been found at the level of the dragonfly second-order neurons (van Kleef et al 2008). In the results presented in this chapter, I found that the directionality of $DNII_2$ was mainly encoded in the compound eye inputs. The ocellar inputs to the neuron were found to produce strong OFF responses to flashes and to enhance the response amplitudes and shorten the response latencies of the ON responses to the flashed stimuli. More importantly, ocellar inputs helped reduce the response times of motion responses. The results suggest that the ocellar signals to the honeybee descending neuron may 'gate' or modify the effect of the compound eye signals.

The results presented in this chapter provide strong support for the view that vertically tuned neurons on the optomotor pathway of the bee not only receive input from green receptors inputs but also from the UV or blue receptors.

Chapter 5

The electrophysiological characteristics of vertically and horizontally tuned motion-sensitive descending neurons in the bee

5.1 Abstract

Honeybees can rotate their head relative to their thorax along three axes known as pitch, roll and yaw. In the previous chapter, the responses of two pitch sensitive honeybee descending neurons ($DNII_2$ and $Locth_3$) suggested that it receives information from both the compound eyes and the ocelli, and that its ability to detect motion relies on both green and short-wavelength photoreceptors. In this chapter, the response characteristics of two roll sensitive neurons ($DNIV_2$ and $DNIV_3$), and one yaw sensitive ($DNVII_1$) descending neuron are reported. The recorded neurons are tested frontally with visual flashes and motion. The results showed that both the vertically tuned motion-sensitive (roll sensitive) neurons were sensitive to short-wavelength and green moving bars. These results suggest that more than one photoreceptor type is involved in the roll detecting system of honeybees. However, in the case of the neuron sensitive to horizontal (yaw) motion, the

directional responses were rather different. The green input provided a clear direction-selective excitatory drive. In contrast, the short-wavelength stimulus generated a non-direction inhibition of the responses. The results suggest a difference in spectral processing between the vertically and horizontally tuned systems.

5.2 Introduction

Chapter 4 introduced readers to the work of Kaiser and colleagues (Kaiser and Liske, 1974; Kaiser, 1975). They demonstrated that optomotor responses to horizontally moving images presented in the ventral visual field of the bee had spectral responses that were almost identical to those of the green photoreceptors that are found in honeybee compound eye and ocellar retinas. Chapter 4 also showed for the first time that direction-selective descending neurons in the bee, that are specifically tuned to detect the optic flow associated with down and frontward head and body pitch, responded equally to short-wavelength and green light stimulation. This finding is at odds with the behavioural work of Kaiser (1975). However, as suggested in the previous chapter it is possible that the green-only input observed behaviourally might be the result of two specific experimental conditions: (a) that the stimuli were presented ventrally and (b) that the stimuli moved only in the horizontal plane. In this chapter I will present the response properties of three direction-selective descending neurons, $DNIV_2$, $DNIV_3$ and $DNVII_1$. The anatomies of these cells were presented in Chapter 3.

Two of the neurons, $DNIV_2$ and $DNIV_3$, are known from previous studies to be highly selective for detecting the optic flow fields that occur during head and body roll (Ibbotson and Goodman 1990). Both neurons are optimally stimulated when moving patterns are presented in the lateral regions of the compound eyes. The optimal combination is upward motion over one eye and downward motion over the other eye, as would occur

when the head rolls. The third neuron, $DNVII_1$ is tuned to detect the optic flow patterns that occur when the body yaws, i.e. it responds optimally when there is regressive motion over one eye and progressive motion over the other (Ibbotson 1991b). Thus, recordings from these three neurons, in combination with the two vertically tuned neurons presented in Chapter 4, offers an opportunity to compare the response characteristics of four vertically tuned, direction-selective descending neurons with a horizontally tuned descending neuron. In so doing, there is an opportunity to compare the sensitivity of the optomotor system of the bee to short-wavelength and green stimulation and to compare these findings with the behavioural work of Kaiser, which was confined to horizontal motion stimulation.

5.3 Methods and materials

The detailed experimental preparation and electrophysiology setup was described in Chapter 4. Briefly, the experiments were conducted on worker honeybees (*Apis mellifera*). Hives were situated at the Australian National University in Canberra, Australia. The bees were collected when returning from foraging at the hive entrance. Each bee was anaesthetised by cooling at 4°C for about 20 minutes. The bee was then placed horizontally (dorsal side up) on a metal holder with the head and thorax secured with low melting point wax (3:1 mixture of beeswax and violin resin). A chlorinated silver wire was inserted into the thorax as the indifferent electrode for the intracellular recordings. The ventral nerve cord was exposed from the dorsal side of the neck so that the recording electrode could be inserted vertically into it (see Figure 4.1 in the previous Chapter for a schematic diagram of the animal preparation).

The visual stimuli generated by the wide-field LED display were described in Chapter 4. Briefly, two types of visual stimuli were applied: flashed stimuli and bar motion stimuli. The flashed stimuli can be further divided into two types: type I: 200 ms flashed light with both short-

wavelength and green LEDs under dark adaptation; and type II: short-wavelength and green LEDs modulated independently to generate single coloured brightness increments or decrements (flash duration: 38 ms). The bar motion stimuli had negative contrast bars (-0.82) that moved across either short-wavelength or green backgrounds.

5.4 Results

In this chapter, the electrophysiological characteristics of three types of honeybee motion-sensitive descending neurons ($DNIV_2$, $DNIV_3$, $DNVII_1$) are described. The cell responses to both flashed stimuli and moving bars of different spectra (either short-wavelength or green) are presented.

5.4.1 Responses of the roll-sensitive neurons, $DNIV_2$ and $DNIV_3$

$DNIV_2$ and $DNIV_3$ are neurons that belong to the DNIV class and, as such, they are morphologically similar (but easy to distinguish based on several criteria revealed in Chapter 3). In this study, each of them was identified as a single fill on 5 occasions. The present account reports the responses of the neurons to flashed and to moving stimuli (both short-wavelength and green) in the frontal visual field.

Flash response

Type I flashed stimulus: The responses of the $DNIV_2$ and $DNIV_3$ neurons to combined short-wavelength and green flashes (200 ms duration) were very similar and very consistent. Figure 5.1 and 5.2 show the flashed responses from 3 anatomically identified $DNIV_2$ and $DNIV_3$ neurons, respectively. It is shown that when both the compound eyes and ocelli were stimulated simultaneously, both $DNIV_2$ and $DNIV_3$ generated an excitatory ON response with two bands of time-locked spikes, and an excitatory OFF response with three bands of time-locked action potentials. However, different response latencies were found between the neuron types. The

latencies for the two bands of time-locked ON responses for $DNIV_2$ were 25.3 ± 7 and 73.3 ±12 ms (mean ± SD, n = 4) while $DNIV_3$ had slightly longer latencies with delays of 33 ± 4.2 and 85.6 ± 16 ms (mean ± SD, n = 5). The differences in latencies shown for the ON responses were not seen in the OFF responses. The latencies for the OFF responses of $DNIV_2$ were 18 ± 3.6, 41.3 ± 11, 67.5 ± 10 ms (mean ± SD, n = 4), and for $DNIV_3$ were 20.2 ± 9.3, 50.2 ± 13.3, 75 ± 15.8 ms (mean ± SD, n = 5).

Type II flashed stimulus: Unlike the responses to the type I flashed stimulus, the neural responses to the type II stimulus were different between $DNIV_2$ and $DNIV_3$. When both compound eyes and ocelli were stimulated simultaneously, $DNIV_2$ responded to brightness increments and decrements for both the short-wavelength and green spectra (Fig 5.3). The mean latency to peak response across 4 $DNIV_2$ cells to the short-wavelength brightness increments and decrements were 36 ± 6, and 32 ± 11 ms (mean ± SD, n = 4), respectively; the latencies to green brightness increments and decrements were 27 ± 5, and 27 ± 11 ms (mean ± SD, n = 4), respectively. $DNIV_3$, however, responded differently to short-wavelength and green flashes (Fig 4.4). The results showed that the $DNIV_3$ neuron responds to green brightness increment flashes, and to short-wavelength brightness decrement flashes. The response characteristics to different spectral flashes did not change when the ocelli were covered.

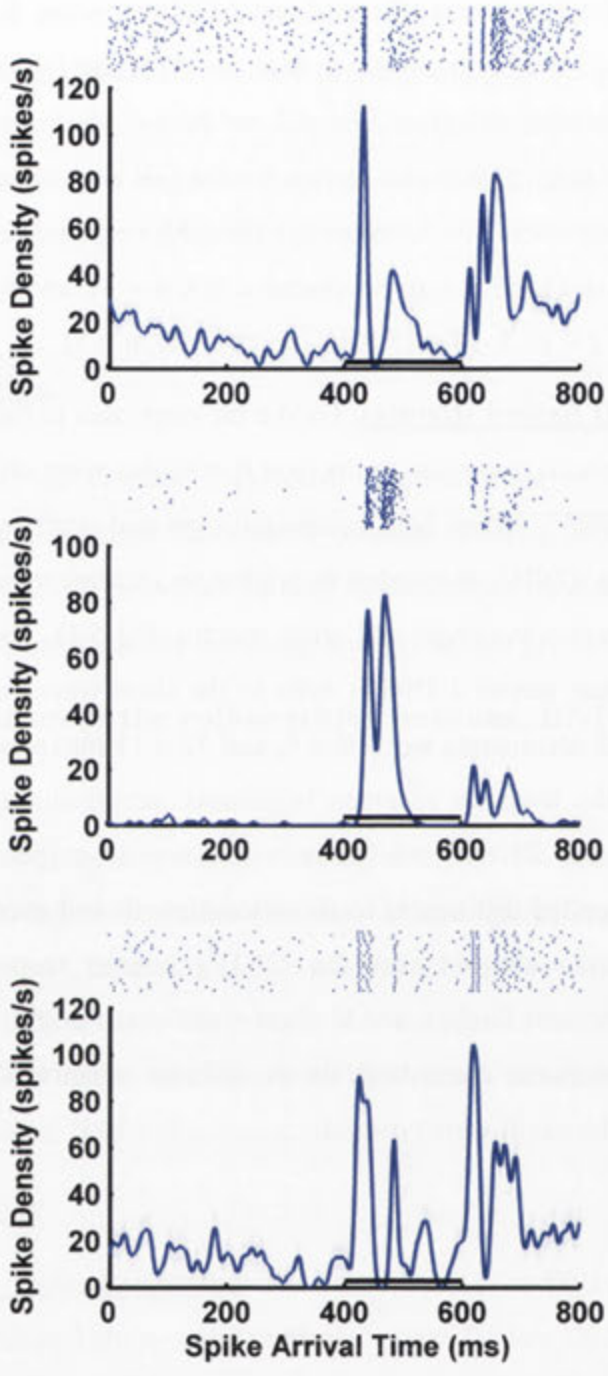

Figure 5.1: Flashed response from three anatomically identified $DNIV_2$ neurons, each of the figures shows the spike density function averaged from 40 trials. The $DNIV_2$ neuron showed a transient ON and OFF response with a band of time-locked spikes. The latency for the ON response was 32.25 ± 7 ms, and 18 ± 3.6 ms for OFF response (mean ± STD, n = 4).

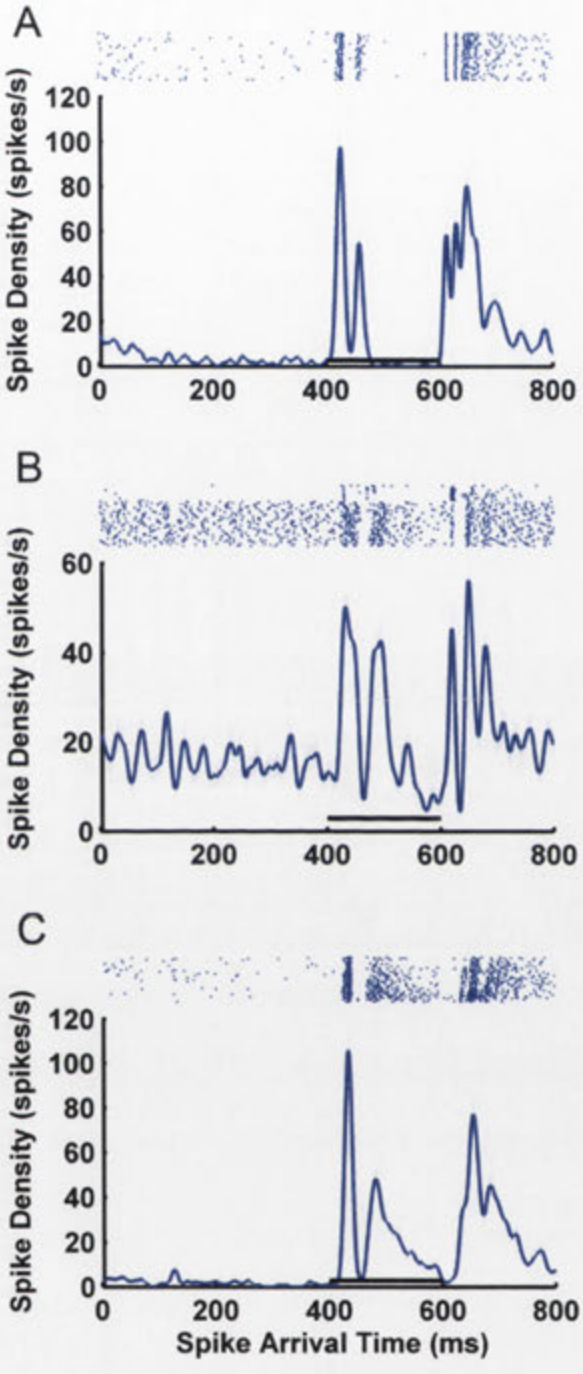

Figure 5.2: Flashed response from three anatomically identified $DNIV_3$ neurons, each of the figures shows the spike density function averaged from 40 trials. The flashed response of $DNIV_3$ appeared to be very similar with those of the $DNIV_2$ neuron; the $DNIV_3$ neuron showed a transient ON and OFF response with a band of time-locked spikes. The latency for the ON response was 33.42 ± 4.2 ms, and 20 ± 9.3 ms for the OFF response (mean ± STD, n = 5).

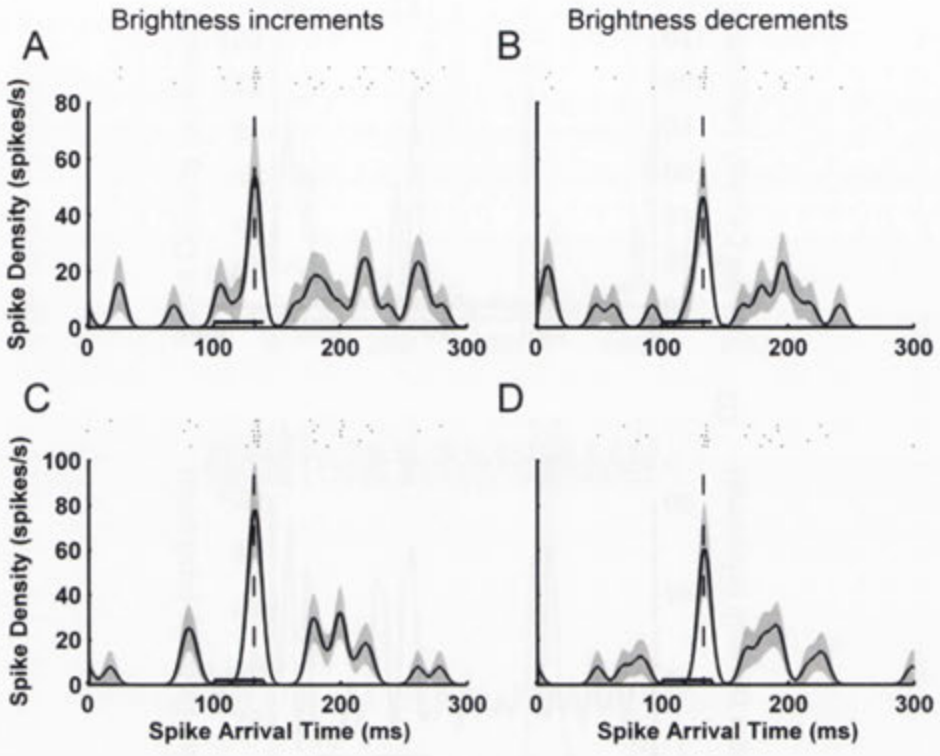

Figure 5.3: The $DNIV_2$ responses to short-wavelength (A,and B) and green (C and D) brightness increment and decrement flashes. The result showed that there was an excitatory response to brightness increments and decrements coloured in either short-wavelength or green.

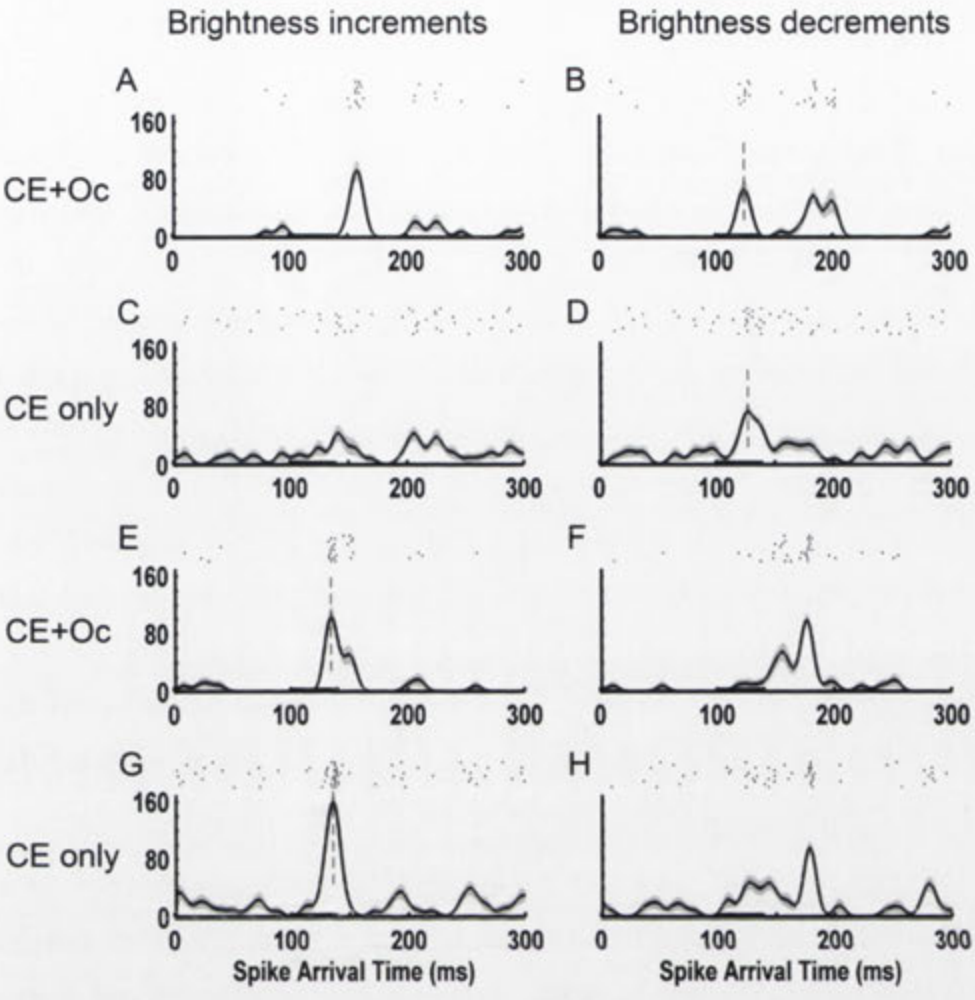

Figure 5.4: The $DNIV_3$ responses to short-wavelength (upper half, A-D) and green (lower half, E-H) brightness increment (left column) and decrement (right column) flashes. The cell responses to compound eye and ocallar stimulation (CE+Oc) and compound eye only stimulation (CE only) appeared to be similar. The result showed that there was an excitatory response to green brightness increments and short-wavelength decrements.

Directional response

$DNIV_2$ and $DNIV_3$ were previously shown to be roll sensitive (i.e. they respond to upward motion over the lateral portion of one eye and downward motion over the lateral portion of the other eye). They respond optimally when there is simultaneous upward and downward motion over the respective eyes (simulating the optic flow that occurs during roll). Wide-field frontal stimulation (via inputs from both eyes) consistently generates a response to upward and downward motion (Ibbotson and Goodman 1990). It is this frontal response that I exploit in the present study. The motion stimuli were restricted to the frontal and dorsal regions of the compound eye, therefore, $DNIV_2$ and $DNIV_3$ showed responses to both upward and downward bar movements (no response was observed to horizontal motion). Although the stimuli used in this study were not optimal for extracting the exact optic flow field sensitivity of the neurons, the results provided the spectral response characteristics of the cells.

$DNIV_2$: Figure 5.5 and 5.6 show the spike density function of a morphologically identified $DNIV_2$ neuron to 4 different speeds of vertical bar movements: the colours of the bars were short-wavelength and green, respectively. It is shown that $DNIV_2$ responds to both up- and downward motion regardless of the colour of the stimuli. Figure 5.8A shows the velocity tuning function from 3 individual identified $DNIV_2$ neurons. It is shown that although all three cells showed motion sensitivity to vertical motion, the response amplitudes and tuning curves varied between preparations. Figure 5.8B shows the result of averaging all 3 cells together after normalising the response to the maximum values obtained with short-wavelength stimulation in the upward moving direction. This average tuning shows that the neuron has a stronger response to downward motion. Ibbotson and Goodman (1990) reported the contrast frequency (CF) function of $DNIV_2$ and showed that the motion-induced excitatory response rate of the neuron increase linearly when stimulating the neuron with motions with 8-11 Hz square-wave gratings (i.e. the angular velocity of the

stimuli were around 90–180°/s). However, in this study, the result does not show velocity dependence based on the tested speeds. There is no significant difference between the short-wavelength and green motion stimuli. It can therefore be inferred that the inputs from both eyes, which respectively provide the response to upward and downward motion, contain both short-wavelength and green inputs.

DNIV$_3$: Figure 5.9 and 5.10 show responses of morphologically identified DNIV$_3$ neurons to 4 different speeds of vertical bar movements. It is shown that DNIV$_3$ responded to both upward and downward motion to both short-wavelength and green motion stimuli. The velocity tuning functions of 3 individual anatomically identified DNIV$_3$ cells are shown in Figure 5.12A. It shows that the cell responses to the upward and downward motions are very similar, and the spectra (short-wavelength or green) of the motion stimuli do not change the directional responses. It can also be seen that although the absolute response rate of each cell is varied between preparations, the response curves remain very similar and the excitatory responses show velocity-dependent characteristics. Figure 5.12B shows the result of averaging all 3 cells together after normalising the response to the maximum values obtained with short-wavelength stimulation in the upward moving direction. Although the result clearly shows velocity-dependent directional responses for DNIV$_3$, the function is quite flat. While responses are stronger at lower speeds, it is very possible that the neuron possesses a low-pass velocity tuning property and the peak response is below the tested speed (312 °/s).

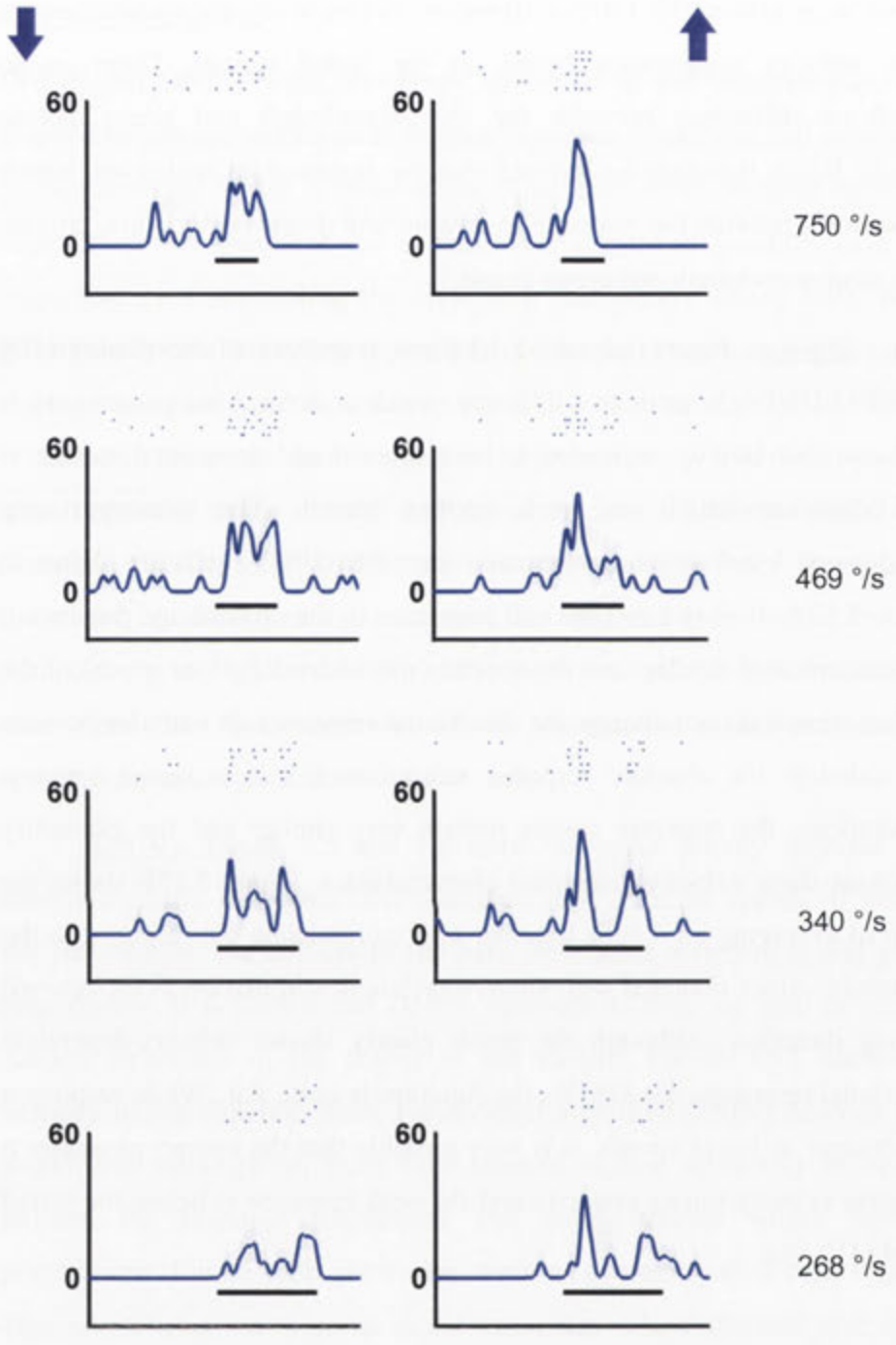

Figure 5.5: Responses of an anatomically identified $DNIV_2$ neuron to vertically moving **short-wavelength** bars. It can be seen that with short-wavelength bar stimuli, the neuron responds to both up- and downward motions.

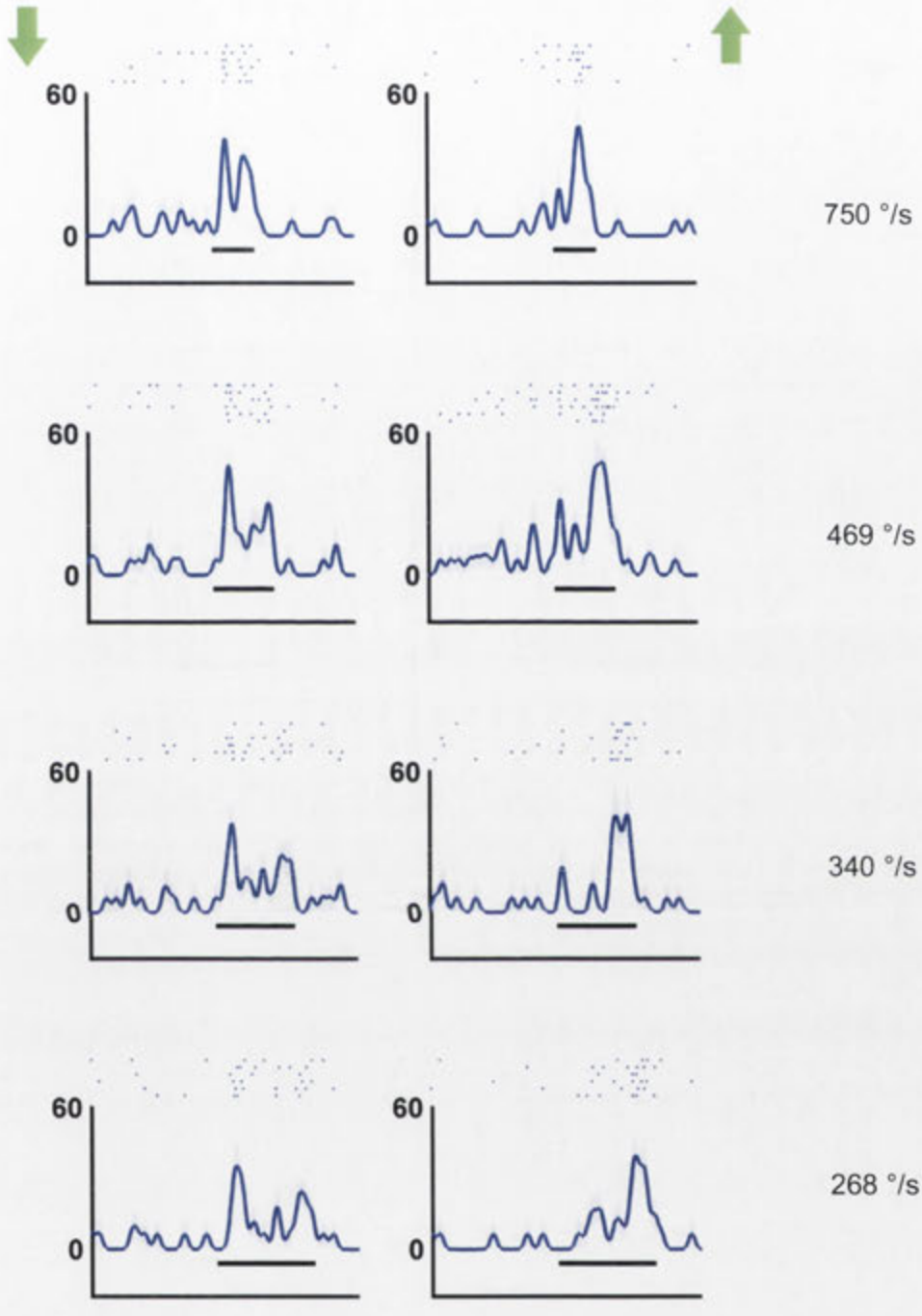

Figure 5.6: Responses of $DNIV_2$ to vertically moving **green** bars. It is shown that the $DNIV_2$ neuron responds to both up- and downward motions of the green stimuli.

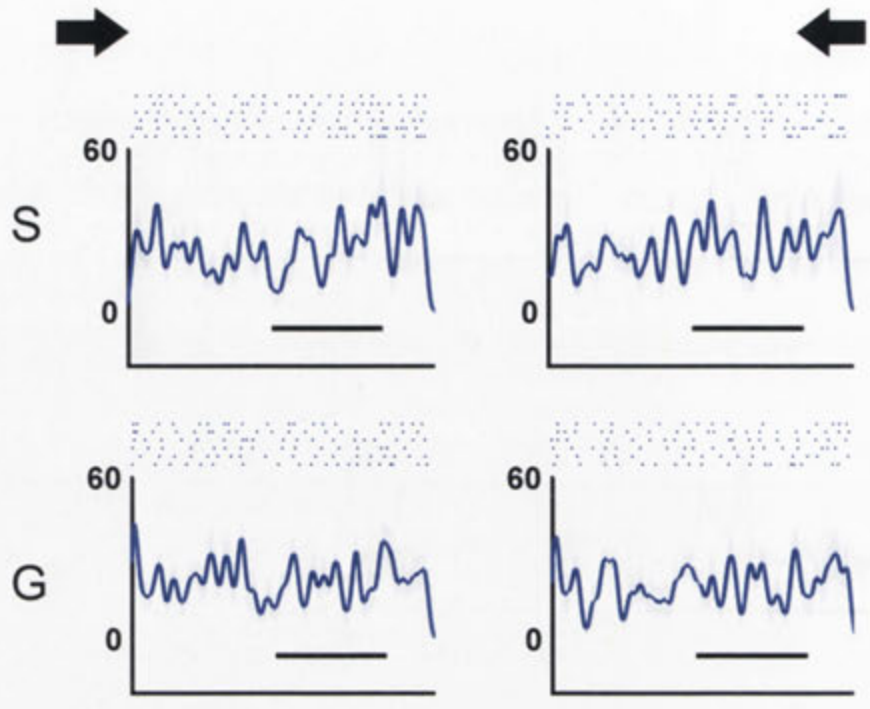

Figure 5.7: Responses of $DNIV_2$ to horizontally moving bars at 536 °/s. In both short-wavelength (S) and green (G) bar stimuli, no response was observed for the horizontal movements.

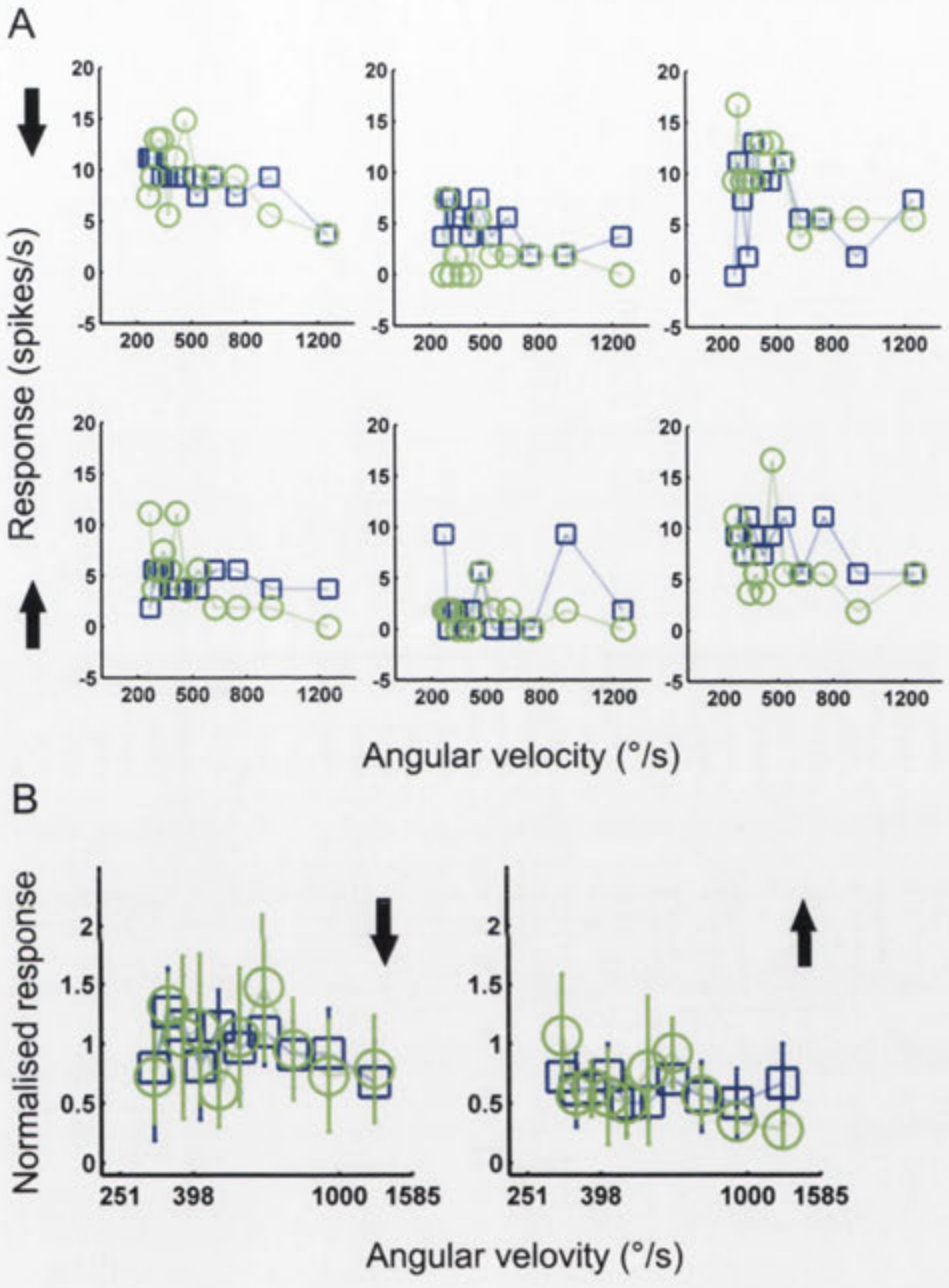

Figure 5.8: The velocity tuning of $DNIV_2$ to vertically moving bars. The black arrows indicate the direction of motion stimuli. The coloured symbols indicate the responses to motion stimuli of two spectra (blue squares: short-wavelength, green circles: green). (A) shows the velocity curves from 3 anatomically identified $DNIV_2$ neurons. (B) shows the results of averaging the 3 individual recordings after normalizing the responses to the maximum values. It is shown that although the $DNIV_2$ neuron clearly responds to both up- and downward motions, the responses of individual preparations varied.

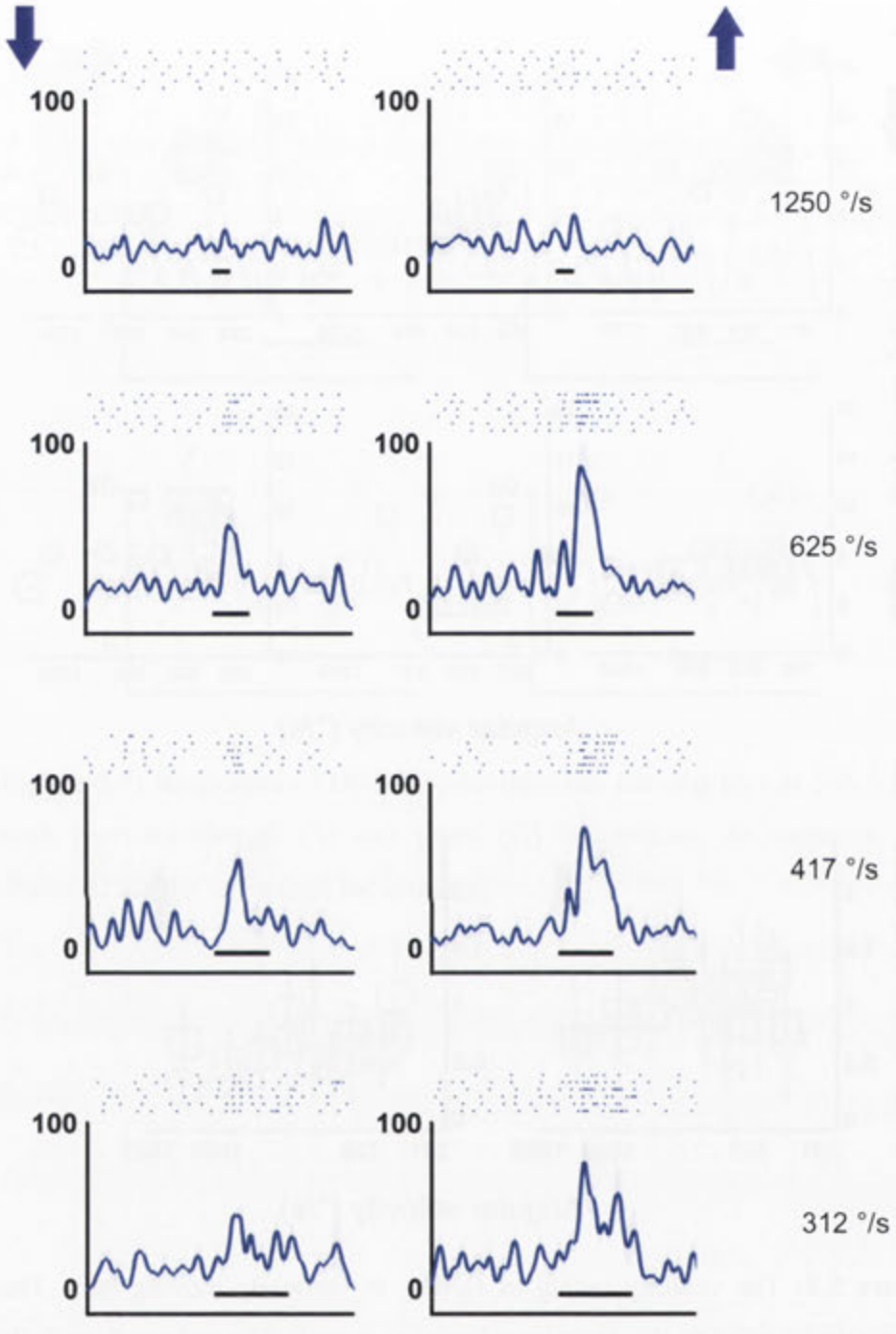

Figure 5.9: Response of an anatomically identified $DNIV_3$ to vertically moving **short-wavelength** bars. It can be seen that the $DNIV_3$ neuron responds to both up- and downward motions to the short-wavelength stimuli. No response was observed when the speeds of motion exceeded 1250°/s.

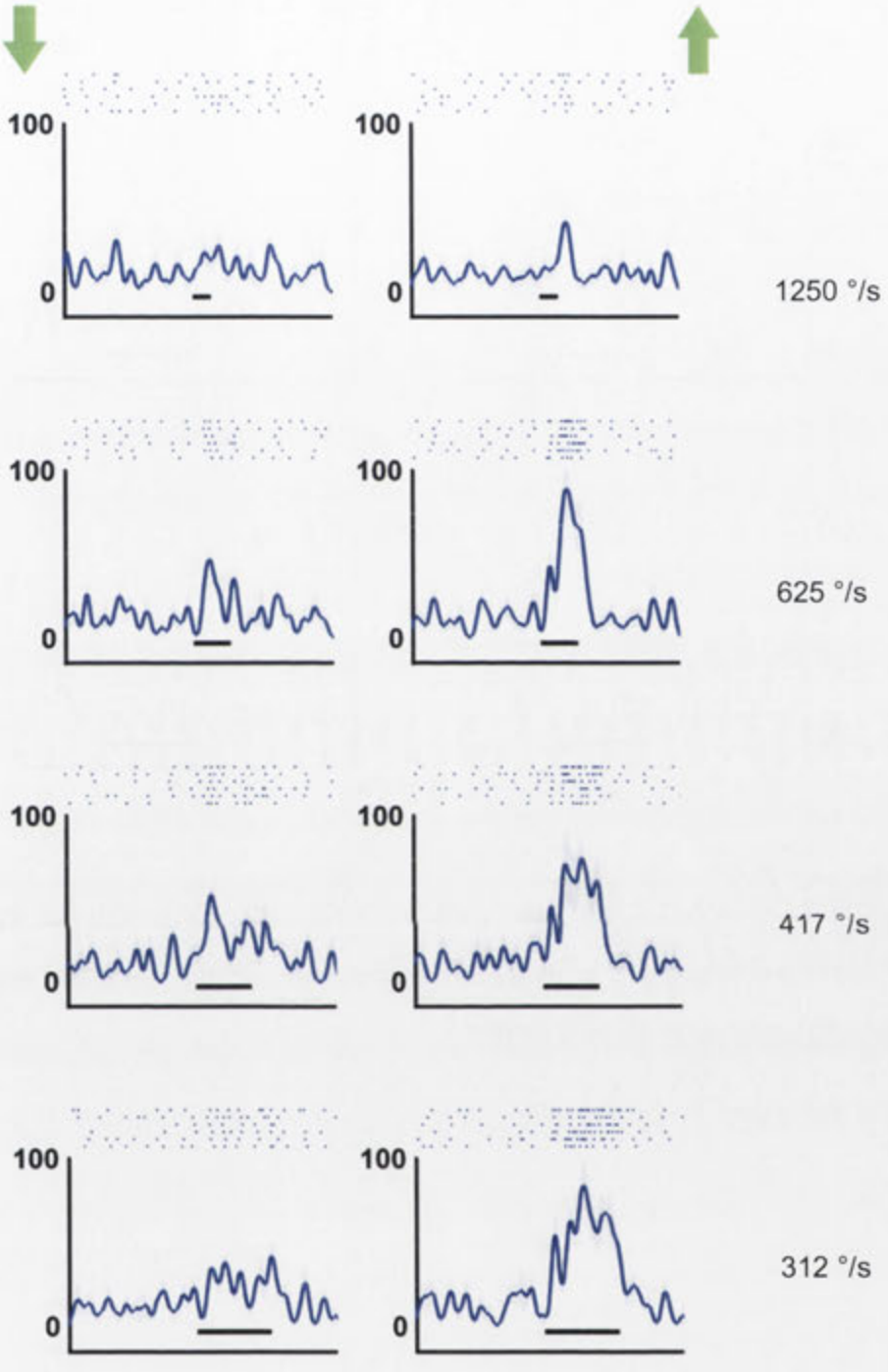

Figure 5.10: Response of $DNIV_3$ to vertically moving **green** bars. It can be seen that the $DNIV_3$ neuron responds to both up- and downward motions of the green stimuli.

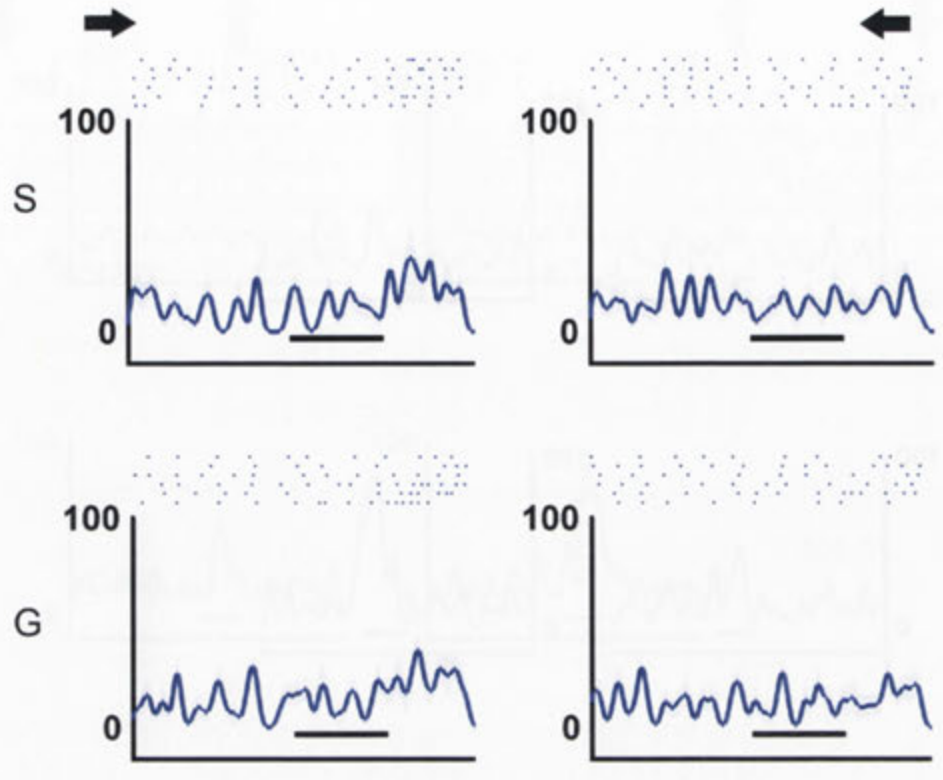

Figure 5.11: Responses of $DNIV_3$ to vertical bars moving at 625 °/s. To both short-wavelength (S) and green (G) bar stimuli, no response was observed to the horizontal movements.

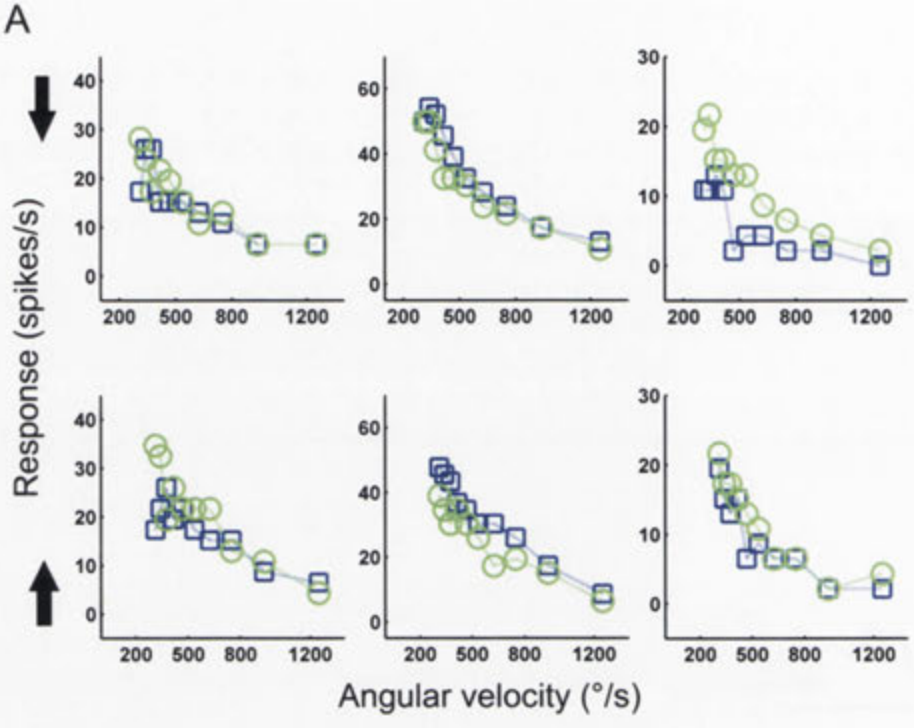
A
Response (spikes/s)
Angular velocity (°/s)
B
Normalised Response
Angular velocity (°/s)

Figure 5.12: The velocity tuning of $DNIV_3$ to vertically moving bars. The black arrows indicate the direction of motion stimuli. The coloured symbols indicate the responses to motion stimuli of two spectra (blue squares: short-wavelength, green circles: green). (A) shows the velocity curves from 3 anatomically identified $DNIV_3$ neurons. (B) shows the results of averaging the 3 individual recordings after normalizing the responses to the maximum values. It is shown that although the individual velocity functions varied with the actual spike numbers, the response curves remained very similar. It is shown that while $DNIV_3$ responds to both up- and downward motions, it has slightly stronger responses to upward motion.

5.4.2 Responses of the yaw-sensitive neuron, $DNVII_1$

Ibbotson (1991b) showed that $DNVII_1$ is sensitive to horizontal movement and the receptive field of the neuron is such that lateral stimulation is optimal. Nonetheless, the neuron does respond to frontal stimulation, albeit in a slightly weaker manner than to lateral stimulation. The neuron is tuned to detect the optic flow that is generated during yawing head and body movements: i.e. regressive motion (back to front) over the ipsilateral eye and progressive motion (front to back) over the other. Therefore, responses to moving stimuli were relatively small for frontal stimulation but did generate sufficient activation to measure the directional responses of the neuron with the two spectral stimuli.

Flashed response

The flashed stimuli (type I and type II) were applied to one anatomically identified $DNVII_1$ neuron. Cell responses to compound eye and ocellar stimulation and compound eye only stimulation were recorded.

Type I flash stimulus: The animal was stimulated with a 200 ms flash, which consisted of both the short-wavelength and green spectra. Figure 5.13 shows the responses of one $DNVII_1$ neuron. The mean and standard deviations shown in the figure were calculated from 40 trials. When both the compound eyes and ocelli were stimulated simultaneously the ON response consisted of two bands of time-locked action potentials: the latency for the first was 67 ms, and for the second was 89 ms (Fig 5.13A). However, when the ocelli were covered, while the latency for the on response was still 67 ms, the second response peak was absent. It can be seen that the cell exhibited a tonic response during the flash period (Fig 5.13B). It is also noted that when the ocelli were covered, the spontaneous response rate was higher than when both the compound eyes and ocelli were stimulated together.

Type II flash stimulus: Figure 5.14 shows the responses of a second anatomically identified $DNVII_1$ neuron to short-wavelength (S, upper half)

and green (G, lower half) brightness increments and decrements. Experiments were carried out under two experimental conditions: compound eyes and ocelli were stimulated simultaneously (CE+Oc), and only the compound eyes were stimulated (CE only). A response was generated in only one stimulus condition. The green flashed stimulus generated a complex spiking response waveform that consisted of a small initial increase in firing rate, a short inhibitory phase where very few spikes occurred and a large excitatory third phase where spike rates increased. The latency from the end of the stimulus flash to the peak of the first phase of the response was 66 ms (bottom right panel).

Another clear feature of the $DNVII_1$ activity pattern was that the spontaneous rate of the cell was found to be higher when the ocelli were covered. This was the case when using both the short-wavelength and green background stimulus (Fig 5.14). Therefore, the ocelli appear to provide a tonic inhibition to the neuron during steady short-wavelength and green stimulation.

Directional responses

$DNVII_1$ showed clear direction-selective responses when stimulated frontally when the green stimulus array was used (Fig 5.15). It produced excitatory responses to motion of a green bar in the preferred direction and no change in activity during anti-preferred direction motion (Fig 5.15A). During motion of a short-wavelength bar in either direction, $DNVII_1$ responded with a brief suppression of the ongoing activity, but clearly no excitatory response (Fig 5.15B). The spectral properties of the background luminance had a major influence on the ongoing activities of $DNVII_1$. With an all-green background the ongoing activity was relatively low (Fig 5.15A). However, with a short-wavelength background the ongoing activity was significantly higher (t-test, $p<0.01$; Fig 5.15B).

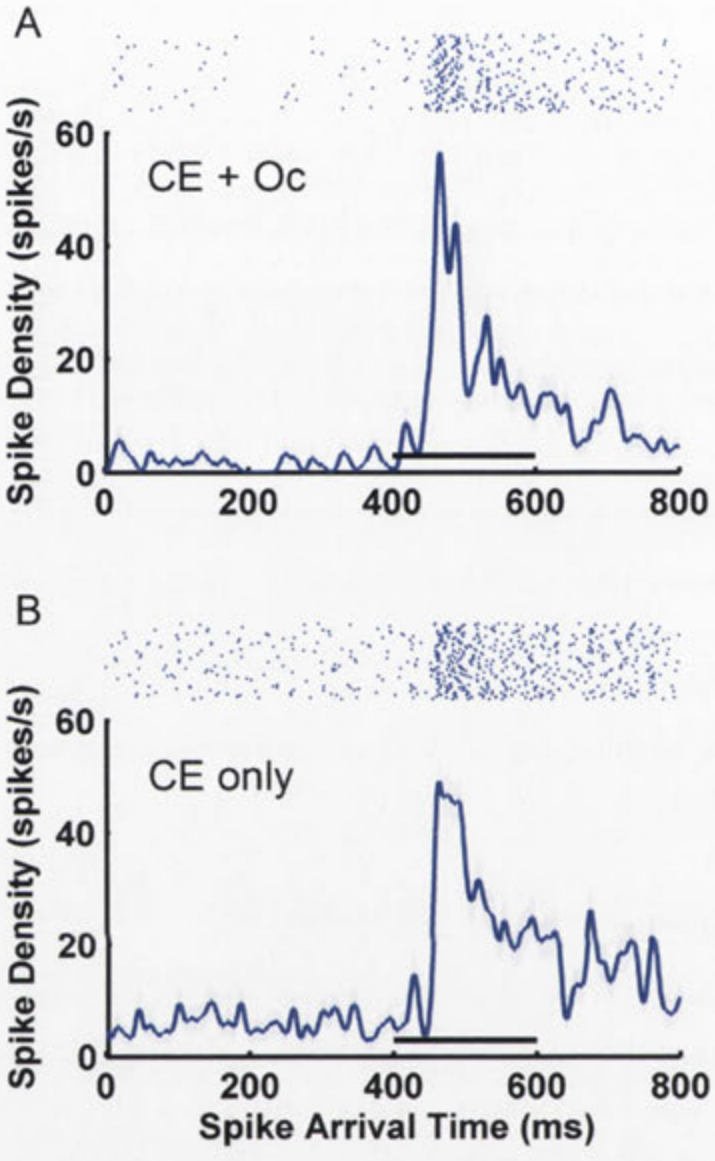

Figure 5.13: Flashed response of an anatomically identified $DNVII_1$ neuron. The results showed that in both conditions (A: compound eyes and ocellar stimulation, CE + Oc; B: compound eye only stimulation, CE only), robust ON responses ocurred with a delay of 67 ms. It is noted that the spontaneous rate (response rate before the stimulus) was higher when ocelli were covered, suggesting that the ocelli may provide a signal that suppresses the background response, thus enhancing the neural sensitivity.

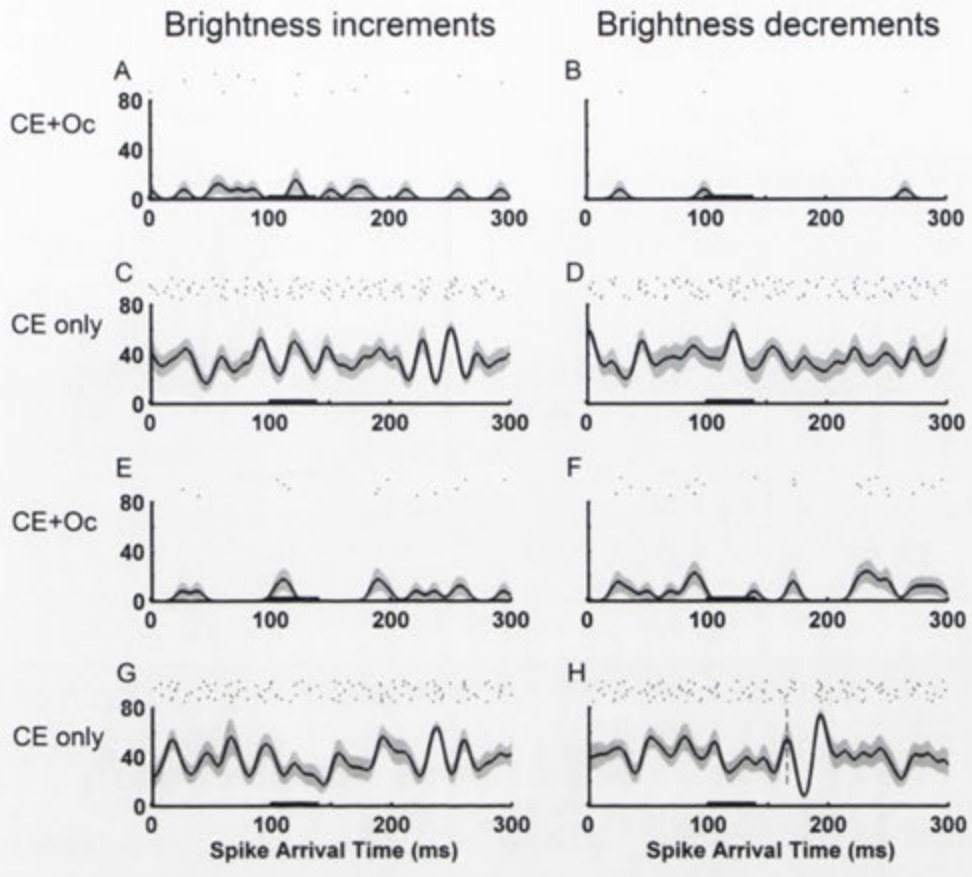

Figure 5.14: Responses of an anatomically identified $DNVII_1$ to short-wavelength (S, upper half) and green (G, lower half) brightness increment and decrement flashes.

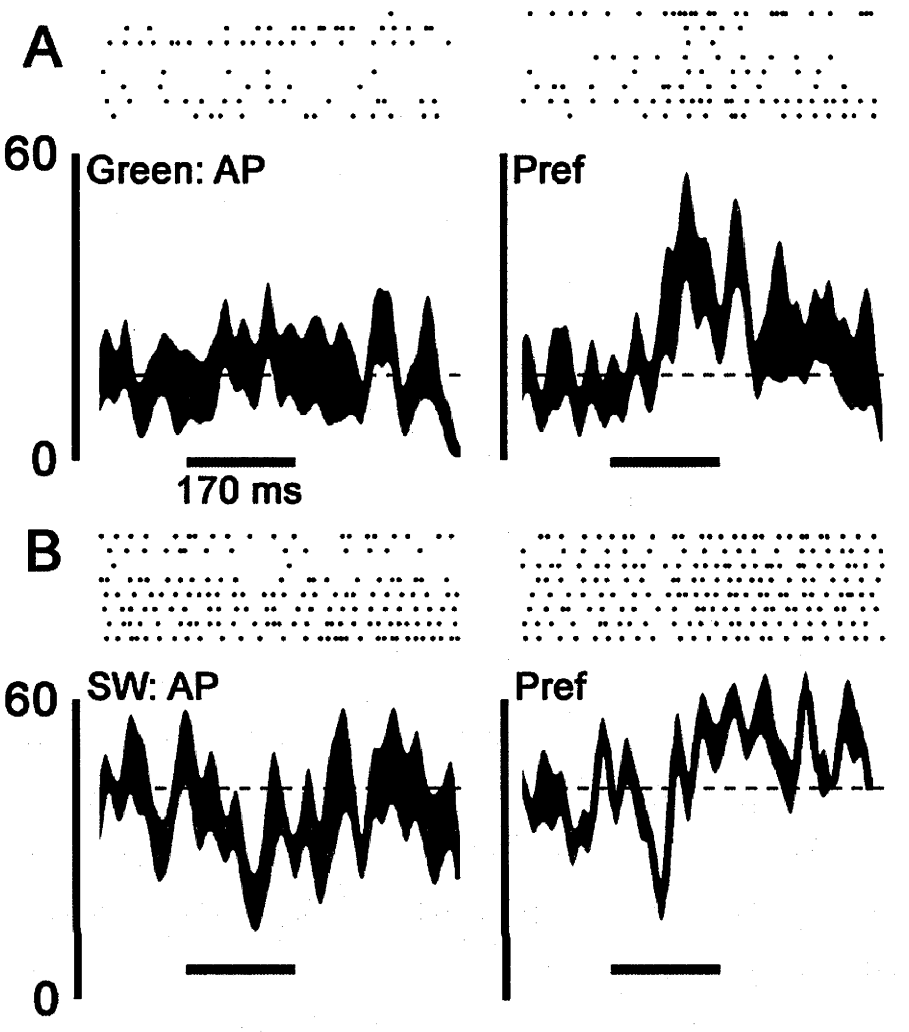

Figure 5.15: Directional responses of an anatomically identified $DNVII_1$ neuron to short-wavelength (SW, lower row) and green (upper row) moving bars (angular speed: 417 °/s). When applying the green bar movement, it is shown that the neuron has an excitatory response in the preferred direction (Pref); no response was observed for motion in the anti-preferred direction (AP). However, when applying the short-wavelength bar movement, the neuron showed an inhibitory response to both Pref and AP directions.

5.5 Discussion

In the 1970s Kaiser (Kaiser and Liske, 1974; Kaiser, 1975) established that, for the honeybee, the behaviourally measured spectral sensitivity of the optomotor response almost exactly matched that of the green photoreceptor found in the bee compound eyes (Autrum and Zwehl, 1964; Menzel and Blakers, 1976; Menzel et al., 1986). This suggested that the optomotor response was exclusively driven by the green photoreceptors. It has also been suggested that motion processing is 'colour blind' and that motion-sensitive interneurons receive inputs from only the green photoreceptors (Zhang and Horridge, 1990). Interestingly, most behavioural studies of optomotor responses have focussed on horizontal optomotor responses (e.g. Kaiser 1975; Yamaguchi et al. 2008). Here, we have shown that a horizontally tuned optomotor neuron in the bee generates increased spiking activity only with green stimulation. Therefore, one of the neurons that is almost certainly involved in driving horizontal optomotor responses in bees (as measured by Kaiser and colleagues) has properties that match the behaviour. However, other neurons that are tuned to detect vertical motion (to detect roll, $DNIV_2$ and $DNIV_3$ in this Chapter; and pitch, $DNII_2$ and $Locth_3$, see Chapter 4) clearly receive excitatory drive from both the green and short-wavelength regions of the spectrum. This demonstrates that selective green-receptor input is reserved for horizontal motion detection, while vertical motion utilises both green and short-wavelengths, at least when stimulated frontally. Behavioural experiments on the optomotor response of the fly *Musca domestica* have shown it to be short-wavelength sensitive when the dorso-frontal regions of the compound eyes were stimulated (Eckert 1971). We can make the prediction that vertical optomotor responses, particularly those driven from the frontal visual field are most likely short-wavelength and green sensitive in the bee.

Another important finding from the present study is that we showed for the first time that the ocelli contribute significantly to the motion responses of both vertical and horizontal tuned optomotor neurons in bees.

For the vertically tuned cells, the ocelli reduce response latencies, slightly increase response amplitudes and are integrated into the directional mechanism that leads to the selective responses of the neuron (see Chapter 4). For the horizontal cell the ocelli had an inhibitory role, sharpening the temporal dynamics of visual responses and tonically influencing the spontaneous activity of the neuron.

Chapter 6

Visual response properties of neck motor neurons in the honeybee

This chapter was published in 2011 by Yu-Shan Hung, Joshua P. van Kleef and Michael R. Ibbotson in the Journal of Comparative Physiology (Vol. 197(12) *pp.*1173–1187)

Yu-Shan Hung and Michael Ibbotson performed and analysed the experiments on the physiology and anatomy of the reported neurons. Joshua van Kleef developed the visual stimuli regarding the LED display. The manuscript was written and edited by Yu-Shan Hung and Michael Ibbotson.

6.1 Abstract

Recent behavioural studies have demonstrated that honeybees use visual feedback to stabilize their gaze. However, little is known about the neural circuits that perform the visual motor computations that underlie this ability. We investigated the motor neurons that innervate two neck muscles (m44 and m51), which produce stabilizing yaw movements of the head. Intracellular recordings were made from five (out of eight) identified neuron types in the first cervical nerve (IK1) of honeybees. Two motor neurons that innervate muscle 51 were found to be direction-selective, with a preference

for horizontal image motion from the contralateral to the ipsilateral side of the head. Three neurons that innervate muscle 44 were tuned to detect motion in the opposite direction (from ipsilateral to contralateral). These cells were binocularly sensitive and responded optimally to frontal stimulation. By combining the directional tuning of the motor neurons in an opponent manner, the neck motor system would be able to mediate reflexive optomotor head turns in the direction of image motion, thus stabilising the retinal image. When the dorsal ocelli were covered, the spontaneous activity of neck motor neurons increased and visual responses were modified, suggesting an ocellar input in addition to that from the compound eyes.

6.2 Introduction

Insects move their heads relative to their bodies for many reasons, some reflexive and others generated from active 'decisions' (e.g. Land 1973; Hengstenberg 1984; Sobel 1990; Baader 1991; Gilbert et al. 1995). Head movements during free flight have an important role in separating the optic flow that occurs across the retina into rotational and translational components, thus mediating good spatial vision during complex locomotion (Kern et al. 2005; Karmeier et al. 2006; Lindeman et al. 2008). This is achieved using a mode of flight in which the animals shift their gaze direction actively using saccade-like movements of the head, followed by a turning movement of the body in the same direction. Immediately after the saccade-like turns there is a period in which the animal flies essentially straight with its head stabilised to minimise rotational signals (flies: van Hateren and Schilstra 1999; honeybees: Böeddeker and Hemmi 2010; Böeddeker et al. 2010). While the image motion during the large saccade-like movements of the head is probably actively 'ignored' using some type of saccadic suppression mechanism (Ibbotson et al. 2008), it is essential to detect any unintended rotations of the head that occur during the straight flight segment (Böddeker et al. 2010). It is well established that such

relatively low-speed rotations can be detected and compensated for using the optomotor head-turning reflex (Hengstenberg et al. 1986). As an example, if an insect's head unintentionally rotates to the left, image motion travels rightward across the retina. To reduce image blur the head is turned to the right to momentarily stabilise the retinal image, as is the case for ocular following in primates (e.g. Ibbotson et al. 2007). Between the saccadic head movements the angular head velocities of flies are reduced to values of 0-100°/s, which is low enough to limit visual blur and maintain a fixed head gaze direction (van Hateren and Schilstra 1999).

To drive head movements it is necessary for the nervous system to detect the direction of wide-field image motion and transfer the signal to the motor neurons that drive appropriate head and body movements. Considerable effort has gone into recording the response properties of direction-selective neurons in insect brains (e.g. fly: Hausen 1982; Krapp and Hengstenberg 1996; Wertz et al. 2009ab; honeybee: Ibbotson and Goodman 1990; Ibbotson 1991). However, with a few notable exceptions in the fly (e.g. Milde et al. 1987; Strausfeld et al. 1987; Gilbert et al. 1995; Huston and Krapp 2008; 2009) and bee (Schröter et al. 2007), there has been relatively little recording of visual responses from the motor neurons that form the final neural output in the neck region. The response properties and connectivity of the motor neurons are interesting because they form the link between the motion signals calculated in the optic lobes and optomotor behaviour. Recordings made from fly neck motor neurons suggest that some behave much like direction-selective neurons in the optic lobes when the eyes are stimulated with wide-field moving patterns (Milde et al. 1987), although binocular interactions become more prominent (Huston and Krapp 2008). It was also noted that many fly motor neurons were multi-sensory, responding to mechanical stimulation of the wings and antennae (Milde et al. 1987) or to simultaneous stimulation of the mechanosensory halteres and the visual motion pathway (Huston and Krapp 2009).

In honeybees many muscles in the thorax are involved in head movements, potentially including those that superficially appear to move the forelegs (Snodgrass 1942; Markl 1966; Berry and Ibbotson 2010). The most obvious muscles that have involvement are muscles 40-44, which connect the thorax and head and are known as direct muscles. Six other muscles (45-51) connect between different parts of the prothorax and deform the exoskeleton in the neck region. These six muscles have a central role in assisting head turns in various planes (Berry and Ibbotson 2010). The neck muscles are controlled via three paired nerves, IK1, IK2 and IN1. Schröter et al. (2007) traced the morphology of the eight motor neurons in the first cervical nerve, IK1, from their cell bodies in the suboesophageal ganglion (SOG) to their terminals in neck muscles 44 and 51, thus providing a baseline for physiological investigation at the single cell level. Muscle 44 is a large direct-muscle that connects the prothorax to the head capsule. Its connections suggest possible involvement in the control of head retraction, in head declination (nose-down pitch) and unilateral adduction (head yaw) control (Fig. 1ab). Muscle 51 is an indirect-muscle that retracts the frontal exoskeleton of the prothorax. It is thought that the direct muscles pull the head firmly against the prothorax while indirect muscles, such as muscle 51, unilaterally retract the front of the prothorax, thus differentially changing the locations of the two horizontally aligned pivot points on which the head sits (the occipital processes: see Fig. 10 and associated text). The combination of these two effects is to give the head a substantial amount of freedom to move in the horizontal plane, as outlined in detail elsewhere (Berry and Ibbotson 2010). It is very likely that muscle 51 is, therefore, involved in controlling yawing movements of the head (Fig. 1bc).

Figure 1c shows reconstructions of the eight motor neurons in the SOG (modified from Schröter et al. 2007). The dendrites of the neurons are all located in the dorso-lateral region of the SOG. While the study by Schröter and colleagues revealed the detailed anatomical connectivity of the motor neurons and showed extracellular evidence that they were visually active, it was not possible to match the identities of particular neurons to

their physiological properties. This limits the interpretation of the directional properties of the cells in the context of the head movements that could be generated reflexively during image motion. That study was also limited to the investigation of visual inputs in general. The present work uses intracellular recording, with subsequent dye filling to assess the relative contributions from the compound and simple eyes (ocelli), revealing that both visual systems provide input. We show recordings from five of the identified neuron types in the first cervical nerve and find that they are visually sensitive and direction-selective. Their directional tuning matches the expected role in driving particular head movements. By conducting intracellular recordings in the present work it was possible to measure not only spiking activity but also the membrane properties of the neurons. We found that profound changes in mean membrane potential occur even in the axons, suggesting an additional role for slow potentials in controlling head movements.

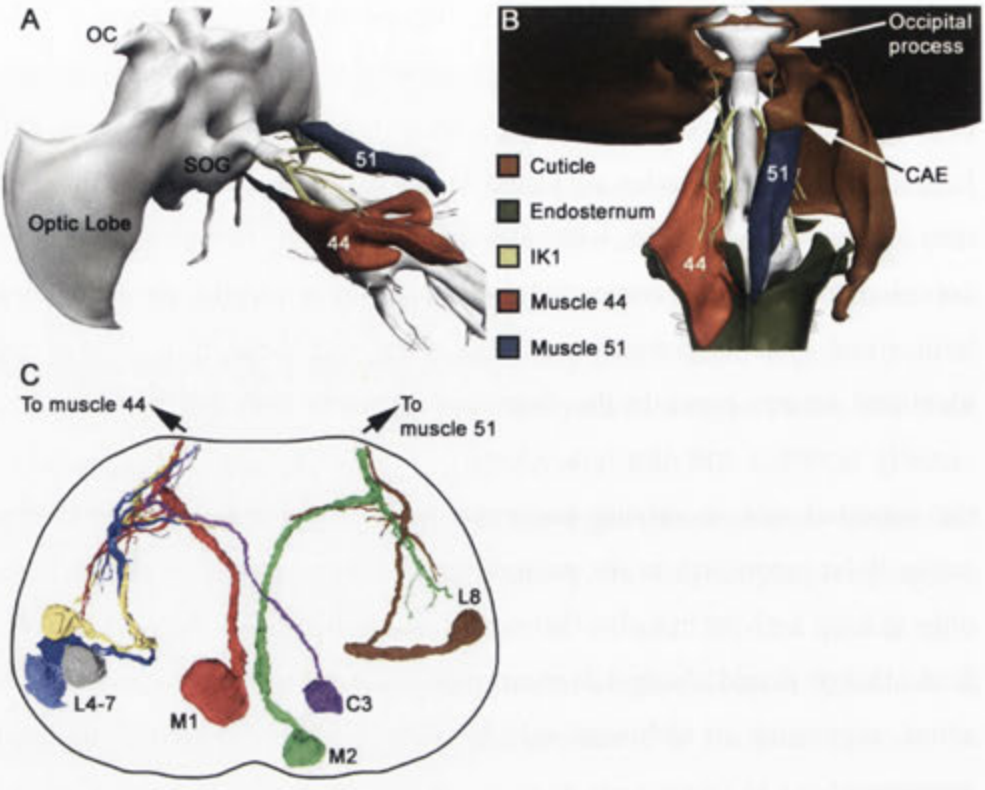

Figure 1: Anatomy of the honeybee neck. (a) Birdseye view of the honeybee brain and ventral nerve cord from the rear left quarter (grey tissue). The ocelli (OC) and subesophageal ganglion (SOG) are labelled. Nerve IK1 is shown in yellow and originates from the nerve cord close to the SOG. Muscle 51 is shown in blue and muscle 44 is shown in orange. (b) A dorsal view of the neck region showing the same structures as in (a) but also with the rear of the head capsule (brown), the right-hand exoskeleton of the prothorax (brown) and the endosternum (green) shown. Muscle 51 connects posteriorly with the endosternum and anteriorly with the cervical apodeme of the endosternum (CAE). When muscle 51 contracts it pulls the CAE inwards, thus also swinging the occipital process inwards (allowing the head to yaw). Muscle 44 connects extensively with the endosternum posteriorly and connects directly to the lower head capsule anteriorly. (c) Three-dimensional reconstructions of motor neurons in the SOG that travel through nerve IK1 (adapted from Schröter et al. 2007. J Comp Physiol A. 193: 289-304). The reconstructions show the main branches of the cells but not the fine dendrites. The black outline shows the outer limits of the SOG.

Muscle 44 is innervated by six motor neurons (M1, C3 and L4-7). These are shown on the left side of the SOG. Muscle 51 is innervated by two motor neurons (M2 and L8), shown on the right of the SOG.

6.3 Materials and Methods

6.3.1 Animals

Experiments were conducted on honeybees, *Apis mellifera*, that had been actively foraging. Hives were situated at the Australian National University. Each bee was lightly anaesthetized by cooling. The wings were then removed, and it was placed dorsal side down into an earthed metal holder. Recordings were made from nerve IK1, which exits the ventral nerve cord between the suboesophageal and prothoracic ganglia (Fig. 1a). The cervical region was exposed by tilting the head backwards by approximately 30°. It was then secured with sticky wax and the episternum, basisternum, fore-legs and neck membrane were removed.

6.3.2 Recording

Bees were inverted and placed in front of a stimulus monitor. The bees were allowed to recover from anaesthesia for at least 20 minutes before electrophysiology began. Recording electrodes were advanced into IK1 from the bee's underside. Intracellular recording and dye injection were performed using microelectrodes pulled from thin-walled filamentous capillary glass (o.d. 1.0 mm, i.d. 0.7 mm; Clark Electromedical GC100TF-10). The electrodes were filled with Lucifer Yellow (5% Lucifer Yellow CH in 0.2 M LiCl; Invitrogen, USA). Electrode tip resistances were approximately 150 MΩ. Chloride coated silver wires were used as the indifferent electrodes and positioned in the exposed thorax just posterior to the prothoracic ganglion. Cell penetration was aided by briefly increasing

the feedback gain in the capacity compensation circuit of the amplifier. Recording periods in individual preparations did not usually exceed 20 minutes, which was the time required to run a subset of experiments, before iontophoretic injection of dye. We were able to obtain stable recordings and fills from 30 cells for the full 20 minutes.

Signals were amplified using a DC-amplifier (Getting Model 5A) and filtered (LP cut-off 1kHz) and then acquired at 25 kHz with a 1401*plus* interface and Spike2 software (Cambridge Electronic Design, Cambridge, UK). The spikes were passed through a Schmitt trigger, producing TTL pulses at the time of each action potential. These pulses were used by Spike2 to generate online peri-stimulus time histograms (PSTHs) of the spiking activity. Offline, data was re-analysed in detail. Isolations were excellent with signal to noise ratios in excess of 10:1. No spike sorting algorithms were required to isolate particular spikes. All presented data are from single cell recordings. The response frequency was calculated relative to the mean ongoing activity of the cell, which was measured in periods before and after each experimental test and subsequently averaged over periods of several minutes.

After isolating a neuron, handheld stimuli were moved around the bee's head to determine if visual responses were present and air was moved over the head by blowing through a straw. Neurons were tested for visual responses quantitatively using custom visual stimuli produced on two devices. Device 1 was a VSG Series 2/5 stimulus generator (Cambridge Research Systems, Cambridge, UK). Stimuli were presented on a gamma-corrected monitor running at 198 Hz (Clinton Monoray, 57 cd/m^2 mean luminance, 600x400 pixels) at a viewing distance of 8 cm. The monitor subtended 134 x 124° at the eye and could be moved such that it covered the frontal visual fields of both eyes (positioned perpendicular to the animals longitudinal axis), or to stimulate either the left or right eye (for arrangement details see Schröter et al. 2007). In the latter case the screen was perpendicular to an axis inclined 45° to the antero-posterior axis of the

head. Stimuli were high contrast (0.6) sine-wave gratings that could be moved back and forth at any angle on the screen. A range of spatial and temporal frequencies was used. The highest temporal frequency used was 48 Hz.

To measure the directional tuning properties of the cells we used moving sine wave gratings (spatial frequency: 0.02 cpd). As the spontaneous activities could fluctuate suddenly, directional and temporal frequency tuning functions were collected quickly. They were most often obtained by measuring the responses to grating movements during time intervals of 500 ms followed by 1 s rest periods. As eighteen directions of image motion were tested, a complete directional tuning function could be achieved in 27 s and this sequence was repeated as often as possible (at least 3 times to produce a valid data set). For low temporal frequencies (<1Hz) it was necessary to increase the stimulus duration to allow the grating to move a reasonable distance across the receptive field. For those experiments the stimulus period was extended to 3 s, with a 3 s rest period.

Device 2 was a custom-built, wide-field stimulus consisting of a display with 9 columns of LEDs, each column containing 12 pairs of UV and green LEDs (Roithner Lasertechnik 380D15 , peak emission at 383 nm; Roithner Lasertechnik B5-433-B525, peak emission at 528 nm). There were 216 LEDs arranged on the surface of a sphere of radius 120 mm. Each bee's head was positioned at the centre of the sphere by locating it at the point of intersection of two aligned laser pointers attached to the stimulus. From the bee's point of view the intervals between LEDs in the vertical direction (elevation) were 6° and in the horizontal direction (azimuth) were 12°. The display subtended 96° in azimuth and 66° in elevation, sufficient to cover a large portion of most receptive fields. While the separation of LEDs was large, the stimuli were typically moved at high speeds and no evidence of aliasing was observed. The directional tuning obtained using device 2 was the same as that obtained using device 1.

The electronic control used the sample-and-hold concept described by Lindemann et al. (2003) and was described in detail previously (Berry et al. 2006). The refresh rate was 625 Hz. The usage of sample-and-hold circuitry allows all LEDs to be switched on continuously, with a maximum intensity of ~10^{14} photons cm^{-2} s^{-1}. This is sufficient to obtain an overall brightness that matches an equivalent patch of daylight sky. We presented moving bars on the screen and at times presented full-field flashed stimuli.

Neuronal responses to individual stimulus presentations were aligned relative to a synchronisation pulse provided by the stimulus generation computer in the blanking interval prior to the first stimulus frame. Responses were measured as the mean number of spikes in the stimulus time window. The mean preferred direction of motion for each cell was obtained by calculating the mean vector angle of the circular histogram (Batschelet 1981; Ibbotson and Goodman 1990).

6.3.3 Staining and histology

Lucifer Yellow was injected into the neurons after recordings using a 3-6 nA hyperpolarizing DC-current. The dye was given 30 minutes diffusion time and then the brains were fixed (2.0 g paraformaldehyde, 17 ml 2.25% NaOH, 83 ml 2.555% $NaHzPO_4$, 2 ml 100 mM $CaCl_2$), dehydrated in an ethanol series, cleared (using methyl salicilate) and viewed on a Nikon Optiphot epifluorescence microscope. When the quality of the filled neuron was acceptable the neuron was optically sectioned on either a BioRad LaserSharp2000 or a Leica SP2 UV confocal microscope (Fig. 2). To allow easy identification of the main features of the cells, without autofluorescence obscuring some of the fine details, we have provided black and white drawings of all cells. These were made in Photoshop by drawing over the photomicrographs produced by the confocal microscope.

6.4 Results

Intracellular recording from motor neurons in IK1 proved a difficult technical challenge. To maintain neural health it was necessary to leave the nerve connected to the muscles, which periodically contracted. The nerve was stabilised to some extent by suspending it over a metal wire that had been glued to the thorax but muscle contractions were still able to move the electrode out of the cell. Holding cells for long enough to record all possible physiological tests and to inject dye was difficult. Recording attempts were made from 157 animals. From these we successfully recorded from and filled 30 neurons sufficiently to determine their identity.

We were able to record from and fill five identified neuron-types in the present study (M1, M2, L5, L7 and L8). We previously determined that the axon diameters of the other three cells were very small (<3μm), which probably explains our inability to record and fill them (i.e. cells C3, L4 and L6). It was possible to use the morphologies of the cells to identify them between preparations. M1 and M2 are similar but M2 has a distinct bend in its neurite close to its dendritic arbours and it soon became evident that the two cells have different physiologies. Anatomically, L8 is easily distinguished from the other lateral cells because its cell body is located more lateral and anterior in the SOG. The only method for distinguishing the remaining lateral cells (L5 and L7) from each other involved dissection of the target muscle to determine which subunit was innervated by a given cell's terminals (Schröter et al. 2007). The difficulty of the latter procedure reduced the number of confirmed fills for L5 and L7. In total, we filled M1 on 10 occasions, M2 on 5 occasions, L5 on 4 occasions, L7 on 3 occasions and L8 on eight occasions.

Figure 2 shows a lucifer yellow fill of M1. The image shows the typically dense dendrites in the ipsilateral neuropile of the SOG. It also illustrates the very large size of the motor neuron cell body. An interesting feature of all the recorded cells was that a small dendrite always crossed into

the dorsal region of the contralateral SOG. This image also shows a common finding when filling medial neurons. Fills of M1 and M2 always led to a second cell body being filled in the ventro-medial region of the SOG. Similar 'shadow-fills' were previously observed using a different fluorescent dye: rhodamine dextran (Schröter et al. 2007). The shadow-filled cell bodies were never associated with a complete neurite, nor was it ever possible to see the associated axon. From these observations we deduced that the additional cell bodies were filled by dye that was transmitted from the recorded cell, presumably through channels in the cell bodies themselves. As these second cell bodies never filled sufficiently to see the associated dendrites, we were never able to determine which neuron had been co-filled. We presume that the medial neurons are connected through gap junctions on the somas that are sufficiently wide to transmit lucifer yellow and rhodamine dextran. We did not see multiple cell bodies when motor neurons with lateral cell bodies were filled.

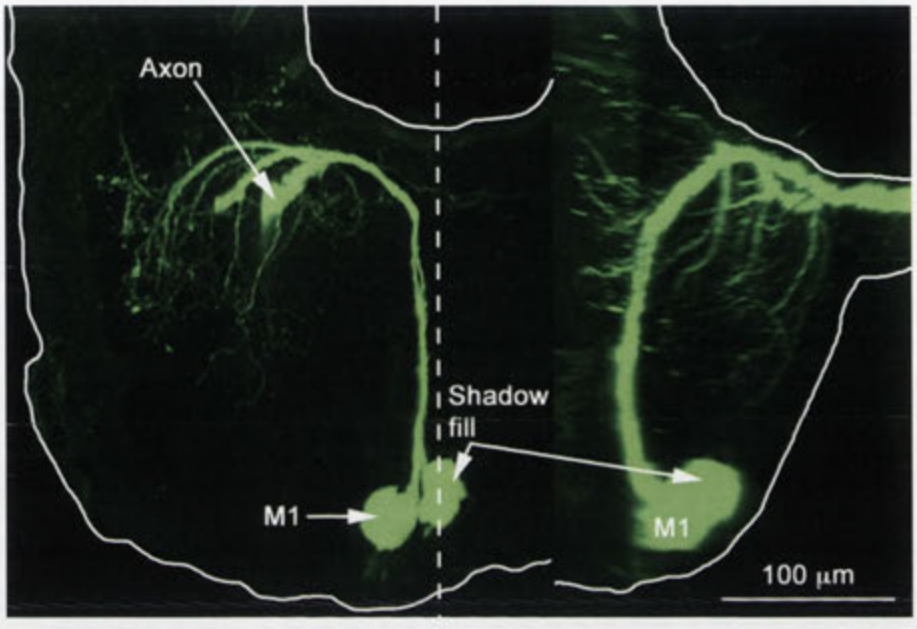

Figure 2: Dye fill of motor neuron M1. On the left is a dorsal view of the suboesophageal ganglion (SOG). On the right is a lateral view. The recorded cell was M1, but another unknown cell was shadow-filled, presumably due to the transfer of dye from M1 at the level of the cell body or neurite. Neither the axon nor the dendrites of the shadow-filled cell could be identified. Fills of both M1 and M2 led to shadow-fills. None of the motor neurons with lateral cell bodies showed shadow-fills.

6.4.1 General physiology

All the action potentials from the motor neurons in IK1 had the same characteristic properties: they tended to be broadly shaped and did not have large hyperpolarizations following the main depolarizing phase of the spike (Fig. 3). The MNs tended to have ongoing spontaneous activities but the actual spike rate could vary during recordings. On occasions a neuron would temporarily become silent, with no spontaneous activity. After a few minutes the spontaneous activity would suddenly return. This spontaneous firing rate is demonstrated for one cell (L8: Fig 3a-c). The spiking activity was regular when present. After a sudden change in firing rate the firing rate usually remained stable at the new rate for some time (usually several minutes). The recordings shown in Figure 3a-c are from the same cell but at different times during the recording session. It is evident that in each case the firing rate is stable. The spontaneous firing rates can also be observed in the raster plots for other MNs (Fig 4 and 5). There were no obvious correlations between the sudden excursions from the regular firing pattern and external stimulation, and firing rates increased as often as they decreased suggesting a normal physiological mechanism rather than a deterioration of recording quality or damage to the cells. The sudden changes in spontaneous activity may reflect internal (locomotor) state changes, which have been recently reported to have an impact on the spontaneous activity in lobula plate tangential neurons in flies (Chiappe et al. 2010; Longden and Krapp 2009; Maimon et al. 2010). The response features outlined above were highly consistent between preparations suggesting real properties and not a problem with the recording technique. Exactly the same electrodes were also used to record from visually active descending neurons in the bee, as have been reported previously (Ibbotson and Goodman 1990). Those recordings consistently revealed action potentials with narrower widths and clear hyperpolarising rebounds. It was also apparent that descending neurons generated higher spike frequencies than motor neurons.

For all cells, we qualitatively tested the sensitivity to air being blown over the head through a straw (by mouth) and to tapping the antennae with wooden tooth picks. All cells responded vigorously to these types of stimulation. Given the qualitative nature of the stimuli we do not present these responses. It is clear that the cells receive input from mechano-sensory receptors and probably also from odour receptors (also see Menzel et al. 1991 for a recording from a motor neuron in a bee that had a cell body in the medial region of the SOG, similar to the cell in Figure 2).

All of the recorded cells showed responses to visual stimulation. Responses consisted of clear fluctuations of the membrane potential. On most occasions there were also changes in the action potential frequency. The mean membrane fluctuation of an M1 neuron in response to a flashed UV and green stimulus (stimulus device 2) is shown (Fig. 4a). There was a transient depolarization when the stimulus came on and a very brief hyperpolarization at the termination of the stimulus. The transient responses were due to a stimulus artefact that had zero delay created by the display (shown inset in Fig. 4a, marked: Stim. Art.). The artefact had no influence on the response of the neuron and was simply a pulse of electrical noise that we could not eliminate using shielding. It only occurred when the stimulus was turned ON or OFF, as clearly demonstrated by the inset figure. We did not subtract this from the response trace as we felt it important to present the raw data. The data show the total mean membrane fluctuation including any spikes that were present. It is evident that a flashed stimulus (light ON, duration 200 ms) leads to a membrane depolarization. The artefact hyperpolarization is then followed by a depolarizing response to light OFF that persists for approximately 200 ms. Below the mean membrane potential we show a raster plot of the spikes (upper, Fig. 4b) and the spike density function from the same spike traces (lower, Fig. 4B). They demonstrate that the depolarizations are accompanied by an increase in spike rate both during light ON and after light OFF. The pattern of responses to flashed UV and green light is generally representative of responses from all the recorded cells, although the relative sizes of the ON and OFF responses varied

between recordings within the same cell types and between cells. It appears that the cells carry information in their axons (which were the recording sites) both in the spike frequency and in slow fluctuations of the membrane potential and that the cells respond both to light ON and OFF.

As mentioned earlier, cells could suddenly (and apparently spontaneously) change their ongoing spiking rate. The recordings shown in Figure 4ab were obtained when the recorded cell had a prominent and regular ongoing firing rate (approximately 10 spikes/s). Several minutes later this cell almost completely stopped producing spikes, yet it was clear that subthreshold responses to flashed stimuli were still present. In this changed state the membrane potential showed the same general properties as had occurred during the previous stimulation, i.e. a depolarization during light ON, a brief hyperpolarization at light OFF and then a robust depolarization that persisted for 150 ms (Fig 4c). However, throughout the trials only one spike was generated (upper, Fig 4d). The data imply a very complex input network in which multiple inputs, perhaps some governed by internal state changes control the spiking behaviour.

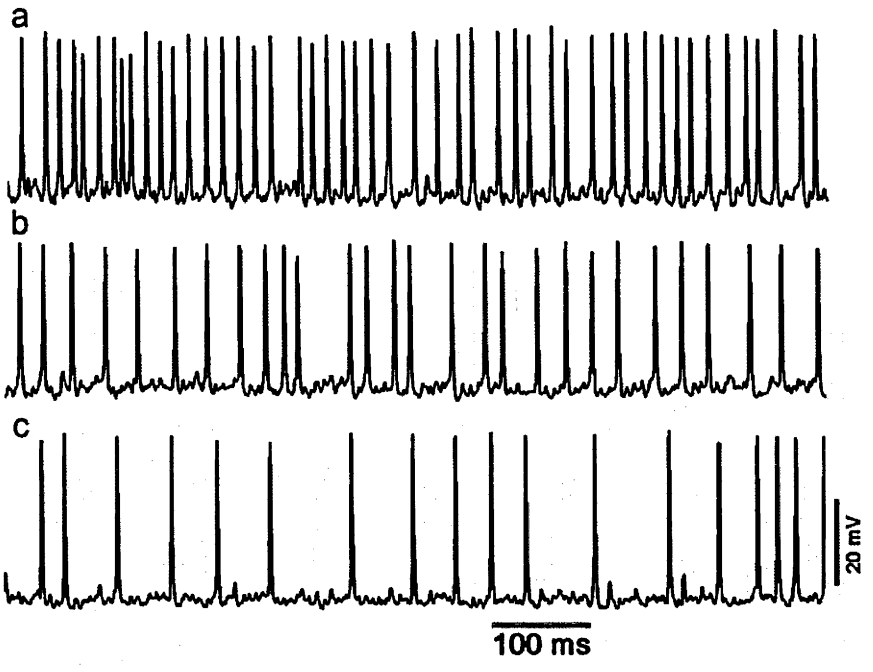

Figure 3: Ongoing spontaneous spiking activity recorded from M1. The spikes in a, b and c were all recorded from the same cell at different times during the recording period. No stimulus was presented during any of the time periods shown. Spike rates tend to be fairly steady for long periods (minutes) but show transient shifts to new firing rates with no external stimulus. The action potentials are relatively broad compared to visual neurons earlier in the visual system. The action potentials are also monophasic (i.e. there is a single depolarization spike but no after-hyperpolarization).

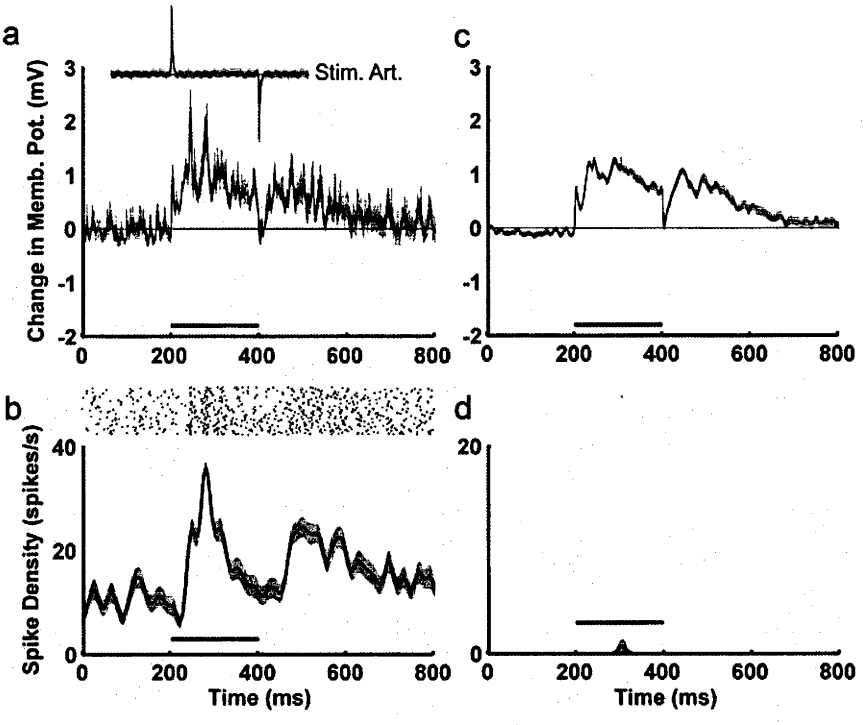

Figure 4: Flash responses of M1. (a) Mean change in membrane potential during and after a 200 ms flash of combined UV and green light, using the LED-stimulus (n=55). There is a short latency followed by a depolarization during the flash. After flash cessation there is a transient hyperpolarization, then a prolonged depolarization. Shown inset (marked Stim. Art.) is a trace collected when the entire visual system was occluded from the stimulator but the stimulator was used as normal. It is clear that a stimulus artefact with zero latency, which could not be removed through grounding, was present. (c) Change in membrane potential for the same cell and the same stimulus, but in this case the cell had stopped spiking. The change in membrane potential appears smoother because there was only one spike included in the averages. The lower rows (b,d) show the spike arrival times (rasters) during 55 repetitions of the stimulus and the associated spike density functions. When the cell was in 'spiking mode' the pattern of spikes was similar (but slightly delayed) compared to the membrane fluctuations. Only one spike was produced during the stimulation shown in d. The grey areas show standard errors.

6.4.2 Ocellar Input

The honeybee has two visual systems, one receiving input from the compound eyes and the other from the three dorsally positioned simple eyes (ocelli) (Cajal, 1918; Ribi 1975a,b; Goodman 1981). We wanted to determine whether both types of eyes (compound and ocelli) provided sensory input. It was not possible to only stimulate the ocelli using our system as stray light always fell on the compound eyes. However, it was possible to completely cover the ocelli with a black cap in such a way that no light fell upon them. We conducted experiments in which we tested the visual responses of the motor neurons with the ocelli covered (stimulus device 2). After results had been obtained we removed the cap over the ocelli and repeated the experiments. Results were consistent between motor neurons, so a representative example is shown. Figure 5a shows the mean change in membrane potential during combined ocellar and compound eye stimulation for neuron M1. There is a clear depolarization during the 200 ms light-ON phase, followed by a hyperpolarization. These membrane changes are accompanied by a significant increase in spike rate during the stimulus (Fig. 5b). After the ocelli had been covered there was a decrease in the amplitude of the membrane depolarization during the light-ON phase (Fig. 5c) and a dramatic difference in the spiking response (Fig. 5b). The spiking response showed virtually no excitation but, instead a suppression of the spontaneous activity. Very importantly, when the ocelli were covered, the spontaneous activity of the motor neuron increased from 30 spikes/s to nearly 50 spikes/s. This was a common observation in the motor neurons and strongly suggests that when the ocelli are illuminated by steady light they provide an ongoing suppressive signal to the motor neurons.

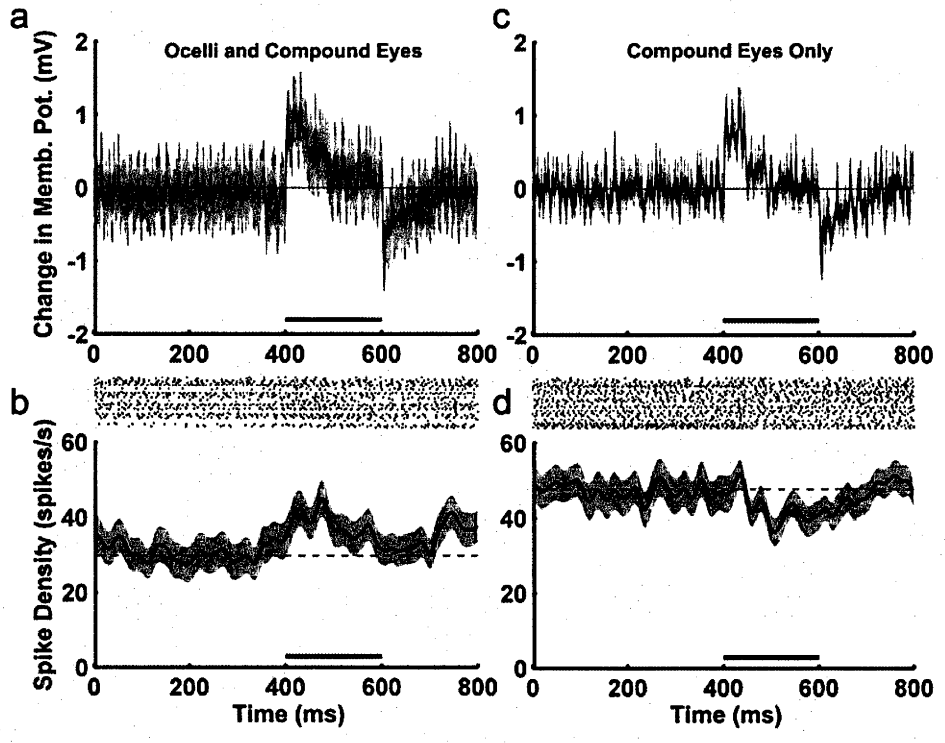

Figure 5: Flash responses of M1, with and without the presence of the ocelli. (a,c) Mean change in membrane potential during and after a 200 ms flashed light stimulus (UV and Green) with either (a) combined ocellar and compound eye, or (c) compound eye only stimulation (n=45). There is a clear depolarization during the 200 ms light-ON phase. The lower rows (b,d) show the spike arrival times (rasters) during 45 repetitions of the stimulus and the associated spike density functions. (b) With combined ocellar and compound eye stimulation, there is a small but significant increase in spike rate during the stimulus compared to the compound eye-only condition. (d) The spiking response shows a suppression of spontaneous activity with only compound eye stimulation. The grey areas show standard errors.

6.4.3 Visual motion responses

The responses to moving visual stimuli that we report were in most cases observed as increases in the ongoing spiking activity for certain selected directions of motion. Motion opposite to the preferred direction did not generally lead to significant inhibition of the spontaneous firing rate. Given that motion in this direction did not lead to inhibition, it is appropriate to use the term 'null direction'. The data presented in Figure 6 show the general properties observed during motion stimulation in all cells. Brief movements of a black bar on a green background in the preferred direction generally led to a small membrane depolarization and an associated increase in spike rate (stimulus device 2, right hand traces, Fig. 6a). When the bar moved in the null direction there was no variation in either the membrane potential or the spike frequency (left hand traces, Fig. 6a).

Throughout the rest of the paper we present quantitative data based on spike frequencies when the bees were stimulated using moving gratings presented on a visual monitor (stimulus device 1). Care was taken to measure the entire directional and temporal tuning during a period of stable spontaneous activity. The data in Figure 6B shows responses to 3 second periods of grating motion in eight different directions for an identified L8 neuron that had its axon on the right hand side of the animal. As was usually the case, the cell had a robust ongoing activity. Motion to the right (progressive motion over the eye) generated a significant increase in firing rate (t-test, $p<0.01$), while motion to the left showed no significant change in firing rate compared to controls (t-test, $p>0.05$). In the example shown, motion downward and to the right (45° down) also led to a significant increase in firing rate (t-test, $p<0.01$). There was no significant change in firing rate relative to the mean ongoing rate for the other directions.

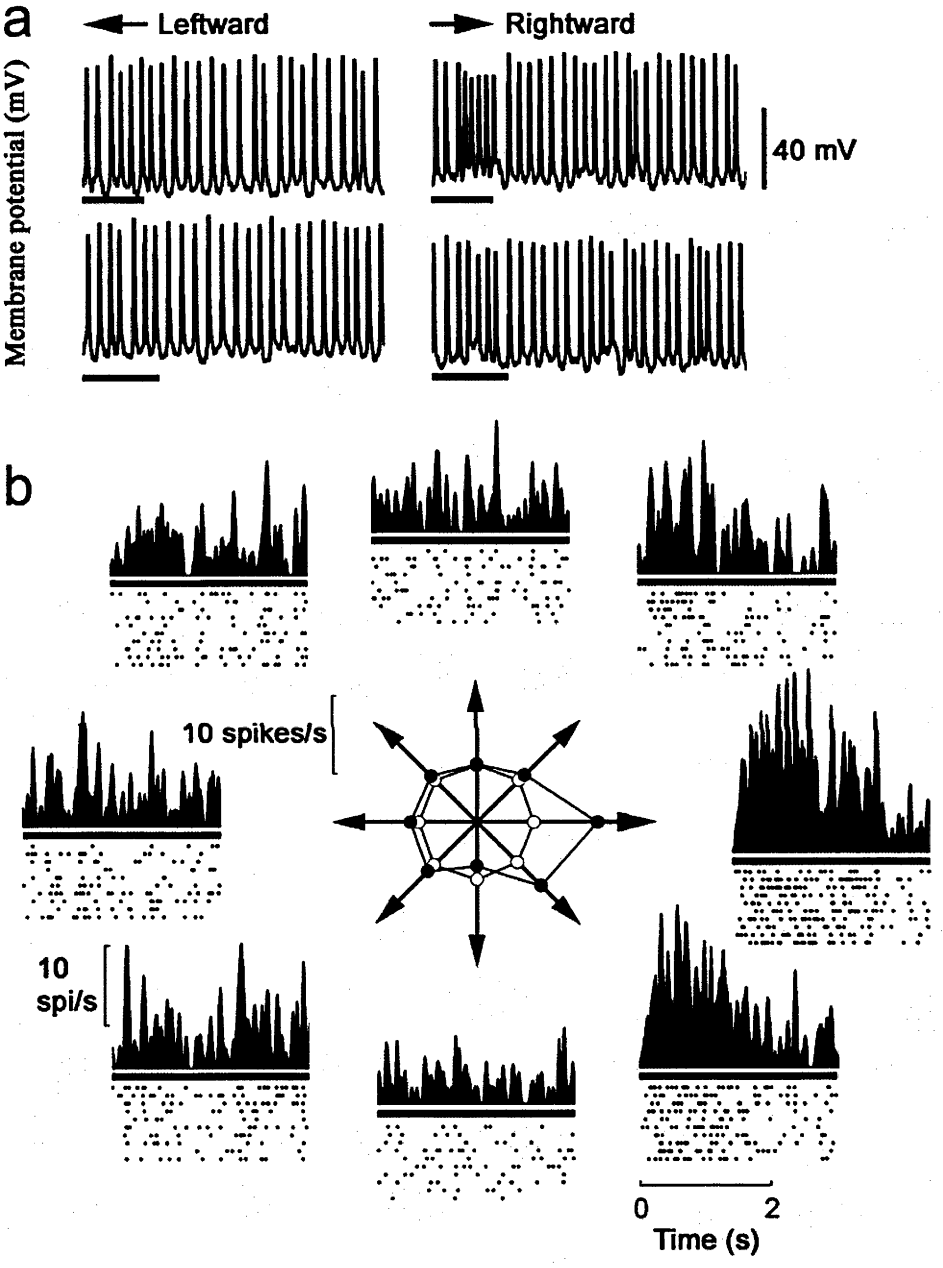
a
Leftward
Rightward
Membrane potential (mV)
40 mV
b
10 spikes/s
10
spi/s
0
2
Time (s)

Figure 6: Motion responses. (a) Spike trains during and after the movement of a vertical green bar that was moved horizontally across the receptive field of L8 to the left (left hand traces) and then to the right (right hand traces). The bar was moved at two speeds (upper, 100°/s; lower, 200°/s). The L8 neuron was on the right hand side of the nervous system. Motion to the right generates an increase in spike rate and a small depolarization of the membrane potential. Motion to the left does not influence the membrane potential or the spike rate. (b) Responses from another L8 neuron, again recorded on the right hand side of the nervous system. Responses to 3 seconds of wide-field grating motion are shown for 8 directions of motion. Both rasters and spike density functions are shown. The inner arrows show the directions of motion and the mean firing rates for each direction of motion (solid symbols). The mean spontaneous rate for this cell during these recordings was 10.2 spikes/s (open symbols). Significant increases in firing rate were obtained from this cell to rightward and rightward-down motion.

6.4.3.1 Directional and temporal tuning of neurons innervating muscle 51

The following convention is used when describing directional tuning. All descriptions are for cells in the left hand side of the body. Rightward motion equates to 0°, upward motion 90°, leftward motion 180° and downward motion 270°. Therefore, 180° is progressive motion over the left eye (i.e. motion from right to left and from front to back).

L8: From the eight L8 neurons we identified anatomically, the directional tuning was measured in full on six occasions. The cell has a lateral cell body and a distinctive long neurite, which makes identification relatively easy (Fig. 7a; Schröter et al. 2007). The ongoing spike rates ranged from 0-28 spikes/s between cells (e.g. Fig. 7). The directional preferences were always for progressive motion over the ipsilateral eye, e.g. leftward motion for a cell with its axon on the left hand side of the nervous system (Figs. 7b). The tuning functions were broad: the stars in Figure 7b show directions of motion that led to significant increases in spiking rate for one cell (t-test, $p<0.01$). The mean preferred direction for the six neurons was 187°±3.0SE (n=6). Stimulation of the contralateral eye with the ipsilateral eye covered produced only very small visual responses. This cell type was maximally sensitive to high TFs, with optima at 8-24Hz (Fig. 7c). The mean TF optimum was 13.3 Hz ±4.6SE (n=6).

M2: While M2 was filled on five occasions in total, we only determined directional tuning in three preparations. It has a ventro-medial cell body location, a distinct kink in its neurite and largely confines its dendrites to the upper regions of the SOG. Its morphology is characteristically different to M1, thus making it possible to identify it with relative ease (Fig. 7d). Spontaneous rates were 6-35 spikes/s in the recorded cells. The cells consistently preferred progressive image motion over the ipsilateral eye,

although the directions of motion that produced increased spike rates were broad (Fig. 7e). The stars in Figure 7E show directions of motion that led to significant increases in spiking rate for one cell (t-test, $p<0.01$). The mean preferred direction for the three neurons was 183°±6.7SE (n=3). Stimulation of the contralateral eye (ipsilateral eye covered) produced only small responses, suggesting that the cell receives mainly ipsilateral eye input. The temporal frequency (TF) tuning showed a preference for high TFs, with a mean peak value of 32 Hz ±16.0SE (n=3) (Fig. 7f).

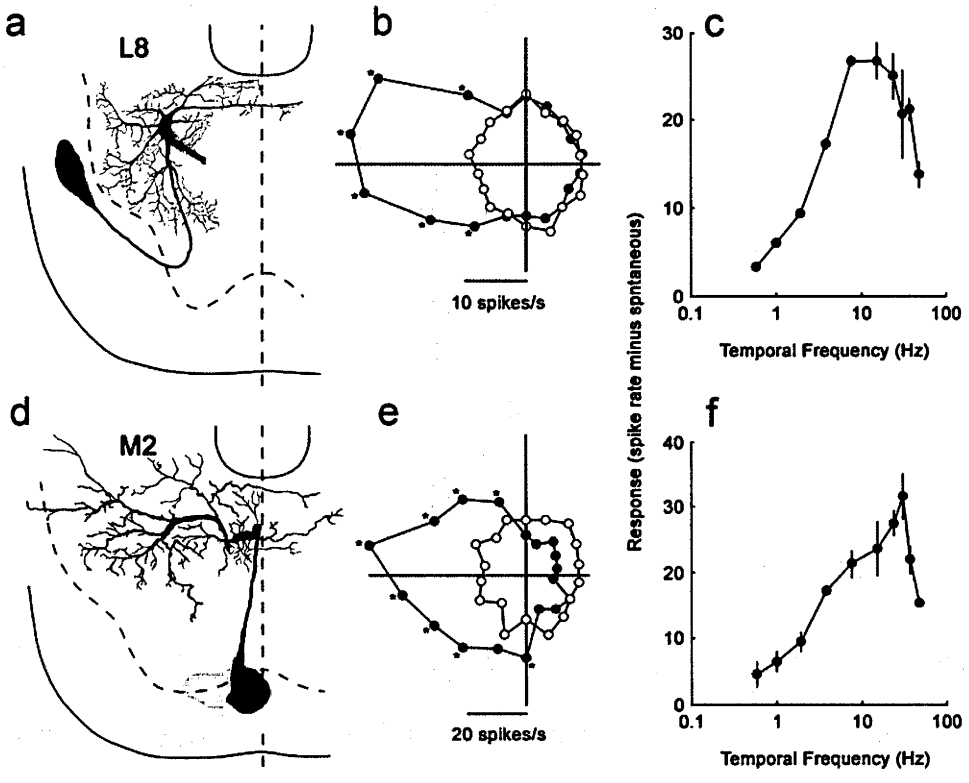

Figure 7: (a) A sketch of an L8 neuron in the SOG. Its directional and temporal frequency tuning are shown in b,c. (d) Sketch of a recorded M2 neuron, along with its directional and temporal tuning (e,f). Both cells respond maximally to progressive motion at high temporal frequencies of (8-24 Hz). Error bars represent standard errors.

6.4.3.2 Directional and temporal tuning of neurons innervating muscle 44

L5: Four confirmed recordings were obtained from this cell type but directional tuning was determined in only two preparations (Fig. 8a). The terminals were located in the dorsal-B subunit of muscle 44, which is what allowed unique identification (Schröter et al. 2007). The spontaneous activities in all cases were high (20-85 spikes/s). There was variation in the ongoing spike rate during each recording but it was relatively minor (30% over time). The directional tuning was consistent, with both cells showing a preference for regressive image motion when the stimulus was positioned frontally (Fig. 8b). The average preferred direction for the two cells was 351° (n=2). Clear responses were observed when the ipsilateral and contralateral eyes were stimulated by regressive motion. The TF tuning was also consistent, with peak TF tuning of 8 and 16Hz in the two cells examined in full (Fig. 8c).

L7: Confirmed recordings were made from this cell type on three occasions (Fig. 8d). The terminals were located in the medial subunit of muscle 44 (Schröter et al. 2007). The spontaneous activities were 0-30 spikes/s between preparations and were highly consistent for individual cells (variation of 10-20% during recordings). The directional tuning of all recorded cells showed high consistency, with all cells preferring regressive motion during frontal stimulation (Fig. 8E). The mean preferred direction was 348°±3.5SE (n=3). A clear characteristic of this cell class was a preference for lower TFs (Fig. 8f). The maximum response was recorded for a TF of 3 Hz ±1.7SE (n=3), while at 24 Hz the cell hardly responded.

M1: Successful recordings and fills from M1 were confirmed in 10 preparations. We were able to determine the directional tuning in six of these preparations. A photograph of one fill is presented in Figure 2 and a

drawing of another fill (Fig. 9a). The cell has three characteristic sweeping dendrites that descend from the dorsal to the ventral SOG. This characteristic, combined with the ventral cell body make identification between preparations particularly easy. M1 had a high spontaneous activity in all recordings, which ranged from 0 to 94 spikes/s. The spontaneous activity fluctuated by as much as 400% from the lowest measured spontaneous rate for prolonged periods during the recording. The fluctuations in spontaneous rate were not always correlated with stimulus manipulations. The cell produced robust responses when presented with full field flashing stimuli and gave weak directional responses when tested with wide-field motion (Fig. 9b). The mean directional tuning was 357°±5.2SE (n=6). The cell responded to stimulation of both eyes. A range of temporal frequencies of motion was tested and responses were most robust at high values (16-32 Hz, Fig. 9c). The mean TF optimum was 16 Hz ±6.5SE (n=4).

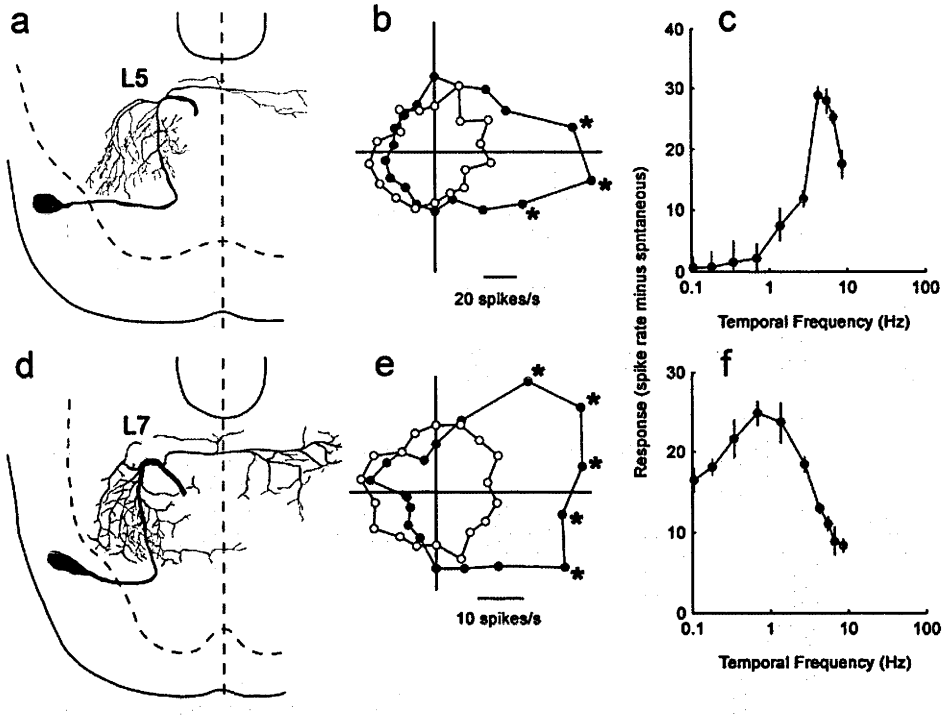

Figure 8: (a) A sketch of an L5 neuron in the SOG. Its directional and temporal frequency tuning are shown in b,c. (d) Sketch of a recorded L7 neuron, along with its directional and temporal tuning (e,f). Both cells respond to regressive motion. L5 responds optimally at high temporal frequencies (5-10 Hz), while L7 responds at lower temporal frequencies (1Hz). Error bars represent standard errors.

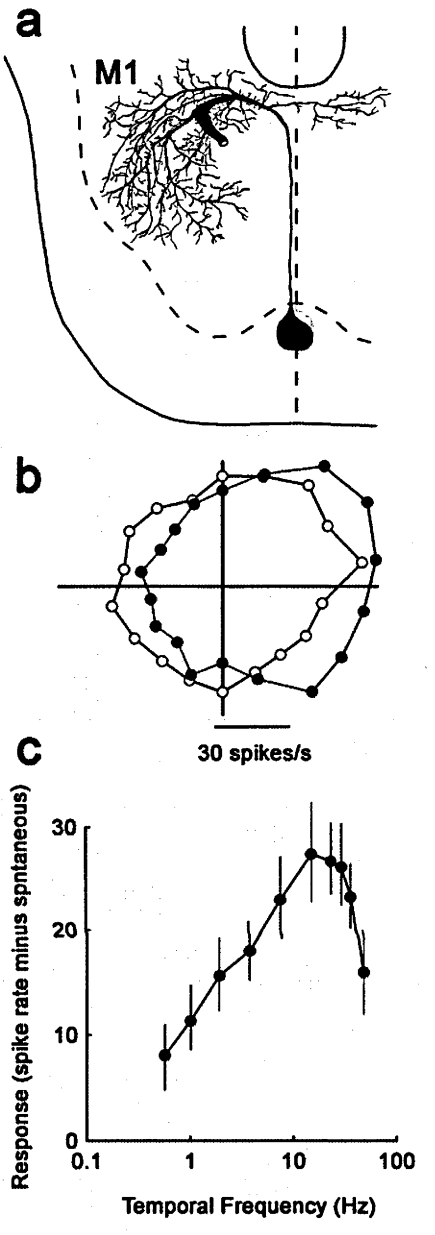

Figure 9: (a) A sketch of an M1 neuron in the SOG. Its directional and temporal frequency tuning are shown in b,c. M1 was optimally sensitive to high temporal frequencies of motion (>16 Hz). Error bars represent standard errors.

6.5 Discussion

Our study has for the first time identified the specific directional tuning characteristics of five uniquely identifiable motor neurons in the honeybee. These neurons innervate two of the muscles found on each side of the body in the neck region. The study revealed that each cell was optimally tuned to detect horizontal image motion at high temporal frequencies. The cells were found to receive input from both visual systems in the bee, the compound eyes and the ocelli. Moreover, all the cells were observed to respond to air currents and tactile stimulation of the head and antennae. Based on this data, we now discuss the relation between the directional tuning of the cells and the potential role of the neurons in driving head movements.

6.5.1 General characteristics

While the main focus of the present study was to investigate visual responses, it is clear that the motor neurons are multisensory, as is the case for fly neck motor neurons (Milde et al. 1987). While our air stimulation technique was not quantitative, it clearly revealed robust responses when air was blown over the heads of the animals. Cells in the bee that anatomically resemble M1 and M2 have been shown to respond to olfactory stimulation, and to have learning capacity (Menzel et al. 1991). Huston and Krapp (2008) have suggested that neck motor neurons in the fly are tuned to activate neck muscles during specific optic flow patterns, which are induced by particular types of self-motion. We did not measure the specific optic flow sensitivities of the motor neurons in the bee but certainly we have found that all five recorded neuron types are sensitive to motion in the horizontal plane, suggesting a role in head yaw stabilization. It is highly likely that the air currents generated by such movements are detected by sensory hairs and that this information is combined with visual input to provide selective stimulation of the neck motor neurons during flight. Descending neurons that connect the brain and thoracic motor centres in the locust have been

shown to accurately coordinate visual and tactile senses to generate turning responses (Reichert et al. 1985; Reichert and Rowell 1986).

The bee, like most insects has two types of eyes, the compound eyes and the simple eyes (ocelli) (shown schematically in Fig. 10). With the ocelli covered visual responses changed and spontaneous activities increased. It is plausible that stimulation of the ocelli needs to roughly match particular rotation axes before sensor fusion between the two visual systems occurs (Parsons et al. 2010). Even if this is the case, we have shown that there is a clear sensory input from both the ocelli and the compound eyes. It is intriguing that with the ocelli uncovered the spontaneous rates went down, suggesting that the ocelli provide a generalised suppression of the ongoing activity when they were exposed to the ambient light conditions in the laboratory. Honeybee ocellar neurons are excited by light off and suppressed by light on (Milde 1981). It appears that ongoing light levels directed at the ocelli drive suppressive signals that reduce the ongoing spiking activities of downstream neurons, including neck motor neurons.

The motor neurons were not disconnected from the muscles and, while the head and prothorax were firmly secured to the thorax with wax, the muscles within the prothorax were able to contract and relax at any time. We presume that the steady firing rates observed during non-stimulation periods (Fig. 3) are most likely position signals that drive a particular muscle contraction state. Under natural conditions this would equate to a particular head position relative to the thorax. The sudden non-stimulus related changes in spiking rates probably signal an internally generated command to change head position. The stability of the ongoing signals resembles the position signals, for example observed in the abducens motor neurons of the primate (Fuchs and Luschei 1970), which drive eye movements for many of the same reasons as the muscles of the bee drive head movements (e.g. to stabilize retinal images). We presume that the sudden increase in the frequency of action potentials generated by our visual stimuli would be sufficient to drive a change in muscle and, therefore, head

position and speed. Gilbert et al. (1995) have shown that electrical stimulation of selected neck muscles in flies leads to movements of the head.

6.5.2 Directional tuning

Two cells innervate muscle 51 (M2 and L8: Schröter et al. 2007). M2 innervates the dorsal subunit of the muscle and L8 innervates the ventral subunit. Both muscle subunits connect the rear of the prothoracic cavity (the endosternum) with the cervical apodeme of the episternum (CAE), which is located at the anterior end of the prothoracic cavity (Fig. 1a,b; Snodgrass 1942; Schröter et al. 2007). Muscle 51 is aligned such that it pulls the CAE inwards towards the centre of the prothorax (Fig. 10). Head turning in bees is a complex process, as recently revealed through 3-dimensional modelling of the head-neck system (Berry and Ibbotson 2010). There are only 5 pairs of muscles that connect the prothorax with the head. These muscles are able to drive head inclination (nose-up pitch) and declination (nose-down pitch) without involvement from other muscles in the thorax. However, head yaw and roll require far more complex interplay between the direct muscles and 12 pairs of indirect muscles that rotate the prothorax relative to the thorax or deform the shape of the prothoracic exoskeleton. The most likely role for the direct muscles during head yaw and roll is to retract the head firmly towards the prothorax (see small arrow close to the head of muscle 44 in Fig. 10B). This retraction effectively fixes the head to the prothorax. The 12 pairs of indirect muscles can rotate the prothorax within the thoracic cavity and, because the head is secured to it, also move the head relative to the thorax. For yaw the head cannot rotate in the horizontal plane because it rests on two horizontally aligned pivot points (the occipital processes). These are indicated in Figure 10 as 'x' and 'y'. For the head to yaw it is necessary for the occipital processes to be differentially retracted. That is, to turn the head to the right, the right hand occipital process (y) needs to be pulled inwards towards the prothorax (as is the case in Fig. 10b). This action 'makes space' for the head so that it can tilt to the right using the left

occipital process (x) as the fulcrum. It is probable that the contracting direct muscles force the head to move into that space. It is muscle 51 that has the most significant effect on retracting the occipital process (Fig. 1a,b). During dissection we attempted to retract the CAE and found that the exoskeleton at the base of the CAE is highly flexible (Berry and Ibbotson 2010).

Both M2 and L8 respond maximally to progressive image motion (motion towards the side containing the innervated muscle). When the image moves progressively, both MNs will respond optimally and provide maximum drive to muscle 51. This activity presumably leads to a muscle contraction, which pulls the ipsilateral occipital process inwards, thus in concert with other muscles turning the head towards that side of the body. A head turn in the direction of image motion acts to stabilize the retinal image and is referred to as an optomotor head turning response (van Hateren and Schilistra 1999). In conclusion, the directional tuning of both M2 and L8 are well suited to a role in driving progressive optomotor head turning in the bee in response to progressive image motion across the retina.

The control of muscle 44 is considerably more complex. This muscle is innervated by six neurons, of which we were able to record from three. All three neurons had consistent directional tuning properties: they all responded optimally to regressive image motion, as did the unit-type 2 reported using extracellular recording (Schröter et al. 2007). In itself, this finding is a surprise because muscle 44 appears to be arranged to activate head declination (nose-down pitch). To find that the cells innervating the muscle have horizontal tuning suggests a far more complex role for the muscle.

The directional tuning makes it possible that muscle 44 is involved in the control of yawing head movements. One role is probably to act with other direct muscles to anchor the head to the prothorax during head yaw. That is, when a horizontal head turn is about to occur, muscle 44 is contracted to retract the head towards the thorax. Muscle 44 connects centrally, medial to the occipital processes (Fig. 10b). Thus even activation

of this muscle on the left side of the nervous system will assist in turning the head to the right if simultaneous deformation of the right hand CAE (via the right hand muscle 51) has made a space for the head to move into. It is presumed that other direct muscles on the ipsilateral side of the body (right hand side in Fig. 10) also contract to drive yawing head movements (Berry and Ibbotson 2010).

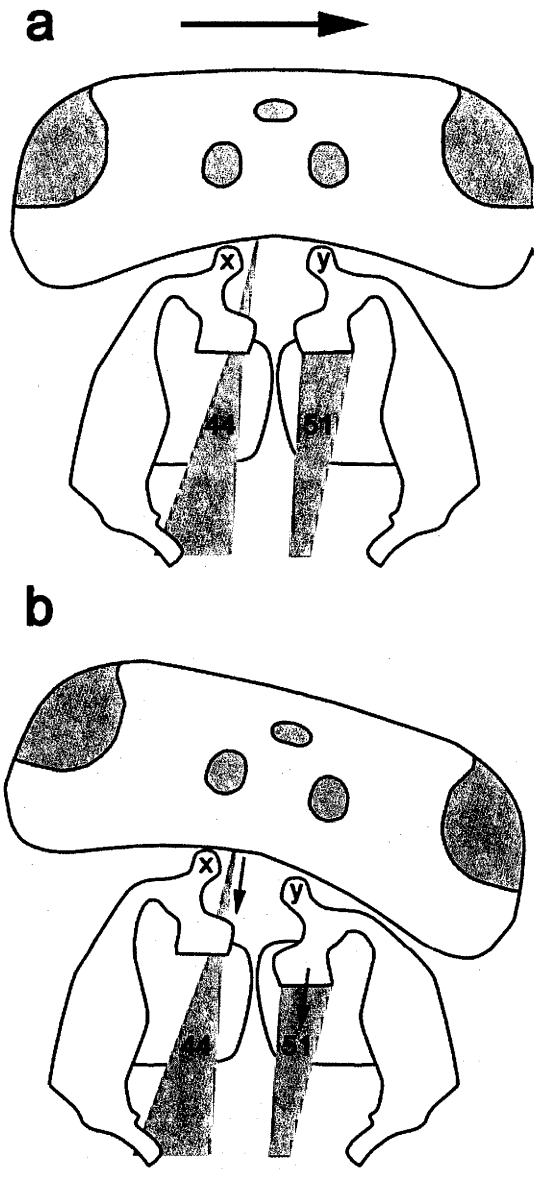

Figure 10: Organisation of yawing head turns in bees. (a) shows the head and prothorax with the head in the normal position, as viewed from above. x and y are the occipital processes and the numbered grey structures are the muscles 44 and 51 that would be involved in a rightward head turn. On the head we have outlined in grey the dorsal regions of the compound eyes and the three ocelli. During image motion to the right (black arrow), optomotor head turning occurs, which drives the head to the right, as shown in (b). To make the head turn to the right muscle 51 contracts, thus pulling the point y inwards. Other direct muscles, including muscle 44 also contract, thus turning the head to the right using point x as the fulcrum.

6.5.3 Temporal frequency tuning

Of the five cell types reported here, four were optimally activated by high temporal frequencies in the range from 8 to 32 Hz. It is interesting to correlate the temporal frequency properties to those of the descending neurons that potentially provide the visual input to the motor neurons. Recordings from descending neurons in the bee have revealed several identifiable neurons sensitive to motion in the same directions as those reported for the motor neurons presented here (Ibbotson and Goodman 1990; Ibbotson 1991). While no actual connectivity between the descending neurons and the motor neurons has been shown, the collaterals of the former clearly intermingle with the dendrites of the MNs in the suboesophageal ganglion. The temporal tuning of these horizontally tuned descending neurons is very similar to that of the MNs, with peaks in the range from 8-20Hz (Ibbotson and Goodman 1990). Direction-selective neurons in the lobula of the bee, which presumably provide input to the descending neurons described above, also exhibit very similar directional and temporal tuning to the motor neurons in IK1 (Ibbotson 1991; O'Carroll et al. 1996). Thus, the potential pathway from lobula to descending neurons to motor neurons in the bee reveals a consistency of temporal tuning. The temporal frequency dependence of optomotor head turning reflexes have not been measured in bees, however, the frequency tuning of optomotor body turning responses have been reported (Kunze 1961). That study revealed a peak temporal frequency tuning of 10 Hz, which again reasonably matches the data from the motor neurons in IK1.

For all the motor neurons reported here, low spatial frequency gratings produced the largest responses, as shown previously with extracellular recordings from IK1 (Schröter et al. 2007). We used a spatial frequency of 0.02cpd for virtually all experiments. Thus, given that speed is the ratio of temporal and spatial frequency, the optimal speed tuning for the cells was very high (400-1600°/s). Based on observations of bees in flight, it appears that they attempt to maintain optic flow speeds of between 200 and

600°/s (Baird et al. 2005; Srinivasan et al. 1996). These speeds were based on the movement of the bee itself and it can be assumed that even more rapid image speeds would be generated when the bee moves its head during flight. In the fly it has been shown that head turns during normal flight can be very fast (hundreds or thousands of degrees per second: van Hateren and Schilistra 1999). The optimum optic flow speed sensitivities observed in the motor neurons of the bee neck appear to be appropriate for the behavioural environment in which bees operate.

One cell type (L5) had consistently lower temporal frequency optima (4 Hz). This equates to 200°/s given a spatial frequency of 0.02cpd, which is lower but not particularly slow. It would appear that some type of speed-related range fractionation exists within the bee motor control system. It has been suggested that it is useful to have cells tuned to lower speeds for behaviours such as hovering close to flowers or scanning outside the nest in certain insect species, including bees (O'Carroll et al. 1996). Certainly it is typical for direction-selective visual neurons in birds and mammals to have a range of speed tuning properties within a given species (Ibbotson and Price 2001; Ibbotson and Mark 1996).

Acknowledgements

To our knowledge the first people to record from neurons in IK1 were Christopher J. Pomfrett and Lesley J. Goodman (unpublished observations). This preliminary work motivated the present study. The LED-based visual stimulator was developed by Dr Gert Stange. Dr Richard Berry developed the 3-Dimensional model of the bee neck used to generate Figure 1A and 1B.

Chapter 7

Summary

7.1 The morphology and anatomy of honeybee ocelli

In **Chapter 2**, I revealed the morphology, anatomy, and optical properties of the honeybee ocelli. A 3-dimensional (3-D) reconstruction model of the honeybee ocelli, including the cuticle, ocellar lenses and the retinas, was developed to understand the ocellar field of view. Anatomically, I showed that each of the three honeybee ocelli have two retinas, each at a different distance from the rear of the ocellar lens. The two retinas in each ocellus are known as the dorsal and ventral retinas. The 3-D reconstruction model of the honeybee ocelli that I developed in this study provided a mechanism for judging the receptive fields of the dorsal and ventral retinas. It is suggested that the dorsal retinas view the sky and above while the dorsal retinas view the horizon for both the median and lateral ocelli.

By using the hanging-drop method, I revealed the optical properties of the ocellar lenses including the back-focal lengths of the lenses. This analysis also revealed the spatial resolving capacity of the ocelli in terms of the number of bars of a grating pattern that could be resolved. It was shown that the lateral ocellus has higher spatial resolution than the median ocellus. It was also shown that the dorsal retinas have a higher spatial resolution than the ventral retinas in both the median and lateral ocelli, consistent with the need to assess spatial detail on the horizon.

7.2 Descending neuron anatomy: motion-sensitive descending neurons

In **Chapter 3**, by using modern fluorescence dye-filling and optical sectioning (confocal microscopy), I presented the detailed neural anatomy of 5 types of honeybee motion-sensitive descending neurons ($DNII_2$, $DNIV_2$, $DNIV_3$, $DNVII_1$, and $DNVII_2$). Among those cells, $DNVII_2$ is a new cell type in which the morphology is reported for the first time. Neural 3-D reconstructions were also made for $DNVII_1$ and $DNVII_2$ for complete comparisons of the morphology of the known cells in the DNVII category. This is also the first time that the depth information of those descending neurons has been reported in the brain. The detailed spatial geometry within the brain presented in this chapter provides a better understanding of the dendritic inputs onto honeybee motion-sensitive descending neurons and the targets of their axonal outputs.

Combining the new knowledge found in the ocellar anatomy (in Chapter 2) I have shown that the dendritic field of ocellar descending neuron $Locth_3$ originates exclusively from the ventral retina of the lateral ocellus.

7.3 Motion and spectral wavelength processing in the honeybee descending neurons

In **Chapter 4**, I showed the responses of two pitch-sensitive neurons, the motion-sensitive descending neuron $DNII_2$ and the ocellar descending neuron $Locth_3$. Both cells are direction-selective to upward motion in the frontal visual field. The responses to the two different spectra showed that they respond equally to both green and the short-wavelength stimulus. Similar spectral results were also observed in two roll-sensitive descending

neurons, $DNIV_2$ and $DNIV_3$ (shown in **Chapter 5**), i.e. they responded equally to both short-wavelength and green motion stimulation. However, for the yaw-sensitive neuron $DNVII_1$, the excitatory responses only occurred for the green stimulus in the preferred direction while the short-wavelength stimulus induced clear inhibitory responses for all tested motion directions. The results suggest that besides green photoreceptors, the ocellar descending neuron $Locth_3$ and the vertically tuned direction-selective descending neurons also receive inputs from the short-wavelength photoreceptors. However, spectral processing is different between the vertically (pitch and roll) and horizontally (yaw) tuned systems: short-wavelength inputs provide excitatory input only to motion detectors tuned for vertical motion.

7.4 Ocellar inputs to motion-sensitive neurons

The honeybee motion-sensitive descending neurons that were previously believed to receive inputs from the compound eyes have now been shown to be multisensory, receiving inputs from both the compound eyes and the ocelli. In **Chapters 4 and 5** I compared the cell responses when both compound eyes and ocelli were stimulated against the case where only the compound eyes were stimulated (i.e. the ocelli were occluded). It was shown that the ocellar inputs contribute a strong OFF response and also enhance the response amplitudes to flashed stimuli. It was also shown that the ocellar inputs led to reduced response latencies to both flashed and motion stimulation. In the case of the $DNII_2$ neuron, although the results suggested that the ocelli provide little input in terms of the amplitudes of the direction-selective responses, a weak but consistent excitatory response after downward motion (anti-preferred direction) was observed only when the compound eyes and ocelli were stimulated simultaneously. The results suggest that the ocelli provide directional inputs to at least one type of motion-sensitive neuron, $DNII_2$.

7.5 Visual response properties of honeybee neck motor neurons

In Chapter 4 and 5 I reported the spectral and motion responses characteristics of the honeybee descending neurons, while in **Chapter 6**, I presented the responses of the neck motor neurons. In insects, the head movements are mediated by the neck motor system. From previous anatomical studies it is believed that insect neck motor neurons are innervated primarily by descending neurons (Gronenberg et al. 1995; Gronenberg and Strausfeld 1990ab; Gronenberg and Strausfeld 1991; Schröter et al. 2007; Hung et al. 2011; also see *Chapter 2*). The recordings were made in five identified motor neuron types (M1, M2, L5, L7 and L8) in the first cervical nerve (IK1). Two motor neurons (L8 and M2) that innervate muscle 51 were found to be direction-selective to horizontal motions moving from the contralateral to the ipsilateral side of the head. Three neurons (L5, L7, and M1) that innervate muscle 44 were tuned to detect motion in the opposite direction (from ipsilateral to contralateral). It is suggested that by combining the directional tuning of the motor neurons in an opponent manner, the neck motor system would be able to mediate reflexive optomotor head turns in the direction of image motion, thus stabilising the retinal image.

Bibliography

Abner BL and Trouth CO (1989) The spectral sensitivity of the ocellar system in the cricket *Gryllus firmus* (Orthoptera: Gryllidae) J Insect Physiol 35:805–808

Autrum H and Stoecker M (1950) Die verschmelzungs frequenzen des Birnauges. Z Naturforsch 5b:38–43

Autrum H and Thomas I (1973) Comparative physiology of color vision in animals. In: Jung R (ed.) Central Processing of Visual Information A: Integrative Functions and Comparative Data (Handbook of Sensory Physiology Vol 7/3A) Springer-Verlag Press, Berlin, Heidelberg, New York. pp. 661–692

Autrum HV and von Zwehl VZ (1964) Spektrale Empfindichkeit einzelner Sehzellen des Bienenauges. Z Vergl Physiol 48:357–384

Baader A (1991) The contribution of some neck and abdominal motoneurons in locust (Locusta migratoria) steering reactions. J Insect Physiol 37:689–697

Baird E, Srinivasan MV, Zhang S and Cowling A (2005).Visual control of flight speed in honeybees. J Exp Biol 208:3895–3905

Barton JS, Sharp JA and Raymond JE (1995) Retinotopic and directional defects in motion discrimination in humans with cerebral lesions. Ann Neurol 37:665–675

Batschelet E (1981) Circular statistics in biology. Academic Press, London

Berry R, Ibbotson M (2010) A three-dimensional atlas of the honeybee neck. PLoS ONE 5:1–14

Berry R, Stange G, Olberg R, and van Kleef J (2006) The mapping of visual space by identified large second-order neurons in the dragonfly median ocellus. J Comp Physiol A 192:1105–1123

Berry RP, Stange G and Warrant EJ (2007a) Form vision in the insect dorsal ocelli: an anatomical and optical analysis of the dragonfly median ocellus. Vision Res 47:1394–1409

Berry RP, Stange G and Warrant EJ (2007b) Form vision in the insect dorsal ocelli: an anatomical and optical analysis of the locust ocelli. Vision Res 47:1382–1393

Berry RP, Wcislo WT and Warrant EJ (2011) Ocellar adaptation for dim light vision in a nocturnal bee. J Exp Biol 214:1283–1293

Bidwell NJ and Goodman LJ (1993) Possible function of a population of descending neurons in the honeybee's visuo-motor pathway. Apidologie 24:333-354

Blondeau J and Heisenberg M (1982) The three-dimensional optomotor torque system of *Drosophila melanogaster*. J Comp Phyiol 145:321–329

Böeddeker N and Hemmi JM (2010). Visual gaze control during peering flight manoeuvres in honeybees Proc Roy Soc B 277:1209–1217

Böeddeker N, Dittmar L, Stuerzl W and Egelhaaf M (2010) The fine structure of honeybee head and body yaw movements in a homing task. Proc Roy Soc B 277:1899–1906

Borst A and Egelhaaf M (1989) Principles of visual motion detection. Tins 12:297–306

Brandt R, Rohlfing T, Rybak J, Krofczik S, Maye A, Westerhoff M, Hege H-C and Menzel R (2005) Three-dimensional average-shape atlas

of the honeybee brain and its applications. J Comp Neurol 492:1–19

Buchner E (1984) Behavioral analysis of spectral vision in insects. In Ali MA (ed.) Photoreception and Vision in Invertebrates. Plenum: New York and London, pp. 561–622

Buchsbaum G, and Gottschalk A (1983) Trichormacy, opponent colours coding and optimum colour information in the retina. Proc R Soc Lond B Biol Sci 220:89–113

Campbell, H. R. (2001). Orientation discrimination independent of retinal matching by blowflies. J Exp Biol 204:15–23

Cajal SR (1918) Observaciones sobre la estructura de los ocelos y vias nerviosas ocelars de algunos insectos. Trab Lab Invest Biol Ubiv Madrid 16:109–139

Cajal SR, Sanchez D (1915) Contribution al conocimiento de los centros nerviosos de los insectos. Trab Lab Invest Biol Univ Madrid 13:1–168

Chappell RL and DeVoe RD (1975) action spectra and chromatic mechanisms of cells in the median ocelli of dragonflies. Journal of General Physiology 65: 399–419

Chiappe M, Eugenia SJD, Reiser MB, Jayaraman V (2010) Walking Modulates Speed Sensitivity in Drosophila Motion Vision. Current Biol 20:1470–1475

Chittka L, Beier W, Hertel H, Steinmann E, and Menzel R (1992) Opponent color coding is a universal strategy to evaluate the photoreceptor inputs in Hymentoptera. J Physiol A 170:545–563

Chittka L, Spaethe J, Schmidt A and Hickeksberger A (2001) Adaption, constraint, and chance in the evolution of flower color and pollinator color vision. *In*: Chittka L, and Thomson JD (eds.) Cognitive

ecology of pollination: animal behaviour and floral evolution. Cambridge University Press, Cambridge pp.106–126

Clifford CWG and Ibbotson MR (2003) Fundamental mechanisms of visual motion detection: models, cells and functions. Progress in Neurobiology. 68:409–437

Collett T (1971) Connections between wide-field monocular and binocular movement detectors in the brain of a hawk moth. Z Vergl Physiol 75:1–31

Collett T and King AJ (1975) Vision during flight. In Horridge GA (ed). The compound eye and vision in insects. Clarendon Press, Oxford, pp 437–466

Cornwell PB (1955) The functions of ocelli of Calliphora (Diptera) and Locusta (Orthoptera). J Exp Biol 32:217–237

Cronin T W, *Marshall NJ, and Caldwell LR (*2000*) Spectral tuning and the visual ecology of mantis shrimps.* Phil Trans Roy Soc B 3551263–*1267*

de Souza J, Hertal H, Ventura DF and Menzel R (1992) Response properties of stained monopolar cells in the honeybee lamina. J Comp Physiol A 170:267–274

de Valois RL (1973) Central mechanisms of color vision. *In*: Jung R (ed.) Handbook of Sensory Physiology, vol. 7/3A. Springer, Berlin. pp. 209-253

DeVoe RD (1980) Movement sensitivities of cells in the fly's medulla. J Comp Physiol 138:93–119

DeVoe RD, Kaiser W, Ohm J, and Stone LS (1982) Horizontal movement detectors of honeybees: Directionally-selective visual neurons in the lobula and brain. J Comp Physiol 147:155–170

DeVoe RD and Ockleford EM (1976) Intracellular cellular responses from ells of the medulla of the fly, *Calliphora erthrocephala*. Biol Cybern 23:13–24

Douglass JK and Strausfeld NJ (1995) Visual motion detection circuits in flies: Peripheral motion computation by identified small-field retinotopic neurons. J Neurosci 15: 5596-5611

Douglass JK and Strausfeld NJ (1996) Visual motion-detection circuits in flies: Parallel direction- and non-direction-sensitive pathways between the medulla and the lobula plate. J Neurosci 16:4451–4562

Dujardin F (1850) Mémorie sur le system nerveux des insects. Annales des Science Naturelles Zoologie B14: 195–206

Dyer AG, Paulk AC and Reser DH (2011) Colour processing in complex environments: insights from the visual system of bees. Proc R Soc B 278:952–959

Eckert H (1971) Die spektrale Empfindlichkeit des Komplexauges von *Musca* (Bestimmung aus Messungen der optomotorischen Reaktion). Kybernetik 9:145–156

Eckert H (1973) Optomotorische untersuchungen am visuellen system der Stubenfliege *Musca domestica* L. Kybernetik 14:1–23

Edwards DM (1982) The cockroach DCMD neuron. II Dynamics of response habituation and convergence of spectral inputs. J Exp Biol 99:61–90

Efler D and Ronacher B (2000). Evidence against retinoptic-template matching in honeybees pattern recognition. Vis Res 40:3391–3403

el Jundi B, Heinze S, Lenschow C, Kurylas A, Rohlfing T and Homberg U (2009) The lost standard brain: A 3D standard of the central complex as a platform for neural network analysis. Front Syst Neurosci 3:21

Emerson RC, Bergen JR, and Adelson EH (1992) Directionally selective complex cells and the computation of motion energy in cat visual cortex. Vis Res 32:203–218

Esch HE. Zhang SW, Srinivasan MV, Tautz J (2001) Honeybee dances communicate distances measured by optic flow. Nature 411:581–583

Fermi G and Reichardt W (1963) Optomotorische reaktionen der fliege Musca domestica. Kybernetik 2:15–28

Flanagan D and Mercer AR (1989) An atlas and 3-D reconstruction of the antennal lobes in the worker honeybee, *Apis mellifera* L. (Hymenoptera: *Apidae*). Int J Insect Morphol Embryol 18: 145–159

Fletcher WA, Goodman LJ, Guy RG and Mobbs PG (1984) Horizontal and vertical motion detectors in the ventral nerve cord of the honeybee, *Apis mellifera*. J Physiol, Lond 351, 15P

Fry SN, Rohreseitz N, Straw AD and Dickinson MH (2009) Visual control of flight speed in *Drosophila melanogaster*. J Exp Biol 212:1120–1130

Fuchs AF, Luschei ES (1970) Firing patterns of abducens neurons of alert monkeys in relationship to horizontal eye movement. J Neurophysiol 33:382–390

Gibson JJ (1979). The Ecological Approach to Visual Perception. Boston: Houghton Mifflin.

Giger AD and Srinivasan MV (1997) Honeybee vision: analysis of orientation and colour in the lateral, dorsal and ventral fields of view. J Exp Biol 200:1271–1280

Gilbert C, Gronenberg W, and Strausfeld NJ (1995) Oculomotor control in calliphorid flies – head movements during activation and inhibition of neck motor-neurons corroborate neuroanatomical predictions. J Comp Neurol 361:285–297

Goldsmith TH and Ruck PR (1958) the spectral sensitivities of the dorsal ocelli of cockroaches and honeybees. J Gen Physiol 41:1171–1185

Goodman C (1974) Anatomy of locust ocellar interneurons: constancy and variability. J Comp Physiol 95:185–201

Goodman CS (1976) Anatomy of the ocellar interneurons of acridid grasshoppers. I. The large interneurons. Cell Tissue Res 175:183–202

Goodman CS and Williams JLD (1976) Anatomy of the ocellar interneurons of acridid grasshoppers. II. The small interneurons. Cell Tissue Res 175:203–225

Goodman LJ (1981) Organization and physiology of the insect dorsal ocellar system. In Autrum H (ed) Handbook of sensory physiology, vol VII/6C. Springer, Berlin Heidelberg New York, pp 201–286

Goodman LJ, Fletcher WA, Guy RG , Mobbs PG and Pomfrett CJD (1987) Motion sensitive descending interneurons, ocellar LD neurons and neck motor neurons in the bee: a neural substrate for visual course control in *Apis mellifera*. *In* Neurobiology and Behaviour of Honeybees ed. Menzel R and Mercer A (Berlin, Heidelberg, New York: Springer-Verlag), *pp* 158–171.

Goodman LJ, Ibbotson MR and Bidwell NJ (1991) Spatial, temporal and directional properties of motion-sensitive visual neurons in the honeybee. *In*: The Behaviour and Physiology of Bees (Goodman L, and Fisher RC eds.) CAB Int, Oxon, UK

Goodman LJ, Ibbotson MR, and Pomfrett CJD (1990) Directional tuning of motion-sensitive interneurons in the brain of insect. *In*: higher order Sensory Processing (Guthrie DM, ed) Manchester Univ Press, Manchester

Gribakin FG (1969a) Types of photoreceptors in the compound eye of the worker honeybee relative to their spectral sensitivity. Cytologia 11:309–314

Gribakin FG (1969b) The distribution of the long wave photoreceptors in the compound eye of the honeybee as revealed by selective osmic staining. Vision Res 12:1225–1230

Gronenberg W, Milde J and Strausfeld NJ (1995) Oculomotor control in calliphorid flies: Organization of descending neurons to neck motor neurons responding to visual stimuli. J Comp Neurol 361:267–284

Gronenberg W and Strausfeld NJ (1990a) Descending neurons supplying the neck and flight motor of Diptera: Organization and neuroanatomical relationships with visual pathways. J Comp Neurol 302:954–972

Gronenberg W and Strausfeld NJ (1990b) Descending neurons supplying the neck and flight motor of Diptera: Physiologycal and anatomical characteristics. J Comp Neurol 302:973–991

Gronenberg W and Strausfeld NJ (1991) Descending pathways connecting the male-specific visual system of flies to the neck and flight motor. J Comp Physiol A 161:413-426

Guitton D (1992) Control of eye-head coordination during orienting gaze shifts. Trends Neurosci 15:174–179

Guy RG, Goodman LJ, Mobbs PG (1979) Visual interneurons in the bee brain: Synaptic organisation and transmission by graded potentials. J Comp Physiol 134:253–264

Haag J, Wertz A and Borst A (2007) Integration of lobula plate output signals by DNOVS1, an identified premotor descending neuron. J Neurosci 27:1992–2000

Haddad D, Schaupp F, Brandt R, Manz G, Menzel R and Haase A (2004) NMR imaging of the honeybee brain. J Insect Sci 4:7

Hammer M and Menzel R (1995) Learning and memory in the honeybee. J Neurosci 15: 1617–1630

Hassenstein B and Richardt W (1956) Systemthoretische Analyse der Zeit, Reihengolgen, und Vorzeichenauswertung bei der Bewegung-sperzeption des Rüsselkäfers Chlorophanus. Z, Naturforsch 11b:513–524

Hausen K (1982) Motion sensitive interneurons in the optomotor system of the fly .2. The horizontal cells – receptive-field organization and response characteristics. Biological Cybernetics 46:67–79

Hausen K, Wolburg-Buchholz K, Ribi WA (1980) The synaptic organization of visual interneurons in the lobula complex of flies. Cell Tissue Res 208:371–387

Heinzeller T (1976) Second-order ocellar neurons in the brain of the honeybee (*Apis mellifera*) Cell Tiss. Res. 171:91–99

Hengstenberg R (1972) Eyes movements in the housefly *Musca domestica.* Datenverarbeitung im visuellen System der Arthopoden, ed Wehner R (Springer, Berlin), *pp* 93–96.

Hengstenberg R. (1984) Roll-stabilization during flight of the blowfly's head and body by mechanical and visual cues. In D. Varju and U. Schnitzler (eds): Localization and orientation in biology and engineering. Berlin: Springer Verlag, pp. 121–134

Hengstenberg R (1993) Multisensory control in insect oculomotor systems. In Visual motion and its role in the stabilization of gaze (eds Miles FA, and Wallman J.), pp. 285–298. Amsterdam, The Netherlands: Elsevier.

Hengstenberg R, Sandeman DC, and Hengstenberg B (1986) Compensatory head roll in the blow fly Calliphora during flight. Proc R Soc London B 227:455–482

Hensler K and Rowell CHF (1990) Control of optomotor response by descending deviation detector neurons in intact flying locusts. J Exp Biol 149:191–205

Hertel H (1980) Chromatic properties of identified interneurons in the optic lobes of the honeybee. J Comp Physiol A 137: 215–231

Hertel H and Maronde U (1987a) The physiology and morphology of centrally projecting visual interneurons in the honeybee brain. J Exp Biol. 133:301–315

Hertel H and Maronde U (1987b) Processing of visual information in the honeybee brain. *In*: Menzel R and Mercer A (eds): Neurobiology and Behavior of Honeybees. Berlin: Springer-Verlag, pp. 141–157

Hickson SJ (1885) The eye and optic tract of insects. Quart J Micr Sci 2, Band XXV

Homann H (1924) Zum Problem der Ocellenfunktion bei den Insekten. Z Vergl Physiol 1:541–571

Horidge GA (1980) Apposition eye of large diurnal insects as organs adapted to seeing. Proc R Soc Lond B 207:387–309

Horridge, A. (2000). Seven experiments on pattern vision of the honeybee, with a model. Vision Res. 40:2589–2603

Horridge A (2009) What does the honeybee see? And how do we know? ANU E Press

Hoyle (1977) Indentified neurons and behaviour of arthropods. Plenum Press, New York

Hung Y-S, van Kleef JP and Ibbotson MR (2011) Visual response properties of neck motor neurons in the honeybee. J Comp Physiol A 197:1173–1187

Huston SJ and Krapp HG (2008) Visuomotor transformation in the fly gaze stabilization system. PLOS Biology 6:1468–1478

Huston SJ and Krapp HG (2009) Nonlinear Integration of Visual and Haltere Inputs in Fly Neck Motor Neurons. J Neurosci 29: 13097–13105

Ibbotson MR (1989) Directionally selective visual interneurons in *Apis mellifera* and *Paravespula vulgaris*: a neural substrate controlling visual orientation. PhD thesis, London

Ibbotson MR (1991a) A motion-sensitive visual descending neurons in *Apis mellifera* monitoring translator flow-fields in the horizontal plane. J Exp Biol 157:573–577

Ibbotson MR (1991b) Wild-field motion-sensitive neurons tuned to horizontal movement in the honeybee, *Apis mellifera*. J Comp Physiol A. 168:91–102

Ibbotson MR (2001) Evidence for velocity-tuned motion-sensitive descending neurons in the honeybee. Proc R Soc Lond B 268:2195–2201

Ibbotson MR, Crowder NA, Cloherty SL, Price NSC, Mustari MJ (2008) Saccadic modulation of neural responses: possible roles in saccadic suppression, enhancement and time compression. J Neuroscience 28:10952–10960

Ibbotson MR, Goodman LJ (1990) Response characteristics of four wide-field motion-sensitive descending interneurons in *Apis mellifera*. J Exp Biol 148:255–279

Ibbotson MR, Maddess T, and Dubois R (1991) A system of insect neurons sensitive to horizontal and vertical image motion connects the medulla and midbrain. J Comp Physiol A 169:355–367

Ibbotson MR, Mark RF (1996) Impulse responses distinguish two classes of directional motion-sensitive neurons in the nucleus of the optic tract. J Neurophysiol 75:996–1007

Ibbotson MR, Price NSC (2001) Spatiotemporal tuning of directional neurons in mammalian and avian pretectum: A comparison of physiological properties. J Neurophysiol 86:2621–2624

Ibbotson MR, Price NSC, Crowder NA, Ono S, Mustari MJ (2007) Enhanced motion sensitivity follows saccadic suppression in the superior temporal sulcus of the macaque cortex. Cerebral Cortex 17:1129–1138

Kaiser W (1975) The relationship between visual movement detection and colour vision in insects. *In*: Horridge A (ed.): The compound Eye and Vision of Insects. Clarendon Press, Oxford, UK

Kaiser W and Bishop LG (1970) Directionally selective motion detecting units in the optic lobe of the honeybee. Z vergl Physiologie 67:403–413

Kaiser W, Liske E (1974) Die optomotoriscen Reaktionen von fixiert fliegenden Bienen bei Reizung mit Spektrallichtern. J Comp Physiol 89:391–408

Karmeier K, van Hateren J H, Kern R, Egelhaaf M (2006) Encoding of naturalistic optic flow by a population of blowfly motion-sensitive neurons. J Neurophysiol 96:1602–1614

Kastberger G (1990) The ocelli control the flight course in honeybees. Physiol Entomol 15:337–346

Kastberger G and Schuhmann K (1993) Ocellar occlusion effect on the flight behaviour of homing honeybees. J Insect Physiol 39:589–600

Kelber A. (1999) Ovipositing butterflies use a red receptor to see green. J. Exp. Biol. 202:2619–2630

Kelber A, Balkenius A and Warrant EJ (2003) Colour vision in diurnal; and nocturnal hawkmoths. Interger Comp Biol 43:571–579

Kelber A, and Pfaff M (1999) True colour vision in the orchard butterfly, *Papillo aegeus*. Naturwissenschaften 86:221-224

Kern R, van Hateren JH, Michaelis C, Lindemann JP, Egelhaaf M (2005) Function of a fly motion-sensitive neuron matches eye movements during free flight. PLOS BIOLOGY 3:1130–1138

Kenyon FG (1896) The brain of the bee. J Comp Neurol 6:133–210

Kein J (1974) Sensory integration in the locust optomotor system. II. Direction selective neurons in the circumesophageal connective and the optic lobe. Vision Res 14:1255–1268

Kien J and Menzel R (1977a). Chromatic properties of interneurons in the optic lobes of the bee. I. Broad band neurons. J Comp Physiol 113:17–34

Kien J and Menzel R (1977b) Chromatic properties of interneurons in the optic lobes of the bee. II. Narrow band and colour opponent neurons. J Comp Physiol 113:35–53

Kolb G, and Scherer C (1982) Experiments on wavelength specific behaviour of *Pieris brassicae* L. during drumming and egg-laying. J Physiol A 149:325–332

Koontz M (1976) Neural pathways from the dorsal ocelli of the house cricket, *Acheta domesticus*. J Morphol 149:105–120

Krapp HG and Hengstenberg R (1996) Estimation of self-motion by optic flow processing in single visual interneurons. Nature 384:463–466

Krauss A and Neumeyer C (2003) Wavelength dependence of the optomotor response in zebrafish (*Danio rerio*). Vision Res 43:1273–1283

Künze P (1961) Untersuchung des Bewegungssehens fixiert fliegender Bienen. Z Vergl Physiol 44:656–684

Land, MF (1973) Head movements of flies during visually guided flight. Nature 243:299–300

Lehrer M (1994) Spatial vision in the honeybee: the use of different cues in different tasks. Vision Res 34:2363–2385

Lehrer M (1998) Looking all around: Honeybee use different cues in different eye regions. J Exp Biol 201:3275–3292

Lehrer M, Srinivasan MV and Zhang SW (1990) Visual edge detection in the honeybee and its spectral properties. Proc R Soc Lond B 238:321–330

Lewen GD, Bialek W, de Ruyter van Steveninck RR (2001) Neural coding of naturalistic motion stimuli. Network 12:317–329

Leydig F (1885) Zum feineren Bau der Arthropoden. Arch Anat Physiol

Lindemann JP, Kern R, Michaelis C, Meyer P, van Hateren JH, Egelhaaf M (2003) Flimax, a novel stimulus device for panoramic and highspeed presentation of behaviourally generated optic flow. Vis Res 43:779–791

Lindemann JP, Weiss H, Moeller R, Egelhaaf M (2008) Saccadoc flight strategy facilitates collision avoidance: closed-loop performance of a cyberfly. Biological Cybernetics 98:213–227

Livingstones MS and Hubel DH (1988) Segregation of form, color, movement and depth: anatomy, physiology and perception. Science 240:740–749

Longden K, Krapp H (2009) State-dependent performance of optic flow processing interneurons. J Neurophysiol 102: 3606–3618

Lowne B (1870) The anatomy and physiology of the blowfly (*Musca vomitoria* Linn.), John Van Voorst (ed), London, pp 121

Maddess T, Dubois RA and Ibbotson MR (1991) Response properties and adaptation of neurons sensitive to image motion in the butterfly *Papilio aegeus*. J Exp Biol 161:171–199

Maimon G, Straw AD, and Dickinson MH (2010) Active flight increases the gain of visual motion processing in Drosophila. Nat Neurosci 13:393–U29

Mares S, Ash L, Gronenberg W (2005) Brain anatomy in bumblebee and honey bee workers. Brain Behav Evol 66:50–61

Markl H (1966) Peripheres Nervensystem und Muskulatur im Thorax der Arbeiterin von *Apis mellifica* L., *Formica polyctena* Foerster und *Vespa vulgaris* L. und der Grundplan der Innervierung des Insektenthorax. Zool Jb Anat 83:107–184

Maronde U (1988) Strukturelle und Funkionelle Charakterisierung visueller Interneuronenpopulationen im Protocerebrum der Honigbiene Apis mellifera. PhD thesis, Freie Universität Berlin

Maronde U (1991) Common projection areas of antennal and visual pathways in the honeybee brain Apis mellifera. J Comp Neurol 309:328–340

McCann GD and Arnett DW (1972) Spectral and polarization sensitivity of the dipteran visual system. J Gen Physiol 59:534–558

Meinertzhagen IA (1976) The organization of perpendicular fibre pathways in the insect optic lobe. Philos Trans R Soc Lond B Biol Sci 274:555–94

Menzel R (1974) Spectral sensitivity of monopolor cells in the bee lamina. J Comp Physiol 93:337–346

Menzel R (1979) Spectral sensitivity and colour vision in invertebrates. *In*: H. Autrum (ed): Comparative physiology and evolution of vision in Invertebrates (Handbook of sensory physiology, Vol.VII/6A). Berlin: Springer, pp. 503-580

Menzel R (2001) Searching for the memory trace in a mini-brain, the honeybee. Learning and Memory 8: 53–62

Menzel R and Backhaus W (1991) Colour vision in insects. In: The perception of colour. Gouras P (ed.) Macmillan Press, London. pp. 262–293

Menzel R and Blakers M (1976) Colour receptors in the bee eye-morphology and spectral sensitivity. J Comp Physiol A 108:11–33

Menzel R, Hammer M, Braun G, Mauelshagen J, and Sugawa M (1991) Neurobiology of learning and memory in honeybees. *In:* L. Goodman, R. Fisher (eds). The behaviour and physiology of bees. Wallingford: CAB International. pp. 323–353

Menzel R and SnyderAW (1974) Polarized light detection in the bee, Apis mellifera. J Comp Physiol 88:247–270

Menael R, Ventura DF, Hertel H, de Souza JM and Greggers U (1986) Spectral sensitivity of photoreceptors in insect compound eyes: comparison of species and methods. J Comp Physiol A 158:165–177

Milde J (1981) Graded potentials and action potentials in the large ocellar interneurons of the bee. J Comp Physiol A 143:427–434

Milde JJ (1984) Ocellar interneurons in the honeybee. J Comp Physiol A 154:683–693

Milde JJ (1987) The ocellar system of the honeybee. In: Menzel R and Mercer A (eds): Neurobiology and Behavior of Honeybees. Berlin: Springer-Verlag, pp. 191–200

Milde JJ and Homberg U (1984) Ocellar interneurons in the honeybee: Characteristics of spiking L-neurons. J Comp A 155:151–160

Milde J, Seyan H, and Strausfeld NJ (1987) The neck motor system of the fly *Calliphora erythrocephala* II. Sensory organization. J Comp Physiol A 160:225–238

Mittelstaedt H (1950) Physiologie des Gleichgewichtssinnes bei fliegenden Libella. Zeitschrift für Naturforschung 32:422–452

Mote MJ, and Rubin LJ (1981) "On" type interneurons in the optic lobe of *Periplaneta amerianan*. J Comp Physiol A 141:395–401

Müller J (1826) "Zur vergleichenden Physiologie des Gesichtssines der Menchen der Tiere". Leipzig, pp 462

Naka KI and Rushton WAH (1966) S-potentials from colour units in the retina of fish (Cyprinidae). J Physiol 185:536–555

Nässel DR and Strausfeld NJ (1982) A pair of descending neurons with dendrites in the optic lobes projecting directly to thoracic ganglia of dipterous insects. 226:355–362

O'Carroll D (1993) Feature-detecting neurons in dragonflies. Nature 362: 541–543

O'Carroll D (2001) Motion adaption and evidence for parallel processing in the lobula plate of the bee-fly *Bombylius major*. *In:* Zanker M and Zeil J (ed) Motion Vision– Computational, Neural, and Ecological Constraints pp 381–394

O'Carroll DC, Bidwell NJ, Laughlin SB, Warrant E (1996). Insect motion detectors matched to visual ecology. Nature 382:63–66

Olberg RM (1981a) Object and self-movement detectors in the ventral nerve cord of the dragonfly. J Comp Physiol A 141:327–334

Olberg RM (1981b) Parallel encoding of direction of wind, head, abdomen and visual pattern movement by single interneurons in the dragonfly. J Comp Physiol A 142:27–41

Olberg RM (1986) Identified target-selective visual interneurons descending from the dragonfly brain. J Comp Physiol A 159:827–840

Olberg RM, Worthington AH and Venator KR (2000) Prey pursuit and interception in dragonflies. J Comp Physiol A 186:155–162

Osorio D (1986a) Directionally selective cells in the locust medulla. J Comp Physiol A 159:841–847

Osorio D (1986b) Ultraviolet sensitivity and spectral opponency in the locust. J Exp Biol 122:193–208

Osorio D (1987) The temporal properties of sustaining cells in the locust medulla. J Comp Physiol A 1612:441–448

Pan KC (1980) The neural organization of the ocellar system and associated pathways in the central system of the worker honey bee. PhD thesis, London

Pan KC and Goodman LJ (1977) Ocellar projections within the central nervous system of the worker honey bee, *Apis mellifera*. Cell Tiss. Res 176:505–527

Pappas LG and Eaton JL (1977) The internal ocellus of *Manciuca sexta*: Electroretinogram and spectral sensitivity. J Insect Physiol 23:1355–1358

Parry DA (1947) The function of the insect ocellus. J Exp Biol 24:211–219

Parsons MM, Krapp HG, Laughlin SB (2006) A motion-sensitive neurone responds to signals from the two visual systems of the blowfly, the compound eyes and ocelli. J Exp Biol 209:4464–74

Parsons MM, Krapp HG, Laughlin SB (2010). Sensor Fusion in Identified Visual Interneurons. Current Biol 20:624–628

Patterson J and Goodman LJ (1974) Relationships between ocellar units in the ventral nerve cord and ocellar pathways in the brain of *Schistocerca gregaria*. J Comp Physiol 95:251–262

Paulk AC, Dacks AM, Phollops-Portillo J, Fellous J-M, Gronenberg W (2009b) Visual processing in the central bee brain. J Neurosci 29:9987–9999

Paulk AC, Dacks AM and Gronenberg W (2009a) Color processing in the medulla of the bumblebee (Apidae: *Bombus inpatiens*). J Comp Neurol 513:441–456

Paulk AC, Phillips-Portillo J, Dacks AM, Fellous JM, Gronenberg W (2008) The processing of color, motion, and stimulus timing are anatomically segregated in the bumblebee brain. J Neurosci 28:6319–6332

Peng H, Chung P, Long F, Qu L, Jenett A, Seeds AM, Myers EW and Simpson JH (2011) BrainAligner: 3D registration atlases of *Drosophila* brains. Nature Methodes 8:493–498

Pfeiffer K and Kinoshita M (2012) Segregation of visual inputs from different regions of the compound eye in two parallel pathways through the anterior optic tubercle of the bumblebee (*Bombus ignitus*). J Comp Neurol 520:212–229

Pichaud F, Briscoe A and Desplan C (1999) Evolution of color vision. Curr Opin Neurobiol 9: 622–627

Portelli G, Ruffier F and Franceschini N (2010) Honeybee change their height to restore their optic flow. J Comp Physiol A 196:307–313

Reader RJ (1975) Competitive relationships of some bog ericads for major insect pollinators. Canadian Journal of Botany 53:1300–1305

Rehder, V (1988) A neuroanatomical map of the suboesophageal and prothoracic ganglia of the honey bee (*Apis mellifera*). Proc. R. Soc. Lond. B. 235:179–202

Reichert H, Rowell CHF, Griss C (1985). Course correction circuitry translates feature detection into behavioural action in locusts. Nature 315:142–144

Reichert H and Rowell CHF (1986) Neuronal circuits controlling flight in the locust: How sensory information is processed for motor control. TINs 9:281–283

Rein K, Zöckler M, Mader MT, Grübel C and Heisenberg M (2002) The Drosophila standard brain. Current Biology 12:227–231

Renner M and Heinzeller T (1979) Do trained honeybees with reliably blinded ocelli really return to the feeding site? J Apicult Res 18:225–229

Ribi WA (1974) Neurons in the first synaptic region of the bee, *Apis mellifera*. Cell Tiss Res 148:277–286

Ribi WA (1975a) The first optic ganglion of the bee. I. Correlation between visual cell types and their terminals in the lamina and medulla. Cell Tissue Res 165:103–111

Ribi WA (1975b) The neurons in the first optic ganglion of the bee (Apis mellifera). Adv Anat Embryol Cell Biol 50:1–43

Ribi WA (1979) The first optic ganglion of the bee. III Regional comparison of the morphology of the photoreceptor-cell axon. Cell Tiss Res 200:345–357

Ribi WA, and Scheel M (1981) The second and third optic ganglia of the worker bee: Golgi studies of the neural elements in the medulla and lobula. Cell Tissue Res 221:17–43

Ribi W, Senden TJ, Sakellariou A, Limaye A, and Zhang S (2008) Imaging honeybee brain anatomy with micro-X-ray-computed tomorgraphy. J Neurosci Methods 171:93–97

Ribi W, Warrant E and Zeil J (2011) The organization of honeybee ocelli: Regional specializations and rhabdom arrangements. Arthropod Struct Dev 40:509–520

Rister J, Pauls D, Schnell B, Ting CY, Lee CH, Sinakevitch I, Morante J, Strausfeld NJ, Ito K, Heisenberg M (2007) Dissection of the peripheral motion channel in the visual system of *Drosophila melanogaster*. Neuron 56:155–170

Robert D (1988) Visual steering under closed-loop conditions by flying locusts: flexibility of optomotor response and mechanisms of correctional steering. J Comp Physiol 164:15–24

Rowell CHF (1989) Descending interneurons of the locust reporting deviation from flight course: What is their role in steering?

Rowell CHF and Reichert M (1986) Three descending interneurons reporting deviation from course in the locust. II. Physsiology. J Comp Physiol 158:775–794

Rushton WAH (1972) Pigments and signals in colour vision. Invited lecture to the physiological society. J Physiol 220:1–31

Rybak J, Kuß A, Lamecker H, Zachow S, Hege H-C, Lienhard M, Singer J, Neubert K and Menzel R (2010) The digital bee brain: integrating and managing neurons in a common 3D reference system. Frontiers in System Neuroscience Vol. 4

Schaerer S and Neumeyer C (1996) Motion detection in goldfish investigated with the optomotor response is "color blind". Vision Res 36:4025–4034

Schlieper C (1927) Farbensinn der Tiere und optomotorische Reaktion. Zeitschrift für Vergleichende Physiologie 6:453–472

Schricker B (1965) Die Orientierung der Honigbiene in der Dämmerung. Zugleich ein Beitrag zur Frage der Ocellenfunktion bei Bienen. Z Verg Physiol 49:420–458

Schuppe H and Hengstenberg R (1993) Optical properties of the ocelli of *Calliphara erythrocephala* and their role in the dorsal light response. J Comp Physiol A 173:143–149

Schröter U, Wilson SLJ, Srinivasan MV, Ibbotson MR (2007) The morphology, physiology and function of suboesophageal neck motor neurons in the honeybee. J Comp Physiol A 193:289–304

Seidl R and Kaiser W (1981) Visual field size, binocular domain and ommatidial array of the compound eyes in the worker honey bees. J Comp Physiol 143:17–26

Singarajah KV (1988) Spectral sensitivity of motion-sensitive units of the butterfly ventral nerve cord. J Insect Physiol 119:1–4

Snodgrass RE (1942) The skeleto-muscular mechanisms of the honey bee. Smithsonian Miscellaneous Collections 103:1–120

Snodgrass RE (1956) Anatomy of the honeybee. New York, Comstock Public Association Cornell University Press

Sobel EC (1990) The locust's use of motion parallax to measure distance. J Comp Physiol 167:579–588

Srinivasan MV (1977) A visually-evoked roll response in the housefly. J Comp Physiol 119:1–14

Srinivasan MV (1985) Shouldn't directional movement detection necessarily be "colour-blind"? Vision Res 25:997–1000

Srinivasan MV and Guy RG (1990) Spectral properties of movement perception in the dronefly *Eristalis*. J Comp Physiol A 166:287–295

Srinivasan MV and Lehrer M (1984) Temporal acuity of honeybee vision: behavioural studies using moving stimuli. J Comp Physiol 297–312

Srinivasan MV, Lehrer M, Kirchner WH and Zhang SW (1991) Range perception through apparent image speed in freely flying honeybees. Vis Neurosci 6:519–535

Srinivasan MV, Zhang SW and Chandrashekara K (1993a) Evidence for two distinct movement-detecting mechanisms in insect vision. Naturwissenschaften 80:38–41

Srinivasan MV, Zhang SW and Rolfe B (1993b) Pattern vision in insects: "cortical" processing? Nature 362:539–540

Srinivasan MV, Zhang SW, Lehrer M and Collett TS (1996) Honeybee navigation en route to the goal: visual flight control and odometry. J Exp Biol 199:237–244

Srinivasan MV, Zhang S, Altwein M, and Tautz J. (2000a) Honeybee navigation: nature and calibration of the 'odometer'. Science 287:851–853

Srinivasan MV, Zhang SW, Chahl JS, Barth E and Venkatesh S (2000b) How honeybees make gazing landing on flat surfaces. Biol Cybern 83:171–183

Stange G (1981) The ocellar component of light equilibrium control in dragonflies. J Comp Physiol 141:335–347

Stange G and Howard J (1979) An ocellar dorsal light response in a dragonfly. J. Exp. Biol. 83:351–355

Stange G, Stowe S, Chahl J, and Massaro A (2002) Anisotropic imaging in the dragonfly median ocellus: a matched filter for horizon detection. J Comp A 188:455–467

Stavenga DC, Chappell RL and Wilson M (1979) Insect pupil mechanisms. II on the pigment migration in dragonfly ocelli. J Com Physiol 129:199–205

Strausfeld NJ (1970) Golgi studies on insects. Part II. The optic lobes of Diptera. Phil Trans Roy Soc B 258:175–223

Strausfeld NJ and Bassemir UK (1985) The origanisation of giant horizontal-motion-sensitive neurons and their synaptic relationships in the lateral deutocerebrum of *Calliphora erythrocephala* and *Musca domestica*. Cell Tissue Res 242:531–550

Strausfeld NJ and Blest AD (1970) Golgi studies on insects. Part I. the optic lobes of Lepidoptera. Phil Trans Roy Lond B 258:81–134

Strausfeld NJ and Gronenberg W (1990a) Descending neurons supplying the neck and flight motor of Diptera: Organization and neuroanatomical relationships with visual pathways. J Comp Neurol 302:954–972

Strausfeld NJ and Gronenberg W (1990b) Descending neurons supplying the neck and flight motor of Diptera: Physiological and anatomical characteristics. J Comp Neurol 302:973–991

Strausfeld NJ and Lee J-K (1991) Neural basis for parallel visual processing in the fly. Vis Neurosci 7:13–33

Strausfeld NJ, Seyan H, Milde JJ (1987) The neck motor system of the fly *Calliphora erythrocephala* I. Muscles and motor neurons. J Comp Physiol A 160:205–224

Suzuki H (1975) Antennal movements induced by odour and central projection of the antennal neurons in the honeybee. J Insect Physiol 21:831–847

Taylor CP (1981a) Contribution of compound eyes and ocelli to steering of locusts in flight. I Behavioural analysis. K Exp Biol 93:1–18

Taylor CP (1981b) Contribution of compound eyes and ocelli to steering of locusts in flight. II. Timing changes in flight motor units. J Exp Biol 93:19–31

Taylor GK and Krapp HG (2008) Sensory system and flight stability: What do insects measure and why? Adv Insect Physiol 34:231–316

Tang R, Wolf R, Xu S and Heisenberg M (2004) Visual pattern recognition in *Drosophila* is invariant for retinal position. Science 305:1020–1022.

Theobald J., Dario LR and Frye MA (2009) Dynamics of optomotor responses in *Drosophila* to perturbations in optic flow. J Exp Biol 213:1366–1375

Toh Y and Kuwabara M (1974) Fine structure of the dorsal ocellus of the worker honeybee. J Morph 143:285–306

Troje N (1993) Spectral categories in the learning behaviour of blowflies. Zeitschrift Für Naturforchung 48:96–104

Wakakuwa M, Kuraswa M, Giurfa M, and Arilawa K (2005) Spectral heterogeneity of honeybee ommatidia. Naturwissenschaften 92:464–467

Warrant EJ (2006) Invertebrate vision in dim light. *In*: Invertebrate vision (Warrant EJ and Nilsson D-E, ed) Cambridge Univ Press, UK. pp. 83-126

Warrant EJ (2008) Seeing in the dark: vision and visual behaviour in nocturnal bees and wasps. J Exp Biol 211:1737–1746

Warrant EJ, Kelber A, Gislén A, Greiner B, Ribi W, and Wcislo WT (2004) Nocturnal vision and landmark orientation in a tropical halictid bee. Current Biology 14:1309–1318

Warrant EJ, Kelber A, Wallén R, and Wcislo WT (2006) Ocellar optics in nocturnal and diurnal bee and wasps. Arthropod Struct Dev 35:293–305

Wehner R (1981) Spatial vision in arthropods. In H. Autrum (ed) Handbook of sensory physiology, vol VII/6C. Springer, Berlin Heidelberg New York, pp 287–616

Wertz A, Borst A, Haag J (2008) Nonlinear integration of binocular optic flow by DNOVS2, a descending of the fly. J Neurosci 28:3131–3140

Wertz A, Gaub B, Plett J, Haag J, Borst A (2009a) Robust coding of ego-motion in descending neurons of the fly. J Neurosci 29:14993–15000

Wertz A, Haag J, Borst A (2009b) Local and global motion preferences in descending neurons of the fly. J Comp Physiol 195:1107–1120

Wilson M (1978) The function organization of locust ocelli. J Comp Physiol 124:297–316

van Hateren, J. H. and Schilstra, C. (1999). Blowfly flight and optic flow. II. Head movements during flight. J Exp Biol 202:1491–1500

van Santen JPH and Sperling G (1985) Elaborated Reichardt detectors. J Opt Soc Am A 2:300–321

van Kleef J, James AC, and Stange G (2005) A spatiotemporal white noise analysis of photoreceptor response to UV and green light in the dragonfly median ocellus. J Gen Physiol 126:481–497

van Kleef J, Berry R, and Stange G (2008) Directional selectivity in the simple eye of an insect. J Neurosci 28:1847–2855

von Frisch K (1914) Der farbensinn und formensinn der biene. Zoologische Fahrbücher. Abteilung für allgemeine Zoologie und Physiologie der Tiere 35:1–188

von Frisch K (1967) The dance language and orientation of bees. Cambridge University Press, Cambridge

von Frisch K (1949) Die Polarisation des Himmelslichtes als orienterener Faktor bei den Tanzen der Bienen. Experientia (Basel) 5:142–148

Vorobyev M and Brandt R (1997) How do insect pollinators discriminate colours? Isr J Plant Sci 45:103–113

Vorobyev M and Menzel R (1999) Flower advertisement for insects: Bees, a case study. *In*: Adaptive Mechanisms in the Ecology of Vision (Archer SN, Djamgoz MBA, Loew ER, Partridge JC and Vallerga S eds.) Dordrecht: Kluwer Academic Publishers. pp. 537–553

Wardill TJ, List O, Li X, Dongre S, McCulloch M, Ting C-Y, O'Kane CJ, Tang S, Lee C-H, Hardie RC and Juusola M (2012) Multiple spectral inputs improve motion discrimination in the *Drosophila* visual system. Science 336: 925–931

Wilson M (1978) The functional organisation of locust ocelli. J Comp Physiol A 124:297–316

Yamaguchi S, Desplan C and Heisenberg M (2010) Contribution of photoreceptor subtypes to spectral wavelength preference in *Drosophila*. PNAS 107:5634–5639

Yamaguchi S, Wolf R, Desplan C and Heisenberg M (2008) Motion vision is independent of color in *Drosophila*. PNAS 105:4910–4915

Yamawaki Y and Toh Y (2009) A descending contralateral directionally selective movement detector in the praying mantis *Tenodera aridifolia*. J Comp Physiol A 195:1131–1139

Yang EC, Lin HC, and Hung YS (2004) Patterns of chromatic information processing in the lobula of honeybee, *Apis mellifera* L. J Insect Physiol 50:913–925

Zanker JM (1996) On the elementary mechanism underlying secondary motion processing. Phil Trans R Soc Lond B 351:1725–1736

Zbikowski B (2005) Fly like a fly. IEEE Spectrum 42:46–51

Zhang SW, Srinivasan MV (1993) Behavioural evidence for parallel information processing in the visual system of insects. Jpn J Physiol 43:S247–S258